

THE UNIVERSITY OF HULL

Optimisation and Control of Muscular Forces to
Maintain Optimal Compression Loading in the Femur

a Thesis submitted for the Degree of Doctor of
Philosophy in the University of Hull

by

Alexander Findlay Brown, BEng (University of Dundee)

September 2014

Abstract

The aims of this study were to investigate the feasibility of maintaining compression in the femur as the dominant state of loading and to explore the impact of changes to the musculoskeletal system on this loading regime. The literature provides a wealth of evidence for the adaptation of bone to its mechanical environment. There is a long standing theory that bone is loaded primarily in compression during routine activities and that this is achieved by coordinated muscle activity.

This study employed a multibody dynamics musculoskeletal model that compared optimisations of muscle loading with, and without, enforced compression in the shaft of the femur. The purpose of these optimisation studies was not to accurately predict patterns of muscle activation *in vivo*, but to comparatively assess the feasibility and cost of maintaining compression in the femur.

The results showed that compression can be maintained in the femur throughout gait by coordinated muscle activity. Loading the shaft of the femur in compression causes a reduction in peak bone stresses. Some increased difficulty in maintaining compressive loading was associated with reduced muscle forces and degraded motor control. These results offer insight into possible mechanisms affecting osteoporosis through incorrect mechanical loading and invite further research.

Acknowledgements

The completion of this work was achieved with the help and support of many people who are deserving of sincere thanks. The work was generously funded by OSPREY and particular thanks are directed towards Syd Howey and Sue Steel for their input and encouragement. The initiation of this research was in large part due to the work of Professor Ulrich Witzel whose insight has been invaluable on this project.

My supervisor, Professor Michael Fagan has shown kindness and patience throughout. His encouragement and optimistic outlook have made this a more enjoyable experience and for this I am grateful. Help has come from many colleagues in many forms. I would like to thank the following people for their constant willingness to help whether I was having software issues, needed help in the lab, or during informal discussions: Amartya Ganguly, Neil Curtis, Steve McCormack, David Lunn, Pete Watson, Anna Chabokdast, Flora Gröning, Catherine Dobson, Junfen Shi, and Sue Taft. It has been a pleasure working with each member of the University of Hull medical engineering research group.

My wife Elizabeth, has gone above and beyond to help in any way possible always without complaint. Without her support this work would never have been completed.

Finally, I would like to offer thanks to my dear friend Tom Chesters. I consider myself genuinely fortunate to have known him.

Table of Contents

Chapter 1 Introduction	1
1.1 Introduction to Bone.....	1
1.2 Methods of Investigation.....	6
1.3 Aims and Objectives of this Study	10
1.4 Thesis Outline.....	11
Chapter 2 Literature Review	13
2.1 Mechanical Loading of Bone.....	13
2.2 Compression Theory of Bone.....	20
2.3 Innervation of Bone	28
2.4 Changes to the Musculoskeletal System	31
2.5 Musculoskeletal Modelling.....	38
Chapter 3 A Multibody Dynamics Musculoskeletal Model	44
3.1 Introduction to the Modelling	44
3.2 Model Development	44
3.3 Final Model Description.....	51
3.4 Sensitivity Studies	67
3.5 Sensitivity Study Results	70
3.6 Discussion.....	74
3.7 Conclusions	76
Chapter 4 Multibody Dynamics Gait Simulation	77
4.1 Introduction	77
4.2 Data Collection.....	77
4.3 Subject Specific Model.....	83
4.4 Simulations Carried Out.....	84

4.5 Results	85
4.6 Discussion.....	102
Chapter 5 Improved Model.....	108
5.1 Introduction	108
5.2 Method.....	109
5.3 Results	111
5.4 Discussion.....	129
Chapter 6 Effect of Limited Muscle Activity on State of Loading in the Femur	132
6.1 Introduction	132
6.2 Method.....	132
6.3 Results	133
6.4 Discussion.....	138
Chapter 7 Discussion.....	140
7.1 Background and Scope of This Study	140
7.2 Limitations of the Study	141
7.3 Compression in the Femur.....	144
7.4 Control of Muscular Loading.....	147
7.5 Ageing and Osteoporosis	149
Chapter 8 Conclusions and Future Work.....	156
8.1 Conclusions	156
8.2 Musculoskeletal Modelling.....	157
8.3 Compression of Bone	159
8.4 Changes to the Musculoskeletal System	160
Appendix A Model Creation.....	173
Appendix B Additional Results	190

List of Figures

1.1	Cross section of a human proximal femur showing trabecular bone encased by cortical bone (Skedros & Baucom 2007).....	2
1.2	Osteoclasts remove old bone leaving a cavity which is filled with new bone by trailing osteoblasts.....	3
1.3	An example of how kinematic and kinetic data is recorded	8
2.1	Diagram of osteocytes embedded in the bone matrix, connected by canalicular tunnels	14
2.2	Comparison of the ordered internal structure of a human femur with the less ordered example of a sloth femur (Tobin 1955, Gregory & Aspden 2008)	16
2.3	The continued decline of muscle and bone following recovery of weight bearing ability in mice (Manske et al., 2011).....	20
2.4	The trabecular structures of the femoral neck and their previously accepted functions (Hammer, 2010)	21
2.5	Cross sectional geometry of the femoral neck (Zebaze et al. 2007)	22
2.6	Stress distribution in a column with increased degrees of bending (Pauwels 1980).....	23
2.7	Stress reduction by adding material (Pauwels 1980)	24
2.8	Stress reduction by counter-bending (Pauwels 1980).....	25
2.9	The FE model used by Sverdlova and Witzel compared with CT scan images on the left (Sverdlova et al. 2010)	26
2.10	The 2-D FE model developed by Rudman showing the proximal femur and acetabulum (Rudman et al. 2006)	27

2.11	The FE model used by Taylor et al. to analyse deflection of the femoral head in different loading conditions (Taylor et al. 1996)	28
2.12	Linear regression plot showing inverse correlation between type II muscle fibre atrophy and BMD in osteoporosis (Terracciano et al. 2013)	37
3.1	Load sensing of interface between two halves of the femur	45
3.2	Simple model with flexible connectors between two parts.....	46
3.3	Simple femur model acted on by one fixed load.....	47
3.4	The model using anatomical data.....	50
3.5	The completed model.....	51
3.6	Torques are measured about 3 axes of the spherical joint at the hip....	53
3.7	Knee joint consisting of two hinges on a single axis	54
3.8	Spherical joint between femur segments constrained by three orthogonal torsional springs.....	55
3.9	Exploded view of the model showing the joints between each segment and the external load applied to the foot.....	56
3.10	Muscle via points	58
3.11	Detailed view of the muscle strands considered in the model	59
3.12	Process flow showing each step of the simulation process with its inputs and outputs.....	61
3.13	Cross sectional dimensions of the cylinder used to calculate maximum allowable stress.....	64
3.14	A representation of a column under axial load	65

3.15	Sagittal view of the knee joint	68
3.16	The direction of the GRF vector in the sagittal plane	69
3.17	Cross section of the cut in the femur	70
3.18	Impact of moving the knee joint in the anterior-posterior direction.....	71
3.19	The axis of rotation of the knee as it sits on the tibial plateau in its original position	72
3.20	Variations in hip, knee, and femur forces with rotation of the knee axis in the transverse plane	72
3.21	Hip, knee, and femur forces with variations in direction of the GRF	73
4.1	Marker setup used for static trials.....	78
4.2	Extension of the hip to test MVC of the gluteus maximus.....	81
4.3	MVC of the gluteus medius tested by abduction of the hip.....	81
4.4	Hamstring MVC tested by flexion of the knee with resistance applied	82
4.5	MVC of quadriceps tested in a seated position by extension of the knee against fixed resistance.....	82
4.6	Gastrocnemius MVC tested by plantarflexion of the ankles against manually applied resistance on the shoulders	83
4.7	Hip joint reaction force across the gait cycle for two constraint conditions.....	86
4.8	Knee joint reaction force across the gait cycle for two constraint conditions.....	87

4.9	Ground reaction forces for the right and left side across the gait cycle	88
4.10	Gluteus maximus EMG profile across the gait cycle from 5 trials with standard deviation	89
4.11	Gluteus maximus activation as predicted by the model with each of two sets of constraints	89
4.12	Gluteus medius EMG profile across the gait cycle	90
4.13	Gluteus medius muscle activity as predicted by the model	90
4.14	Gluteus medius anterior muscle activity as predicted by the model	91
4.15	Gluteus medius posterior muscle activity as predicted by the model	91
4.16	Tensor fascia lata EMG profile across the gait cycle	92
4.17	Tensor fascia lata muscle activity as predicted by the model	92
4.18	Rectus femoris EMG profile across the gait cycle	93
4.19	Rectus femoris muscle activity as predicted by the model	94
4.20	Vastus intermedius muscle activity as predicted by the model	94
4.21	Vastus lateralis EMG profile across the gait cycle	95
4.22	Vastus medialis EMG profile across the gait cycle	95
4.23	Vastus lateralis muscle activity as predicted by the model	96
4.24	Vastus medialis muscle activity as predicted by the model	97
4.25	Semitendinosus EMG profile across the gait cycle	97
4.26	Semitendinosus muscle activity as predicted by the model	98
4.27	Biceps femoris EMG profile across the gait cycle	99

4.28	Biceps femoris muscle activity as predicted by the model.....	99
4.29	Gastrocnemius medialis EMG profile across the gait cycle	100
4.30	Gastrocnemius medialis muscle activity as predicted by the model ...	100
4.31	Gastrocnemius lateralis EMG profile across the gait cycle.....	101
4.32	Gastrocnemius lateralis muscle activity as predicted by the model	101
4.33	GRF measured in 18 adult males by Hunt et al. (2001)	103
4.34	Simplified diagrams of two options for modelling of the ITB imagined from a sagittal perspective	106
5.1	Hip and knee joint loads at 50% of gait comparing the 67 and 31 strand models.....	109
5.2	Hip joint reaction forces across the stance phase of gait with and without enforced compression	112
5.3	Knee joint reaction forces across the stance phase of gait with and without enforced compression.....	113
5.4	Gluteus maximus muscle activation across the stance phase of gait with and without enforced compression.....	113
5.5	Gluteus maximus activation with compression enforced in both the 31 and 67 strand models	114
5.6	Gluteus medius posterior muscle activation across the stance phase of gait with and without enforced compression.....	115
5.7	Gluteus medius anterior muscle activation across the stance phase of gait with and without enforced compression	115
5.8	Gluteus medius posterior activation with compression enforced in both the 31 and 67 strand models	116

5.9	Gluteus medius anterior activation with compression enforced in both the 31 and 67 strand models	116
5.10	Tensor fascia lata muscle activation across the stance phase of gait with and without enforced compression.....	117
5.11	Rectus femoris muscle activation across the stance phase of gait with and without enforced compression.....	118
5.12	Vastus medialis muscle activation across the stance phase of gait with and without enforced compression.....	119
5.13	Vastus lateralis muscle activation across the stance phase of gait with and without enforced compression.....	119
5.14	Semitendinosus muscle activation across the stance phase of gait with and without enforced compression.....	120
5.15	Biceps femoris muscle activation across the stance phase of gait with and without enforced compression.....	120
5.16	Gastrocnemius lateralis muscle activation across the stance phase of gait with and without enforced compression	121
5.17	Gastrocnemius medialis muscle activation across the stance phase of gait with and without enforced compression	122
5.18	The sum of muscle stresses cubed across the stance phase of gait with and without enforced compression.....	123
5.19	Maximum principal stress at the cut in the femur with and without compression enforced	124
5.20	Hip joint reaction forces across the stance phase of gait compared using three different cost functions	125

5.21	Knee joint reaction forces across the stance phase of gait compared using three different cost functions	125
5.22	Gluteus maximus muscle activation across the stance phase of gait compared using three cost functions	126
5.23	Gluteus medius muscle activation across the stance phase of gait compared using three cost functions	126
5.24	Tensor fascia lata muscle activation across the stance phase of gait compared using three cost functions	127
5.25	Rectus femoris muscle activation across the stance phase of gait compared using three cost functions	127
5.26	Semitendinosus muscle activation across the stance phase of gait compared using three cost functions	128
5.27	Semimembranosus muscle activation across the stance phase of gait compared using three cost functions	128
6.1	Hip joint loads across the stance phase of gait with and without limitations to maximum muscle forces.....	134
6.2	Knee joint loads across the stance phase of gait with and without limitations to maximum muscle forces.....	134
6.3	Activation of the anterior muscles of the thigh at 45% of gait with and without limitations to maximum muscle forces.....	136
6.4	Activation of the muscles surrounding the hip at 45% of gait with and without limitations to maximum muscle forces.....	137
6.5	Maximum principal stress in the femur with and without limitations to maximum muscle forces	138

7.1	Gluteus medius anterior and TFL showing disparate lines of action which may not be replicated in vivo	146
7.2	A suggested double feedback loop for the regulation of healthy bone mass	148
7.3	Hip joint reaction force across the stance phase of gait	152
7.4	Knee joint reaction force across the stance phase of gait.....	153
7.5	Maximum principal stress at the cut in the femur across the stance phase of gait	154

List of Tables

2.1	Muscles crossing the hip and knee joints with their respective points of origin, insertion, and actions (Moore et al. 2011)	33
3.1	List of 32 muscles, the number of strands used for each, and the abbreviations	57
3.2	Summary of cost functions investigated during optimisation studies ...	66
3.3	Summary of constraints applied to the model	66
3.4	Impact on knee joint reaction force of moving the spherical joint between femur segments in the transverse plane	74
4.1	List of marker locations and their inclusion in static/motion trials.....	79
4.2	EMG data collected from 10 muscles using 8 channels over 2 sets of trials	80
5.1	Optimisation studies carried out using 67 strand model	111

Chapter 1

Introduction

1.1 Introduction to Bone

The extensive variety of human movements is made possible by a complex musculoskeletal system. Muscles provide the forces which move the body and bones provide the structure which allows these forces to be effective. From the precision of a pianist to the sweeping grace of a gymnast, the musculoskeletal system is capable of adapting to a staggering range of tasks. This is made possible by training of the neurological control system which activates the muscles as well as strengthening of the muscles and bones themselves. Athletes know that increased endurance or stronger contractions requires training of the muscles so that they increase in size and force-producing capability. It naturally follows that larger forces require stronger supporting structures and so bones adapt according to the loads placed upon them. Bone adaptation was first described by Roux (Roux 1885) and later by Wolff (Wolff 1986), with the theory that describes bone's adaptation to mechanical usage now commonly known as Wolff's law. A good example of this adaptation is seen in tennis players whose racquet arms are routinely exposed to higher stresses than their other arm. There is a corresponding difference in bone mass between the two arms, with the racquet arm having thicker bones (Calbet et al. 1998). It is also true that reduced loading results in a loss of bone mass. For example, astronauts in a weightless environment experience a dramatic loss of bone due to unloading of the skeleton (Baldwin et al. 1996, Carmeliet et al. 2001). The same is true of those who are bedridden for long periods or have a limb in a cast (Gross & Rubin 1995).

Bones consist of an outer shell of compact material known as cortical bone. This outer shell is supported from within by a latticework of small columns known as trabecular or cancellous bone. The structure is often described as being similar to that of a sponge. This spongy inner structure allows the skeleton to remain relatively light whilst maintaining sufficient strength. A cross-sectional view of a proximal femur demonstrates this lightweight structure in Figure 1.1.

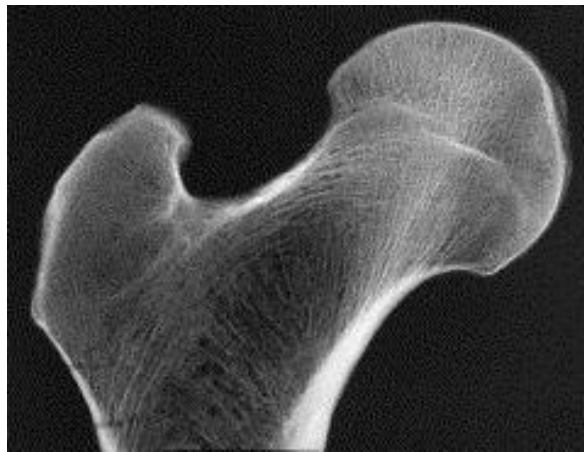


Figure 1.1 - Cross section of a human proximal femur showing trabecular bone (the darker “spongy” looking texture at the interior of the bone) encased by cortical bone (the bright areas at the bone surface) (Skedros & Baucom 2007).

The mechanisms by which bones change are known as modelling and remodelling as first described by Frost (Frost 1963, Robling et al. 2006). Old bone is removed by cells called osteoclasts, in a process called resorption. Formation of new bone is accomplished by osteoblast cells. The bone modelling process is primarily operative during growth of the skeleton or where adult bone geometry is to be altered. This may be in response to changes in mechanical stimuli or in pathological conditions. Modelling consists of resorption in one area and formation in another, but not in the same place. For example, if the diameter of a tubular bone was to be increased, bone would be removed at the inner surface and deposited at the outer surface. In this way bones are capable of growth and adaptation. Remodelling is a

continually occurring cycle in which osteoclasts and osteoblasts work in tandem to renew the skeleton as shown in Figure 1.2. Cells are arranged into basic multicellular units or BMUs. These BMUs are led by osteoclasts which carve their way through the bone leaving a cavity to be filled with new bone by the trailing osteoblasts. This allows the reparation of microdamage and conservation of healthy bone. Resorption and formation ideally occur in equal measure but in some disease states there can be an imbalance in the way bone is remodelled (Robling et al. 2006). Bone remodelling in response to mechanical loading is regulated by biochemical signals originating from osteocytes which are cells residing within the bone matrix. Osteocytes monitor the habitual loading conditions of bone and send signals to the bone surface which initiate or inhibit bone remodelling activity (Bonewald 2007, Chen et al. 2010).

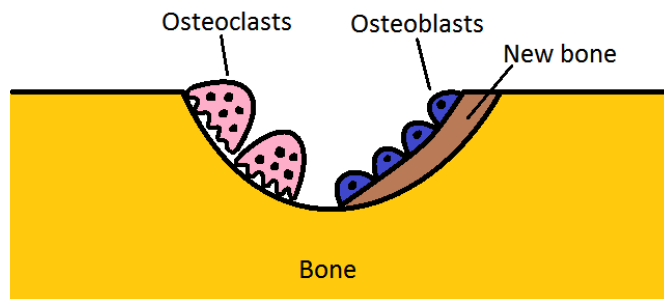


Figure 1.2 - Osteoclasts remove old bone leaving a cavity which is filled with new bone by trailing osteoblasts.

The precise interaction of the many factors influencing bone remodelling is complex and as yet, not fully understood. It is clear however that in addition to the mechanical influences mentioned previously, diet, hormones and age play a part. Calcium and vitamin D levels have long since been associated with bone mass regulation (Salamoun et al. 2005, Grados et al. 2003) and in general a healthy diet containing fruit and vegetables has been found to influence bone mass positively (Chapuy et al. 1992, Brazier et al. 1995). The effects of various hormones have been researched extensively. For example, an excess

of thyroid hormone has been found to contribute to bone loss (Auwerx & Bouillon 1986), while hormonal changes which take place following menopause are a strong contributor to the onset of osteoporosis in post-menopausal women.

Osteoporosis is a weakening of the bones caused by deterioration of trabecular structures and thinning of the cortex, and occurs as a result of an imbalance in the way bone is remodelled. Humans reach their peak bone mass in their mid-twenties, then from around the age of 40, everyone will experience some bone loss due to the increased prevalence of resorption over formation. Depending on the various factors involved in bone mass regulation, this imbalance can become exaggerated resulting in weak bones and a risk of fragility fractures. Even if the rate of bone loss is not excessive osteoporosis can still develop if peak bone mass is too low. Among the many disorders affecting bone, osteoporosis is perhaps the most common, and is more common among women, although men are also at risk.

It has been reported that 50% of women aged 50 will suffer a fracture in their lifetime, most likely due to osteoporosis (Van Staa et al. 2001). Osteoporotic fractures occur most frequently in the wrist, hip and spine, with hip fractures regarded as the most serious due to high mortality rates and reduced quality of life post-fracture. Cooper reported that one year after fracture, 60% of hip fracture patients are limited in at least one task of daily living such as dressing or toileting (Cooper 1997). The rate of hip fractures in the UK is predicted to reach 117,000 in 2016 according to a 2005 study (Dennison et al. 2005). With such an increasing problem, it is important that our understanding of osteoporosis continues to deepen, with a view to developing more effective treatments and management strategies.

One of the difficulties in treating osteoporosis is that a fractured bone is often the first symptom of the disease. Those at high risk of having or developing osteoporosis are often given DEXA (dual-energy X-ray absorptiometry) scans. These allow those with low bone mineral density (BMD) to be identified and

where appropriate, treated. Only a very brief overview of those treatments available will be given here.

Current treatments include bisphosphonates and calcitonin which serve to inhibit osteoclast activity, thus tipping the balance of bone turnover more favourably towards formation. Parathyroid hormone (PTH) stimulates osteoblasts and can increase bone density. Both osteoblasts and osteoclasts are affected by strontium ranelate which is used as an alternative treatment where bisphosphonates are not a viable option.

Owing to the effect of calcium and vitamin D deficiencies on BMD, these are also often given as dietary supplements to those at risk of or suffering from osteoporosis. Furthermore, the effects of post-menopausal osteoporosis can be treated by hormone replacement therapy (HRT) or selective estrogen receptor modulators (SERMs).

Bisphosphonates are the most commonly used front-line treatment and evidence shows their success in reducing fracture risk, along with the other treatments mentioned (MacLean et al. 2008, Chen & Sambrook 2012). It should be noted however, that all of these treatments are associated with some undesirable side effects.

Although most of the treatments currently in use act by limiting or accelerating the work of bone remodelling cells, a strong case has been made recently for the benefit of exercise regimes such as Tai Chi (Murphy & Singh 2008, Lee et al. 2008). These not only provide physical stimulation of the bone, but lead to improved balance and postural stability. This greatly reduces the risk of falls, which are often the cause of fractures.

Fractures occur when bones are subjected to loads for which they are not adapted. Poorly adapted bones are therefore more susceptible to fractures. As bones adapt to their mechanical environment, it follows that one of the main contributors to poorly adapted bones is incorrect mechanical loading (Frost 1988, Prendergast & Huiskes 1995, Saporin et al. 2011). A question remains

over what constitutes correct mechanical loading of bone. Bone is well known to be strongest in compression (Savvidis and Stabrey, 1996). Some investigators have made the case for compressive loading of long bones achieved by synergistic agonist-antagonist muscle activity (Pauwels 1980, Sverdlova & Witzel 2010, Taylor et al. 1996). This school of thought states that tensile loads arising from large amounts of bending are reduced by counter bending loads, which create a compressive and more even stress distribution.

Degradation of neuromotor control which occurs as a consequence of ageing and some pathological conditions not only causes postural instability, but also limits the ability of muscles to habitually provide appropriate loading of the long bones (Martelli et al. 2011).

The main hypothesis of this current research is that the body naturally prefers to load the bone in compression, and where possible creates the appropriate muscle activity to do so. The work aimed to determine initially whether the musculature of the thigh was capable of maintaining such a loading regimen in the femur during the entire gait cycle. This capability was then assessed under conditions of limited muscle activity, to simulate ageing or impaired neuromuscular control. The purpose of these investigations was to clarify the extent to which bone pathologies, such as osteoporosis, might be influenced by muscular malfunction, and to prompt development of appropriate treatments.

1.2 Methods of Investigation

Understanding precisely how muscular loading is applied to bone presents a challenge. The loading surrounding the femur for example, is highly complex, with 30 muscles crossing the hip and knee joints. In addition, several of these muscles have wide attachments and separate into superior and inferior portions and there are various ligaments connecting the bones as well. It is therefore very difficult to predict how changes to the complex patterns of muscle activity might affect the loading of the bone. In order to assess the possible relationship between mechanical factors and the onset or promotion

of osteoporosis, ideally the forces produced in each muscle and the resulting strain distribution in the bone need to be measured simultaneously. However, standard engineering methods of force and strain measurement are unsuitable for use *in vivo*. Alternative methods must therefore be sought.

Strains in bone cannot be measured non-invasively although valuable joint loading data has been collected using instrumented prostheses (Bergmann et al. 2001). Perhaps the most common examples of these are hip and knee replacements fitted with strain gauges or pressure transducers. These can provide strain data at specific locations in post-operative patients and thus yield information on the total force through the prosthesis. Such measurements are extremely useful in the validation of mathematical models predicting joint loading. Comparison of loading patterns during different activities is also useful in determining when and how peak loads occur. It is important to note however that the data collected is post-operatively from patients who have undergone a significant invasive procedure requiring sizeable sections of bone to be removed, inevitably leading to some modification of, and possibly damage to, the neuromuscular control system. Thus, the measured loads from the instrumented implants are likely to differ from normal physiological loading. Another limiting factor is that the results obtained provide only the strain in the prosthesis and so estimations of strain distribution throughout the femur must still be provided theoretically using mathematical models.

The external forces acting on the body are bodyweight and ground reaction forces. These may be measured and used as inputs to mathematical models. Bodyweight measurement is a routine activity which can be accomplished using bathroom scales, but the measurement of ground reaction forces during locomotion requires the use of specialised force plates (Sutherland 2005). Modern force plates are capable of measuring force in 3 directions and moments about 3 axes. This can be accomplished using strain gauges and often piezoelectric sensors. Force plates are usually used in conjunction with motion capture systems for gait analysis. Most motion capture systems used in

biomechanical analyses use reflective markers placed over bony landmarks which are tracked by infra-red cameras (Figure 1.3). The kinematic data from the system then reveals the instantaneous positions and movement of the body segments. Combined motion capture and force plate measurements allow correlation to be made between external forces acting on the skeleton and their concurrent movements. For the loads on a bone to be accurately represented however, muscle forces must also be taken into account.

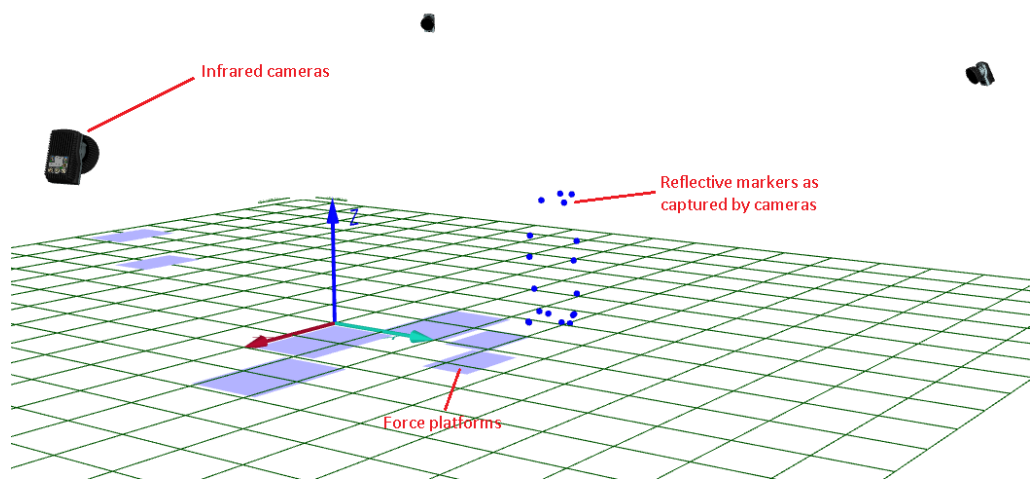


Figure 1.3 - An example of how kinematic and kinetic data is recorded. The image above shows part of our lab setup as represented in the data collection program (Qualysis Track Manager).

Muscle forces cannot be measured directly, but electromyography (EMG) can offer information on when and to what extent muscles are firing. A small electrical signal is produced when muscles contract. Measuring this signal can yield information on muscle activation. There are two ways in which EMG measurements are collected. These are surface EMG and fine-wire EMG (Sutherland 2001). In surface EMG, electrodes are placed on the skin over the belly of the muscle and electrical activity is monitored. This technique can only be applied to superficial muscles and there is some risk of cross-talk from other muscles if electrodes are not placed correctly (De Luca 1997). Fine-wire EMG involves the insertion of electrodes into the muscle tissue using needles. Activity of deep muscles can be monitored in this way but the procedure is

somewhat invasive and EMG signals are only measured at a very specific point within the muscle. Most laboratories use only surface EMG owing to its non-invasive application when compared with fine-wire EMG and the relative ease with which data can be collected (Sutherland 2001). Unfortunately the electrical activity measured by EMG is not necessarily proportional to muscle force production. It offers an indication of the level of muscle activity during a particular movement. Care must then be taken in the processing and interpretation of data.

A useful alternative to the above methods is to simulate models of the musculoskeletal system using numerical methods. A range of musculoskeletal models have been developed to predict muscle forces, joint loads, strains in bone, and countless other parameters. These models are designed to replicate the systems of the body as closely as possible. Dissection studies and modern scanning methods such as CT and MRI may be used to provide anatomical data with which to recreate body parts (Blemker et al. 2007), and software is available which can translate medical images into 3D objects ready for use in engineering simulation software. Inevitably limitations on computing power and gaps in the available data require that some simplifications be made to musculoskeletal models and boundary conditions applied. These must be very carefully designed so as not to invalidate the results of the study by straying too far from conditions *in vivo*. The input and boundary conditions required depends on the aim of the particular study.

The primary challenge facing researchers in this area is and always has been validation. Great care must be taken to build accurate models, including considerations of the precise location of joint centres of rotation, load distribution and direction, material properties, and many others. Regrettably there is still no absolute way to prove that results obtained by numerical methods are wholly representative of conditions *in vivo*. Fortunately however there are some limited means to prove that the results are reasonable, such as those previously mentioned: instrumented prostheses and EMG. These may

be compared to joint loads and muscle activation patterns predicted by a model. If agreement is found, a case can be made for the validity of the model.

A growing body of evidence supports the value of musculoskeletal modelling. Continued development of these numerical methods will allow engineers to make increasing contributions in the medical field and provide medical professionals with better information. Computerised models are widely used in the engineering industry to test designs quickly and cheaply. Now and in the future there is a definite role to play for these methods in medical engineering. The ability to simulate the outcome of a treatment accurately will allow treatments to be improved greatly and administered with far less risk to the patient. The primary means of investigation in this current research will be the application of such a computerised model of the mechanical environment surrounding the human femur.

1.3 Aims and Objectives of this Study

The aims of this research were to better understand muscular loading of the femur and its impact on bone health particularly as it relates to osteoporosis. Where previous studies on compressive loading of bone have examined loading at particular points or postures, this study considered the entirety of the gait cycle.

There were two key objectives. The first was to determine whether it is possible to maintain compression in the shaft of the femur during gait. A multibody dynamics model was used to simulate the bones and muscles of the thigh. Muscle forces were optimised to maintain equilibrium in the hip and knee joints whilst minimising a cost function. These optimisation studies were then repeated, while including compression in the shaft of the femur as an added simulation objective. As the mechanisms guiding muscle activation are unknown, several cost functions were applied in turn. The degree to which compression can be maintained throughout gait by the combination of muscle forces was a point of key interest in this study.

The second objective was to undertake an investigation into the effects of limiting muscle activity. Age and infirmity can cause muscles to function incorrectly or with greater limitations. Using the model developed previously, simulations were designed to determine to what extent muscles can maintain compression in the femur when muscle activity is limited.

Peak stresses in the shaft of the femur were calculated for each loading condition. These calculations yielded information on how the modified loading affects the stress distribution in the femur. This has implications for the way in which the bone adapts and to what degree limitations in muscle activity may influence the development of osteoporosis.

1.4 Thesis Outline

The structure of this thesis is as follows:

- **Chapter 2** is a literature review discussing bone adaptation in response to its mechanical environment. The following points are addressed:
 - Mechanical loading of bone – the ways in which bone reacts to mechanical stimuli.
 - Compression theory of bone – the theory is presented along with evidence from previous studies.
 - Innervation of bone – the role of nerves on bone mass regulation.
 - Changes to the musculoskeletal system – those which occur as a consequence of ageing.
 - Musculoskeletal modelling – key points to consider in musculoskeletal models as well as some previous examples.
- **Chapter 3** describes the development of a multibody dynamics model of the femur including its surrounding muscles and bones. The incremental process of model development is explained before giving a detailed description of the final model and presenting the results of studies designed to test the sensitivity of the model to certain key parameters.
- **Chapter 4** gives an account of the collection of gait data including EMG. The process of adapting the model to be subject specific is described. A

series of simulations is presented in which muscle forces were calculated to maintain compression in the femur using a minimum muscle stress optimisation. Simulations were performed in 20 positions spread evenly across the gait cycle. The recorded EMG is used as a reference and model results are compared both with and without compression in the femur.

- **Chapter 5** explains a change to the model which allowed more muscle strands to be included. Simulations were repeated in 13 positions across the stance phase of gait using the new model and these results are presented. Further simulations were carried out in 5 positions across the stance phase of gait using different optimisation cost functions. The results from each cost function are compared.
- **Chapter 6** introduces the problem caused by weakened or malfunctioning muscles. Some of the simulations described in chapter 5 were repeated with limitations placed on muscle activity and the results from this and the previous chapter are compared to determine the effect of limiting muscle activity on the ability to maintain compression.
- **Chapter 7** presents a discussion of the limitations of the study and reviews the results in the context of the aims and objectives outlined in Section 1.3. Comment is made regarding maintaining compressive loading of the femur and neuromotor control of muscular loading. The final section contains a discussion of the results in terms of their implications for ageing and osteoporosis.
- **Chapter 8** presents conclusions drawn from this work and offers suggestions for future research. These are given under three headings; musculoskeletal modelling, compression of bone, and changes to the musculoskeletal system.

Chapter 2

Literature Review

This chapter contains a review of literature relevant to the current study. The study aimed to determine whether or not compression is viable as the dominant state of loading of the femur during gait. Research relating to this theory was reviewed as well as more general work relating to bone's adaptation to mechanical loading. Age-related neuromuscular changes were also investigated with respect to their impact on skeletal loading. The final section of this review focuses on proposed methods for studying changes to the musculoskeletal system.

2.1 Mechanical Loading of Bone

Of the many factors affecting bone turnover mechanical strain is among the most important (Frost 1988, Robling et al. 2006). Previously cited studies highlight the dangers of under-loading the skeleton and the bone mass gains which result from increased loads (Baldwin et al. 1996, Carmeliet et al. 2001, Gross & Rubin 1995, Calbet et al. 1998). Research continues into the mechanisms by which bone senses and reacts to loads as well as the mode of loading. This section presents a discussion of some of the relevant research in this area.

The literature shows a role for osteocytes as mechanosensors in bone (Rubin et al. 2006, Bonewald 2007, Tatsumi et al. 2007, Robling et al. 2006, Chen et

al. 2010). Osteocytes are mature osteoblasts, housed within cavities known as lacunae buried in the bone matrix and connected by tunnels called canaliculi. Osteocyte cell processes extend along canaliculi, suspended centrally to their cross section. Such an arrangement is made possible by tethering filaments between the cell process and canalicular wall (You et al. 2001). Strains applied to the bone are transferred to osteocyte cell processes, prompting a biochemical response which serves to inhibit osteoclast activity or to activate osteoblasts (Chen et al. 2010). Transfer of loads from the mineralised bone matrix to osteocytes has been a point of some interest, owing to the discovery that the strains required to provoke a response in osteocytes are one to two orders of magnitude higher than bone strains arising from routine activities (You et al. 2000). You et al. (2001) presented a model to address this discrepancy (You et al. 2001). They modelled the drag force placed upon the tethering filaments of osteocyte cell processes by fluid flow within the canalicular network. It was found that within the loading range of 1-10MPa and frequency range 1-20Hz, strains may be produced which are 100 times larger than those in the bone matrix. The study also demonstrated that strain induced by drag force on the tethering filaments may be several times larger than strains caused by fluid shear on the cell membrane.

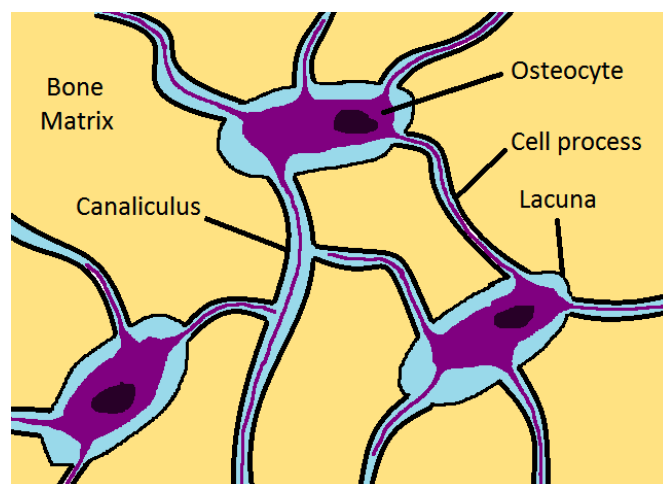


Figure 2.1 - Diagram of osteocytes embedded in the bone matrix, connected by canalicular tunnels.

In a 2007 study, 70-80% of osteocytes were killed in mice by injecting diphtheria toxin designed specifically to target osteocytes (Tatsumi et al. 2007). Mice injected with the toxin experienced bone loss due to interruption in the osteocyte network. The effects appeared to be similar to osteocyte apoptosis observed in the elderly (Bonewald 2007). Interestingly, injected mice were resistant to unloading-induced bone loss, suggesting that osteocytes promote resorption during unloading. One test group were subjected to 7 days unloading then given an injection before reloading. These mice experienced normal bone loss during unloading and normal or in some cases slightly enhanced recovery upon reloading, suggesting a lack of osteocyte influence on bone recovery following unloading.

Some of the earliest observations on the functional adaptation of bone were made by Wolff who noticed that the orientation of trabecular structures follows the direction of the maximum stresses, making bone a highly anisotropic material (Prendergast & Huiskes 1995). A more recent study demonstrated this principle by examining trabecular structures in the proximal femora of primates with different locomotor behaviour (Saparin et al. 2011). The wild primates were grouped according to primary locomotor behaviour in the following categories; quadrupedal walkers, brachiators, climbers, and springers. High resolution CT images were recorded and analysed. The images showed thicker trabeculae in highly stressed areas compared with less trabeculae in less stressed areas. Orientation and distribution of the trabecular structures varied according to locomotor behaviour, providing strong evidence for the functional adaptation of trabecular bone based on habitual loading conditions.

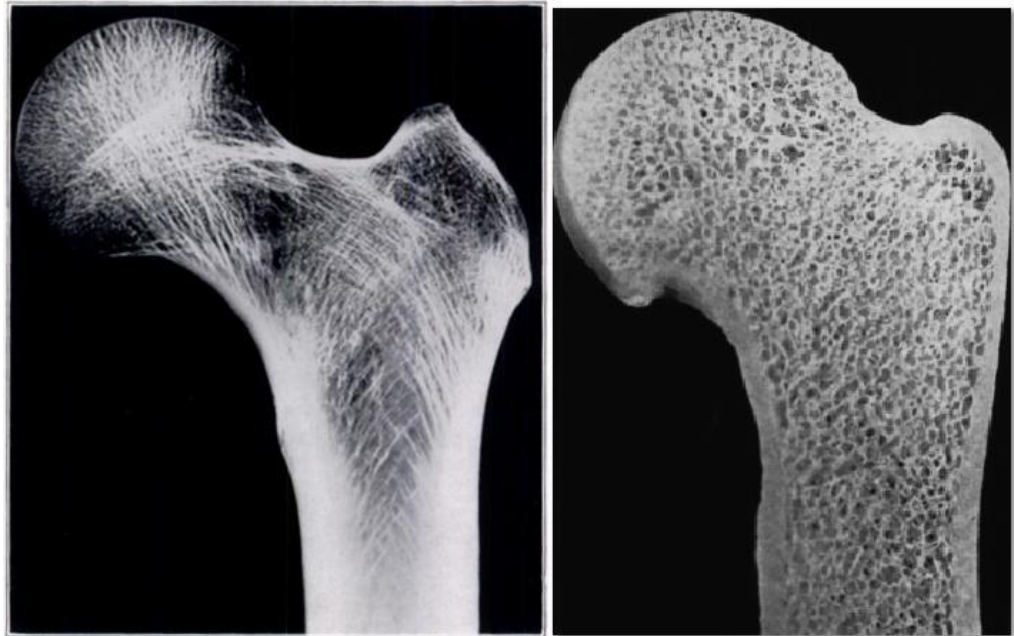


Figure 2.2 - Comparison of the ordered internal structure of a human femur (left) with the less ordered example of a sloth femur (right) (Tobin 1955, Gregory & Aspden 2008).

Frost also suggested that bone adapts to habitual rather than one time loads, suggesting an ability to monitor loading history (Frost 1988). The adaptation which takes place is according to that loading history. The size and structure of the tissue is varied such that strain is kept below a certain threshold. Frost called this threshold the minimum effective strain (MES); the value above which remodelling will vary the geometry of the bone to reduce strain and below which normal bone turnover will be maintained. Following discussion of several studies on the fatigue strength of bone, Frost concluded that the level of MES is set to limit strains such that fatigue life is long enough for any microdamage to be repaired by normal bone turnover. This is evidenced by the fact that bones are capable of carrying momentary loads ten times greater than the MES but even a small increase above the MES would reduce fatigue life enough to seriously threaten bone integrity.

Further work on the subject has revealed that there is an optimum range of loading for maximum bone gains (Robling et al. 2006). This is the range in

which remodelling activity is minimised and new periosteal bone formation increases the second moment of area of the cross section, resulting in increased stiffness.

Not only is there an optimum magnitude for loading of bone but frequency and loading rate are also important (Robling et al. 2006, Hert et al. 1971). In fact static loads appear to have no effect on bone remodelling whatsoever (Lanyon & Rubin 1984).

This understanding of bone's response to mechanical loading has led to the development of treatments aimed at inducing strains of appropriate magnitude, frequency, and duration to stimulate bone formation. These include vibrating platforms and dynamic muscle stimulation. Vibrating platforms have been shown to be effective at stimulating bone formation and can be used with varying frequency and magnitude of vibrations (Judex & Rubin 2010). A year long study in post-menopausal women showed that those who stood on a vibrating platform for two 10-minute periods per day conserved BMD in the femoral neck (Rubin et al. 2004). This is compared with a loss of 2.1% in controls. A similar study was conducted in young women which showed a 3.9% increase in spinal trabecular bone and 3.0% in femoral cortical bone (Gilsanz et al. 2006). Additionally, muscle mass was measured and increases were observed in the psoas, quadratus lumborum, and erector spinae muscles. Judex and Rubin reviewed the findings of various studies to assess whether or not the external vibrations stimulate the skeleton directly or via muscle stimulation (Judex & Rubin 2010). They concluded that vibrations are effectively transmitted through the skeleton up to frequencies of 30Hz and that bone cells are capable of responding directly to the externally applied mechanical stimulus.

Dynamic muscle stimulation is achieved by electrical excitation of the muscles. This technique has been developed and tested as a means to combat disuse osteopenia. Studies have shown that if applied correctly, dynamic muscle stimulation can prevent bone loss due to disuse (Qin et al. 2010, Chapuy et al.

1992, Lam & Qin 2008). Loading frequency has emerged as a key factor in the effectiveness of muscle stimulation, with frequencies of 20-50Hz being most effective (Lam & Qin 2008). A study on hind-limb-suspended rats demonstrated that there is an optimum contraction-to-rest ratio at which bone formation is maximised (Lam et al. 2011).

When applying external loads either directly on the skeleton or via muscle activation, considering bone safety and other health implications is of paramount importance (Judex & Rubin 2010, Muniñ & Kralj 1997). Artificial loading systems lack the in-built feedback system of the body. The problem is similar in principle to the case of a robot gripping a crushable object. There must be some kind of control in place to prevent the force exerted exceeding the allowable force upon the object. This is particularly pertinent in cases where loads are oft repeated such as high frequency loading treatments on the musculoskeletal system. Research has shown that sub-optimal patterns of muscle activation can result in greatly increased bone loading (Martelli et al. 2011) and where bones are weakened by osteoporosis, spontaneous fractures can result (Viceconti et al. 2012).

In understanding how best to improve treatments involving mechanical stimulation, a more complete picture of how bone is loaded under ideal conditions is required.

There is ongoing debate regarding the types of loads that have the greatest influence on the mechanical adaptation of bone (Robling 2009, Judex & Carlson 2009, Poliachik et al. 2010, Manske et al. 2011). Muscle and gravitational forces both play a part although it is difficult to separate the two and quantify their impact as in many ways they are dependent on each other. Muscles are activated to provide locomotive forces and to support joints experiencing ground reaction forces. Judex and Carlson drew upon the findings of various studies to demonstrate the importance of gravitational forces on bone adaptation while Robling produced a similar review in favour of muscle loading (Judex & Carlson 2009, Robling 2009). Both studies admitted that

gravitational and muscular loads are equally required to maintain bone homeostasis. It was also noted however, that bone adapts to the highest loads to which it is habitually subjected and these highest loads arise from muscle activity.

The importance of muscle in maintaining bone mass was highlighted by Poliachik (2010) and colleagues who observed that in various models of disuse seen in animal studies, bone loss was always accompanied by muscle atrophy (Poliachik et al. 2010). They used an injection of botulinum toxin into the calves of mice to cause temporary muscle paralysis. In addition to muscle atrophy, there was a rapid reduction in bone volume fraction and cortical bone volume in the tibia. Muscle cross sectional area and cortical bone volume were mostly recovered 84 days following injection. Trabecular bone loss progressed more rapidly following injection and recovered slower than cortical bone. The authors concluded that normal muscle function plays an essential role in the homeostasis of an adjacent bone.

A recent study used a similar method of botulinum toxin injection with the addition of measuring ground reaction forces by training the mice to run over force platforms (Manske et al. 2011). The team hypothesised that weight bearing ability would recover sooner than muscle and bone volume. An initial loss of weight bearing ability in the injected limb was observed and took 14-21 days to recover. This recovery was not mirrored in muscle and bone volume which continued to decrease (see Figure 3), showing that bone mass cannot be maintained by ground reaction forces alone. The fact that gait patterns were restored before muscle recovered indicates some sort of compensatory action. Compensation by non-injected muscle groups or unaffected fibres within the injected muscles were offered as possible explanations. It was also noted that slow-twitch fibres have been shown to recover sooner than fast-twitch fibres following botulinum toxin injection (Duchen 1970). Combined with the fact that higher frequency muscle loading declines with old age these findings may suggest that fast-twitch muscle activity is essential for bone maintenance (Huang et al. 1999). Previously cited studies relating to dynamic

muscle stimulation would seem to confirm that low frequency muscle activation patterns are not effective in preventing bone loss (Qin et al. 2010, Chapuy et al. 1992, Lam & Qin 2008). This is particularly significant in relation to age-related bone loss due to the fact that fast-twitch muscle activity reduces with age whereas slow-twitch muscle activity is maintained (Huang et al. 1999).

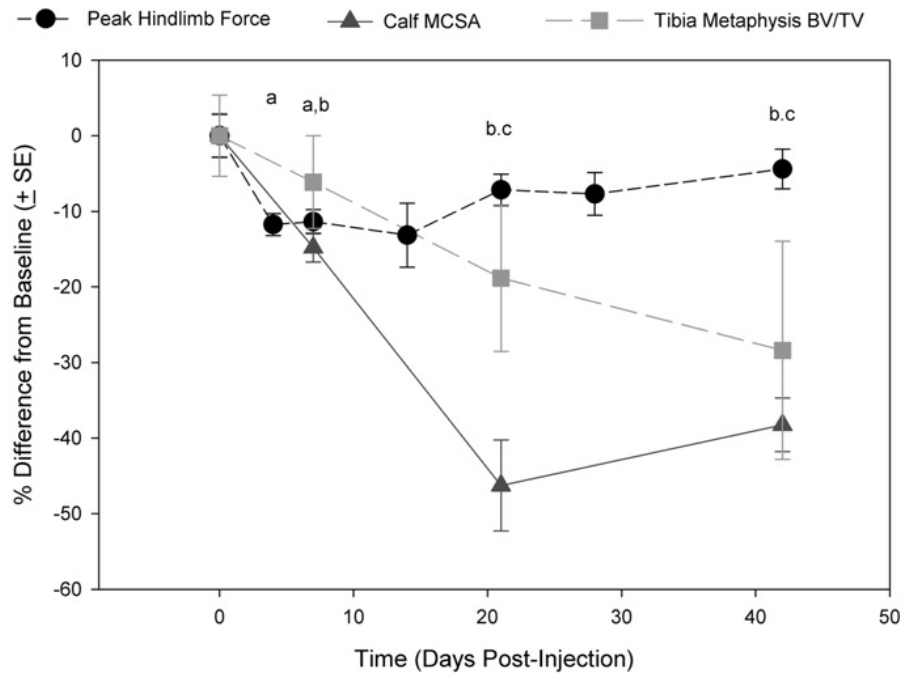


Figure 2.3 - The continued decline of muscle and bone following recovery of weight bearing ability in mice (Manske et al., 2011).

To summarise; bone adapts to the strain it experiences. Its geometry and strength are determined by the magnitude, direction, frequency, and rate of recurrence of that strain. The main influence on these factors is the forces produced by skeletal muscle. It is imperative then to determine how muscles act in the physiological condition in order to understand how muscle malfunction may contribute to bone pathology.

2.2 Compression Theory of Bone

The long bones of the lower limb rarely fail due to pure tension or compression, but most frequently under bending and torsional loads (Muller

& Nazarian 1981, Courtbrown & McBirnie 1995, Ebacher et al. 2007). Logic would assume then that these types of loads induce high peak stresses to which bones are mal-adapted, are therefore undesirable, and should be minimised. However, an examination of the shape of the femur with the force of bodyweight applied to the femoral head would suggest that the bone habitually carries a bending load. Much information on the predominant state of bone loading can be gleaned from an examination of bone geometry as bone is known to be highly anisotropic, adapting to habitual loads. For example, the human proximal femur is supported by a column of thick trabeculae which runs from the point of application of the hip load down through the femoral neck in the direction of the principal compressive stress experienced during upright activities (see Figure 2.4).

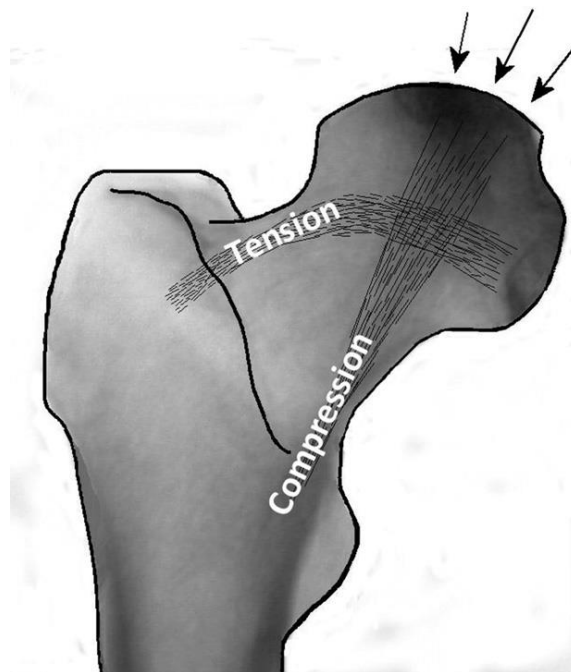


Figure 2.4 - The trabecular structures of the femoral neck and their previously accepted functions (Hammer, 2010).

Scrutiny of the material distribution in the femoral neck as shown in Figure 2.5, unveils a non-uniform cross section resulting in an off-centre neutral axis. This material distribution reduces the angle between the neutral axis and the hip load line of action, thus minimising bending.

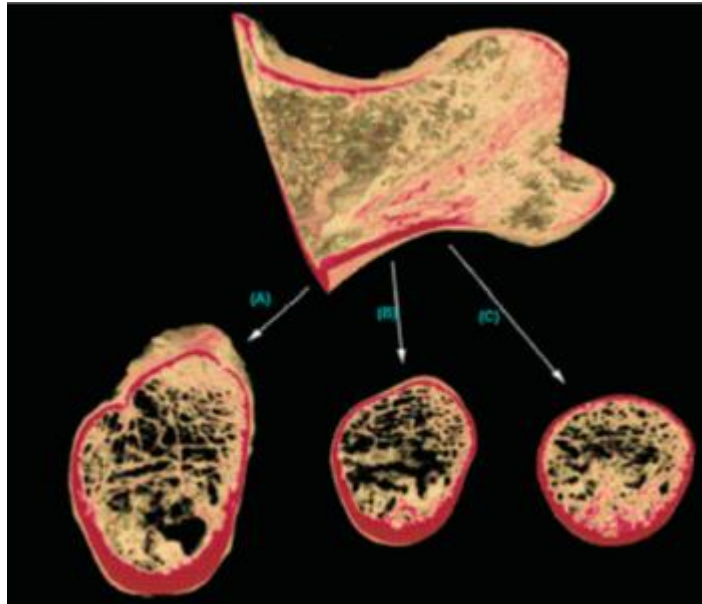


Figure 2.5 - Cross sectional geometry of the femoral neck (Zebaze et al. 2007). The cross-sectional views show a non-uniform distribution of mass.

There is also a horizontal trabecular column which intersects the vertical column at right angles and has long since been viewed as carrying tensile loads (Tobin 1955). Hammer conducted a detailed dissection of the proximal femur which lead to the conclusion that the horizontal trabecular column carries compressive rather than tensile loads as was the previously accepted view (Hammer 2010). The study showed that the horizontal trabecular column lies anteriorly within the femoral neck, too far off centre to effectively carry tensile loads during standing. Analysis of these findings prompted the suggestion that the horizontal trabecular column carries compressive loads when the hip is flexed during activities such as stair climbing and squatting.

The work of Roux and later Wolff showed that bone is a lightweight optimised structure, meaning that bones are adapted not only to carry habitual loads but to do so with the minimum volume of material (Erdemir et al. 2007, Abrahamsen 2012). This being the case, it follows that the musculoskeletal system should be organised in such a way as to minimise stress and therefore require less material. Pauwels presented evidence for this theory as outlined below (Pauwels 1980).

A column under axial compression will experience compressive stress which will increase in magnitude with increasing load. If the load increases to the point where the stresses exceed the yield stress of the material, permanent deformation will occur and eventually failure of the material. To avoid this occurrence, maximum stresses should be far below the yield stress of the material. In engineering applications, the yield stress of the material should be a multiple of the maximum expected stress. This multiple is known as the factor of safety. For example; the stress experienced by a column with a factor of safety of three should never exceed one third of the yield stress.

When stresses in bone exceed an acceptable level (MES as described by Frost) remodelling alters the geometry of the bone to reduce stresses and maintain bone's natural factor of safety. Considering that high stresses mean adding new material, stress minimisation becomes a priority.

A column under axial compression will have an even stress distribution across its cross section. If the source of loading is offset from the neutral axis of the column, bending stresses will result. The sum of stresses through the cross section will remain the same but the peak stresses at the edges of the column will be much higher than in the purely axially loaded case (see Figure 2.6). This illustrates the danger of bending loads for the long bones and demonstrates why femoral fractures occur most frequently under bending.

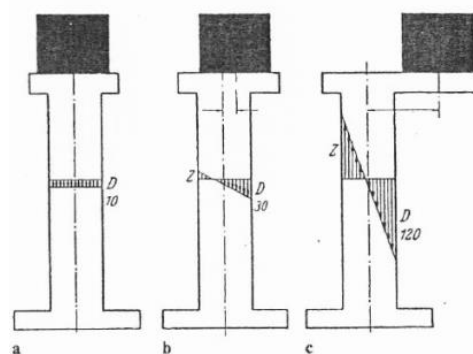


Figure 2.6 - Stress distribution in a column with increased degrees of bending (Pauwels 1980).

In order to compensate for increased peak stresses, material must be added to the column as in Figure 2.7. This is an undesirable solution if a lightweight optimised structure is to be achieved as in the human skeleton. Pauwels used simple column examples to show how bending stresses can be eliminated by applying an equal bending load in opposition to the original load, resulting in overall compression (see Figure 2.8). Pauwels called this counter-bending. The counter-bending force essentially applies another bending load – equal and opposite to the original load. This has a cancelling effect on the peak stresses and results in an even stress distribution. Although the sum of stresses throughout the cross section is higher, the peak loads are greatly reduced and this is therefore a much preferred loading scenario.

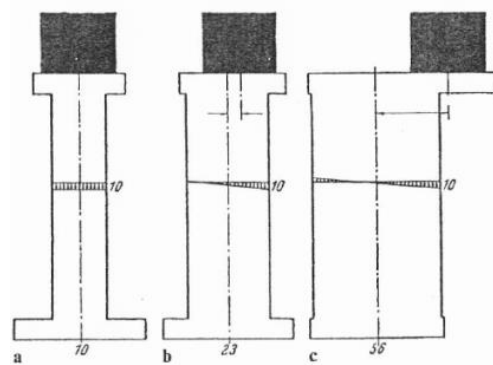


Figure 2.7 - Stress reduction by adding material (Pauwels 1980).

As an alternative to using a counterweight as in Figure 2.8, a tension band may be used to provide a counterbending force. In the human locomotor system, ligaments act as tension bands and synergistic agonist-antagonist muscle activity provides bending and counterbending loads which result in overall compressive stresses. An example of a tension band in the human body is the force exerted by the iliotibial tract on the femur which counteracts the bending load created by bodyweight during single leg stance (Sverdlova & Witzel 2010).

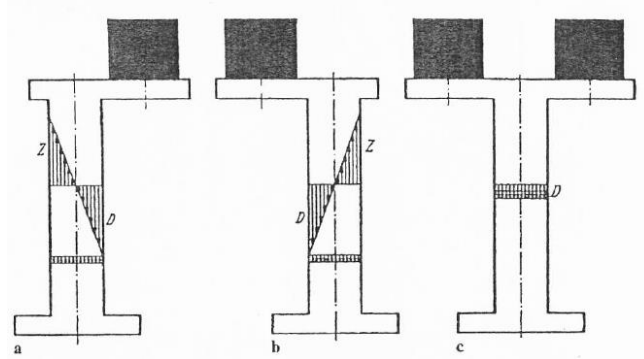


Figure 2.8 - Stress reduction by counter-bending (Pauwels 1980).

The idea that muscles act to minimise bending was called the “active unloading” principle by Munih, Kralj, and Bajd (Munih et al. 1992). Their analysis of two standing postures included a detailed dissection of the leg, optimisation of muscle forces for minimised bending, and EMG measurements. Agreement between the results of the optimisation and EMG patterns confirmed their hypothesis that synergistic muscle activity reduces bending. This theory was supported by the work of Sverdlova and Witzel who developed an optimised load case for minimised bending in the femur (Sverdlova & Witzel 2010). A finite-element (FE) analysis of their results showed a strain distribution which matched the physiological condition (see Figure 2.9).

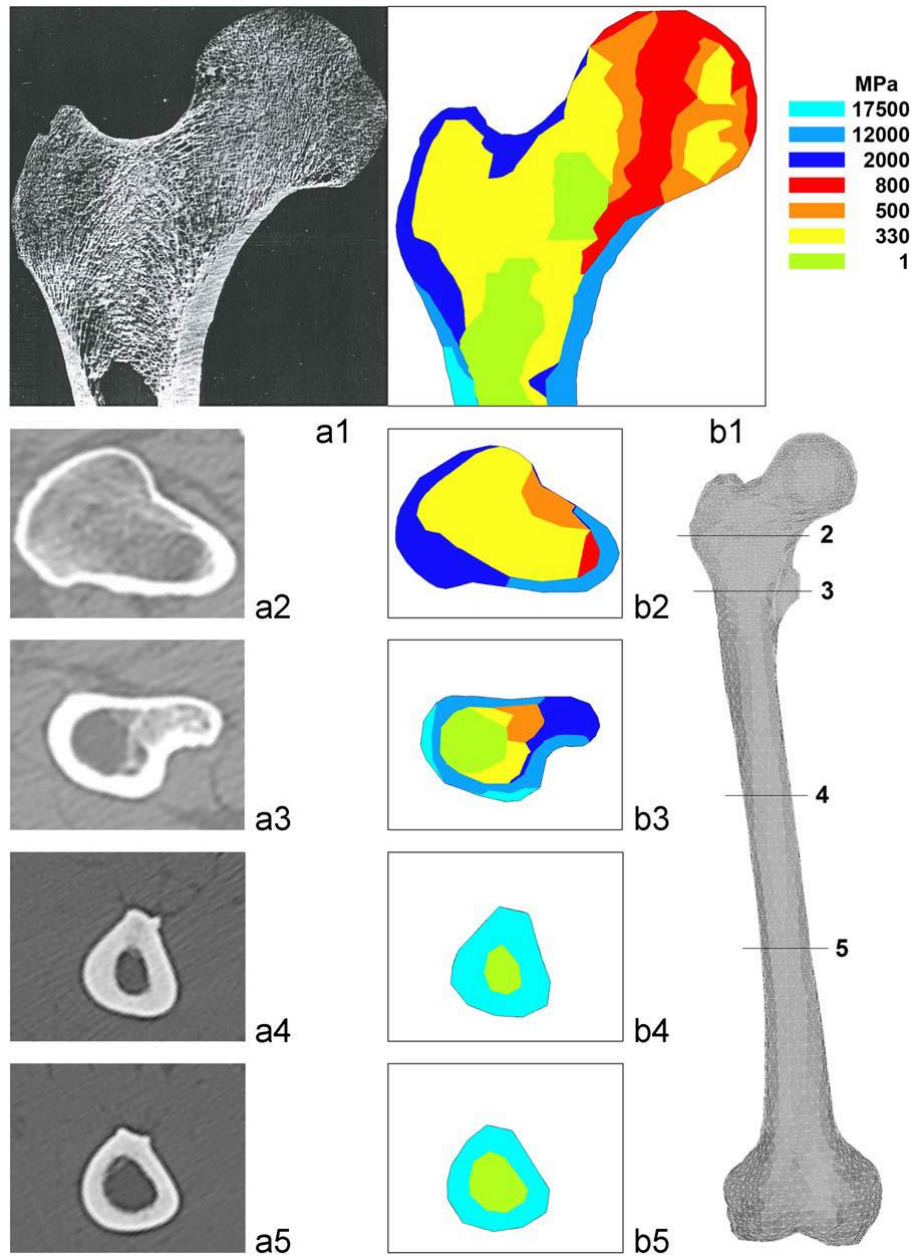


Figure 2.9 – The FE model used by Sverdlova and Witzel (b1-b5) compared with CT scan images on the left (a1-a5)(Sverdlova et al. 2010).

Rudman and colleagues created a 2-D FE model of the proximal femur (as shown in Figure 2.10) including muscle and ligament forces (Rudman et al. 2006). Although the hip reaction force alone caused bending in the femoral neck in the frontal plane (compression on the inferior surface and tension on the superior surface), it was noted that the ligaments of the hip joint are pre-tensioned in the standing position and pull the femur towards the pelvis. This

serves to reduce tension in the femoral neck. Addition of muscle loads eliminated tensile loads in the femoral neck, leaving a small amount of tension on the lateral aspect of the greater trochanter and the remainder of the proximal femur loaded in compression.

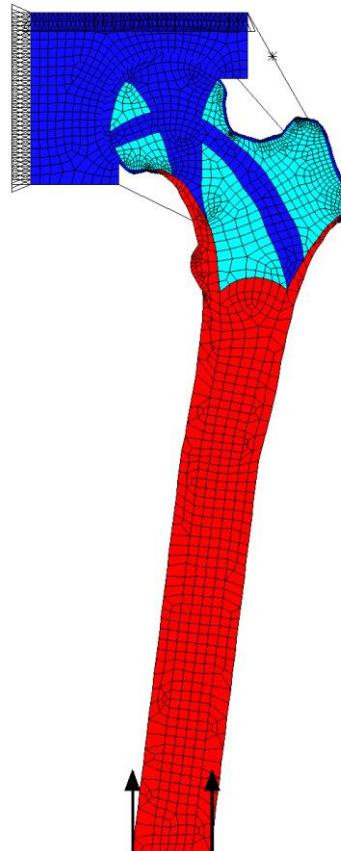


Figure 2.10 – The 2-D FE model developed by Rudman showing the proximal femur and acetabulum (Rudman et al. 2006).

In a 1996 study X-rays were carried out to measure the deflection of the femoral head in the loaded and unloaded conditions (Taylor et al. 1996). This was combined with a finite-element analysis which showed large deflections of the femoral head (13-20mm) in the case of bending and minimal deflection for the compressive load case. The results of the X-rays showed minimal deflection of the femoral head, providing evidence for compressive loading. The FE model used is shown in Figure 2.11.

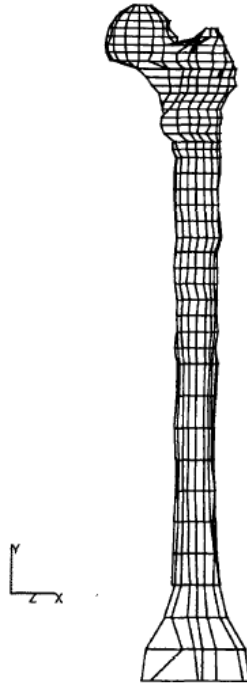


Figure 2.11 – The FE model used by Taylor et al. to analyse deflection of the femoral head in different loading conditions (Taylor et al. 1996).

If indeed muscle activity is coordinated to reduce bending, there must be some means of load sensing feedback from bone to muscle. It is postulated that this feedback originates from nerves in bone. The following section reviews research relating to the influence of innervation on bone mass.

2.3 Innervation of Bone

Recent technological advancements have made possible the detection of nerves in bone, showing that nerve endings are found most abundantly at the periosteal surface and in the most highly stressed areas (McCredie 2007). This would suggest that nerves play a role in the sensing of mechanical loads. This is a topic of debate however, as no means of signal transmission from nerve to bone cells has been identified (Chenu 2004), and it has been shown that isolated bone cells are sensitive to mechanical stimuli without the need for neurological control (Pitsillides et al. 1995). Furthermore, a comparison of innervated and denervated rabbit tibias loaded in axial compression showed no difference in the way they reacted to loading (Hert et al. 1971).

Although these findings suggest that bone's response to mechanical loading is locally controlled, a more recent study challenged this view (Sample et al. 2008). In this study loading was applied to ulnas of young rapidly growing rats and found increased bone formation not only in the loaded bone but in the contralateral limb and unloaded bones of the loaded limb. Chemical blockade of the nervous system cancelled this effect, suggesting centrally controlled cross-talk between limbs in response to mechanical loading. At lower strain magnitudes however, the effect of loading on remote bones was diminished. The findings of Hert et al. were supported by a group at the University of London who found no significant difference in contralateral and adjacent bones following loading of the rat hind-limb (Sugiyama et al. 2010). They noted that the loads applied in their own experiment were within the physiological range whereas the cross-talk effect observed by Sample et al. occurred at higher loads. This may have been due to a neuronally regulated trauma response or changes in blood flow at higher strain magnitudes. It was highlighted that these effects would be more pronounced in rapidly growing rats as used by Sample et al. (2008) compared with the skeletally mature rats used in the study by Sugiyama et al. (2010).

Changes to the nervous system caused by spinal cord injury often result in severe osteoporosis (Chenu 2004, Morse et al. 2008). Skeletal unloading caused by disuse is an obvious culprit, although a 2008 study suggested a neural contribution (Liu et al. 2008). A hind-limb cast immobilisation (HCI) model was compared with bone loss induced by spinal cord injury (SCI). All measured properties were lower in the SCI group including BMD, cortical thickness, ultimate compressive load, and Young's modulus. These results show an additional mechanism for bone loss over and above that which results from disuse. It is worth noting however that the HCI model allows some limited continuation of muscle activity which may explain why bone loss was less severe than in the SCI group.

Sciatic neurectomy (SN) has been suggested as a more suitable disuse model than hind-limb suspension (HLS) due to the confounding factors originating

from stress experienced by the animal in HLS (Huang et al. 2011). De Souza et al. (2005) applied cyclic loading to mouse tibias 5 or 100 days after SN (de Souza et al. 2005). It was shown that cortical bone formation in response to loading was increased following SN and more so when loading was applied later. This implies that bone's sensitivity to mechanical loading is increased following unloading and that this effect is increased with a longer period of unloading. Another facet of the study was blockade of the sympathetic nervous system (SNS) using propranolol administered via drinking water. This was found to have no measurable effect, suggesting that increased cortical formation following SN is not regulated by the SNS.

A strong case has been made in the literature for the role of the SNS in regulation of bone metabolism (Chenu & Marenzana 2005, Elefteriou 2005, He et al. 2011). An important factor appears to be the influence of leptin (Elefteriou et al. 2005). Leptin is a hormone produced by fat cells which contributes to the regulation of bone remodelling by acting on hypothalamic neurons (Chenu & Marenzana 2005). This triggers release of epinephrine and norepinephrine by the SNS. The former stimulates osteoclastogenesis and the latter binds with β 2-adrenergic receptors (β 2-AR) expressed in osteoblasts to inhibit bone formation (He et al. 2011). Mice lacking the necessary β 2-AR receptor were found to be immune to the bone reducing effect of leptin (Elmqvist & Strewler 2005). It was also noted that the β 2-AR deficient mice had higher baseline bone mass, suggesting that the SNS helps regulate bone mass in normal conditions. In addition β 2-AR deficient mice showed no bone loss after ovariectomy, suggesting that post-menopausal bone loss could be influenced by the SNS (Elefteriou 2005). The involvement of the SNS was further evidenced by reduced innervation of bone following ovariectomy in rats (Burt-Pichat et al. 2005).

The precise mechanism by which the SNS is involved in bone metabolism remains a topic for investigation. Using chemical interventions to block β 2-AR receptors has been found to have a preventative effect on bone loss in a variety of conditions (Bonnet et al. 2006, Zhang et al. 2007, Huang et al. 2011).

Some investigators however, have produced conflicting results in the use of propranolol as a β -blocker (Marenzana et al. 2007, Bouxsein et al. 2009). Other studies have suggested that dosage may be an important factor as high doses of propranolol can cause a double-deletion effect whereby β_1 and β_2 receptors are blocked causing overall bone loss (Bonnet et al. 2008, Pierroz et al. 2012). A lower dosage allows β_2 receptors to be targeted more accurately and promote bone formation (Huang et al. 2011). The role of the nervous system in bone mass regulation it seems is not simple, and research is ongoing

Many of the studies cited in the paragraph above have investigated how neural control regulates bone's response to loading. There is not so much evidence however, for the potential role of nerves as regulators of bone's mechanical environment via the muscles. If muscle activity is indeed coordinated to minimise bending of the long bones, there must needs be some means by which the state of loading in bone is detected, be it tension or compression. It would be wholly impossible for muscle activity to minimise bending in bone without an appropriate feedback mechanism.

The study conducted on rabbit tibias by Hert and colleagues applied loads under general anaesthesia, ruling out any effect of muscle activity (Hert et al. 1971). The loads applied to innervated and denervated tibias were the same. Thus it would be expected that the remodelling signals coming from osteocytes in both cases would also be identical. Where loading of the bones is automatically regulated *in vivo*, the absence of nerves results in unloading and therefore bone loss. Even if nerves do not directly regulate bone remodelling, they may be involved in the regulation of muscle loads – the loads to which the bone adapts via the remodelling cycle.

2.4 Changes to the Musculoskeletal System

Having established the importance of muscular loading for bone health, it is important to understand how changes to muscle function occur, what is their impact on bone mass, and what interventions are effective. Skeletal muscle contractions originate as electrical impulses delivered through the nervous

system to the neuromuscular junction. There, chemical processes are activated which cause muscle contraction by shortening of the muscle fibres. The amount of force produced by a muscle depends on the size and number of fibres which are recruited as well as the frequency of the signals arriving from the nervous system.

There are 30 muscles crossing the hip and knee joints which are responsible for loading the femur. The location and function of each muscle is shown in Table 2.1. The current work is concerned with how age-related changes to skeletal muscle influence bone health. The effect of ageing on muscle is well documented and a summary will be presented here.

A reduction in force producing capability has been shown with ageing. This reduction comes by several mechanisms, namely, changes in muscle cross sectional area (CSA), changes to the amount of contractile tissue within muscle, and changes to neural control of muscle firing. There is also evidence to suggest that muscle fibre atrophy is more pronounced in fast-twitch type II fibres.

A longitudinal study examined muscle size and strength initially in 12 healthy sedentary men (aged 65.4 ± 4.2 years) and followed up 12 years later with 9 of the participants (Frontera et al. 2000). The researchers observed a 20-30% loss of muscle strength of knee extensors and flexors. This corresponded with an overall 14.7% reduction in CSA in all thigh muscles. It was concluded that reduction in muscle CSA is one of the main contributors to age related muscle strength losses. It has been reported that reduction in whole muscle size is small (10%) between the ages of 24 and 50, and much more pronounced (30%) between 50 and 80 years of age (Lexell et al. 1988). The cause of these changes appears to be a reduction in fibre number, with a 35% drop being reported between the ages of 52 and 77 (Lexell et al. 1986). The amount of contractile tissue within muscle has also been shown to be reduced in elderly subjects, although the percentage of non-contractile area was reported to be linearly related to physical activity (Kent-Braun et al. 2000).

Table 2.1 - Muscles crossing the hip and knee joints with their respective points of origin, insertion, and actions (Moore et al. 2011)

Muscle	Origin	Insertion	Actions
Adductor Brevis	Body and inferior ramus of pubis	Pectineal line and proximal part of linea aspera of femur	Adducts thigh and to some extent flexes it
Adductor Longus	Body of pubis inferior to pubic crest	Middle third of linea aspera of femur	Adducts thigh
Adductor Magnus	Adductor part: inferior ramus of pubis, ramus of ischium. Hamstring part: ischial tuberosity	Adductor part: gluteal tuberosity, linea aspera, medial supracondylar line. Hamstring part: adductor tubercle of femur	Adducts thigh; its adductor part also flexes thigh, and its hamstring part extends it
Biceps Femoris Caput Breve	Linea aspera and lateral supracondylar line of femur	Lateral side of head of fibula	Flexes leg and rotates it laterally when knee is flexed; extends thigh
Biceps Femoris Caput Longus	Ischial tuberosity	Lateral side of head of fibula	Flexes leg and rotates it laterally when knee is flexed; extends thigh
Gastrocnemius Lateralis	Lateral aspect of lateral condyle of femur	Posterior surface of calcaneus	Plantarflexes ankle when knee is extended; raises heel during walking, and flexes leg at knee joint
Gastrocnemius Medialis	Popliteal surface of femur, superior to medial condyle	Posterior surface of calcaneus	Plantarflexes ankle when knee is extended; raises heel during walking, and flexes leg at knee joint
Gemellus Inferior	Ischial tuberosity	Medial surface of greater trochanter of femur	Laterally rotates extended thigh; abducts flexed thigh; stabilises hip joint
Gemellus Superior	Ischial spine	Medial surface of greater trochanter of femur	Laterally rotates extended thigh; abducts flexed thigh; stabilises hip joint
Gluteus Maximus	Ilium posterior to posterior gluteal line; dorsal surface of sacrum and coccyx; and sacrotuberous ligament	Most fibers end in iliotibial tract, which inserts into lateral condyle of tibia; some fibers insert on gluteal tuberosity of femur	Extends thigh and assists in its lateral rotation; steadies thigh and assists in rising from sitting position

Muscle	Origin	Insertion	Actions
Gluteus Medius	External surface of ilium between anterior and posterior gluteal lines	Lateral surface of greater trochanter of femur	Abducts and medially rotates thigh; keeps pelvis level when opposite leg is raised
Gluteus Minimus	External surface of ilium between anterior and inferior gluteal lines	Anterior surface of greater trochanter of femur	Abducts and medially rotates thigh; keeps pelvis level when opposite leg is raised
Gracilis	Body and inferior ramus of pubis	Superior part of medial surface of tibia	Adducts thigh; flexes leg, and helps rotate it medially
Iliacus	Iliac crest, iliac fossa, ala of sacrum, and anterior sacro-iliac ligaments	Tendon of psoas major, lesser trochanter, and femur distal to it	Flexes thigh at the hip and stabilises hip joint; helps control deviation of the trunk during standing
Obturator Externus	Margins of obturator foramen and obturator membrane	Trochanteric fossa of femur	Laterally rotates thigh; steadies head of femur in acetabulum
Obturator Internus	Pelvis surface of ilium and ischium; and obturator membrane	Medial surface of greater trochanter of femur	Laterally rotates extended thigh; abducts flexed thigh; stabilises hip joint
Pectineus	Superior ramus of pubis	Pectineal line of femur, just inferior to lesser trochanter	Adducts and flexes thigh; assists with medial rotation of thigh
Piriformis	Anterior surface of the 2nd-4th sacral segments; superior margin of greater sciatic notch and sacrotuberous ligament	Superior border of greater trochanter of femur	Laterally rotates extended thigh; abducts flexed thigh; stabilises hip joint
Plantaris	Inferior end of lateral supra-condylar line of femur and oblique popliteal ligament	Posterior surface of calcaneus	Weakly assists gastrocnemius in plantarflexing ankle
Popliteus	Lateral surface of lateral condyle of femur and lateral meniscus	Posterior surface of tibia, superior to soleal line	Weakly flexes knee and unlocks it by laterally rotating femur on fixed tibia, or medially rotating tibia of unplanted limb

Muscle	Origin	Insertion	Actions
Psoas Major	Sides of T12-L5 vertebrae and discs between them; transverse processes of all lumbar vertebrae	Lesser trochanter of femur	Flexes thigh at the hip and stabilises hip joint; helps control deviation of the trunk during standing
Quadratus Femoris	Lateral border of ischial tuberosity	Quadratus tubercle on intertrochanteric crest of femur and area inferior to it	Laterally rotates thigh; stabilises hip joint
Rectus Femoris	Anterior inferior iliac spine and ilium superior to acetabulum	Base of patella; indirectly via patellar ligament to tibial tuberosity	Extends leg at knee joint; steadies hip joint and helps flex thigh
Sartorius	Anterior superior iliac spine and superior part of notch inferior to it	Superior part of medial surface of tibia	Flexes, abducts, and laterally rotates thigh at hip joint; flexes leg at knee joint
Semimembranosus	Ischial tuberosity	Posterior part of medial condyle of tibia	Extends thigh; flexes leg and rotates it medially when knee is flexed
Semitendinosus	Ischial tuberosity	Medial surface of superior part of tibia	Extends thigh; flexes leg and rotates it medially when knee is flexed
Tensor Fascia Lata	Anterior superior iliac spine; anterior part of iliac crest	Iliotibial tract, which attaches to lateral condyle of tibia	Flexes thigh
Vastus Intermedius	Anterior and lateral surfaces of shaft of femur	Base of patella; indirectly via patellar ligament to tibial tuberosity	Extends leg at knee joint
Vastus Lateralis	Greater trochanter and lateral lip of linea aspera	Base of patella; indirectly via patellar ligament to tibial tuberosity	Extends leg at knee joint
Vastus Medialis	Intertrochanteric line and medial lip of linea aspera of femur	Base of patella; indirectly via patellar ligament to tibial tuberosity	Extends leg at knee joint

In addition to a loss of muscle fibres, muscle atrophy of individual fibres has been observed in the elderly (Lexell et al. 1988, Hortobagyi et al. 1995). Although changes to fibre number occur equally in type I and type II fibres, age-related fibre atrophy only affects type II fibres (Lexell et al. 1988). The work by Lexell et al. (1988) showed no change to CSA of type I fibres but type II fibres exhibited a 26% reduction between 20 and 80 year olds. Type II fibres are more commonly known as fast-twitch fibres and are responsible for producing “explosive” power by means of rapid contractions. They are separated into moderately fast type IIa fibres and very fast type IIb fibres. Type I fibres are often referred to as slow-twitch fibres. They contract more slowly and are more fatigue-resistant. Coggan et al. found that atrophy is more pronounced in type IIb fibres than type IIa (Coggan et al. 1992a). They compared muscle fibre size in young and elderly men and women. Type IIa fibres showed 13% atrophy in men and 24% in women, while type IIb fibres exhibited 22% atrophy in men and 30% in women.

The reported atrophy of type II fibres is of particular interest in connection with the previously cited work on loading rate as an essential factor for bone maintenance. It may be that the loading rate of type I fibres on bone is insufficient to stimulate bone effectively and type II atrophy therefore plays a significant role in the development of osteoporosis. Terracciano et al. compared muscle fibre atrophy in age matched subjects with osteoporosis and osteoarthritis and found type II atrophy to be prevalent in osteoporosis, whereas atrophy in osteoarthritis was evenly spread between fibre types (Terracciano et al. 2013).

In the osteoarthritis group, the degree of muscle atrophy corresponded with the level of disuse imposed by the disease severity and duration. This was not the case in the osteoporotic group as no limitations to regular physical activity had been reported. Data collected from the osteoporotic subjects showed an inverse correlation between type II fibre atrophy and BMD (see figure 2.12). This reinforces the evidence for the role of muscles – particularly type II fibres – as an essential part of maintaining bone mass. It was also found that levels of Akt were reduced in osteoporotic subjects as a result of changes to circulating hormones in ageing. Akt is a protein kinase which helps regulate muscle protein synthesis (Perrini et al. 2010). The results of Terracciano et al. show a mechanism for osteoporosis-related muscle atrophy, independent of age-related or disuse-induced changes, and highlight a close relationship between muscle atrophy and

BMD (Terracciano et al. 2013). This relationship has also been demonstrated in a study showing reduced back flexor/extensor strength in women with spinal osteoporosis compared to those without (Cunha-Henriques et al. 2011).

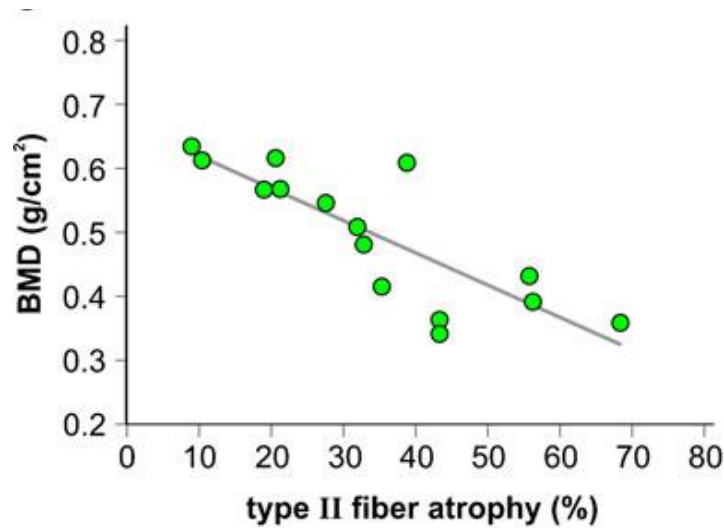


Figure 2.12 - Linear regression plot showing inverse correlation between type II muscle fibre atrophy and BMD in osteoporosis (Terracciano et al. 2013).

With a reduction in fast-twitch fibre strength, muscle power is reduced more than overall muscle strength (Izquierdo et al. 1999). This is of particular interest in considering osteoporosis, as risk of falling (the main cause of osteoporotic hip fractures (Carter et al. 2001)) relates to loss of muscle power in the elderly (Skelton et al. 2002).

Another age-related change to muscle contractile properties occurs in the number and size of motor units (MU's). Older people have fewer overall MU's although they are often larger due to reinnervation of denervated muscle fibres by nearby MU's (Campbell et al. 1973, Roos et al. 1997). Some variability has been observed in MU firing rates, which may be due to reinnervation of type II fibres by type I MU's (Roos et al. 1997). This produces potential deficiencies in motor control (Williams et al. 2002).

Exercise has been shown to mitigate loss of muscle strength and power to some extent, depending on the type and duration of exercise program (Coggan et al. 1992b, Rogers & Evans 1993, Hurley & Hagberg 1998). Modest gains in muscle CSA are often associated with much larger gains in force-producing capability (Williams et al. 2002). This is attributed to the fact that most studies have been conducted with untrained individuals,

and neural adaptations cause the greatest gains in force production during the early stages of training (Kraemer et al. 1996). Increased muscle strength and power due to training have been associated with positive effects on BMD (Sinaki et al. 1996, Nguyen et al. 2000)

If compression is the dominant form of loading on bone, this study is interested in what age-related changes to muscle activity mean for the maintenance of overall compression. Degradation of neuromotor control and firing rate of muscles must surely inhibit the ability to reduce bending through synergistic muscle activity. The following section presents a review of some proposed techniques for studying the effect of changes to muscle loading on bone.

2.5 Musculoskeletal Modelling

As outlined in the previous chapter, a detailed study of muscular loading on bone requires the use of numerical methods. Early models consisted of two-dimensional studies of idealised joints using very few muscle strands. The development of computer technology and advanced computer modelling techniques has allowed increasingly complex models to be developed. A number of ambitious projects are underway which aim to make accurate and reliable modelling of the human musculoskeletal system a reality (Delp et al. 2007, Andersen et al. 2009). A general description of common features and considerations in musculoskeletal modelling will be given in this section.

Typically, external loads (such as gravitational loads) are applied to an anatomically accurate model of the system being studied, and muscle loads are calculated to maintain static equilibrium or produce a desired movement (Sverdlova & Witzel 2010, Modenese et al. , Modenese et al. 2013). Due to the complexity of the human musculoskeletal system, this creates a large number of possible muscle activation patterns, each capable of producing the required resultant joint moments. In order to produce a single optimal solution, a cost function related to some aspect of muscle performance must be included (Crowninshield & Brand 1981, Praagman et al. 2006, Ojeda et al. 2011).

The factors guiding optimal muscle activation patterns in vivo are unknown and may depend on the goal of a particular movement. A large number of optimisation cost functions have been tested during a wide variety of movements and isometric

contractions, often being compared with EMG patterns or validated using recorded joint reaction forces (Erdemir et al. 2007). Some of the simplest and most commonly used among these include minimising total muscle force, or the sum of muscle stresses (Crowninshield & Brand 1981, Glitsch & Baumann 1997).

Calculating muscle stress requires measurement of the physiological cross-sectional area (PCSA) of each muscle. This is usually obtained by CT, MRI, or cadaver studies. Brand et al. predicted muscle forces by optimisation using 3 different sets of PCSA values (Brand et al. 1986). They reported a high level of sensitivity of muscle force predictions to PCSA. Percentage activation requires some estimate of the maximal muscle force. This is often based on PCSA data and combined with force-length-velocity characteristics to provide a maximum potential activation at each given moment (Arnold et al. 2010).

Other cost functions are more complex and include consideration for the distribution of muscle fibre types, muscle energy consumption, and fatigue (Prilutsky et al. 1997, Praagman et al. 2006). Prilutsky et al. compared six cost functions in a model of force sharing in cat ankle extensor muscles (Prilutsky et al. 1997). In addition to functions involving total muscle force and stress, they investigated a function for minimising muscle fatigue developed by Dul et al. (Dul et al. 1984). This last function was shown to predict muscle force sharing most accurately, favouring fatigue resistant muscles with a high percentage of type I fibres.

Praagman and colleagues used near infrared spectroscopy to measure muscle oxygen consumption as a measure of muscle energy expenditure (Praagman et al. 2006). They compared two cost functions (the sum of muscle stresses squared and a newly developed energy-related function) with the experimental results using an inverse-dynamic shoulder and elbow model. The muscle stress cost function showed good correlation with recorded data for the elbow extensors but differed significantly from the flexor muscles. The proposed energy-related cost function demonstrated better correspondence with recorded data. This function was based on the two major energy consuming processes in muscle namely detachment of cross-bridges and re-uptake of calcium. For full details of the derivation of this function the reader is referred to the original work. The function used is given below where the constants c_1 and c_2 are such that the contribution of each term is 50-50 at 50% of muscle activation.

$$\sum_{m=1}^n m_m \left\{ c_1 \frac{F_m}{PCSA_m} + c_2 \left(\frac{F_m}{PCSA_m \sigma_{max}} \right)^2 \right\}$$

Before formulating the optimisation problem, the system to be studied must be accurately modelled in an appropriate format depending on the desired output. Several dedicated musculoskeletal modelling packages are available for this purpose. OpenSim is an open-source software system for the development of musculoskeletal models which aims to foster collaboration within the biomechanics community (Delp et al. 2007). This modelling system is commonly used in gait simulations (Viceconti et al. 2012, Lerner et al. 2014). The AnyBody Modelling System (AnyBody Technology, Aalborg, Denmark) is a commercial product originally developed at the University of Aalborg, Denmark. The managed model repository is ever developing and contains a detailed lower extremity model based on cadaver data which is fully scale-able for subject specific models (Andersen et al. 2009, Schwartz et al. 2010).

Multibody Dynamics Analysis (MDA) is a more generally applied computer modelling technique which allows rigid body simulations of large movements and complex systems. Its suitability for musculoskeletal analysis is evidenced by its ability to model complex interactions between a large number of forces and rigid bodies without requiring a great deal of computing power. This becomes essential as complexity of models increases. Using rigid bodies does not allow simulation of stress and strain in an object. Fortunately most MDA packages allow models to be exported for finite element analysis.

MDA has been used extensively within our research group for modelling of bite forces and muscular loading in lizard and macaque skulls (Moazen et al. 2008, Curtis et al. 2008, Groning et al. 2013). Sellers and Compton used MDA to study human bite forces and highlighted the importance of conducting sensitivity studies on models to identify which outputs can be relied upon (Sellers & Crompton 2004). In demonstration of this principle, Gröning and colleagues carried out a study on lizard skulls and concluded that accurate muscle measurements are crucial to building realistic models (Groning et al. 2013). Carbone used the AnyBody lower extremity model to assess the effects of errors in muscle origin and insertion points (Carbone et al. 2012). The effect of small errors in muscle geometry on muscle force predictions was found to be significant.

Knowledge of musculoskeletal modelling continues to increase and new data collection methods allow models to be improved. As musculoskeletal models become more widespread, a need has been identified for development of standardised validation methods (Lund et al. 2012). If suitably robust models exist with appropriate validation procedures, there exists a wealth of possibilities for development of targeted subject specific treatments of musculoskeletal disorders.

Following collection of anatomical data, conversion of that data into a model, and selection of a suitable cost function, there remains a choice to be made on appropriate optimisation techniques. In simple terms, optimisation consists of finding the solution to a problem which best meets a defined objective. This typically means finding the maximum or minimum of the objective function by adjusting input variables. It is normally desirable to do this with the minimum number of iterations and this is achieved by using an optimisation algorithm to guide perturbations of the variables towards an improved solution until no more improvement can be made. This process is complicated in some instances by inclusion of a large number of inter-dependent variables, multiple objectives, and constraints.

The weight of calculation required in optimisation of a complex system can be lightened by application of response surface methodology (RSM) (Bezerra et al. 2008). RSM is a set of techniques which involves approximation of a system response by relating inputs to outputs directly using a series of polynomials. These polynomials are based on a best-fit of the true system response. Before the system can be approximated, a series of sample simulations must be completed which build up a picture of system response across the range of variables under study. A mathematical approximation of a system is in a format which can be more easily interrogated by an optimisation algorithm and thus allows optimisation studies to be carried out more quickly as opposed to direct optimisation which requires a new simulation to be run each time input variables are perturbed.

This time saving at the optimisation stage comes at the cost of an earlier investment when sample simulations must be run. Variable values for these simulations are determined by a selected sampling method. These sampling methods are often referred

to as experimental designs and are a way of ensuring that the data collected is sufficient to provide a complete picture of the system response.

Monte Carlo sampling methods take a pseudo-random sampling of factor values for each simulation run with the aim to determine the effect of real world variations on the performance of the system. Latin Hypercube sampling is similar but stratifies the data such that each variable is sampled across the full range of available values (McKay et al. 1979). Latin Hypercube sampling is popular with computationally demanding models and is more efficient than Monte Carlo methods – requiring less simulation runs to model the system response (Helton & Davis 2003, Helton et al. 2006).

Whether optimising directly or via a response surface, a number of optimisation algorithms are available depending on the problem being studied. The generalised reduced gradient method was developed by Lasdon in 1974 (Lasdon et al. 1974). This method consists of creating a linear approximation of the objective function at the point under study and moving towards minimisation of this linear function. The selection of an optimisation algorithm is dependent upon the problem to be optimised and some algorithms may perform better than others for a given problem or throughout the course of an optimisation study. A recently developed algorithm employs numerous methods simultaneously to a single optimisation problem and intelligently selects the most suitable method at each optimisation stage. This algorithm is known as SHERPA and is the main feature of HEEDS optimisation software (Red Cedar Technology, USA). Such developments show the promise of improved results and reliability over any single optimisation algorithm.

In summary, this review has brought together research on a range of topics relevant to the current study. It was demonstrated that bone adapts to its mechanical environment and that many factors play a role in this adaptation including health of the osteocyte network, frequency of loading, and rate of loading. There is a body of evidence to suggest that bone is loaded primarily in compression and this work aims to further investigate that theory.

It is clear that nerves play a role in the maintenance of bone health although work is ongoing to clarify this. Nerves may affect bone indirectly by regulating muscle activity and degradation of muscular health is inseparably connected with declining bone

health. These effects occur during aging but can be reduced or stopped by muscle strengthening activity.

The musculoskeletal system has been studied extensively using computer simulation and although these studies face limitations, advances in this field are allowing for ever more complex models and increasing confidence in model based results.

Chapter 3

A Multibody Dynamics

Musculoskeletal Model

3.1 Introduction to the Modelling

This chapter describes the development of a multibody dynamics musculoskeletal model of the lower limb. The model was developed to determine whether it is possible to maintain compression in the shaft of the femur during gait, and if it was, to investigate the resulting muscle activation patterns. This was explored by carrying out a series of static simulations at various points in the gait cycle in which muscle forces were optimised according to a cost function in order to reduce the resultant torques in the hip and knee joints to zero, and maintain compression at a given point in the shaft of the femur.

The model development process began with simple models to test the optimisation method and model features. Accurate anatomical data was obtained, and a more complex model was subsequently developed, and further increased in complexity until it was deemed that the level of anatomical accuracy in the model and its operation was acceptable. Sensitivity studies were carried out, the results of which are presented here.

3.2 Model Development

The model was developed using ADAMS multibody dynamics software (MSC Software Corp, USA). The software allows representation of 3D shapes as rigid bodies and the

modelling of complex mechanical systems. ADAMS is an industry-leading multibody dynamics tool which has previously been used for biomechanical analysis (Moazen et al. 2007, Moazen et al. 2008, Curtis et al. 2008, Shi et al. 2008, Shi et al. 2009). Of particular use in this study was ADAMS Insight which is an integrated tool for experimental design and optimisation. The experimental design capabilities allowed an approximation of model behaviour to be represented mathematically, so that optimisation studies could be carried out quickly. This provided the option of varying objective values and constraints without having to repeat simulation runs.

The input to the model was the external (non-muscular) loads acting on the femur. The purpose of the model was to vary muscle forces in order to balance external loads and maintain compression in the shaft of the femur. In order to determine whether or not the femur was in compression, the proposed femur model included a cut mid-shaft, creating two separate parts with sensors used to detect the state of loading at the interface between those parts. This is illustrated in Figure 3.1.

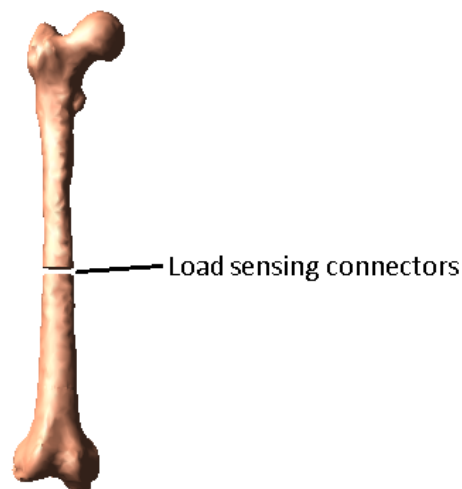


Figure 3.1 - Load sensing of interface between two halves of the femur. The femur was cut into two parts which were joined using force sensing connectors to monitor the state of loading, and thereby allowing compression to be monitored/enforced. Several types and configurations of force sensors were used. These are discussed later in this chapter.

Test Model 1

Simulations using simple shapes were carried out initially to become familiar with the operation of the software and as a means of testing the simulation/optimisation methods. This simple model consisted of two cuboids on top of one another, representing the two parts of the femoral shaft. They were connected with flexible force-sensing connectors (see Figure 3.2) which allowed the load distribution between the parts to be monitored. The bottom part was fixed in position and several forces were applied to the top part as shown by the red arrows in Figure 3.2. The forces were optimised using a sum of forces cubed cost function such that the load transferred between the two parts was evenly distributed between the connectors, resulting in axial compression. Due to the simplicity of this system, the results produced by the optimisation method were easily verifiable by observation and found to be correct. This confirmed that the method of sensing and optimising loads worked well in a simple model. This allowed a more complex test model to be created with confidence that the results would be accurate.

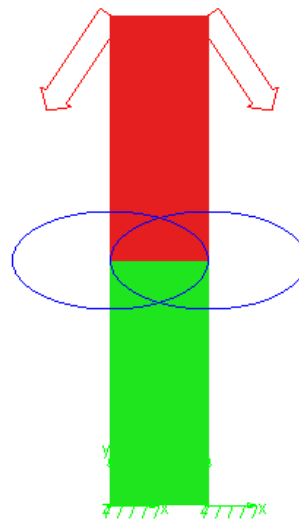


Figure 3.2 - Simple model with flexible connectors (blue ovals) between two parts, with two forces (red arrows) acting on the upper block.

Test Model 2

Geometry of a femur was obtained from the BEL Repository (Christian Desmarais-Trépanier, composite femur 3rd gen solid model; BEL Repository, www.tecno.ior.it/VRLAB/)

and used for a model in which a small number of forces were optimised to balance the femur about a supporting structure of springs on its shaft (see Figure 3.3). The forces applied at this point were representative of the hip joint load and a few muscle groups. The points of application and direction of the forces were approximated and did not come from any specific measured data.

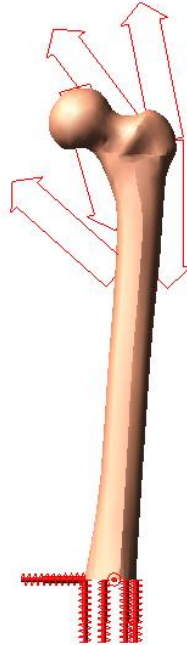


Figure 3.3 - Simple femur model acted on by one fixed load representing the hip joint reaction force, and four variable muscle forces, supported at its base by springs.

Six vertical springs were arranged in a ring centred on the centre of geometry of the cross section of the femoral shaft. Additional horizontal springs were added to stabilise the structure. It was supposed that an even distribution of load across the vertical springs would indicate axial compression.

The model was increased in complexity by adding more muscle forces. This was done initially somewhat arbitrarily in order to prove the functionality of the model. The goal of adding muscle forces to the model at this stage was to ensure that solutions could be reached under more complex loading scenarios. When this was accomplished, attention was shifted towards developing a more realistic model.

Test Model 3

Any output predicted by a model is only of value if the model can be validated successfully. With this in mind, the next step was to build an anatomically accurate model. Anatomical data was not collected as part of this study and so an appropriate data set was sought which would include the following:

- Bone geometry (pelvis, femur, patella, tibia)
- Muscle origin/insertion points
- Path of muscles wrapping around bony structures
- Muscle physiological cross sectional areas (PCSA)
- Gait motion data
- Ground reaction forces

The Twente Lower Extremity Model (TLEM) consists of a complete data set collected from a single cadaver including muscle geometry and bony landmarks of the lower limb (Klein Horsman et al. 2007). This is the data set used in the creation of the Gait Lower Extremity Model for the AnyBody modelling system (AnyBody Technology, Aalborg, Denmark)(Andersen et al. 2009). The AnyBody model includes all muscles of the lower limbs which have their insertion on the femur or below. Each muscle is divided into a number of strands with larger muscles comprising a larger number of strands. Unfortunately the bone geometry included in the dataset is representative of the bony structures, but does not correspond to the exact bone geometry of the original subject. This fact will be discussed in more detail later as it relates to the final model.

Thus Test Model 3 was the first multibody dynamics model developed as part of the current research which used accurate anatomical data. It was created using the default gait data stored in the AnyBody model repository as part of the Gait Lower Extremity model (AnyBody Managed Model Repository version 1.4.1). Bony geometries were exported from AnyBody as .stl files which can be imported directly into ADAMS. Muscle origin and insertion points were exported as lists of coordinates which were used to create markers in ADAMS to which muscle strands were then attached. By this method, the model was created in ADAMS based on the TLEM data set.

Positions of the bones and muscles at each point of interest throughout the gait cycle were obtained by stopping the AnyBody simulation at the appropriate time step and exporting the data. Models were created at 5% increments from 0 to 100% of gait. PCSA (Physiological Cross-Sectional Area) values recorded in the TLEM data set were used to calculate the maximum force producing capability of each muscle strand as per the literature (Brand et al. 1986, Sverdlova & Witzel 2010). This calculation involved multiplying the recorded PCSA values by an experimentally obtained intrinsic stress value, which in this case was $50\text{N}/\text{cm}^2$ (Sverdlova & Witzel 2010).

Test Model 3 followed the same loading and constraint regime presented in figure 3.3, where the load through the shaft of the femur was distributed over six springs. For simplicity, the tibia, patella, and foot in this model were represented by a single red block which provided a reference point for attaching muscle insertion points. This part was fixed in position. The pelvis was constrained to the femur at the hip using a spherical joint, and the femur was constrained by the springs along its shaft. The springs on the shaft of the femur were anchored to another reference object (the green disc in Figure 3.4) which could be moved with the femur to ensure the springs were always parallel to the femoral shaft. A bodyweight load was applied to the centre of mass of the pelvis, and muscle forces were optimised to balance the load evenly across the springs at the cross-section of the femur.

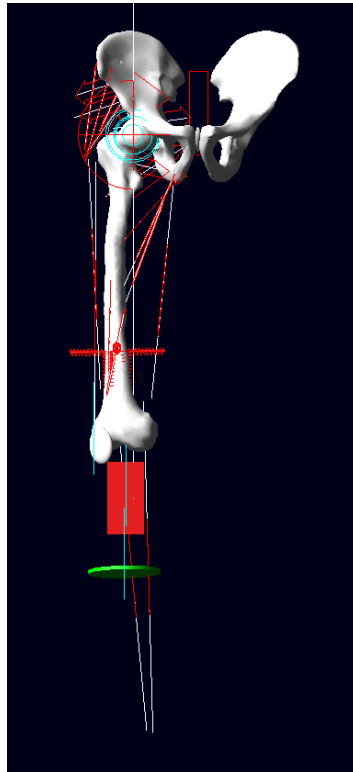


Figure 3.4 - The model using anatomical data where the red block represents the tibia/patella and the green disc is a reference object to allow springs to remain parallel to the femur when in different positions.

When results from this model were analysed, the spring method of load sensing was found to be inadequate, inasmuch as torsional loads could not be accounted for. No resistance to torsional loading was provided and so the structure of springs was free to twist, leaving the springs no longer parallel to the shaft of the femur. The axial forces measured by the springs were consequently not an accurate representation of the axial force acting through the shaft of the femur.

Further consideration of the constraints applied to the femur led to the conclusion that in order to accurately model loads through the femur, the knee joint reaction force had to be included. This would allow the reaction force from the tibial plateau to act on the femur and the knee joint reaction to be monitored as a potential means of validation. It was also concluded that adding a non-physiological constraint on the femur, such as the springs, would alter muscle action and invalidate the model. This led to the decision to separate the femur into two parts and monitor the state of loading at the cut between

the two parts. This meant that the femur as a whole was only constrained about the hip and knee joints, allowing muscle actions to be represented more accurately.

Adding the knee joint to the model also required the addition of the patella to allow load produced in the quadriceps to be transferred across the knee. The model was enhanced further by the addition of more muscle strands and in the interests of visualisation, the tibia and foot segments were added.

As results were collected and analysed, further refinements to the model were made. Details of these refinements and a description of the final model is presented in the following section.

3.3 Final Model Description

The completed model as shown in Figure 3.5, consisted of six rigid body segments; pelvis, proximal femur, distal femur, patella, tibia, and foot. The pelvis was fixed in position with the measured ground reaction force being applied to the foot.



Figure 3.5 - The completed model, frontal view, consisting of six rigid body segments; pelvis, proximal femur, distal femur, patella, tibia, and foot.

With earlier versions of the model, the foot was fixed and **input to the model** was provided by a force representing bodyweight applied to the pelvis. However, as the model includes only one leg, that loading scenario was only valid during the single leg stance phase of gait unless compensation was included during the double leg stance phase to account for the load carried by the other leg.

Possible solutions included adjustment of the magnitude and position of the 'bodyweight' force, or application of a compensatory load to the pelvis to represent the load carried by the missing leg, however it would have been difficult to determine how these loading adjustments should be carried out during the gait cycle. Perhaps the most obvious solution was to model both legs, but this would have added additional complexity to the model, increasing simulation time and still requiring adjustment of the bodyweight load.

Aside from bodyweight, the only other measurable external load is the ground reaction force, which is measured routinely using force plates during the collection of gait data. It gives an accurate measure of the reaction force applied under one foot and consequently the force transferred through one leg. Fixing the pelvis and applying an experimentally measured ground reaction force to the foot, ensures that only the load transferred through the right leg is applied to the model. This approach was therefore adopted here.

The **hip joint** was represented by a spherical joint with the location of the hip centre obtained computationally in AnyBody by finding the centre of rotation between the pelvis and thigh segments. Three orthogonal torsional springs were applied in ADAMS, centred on the hip joint, allowing the joint torque about each axis of the joint to be monitored and specified as a design constraint during optimisation (see Figure 3.6).

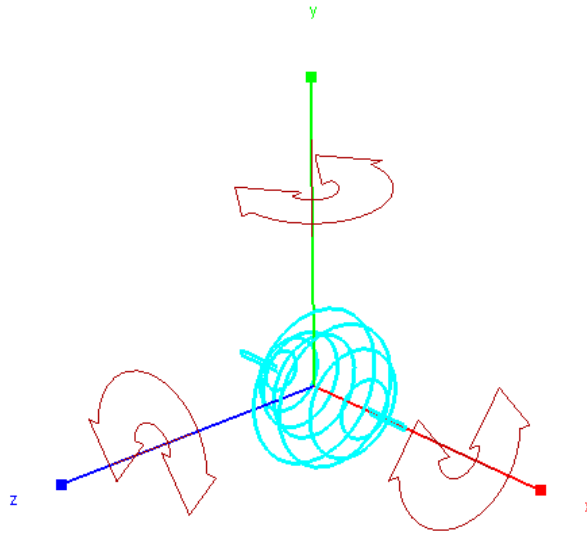


Figure 3.6 - Torques (red arrows) are measured about 3 axes of the spherical joint at the hip (light blue wireframe sphere). The same torque sensing method was used in the spherical joint between the proximal and distal femur segments.

The **knee joint** was represented by a revolute (simple hinge) joint which was positioned initially according to the AnyBody data, which unfortunately happened to be shifted posteriorly and proximally from the joint surface. In this position, equilibrium of the knee joint was only possible by near full activation of the gastrocnemius muscles, and as a result, the resulting knee joint load was unrealistically large. It was decided therefore that the knee joint load would be more appropriately measured at the point of contact at the joint surface. This was to allow a more reasonable comparison to be made between the loads predicted by the model, and those measured by instrumented prostheses. The knee joint position was determined by placing two markers on the tips of the femoral condyles at the points where the gap between each condyle and the tibial plateau was observed to be narrowest. The line between these two markers was specified as the axis of rotation about which the knee was to be placed in equilibrium. Two revolute joints were placed along the axis, each joint placed under a condyle as shown in Figure 3.7. Although the use of two joints introduces mechanical redundancy in terms of the knee rotation, it does allow the distribution of force through each condyle to be recorded. A single torsional spring at the knee also allows the joint torque to be monitored and controlled as with the hip.

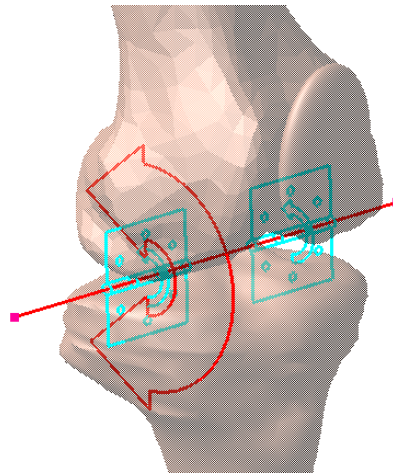


Figure 3.7 - Knee joint consisting of two hinges (light blue) on a single axis (red line) constrained by a single torsional spring (red arrow indicating direction of torque about the axis).

The **patella** was also included and allowed to slide over the distal femur by means of a translational joint placed on the posterior surface of the patella over its centre of mass. Initially a hinge joint was used to link the patella to the distal femur, with the joint positioned according to the Anybody data, but again this proved to be problematic as the knee mechanism was prone to “locking up”, causing simulations to terminate in error. The final configuration also had the benefit that it allowed the quadriceps muscle loads to be transferred across the patella, without causing errors.

The **two femur segments** were united by a spherical joint placed at the centre of mass of the cross section at the point of interface as shown in Figure 3.8. This joint, as with the hip, was spanned by three torsional springs to allow sensing of sagittal bending, frontal bending, and torsion. This arrangement proved to be much more reliable and accurate than the earlier system that used a circle of evenly spaced springs to record the state of compression, since it easily allowed the calculation and monitoring of all loads at the femur cross-section.

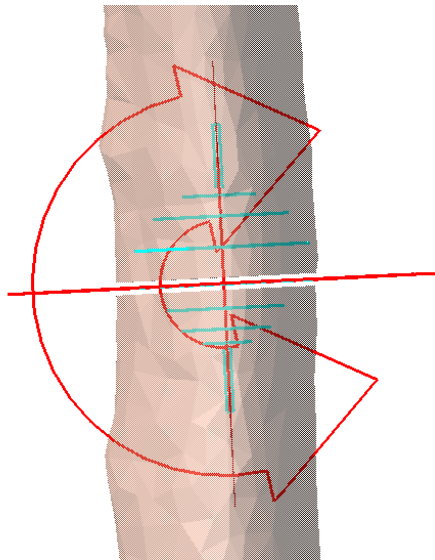


Figure 3.8 - Spherical joint between femur segments constrained by three orthogonal torsional springs.

The stiffness and damping coefficients of the **torsional springs** crossing the joints were determined by trial and error and effectively set sufficiently high to limit any movement at the joint (stiffness: 1×10^{12} N/mm, damping: 1×10^{12} N/mm/s). It was found that any slight deviation in the line of action of the muscles, caused an oscillatory behaviour in the model and made it impossible to reconcile the results at the optimisation stage. As a result, significantly higher or lower coefficients resulted in simulation errors.

The **foot** segment was attached to the tibia using a fixed joint. This study was only concerned with the loading on the femur, and so the muscles selected were only those crossing the hip and knee joints, *i.e.* those which only directly impacted the loading on the femur. For this reason, it was not deemed necessary to model the ankle joint. A summary of the segments and joints included in the model is given in Figure 3.9.

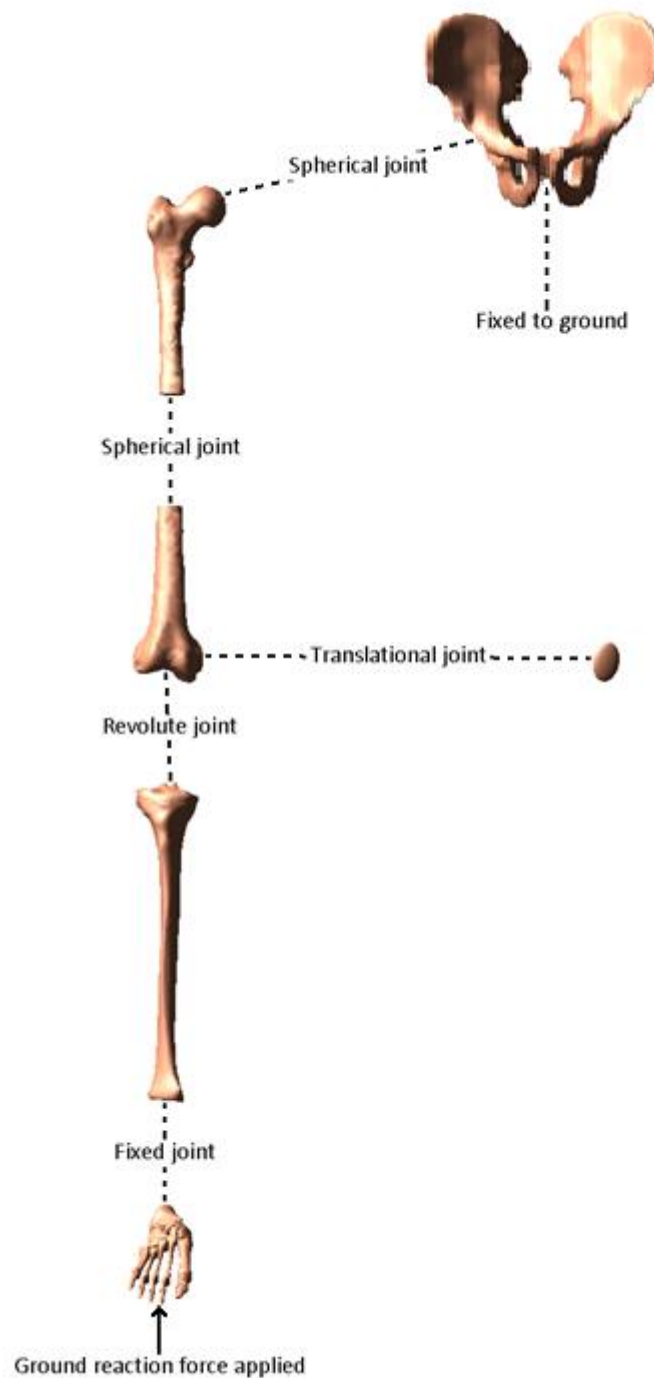


Figure 3.9 - Exploded view of the model showing the joints between each segment and the external load applied to the foot.

Overall the model included 32 **muscles** as shown in Table 3.1, which were divided into 65 strands. Each strand was referenced to a design variable with limits determined by the PCSA of each muscle, as reported by Klein Horsman (Klein Horsman et al. 2007). A

description of the specific muscles, their points of attachment, and main function, was given in Table 2.1.

Table 3.1 - List of 32 muscles, the number of strands used for each, and the abbreviations used. Muscle PCSA and maximum muscle force are included, as well as the abbreviation used for the (passive) ligamentous Iliotibial band

Muscle (# of strands)	Abbreviation	PCSA (cm²)	Maximum Force (N)
Iliotibial band (2)	ITB		
Psoas major (0)	PM	19.5	975
Iliacus (1 – includes PM)	IL	27.2	1360
Gluteus maximus inferior (3)	GMax-Inf	22.5	1125
Gluteus maximus superior (3)	GMax-Sup	49.7	2485
Gluteus medius anterior (3)	GMed-Ant	37.9	1895
Gluteus medius posterior (3)	GMed-Post	60.8	3040
Gluteus minimus medial (1)	GMin-Med	14.05	702.5
Gluteus minimus lateral (1)	GMin-Lat	11.45	572.5
Tensor Fascia lata (1)	TFL	8.8	440
Piriformis (1)	Piri	8.1	405
Obturator externus inferior (1)	OEI	5.5	275
Obturator externus superior (2)	OES	24.6	1230
Obturator internus (1)	OI	25.4	1270
Gemellus inferior (1)	GI	4.1	205
Gemellus superior (2)	GS	4.1	205
Quadratus femoris (3)	QF	14.6	730
Pectineus (3)	Pect	6.8	340
Adductor brevis (3)	AB	10.5	525
Adductor longus (3)	AL	15.1	755
Adductor magnus (9)	AM	53.6	2680
Rectus femoris (1)	RF	28.9	1445
Sartorius (2)	S	5.9	295
Gracilis (2)	G	4.9	245
Vastus medialis (3)	VM	59.9	2995
Vastus intermedius (1)	VI	38.1	1905
Vastus lateralis (3)	VL	69.7	3485
Semitendinosus (1)	ST	14.7	735
Semimembranosus (1)	SM	17.1	855
Biceps femoris caput longus (1)	BFL	27.2	1360
Biceps femoris caput breve (3)	BFB	11.8	590
Gastrocnemius medialis (1)	GM	43.8	2190
Gastrocnemius lateralis (1)	GL	24	1200

Of the 65 muscle strands, 55 pass in a straight line from origin to insertion. The remaining 10 were connected using via points attached to rotational bodies which allowed the strands to wrap around bony structures and other muscles (see Figure 3.10).

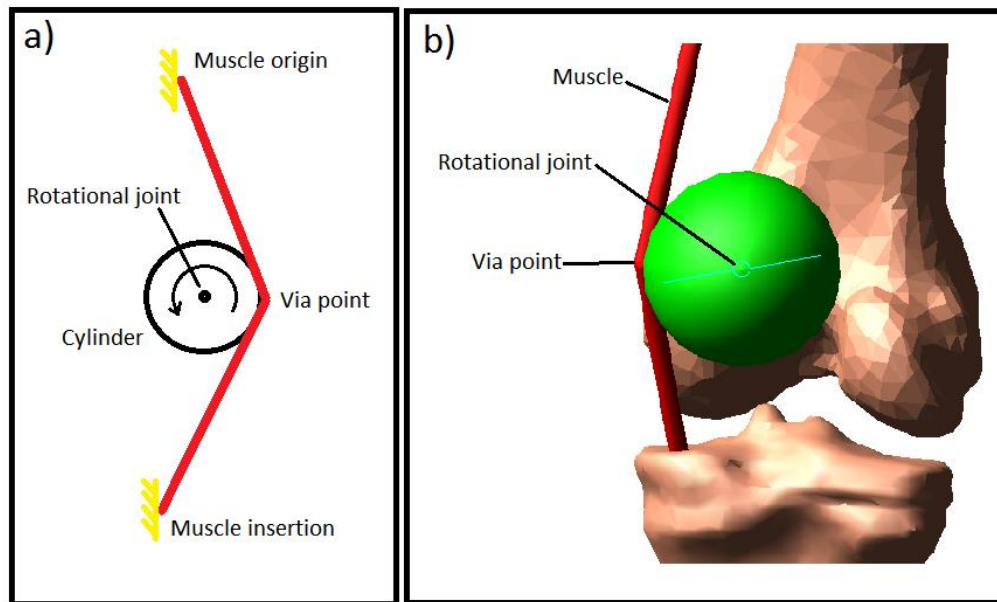


Figure 3.10 - Muscle via points were used for muscle strands which do not pass from their origin to insertion in a straight line. This allows for wrapping around bones or other muscles. a) Muscle via point schematic. b) Example of a muscle via point in the model.

The muscles that were considered, were those that crossed the hip and/or knee joints and which influence the state of loading of the femur. The plantaris muscle was not included as its influence is small and its action is similar to the much larger gastrocnemius. The popliteus muscle was also excluded from the model. Its function as a knee flexor is weak and its role in rotating and unlocking the knee is irrelevant in the hinge knee model used. The table shows that the psoas major and iliacus muscles were modelled as a single strand. Although these are both large muscles which merit the use of several strands, their distal portions run together from their point of wrapping around the anterior inferior iliac spine to their attachment on the lesser trochanter of the femur. As the trunk in this model is in a fixed position, the wider spread of the proximal muscle attachments across the ilium and lumbar vertebrae would have no influence on the action created on the femur and so a single strand was considered sufficient.

Modelling of the **ilio-tibial band** (ITB) was a matter which required some attention as the Klein Horsman dataset did not include an accurate description of the ITB anatomy. The ITB however is important as it has been implicated as a tension band for maintaining compression in the femur (Sverdlova & Witzel 2010). It is a thick ligamentous band on the lateral thigh into which the tensor fascia latae (TFL) muscle inserts as well as a portion of the gluteus maximus. The ITB inserts on both the lateral condyle of the femur and the lateral condyle of the tibia (Vieira et al. 2007). The ITB in this model was represented by 3 strands. One a continuation of the TFL muscle from its point of origin to the ITB insertion point. The other two connected the insertion of the gluteus maximus to the ITB insertion point as shown in Figure 3.11. One strand originated in the centre of the insertion of the superior portion of the muscle, and the other attached similarly to the inferior portion. The ITB insertion point was placed on the lateral femoral condyle. Although, the ITB also attaches on the tibia, the proportion attached to each bone is unknown and since the action on the femur is of primary concern in this study, only a femoral attachment was considered.

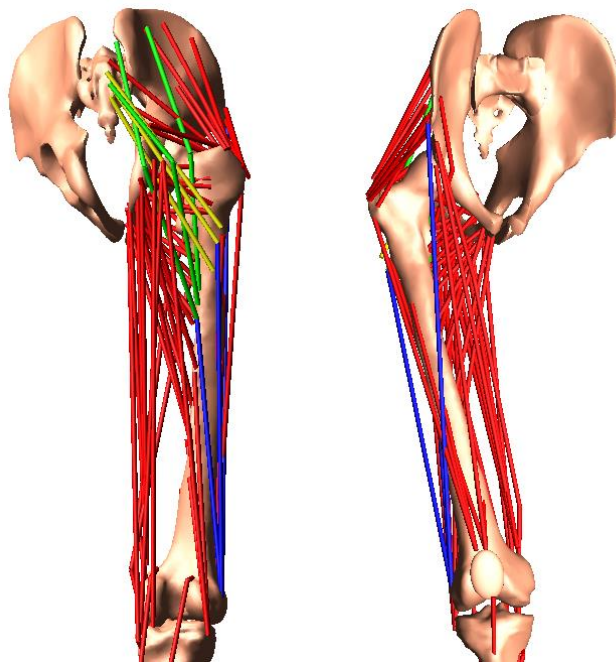


Figure 3.11 - Detailed view of the muscle strands considered in the model. The posterior view, on the left, shows the superior GM in green and the inferior GM in yellow. Two of the three ITB strands (blue) can be seen extending from the insertion points of the GM to the lateral condyle of the femur. The anterior-lateral view, on the right, shows the TFL-ITB strand originating at the anterior superior iliac spine.

Simulation Method

Briefly, the simulation method works as follows: Optimisation objectives and constraints are defined in the model. The relevant model variables and output measures are selected and used to create a DOE (Design of Experiment) study which involves a series of simulation runs. The simulation results are compiled and used to create a response surface. An optimisation is then carried out using the response surface to find an approximation of the optimal solution. Finally, the approximation is used as the starting point in a direct optimisation study. A process flow showing the entire simulation process from recorded gait data to an optimised muscle loading pattern is shown in Figure 3.12. This method was the product of some development work which is described below.

A number of additional model parameters, referred to as factors and responses, had to be defined before the simulations and optimisation analysis could be undertaken. The factors or design variables were in this case, muscle force values. The responses were the objectives to be examined during the optimisation. These included joint torques and reaction forces (including the joint between the two femur segments). The relevant cost functions described later in this section were also defined as responses. A Latin Hypercube sampling method was used, as this approach allows the full range of factor values to be tested against each other in random order across a series of runs (McKay et al. 1979). A response surface was then defined using cubic polynomials to relate the factors to the responses, with ADAMS Insight using a least-squares fit of the polynomials. The response surface then allows rapid calculation of optimal muscle activation patterns for a given set of output conditions specified during the optimisation, with the optimisation tool searching the response surface using a generalised reduced gradient (GRG) method (Lasdon et al. 1974). Other approaches, such as sequential quadratic programming and stochastic design improvement methods, are also available in ADAMS Insight, but GRG is the default search method and was selected as the most robust and the one which produced the best results. All three approaches were tested and GRG converged upon a solution using less iterations than the other two methods.

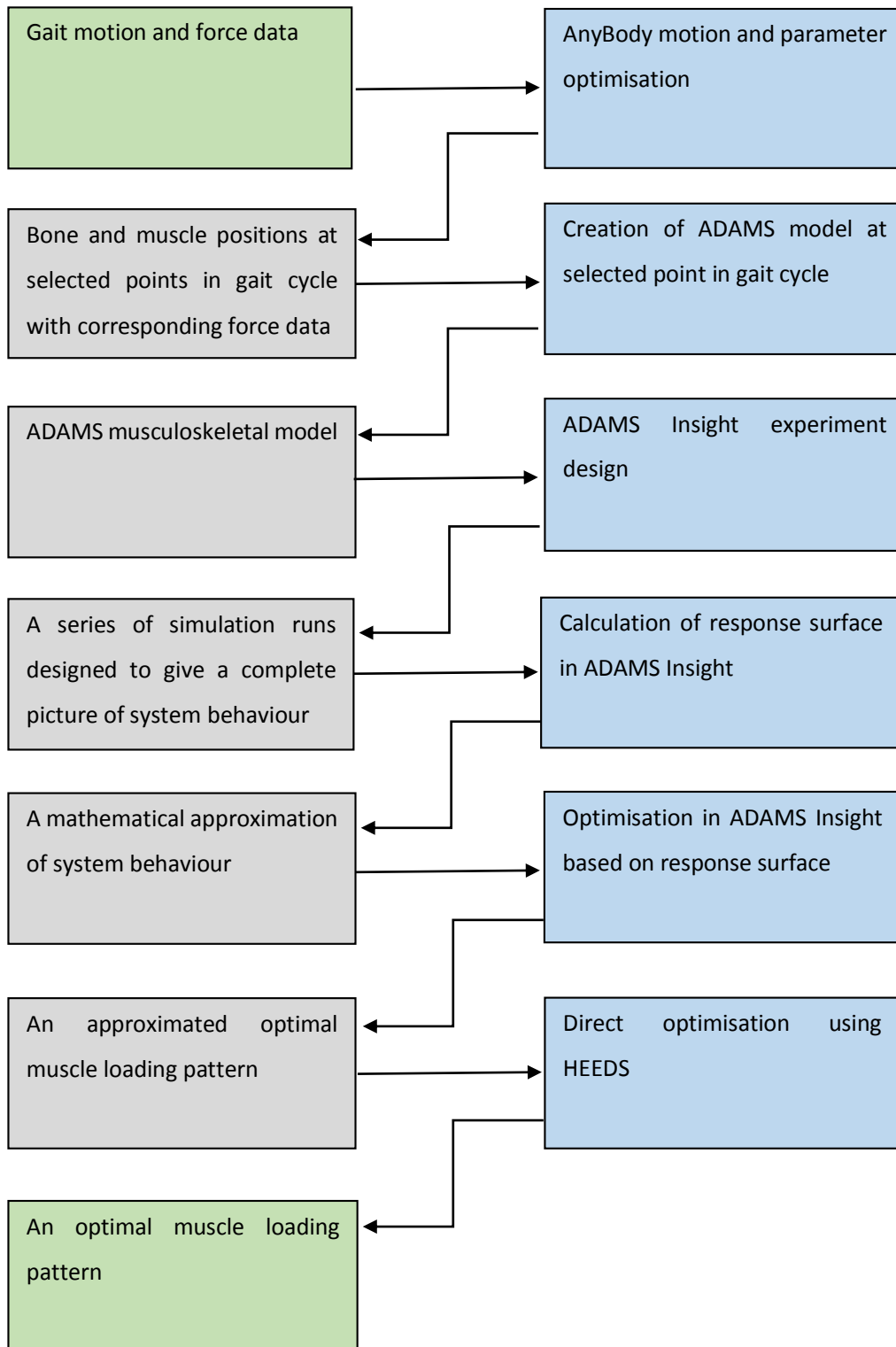


Figure 3.12 – Process flow showing each step of the simulation process with its inputs and outputs. The main input and output of the process are displayed in the green boxes. Process steps are shown in blue and the input/output of each step is shown in grey.

Although the response surface method was extremely useful for optimising the system in many different ways quickly, there were some issues to contend with. Firstly, as the number of factors included in the simulations increased, the number of runs required to generate an accurate response surface increased significantly. This made the use of large numbers of variables (i.e. muscle strands) impractical. Additionally it must be remembered that the response surface represents an approximation of the system and not the true system response. Although in most cases the response surface provided a very good approximation of system behaviour, the inclusion of certain more complex functions – such as those used to monitor the resultant state of loading in the femur – caused a reduction in response surface accuracy, invalidating the results.

To combat these problems, a direct optimisation method was applied. HEEDS (Red Cedar Technology, USA) is a piece of optimisation software which uses the SHERPA algorithm. SHERPA stands for Simultaneous Hybrid Exploration that is Robust, Progressive and Adaptive. SHERPA simultaneously uses multiple search methods, both local and global, to hone in on an optimal solution. The most effective search methods for a given problem are selected automatically as the algorithm “learns” about the design space.

The benefit of direct optimisation is that the simulation is run directly in the ADAMS solver without approximating the system response, allowing more complex objective functions to be calculated accurately, and a large number of variables to be included. One drawback is that simulations must be re-run for each set of optimisation criteria, increasing the amount of time taken when multiple optimisations are to be performed. Using the response surface method to obtain an initial approximation as a starting point for each optimisation helped to speed up the process and find better solutions faster.

ADAMS is capable of running optimisation studies in the ADAMS View environment, without the need for additional software. Before electing to use HEEDS, this functionality was investigated thoroughly, however, experimentation with each of the 5 available algorithms and various settings did not lead to a single feasible solution. These difficulties arose due to the large design space and extremely high ratio of infeasible to feasible designs, and led to the decision to use the dedicated optimisation software, capable of dealing with such complex optimisation problems.

Simulation Objectives and Constraints

The following section describes the constraints applied to the model, including their derivations, and the cost functions that are minimised during the optimization.

The aim of the constraints placed upon the hip and knee joints was to maintain static equilibrium about those joints by coordination of muscle forces. This was implemented in the model by applying limits to the torque in the torsional springs. If the torsional springs crossing each joint were carrying close to zero torque, then equilibrium in the joint was being maintained by muscle forces. The limits were set as the point at which the torque in the joint (T) - as measured in the torsional springs - was equal to the minimum torque required to overcome the static friction and cause movement in the joint. The static friction was calculated as a function of the joint reaction force (F_j), using a coefficient of static friction (μ) reported in the literature (Caligaris & Ateshian 2008). This yielded the following for each joint:

$$T - \mu F_j d < 0 \quad (\text{Constraint 1})$$

where d is the distance from the joint surface to the joint centre of rotation. This was approximated as 30mm for both the hip and knee joints, based on a visual assessment of the model. With this and the other constraints applied to the model, muscle forces were free to violate the constraints, but the muscle force combinations which did so were discarded as infeasible.

A guideline value of maximum stress for the combined bending and axial load was calculated based on a hollow cylinder with outer diameter 20mm and inner diameter 10mm as shown in Figure 3.13, being an approximate representation of the femoral shaft. The cylinder was given a Young's modulus of 18.6GPa in accordance with values reported for cortical bone in the literature (Cuppone et al. 2004). The maximum allowable stress was calculated as follows based on a maximum strain value of $3000 \mu\epsilon$, this being the upper limit of the envelope of minimum effective strain as defined by Frost (1988).

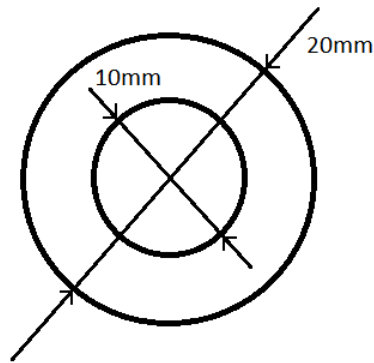


Figure 3.13 - Cross sectional dimensions of the cylinder used to calculate maximum allowable stress.

The maximum allowable principal stress is given by: $\sigma_{pmax} = E \varepsilon_{max}$

Substituting in values: $\sigma_{pmax} = (18.6 \times 10^9) \times (3 \times 10^{-3}) = 55.8MPa$

The maximum stress on the femoral shaft is a combination of axial (σ_a), bending (σ_b) and torsional stresses (τ). These are given as follows:

$$\sigma_a = \frac{F_a}{A} \qquad \sigma_b = \frac{M_T r}{I} \qquad \tau = \frac{M_t r}{J}$$

Where A, r, I, and J are respectively the area, outer radius, second moment of area and polar moment of area of the cross section of the approximated femur. F_a is the axial force measured through the joint in the femur; M_t is the torsional moment measured by the torsional spring in the transverse plane at the cut in the femur; and the resultant bending moment M_T is given as: $M_T = \sqrt{M_s^2 + M_f^2}$, where M_s and M_f are measured by the torsional springs at the cut in the femur in the sagittal and frontal planes respectively.

The maximum combined axial and bending stress is given as: $\sigma_{max} = \sigma_a + \sigma_b$

Thus, the maximum principal stress can be obtained by:

$$\sigma_{pmax} = \frac{\sigma_{max}}{2} + \sqrt{\left(\frac{\sigma_{max}}{2}\right)^2 + \tau^2}$$

This leads to the constraint:

$$55.8 \times 10^6 \geq \frac{\sigma_{max}}{2} + \sqrt{\left(\frac{\sigma_{max}}{2}\right)^2 + \tau^2} \quad (\text{Constraint 2})$$

The degree of bending in the shaft of the femur was constrained in order to maintain overall compression in the bone. To achieve this, the maximum allowable bending stress was set equal to the axial stress. Thus, the combination of axial and bending stress always resulted in overall compression.

Figure 3.14 shows how bending and axial loads are combined. The minimum combined bending and axial stress is given by: $\sigma_{min} = \sigma_a - \sigma_b$

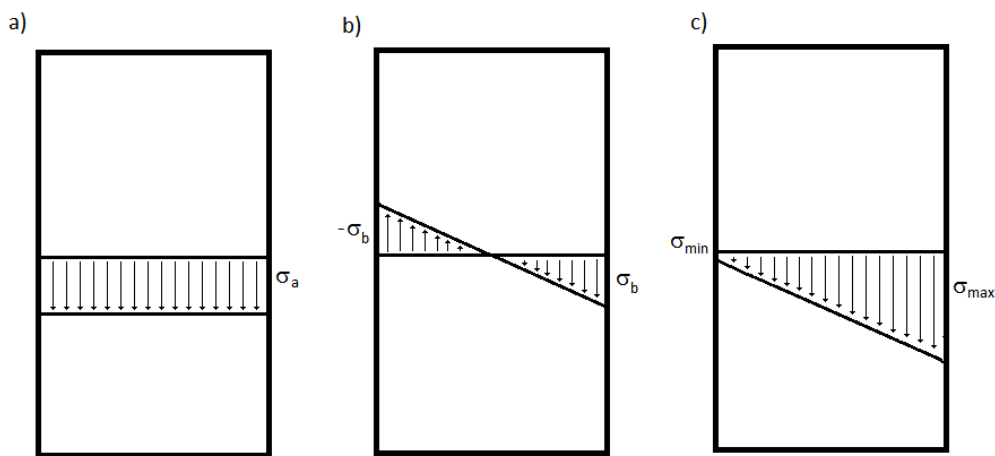


Figure 3.14 - a) A representation of a column under pure axial load where the axial stress is represented by σ_a b) A cylinder under pure bending with maximum load σ_b at the outer surface. c) Column under combined axial and bending load.

In order to maintain compression in the femur σ_{min} must be greater than or equal to zero, i.e. $\sigma_a \geq \sigma_b$

Substituting for σ_a and σ_b , we obtain: $\frac{F_a}{A} \geq \frac{M_T r}{I}$

And thus: $(M_T)_{max} = \frac{IF}{Ar}$

The constraint becomes: $0 > M_T - \frac{IF}{Ar}$ (Constraint 3)

With these constraints in place a variety of minimisation cost functions were applied in turn to find the optimum muscle loading patterns. These included minimising the force

through the hip and knee joints, minimising the sum of muscle stresses cubed and minimising muscle energy expenditure using the function described by Praagman et al. (2006). A summary of the cost functions and constraints used in the model is given in Tables 3.2 and 3.3 respectively.

Table 3.2 - Summary of cost functions investigated during optimisation studies

Cost function	Function
Joint reaction forces	Hip and knee joint reaction forces both set up as objectives with equal weighting
Muscle stress cubed	$\sum_{m=1}^n \left(\frac{F_m}{PCSA_m} \right)^3$
Muscle energy expenditure	$\sum_{m=1}^n m_m \left\{ c_1 \frac{F_m}{PCSA_m} + c_2 \left(\frac{F_m}{PCSA_m \sigma_{max}} \right)^2 \right\}$

Only one cost function was used at any one time. Simulations minimising muscle stress cubed were carried out across the entire gait cycle, whereas investigations using the other cost functions were only completed at select points during gait.

Table 3.3 - Summary of constraints applied to the model

Constraint	Function	Simulation type	
		Unconstrained femoral loading	Compression enforced
Hip joint torque	$T_{hip} - \mu F_{hip} d < 0$	Yes	Yes
Knee joint torque	$T_{knee} - \mu F_{knee} d < 0$	Yes	Yes
Maximum stress in femur	$55.8 \times 10^6 \geq \frac{\sigma_{max}}{2} + \sqrt{\left(\frac{\sigma_{max}}{2} \right)^2 + \tau^2}$	No	Yes
Compression at cut in the femur	$0 > M_T - \frac{IF}{Ar}$	No	Yes

Note: Constraints were selected for each simulation type depending on whether or not compression in the femur was enforced.

The model was tested for sensitivity to certain key parameters as described in the following section. All simulations described here were carried out using the minimum muscle stress cost function.

3.4 Sensitivity Studies

Four sensitivity studies were carried out at 15% of gait on the following model parameters:

- **Study 1:** anterior-posterior position of the knee point of contact.
- **Study 2:** rotational position of the knee joint in the transverse plane.
- **Study 3:** direction of the ground reaction force in the sagittal plane.
- **Study 4:** position of the spherical joint between femur segments in the transverse plane.

Studies 1-3 were carried out under conditions of enforced compression as outlined in the right hand column of Table 3.3. Study 4 was carried out under a similar set of constraints except that instead of Constraint 3 (enforcing compression in the femur), bending in the femoral shaft was reduced to zero. This was done to ensure that sensitivity to variations in the position of the spherical joint between femur segments was not compensated for by varying degrees of bending across the joint.

In Study 1, the position of the hinge joint representing the knee was varied in the x-direction (as shown in Figure 3.15), because the precise points of contact in the knee throughout gait were not known. Therefore they had to be approximated by visually identifying the position of the narrowest gap between each femoral condyle and the tibial plateau, as previously described. This was identified as a potential source of error in the model.

The rotational position of the knee joint in the transverse plane was also varied (Study 2) through a series of simulations for the same reason. Both hinge joints were rotated about the green highlighted y-axis shown in Figure 3.15.

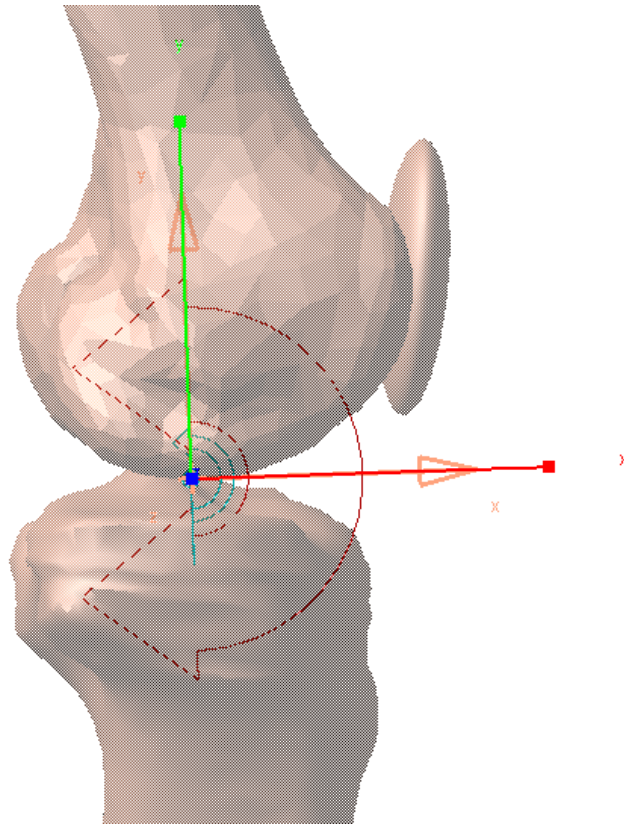


Figure 3.15 - Sagittal view of the knee joint showing the x-axis along which the knee joint was moved in the sensitivity study, and the green y-axis about which it was rotated.

As the ground reaction force (GRF) provides the only input to the model, sensitivity to variations in its line of action was also of interest, to determine the importance of precise GRF measurements. The line of action of the force was rotated in the sagittal plane about its point of application by 5° in each direction (Study 3). This is illustrated in Figure 3.16.

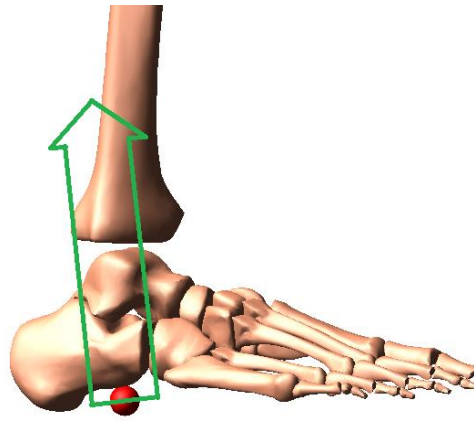


Figure 3.16 - The direction of the GRF vector in the sagittal plane is represented here by the green arrow. The direction vector shown reflects the GRF data recorded in AnyBody at 15% of gait. The red circle under the foot represents the centre of pressure (COP), also being the point at which the GRF was applied to the model. The direction vector was rotated about the COP in the sagittal plane. The anti-clockwise direction was taken as positive.

Finally, in Study 4 the position of the spherical joint between the two halves of the femur was recognised as a potential error in the model. This arose from the fact that the femur was obtained as a solid shape, not hollow as is the case in reality. The joint was placed at the centre of mass of the cross section so as to correspond with the neutral axis of bending. However, it was noted that without accounting for the medullary cavity, this did not represent the true centre of area of the cross section of a real femur. Furthermore, the bone geometry used in this model did not match the cadaver from which the TLEM dataset was collected. Thus the joint was moved in the transverse plane through the cross section of the femur positively and negatively in the z and y directions as shown in Figure 3.17.

All of the above sensitivity studies were carried out at 15% of the gait cycle, where the first peak loads typically occur. The minimum muscle stress cost function was used in all cases.

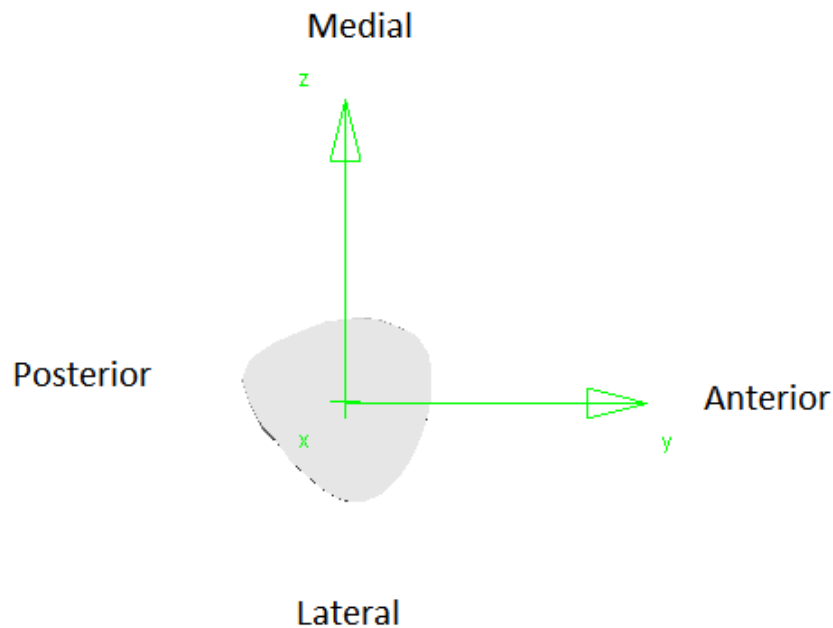


Figure 3.17 - Cross section of the cut in the femur showing the local coordinate system within which the position of the joint between the femur segments was moved.

3.5 Sensitivity Study Results

The performance of each simulation was based on how well it met the constraints and minimised the value of the sum of muscle stresses cubed. As the actual value of the cost function is difficult to relate directly to any real-world parameter, joint reaction forces were selected as a convenient way to evaluate results, and are presented as multiples of bodyweight as per the standard approach. Lower values of joint reaction forces equate to lower overall muscle stress and therefore improved performance. The utility of using joint reaction forces as a means of evaluating results was further enhanced by the fact that comparative data exists in the literature. The force passing through the femoral shaft at the cut in the femur was also measured and recorded as an additional output.

Study 1: Anterior-posterior position of the knee point of contact.

The results of Study 1 are shown in Figure 3.18. The means of determining the original position of the rotational joint at the knee has been described previously. When the joint was moved from this position 10mm anteriorly, it resulted in a slightly increased hip

joint reaction force, and an increase in knee joint and femoral shaft forces of more than 1 times bodyweight. A posterior shift in the knee joint position had little impact on the hip joint reaction force, but led to a reduction on the knee and femur forces of approximately 0.5 times bodyweight per 10mm across the range studied.

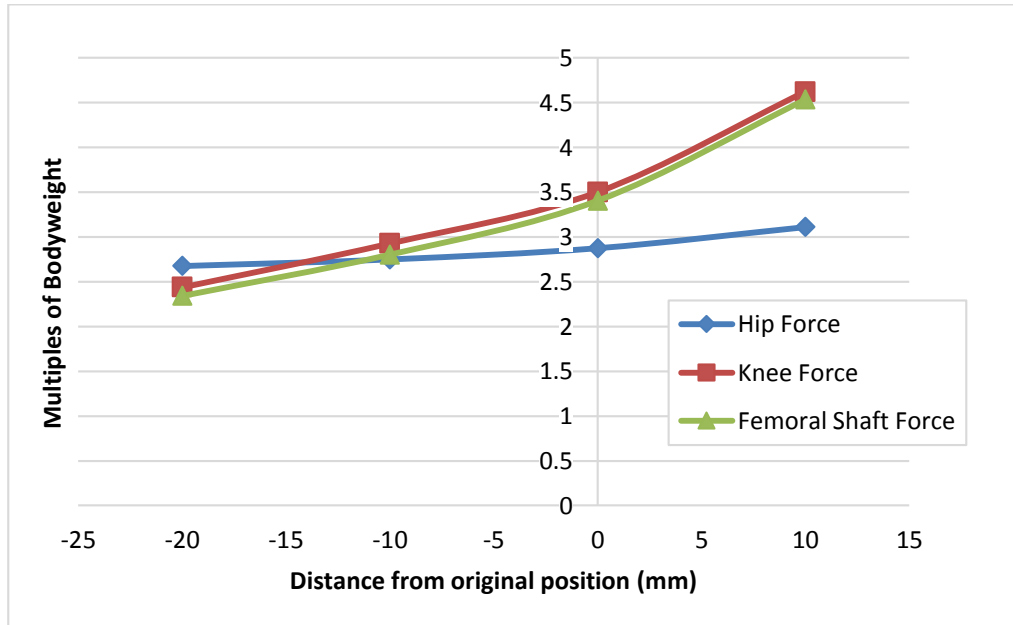


Figure 3.18 - Impact of moving the knee joint in the anterior-posterior direction, where anterior is positive.

Study 2: Rotational position of the knee joint in the transverse plane.

Figure 3.19 shows how the axis of rotation of the knee was varied in the transverse plane for Study 2. The impact of this variation on joint and femur forces is shown in Figure 3.20. A positive rotation of 5° had very little impact on hip, knee and femur forces. Similarly, a negative rotation had little impact on hip forces, but caused an increase in knee and femur forces of approximately one quarter of bodyweight.

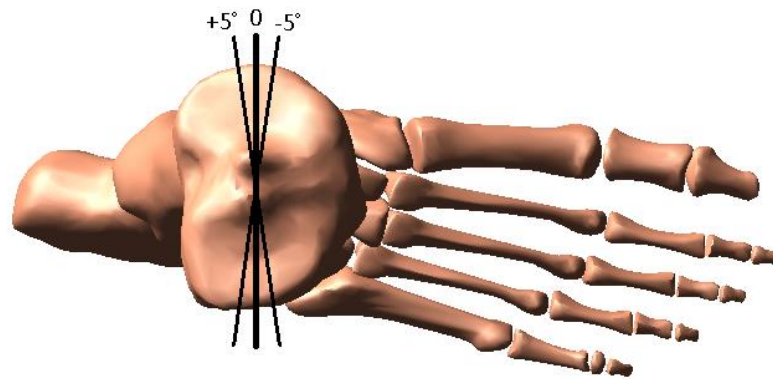


Figure 3.19 - The axis of rotation of the knee as it sits on the tibial plateau in its original position (0) and showing how it was rotated in the transverse plane.

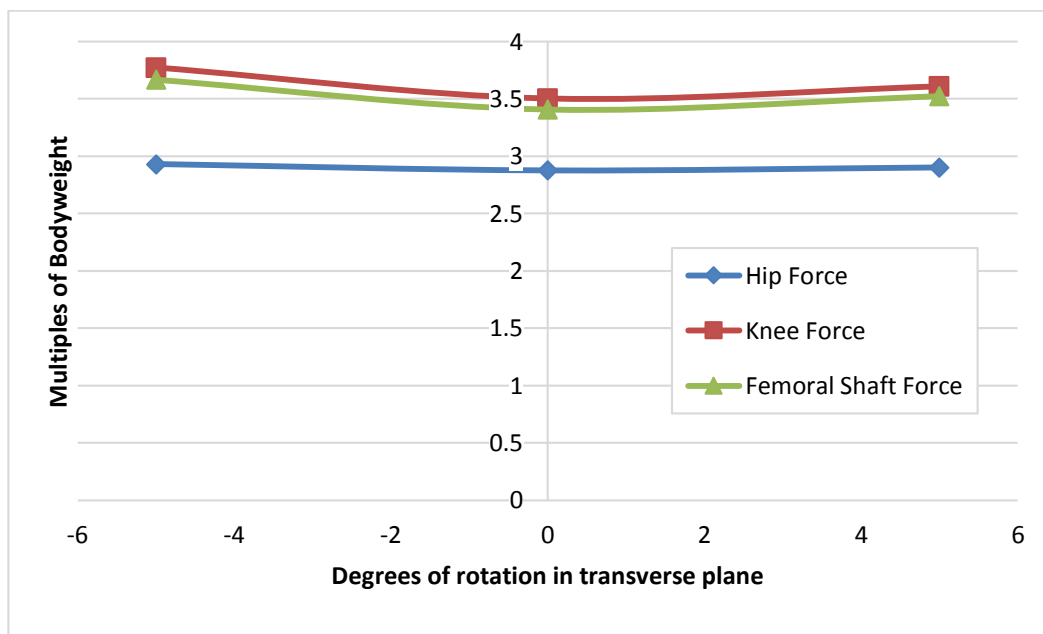


Figure 3.20 - Variations in hip, knee, and femur forces with rotation of the knee axis in the transverse plane (see Figure 3.19).

Study 3: Direction of the ground reaction force in the sagittal plane.

The results of Study 3 are shown in Figure 3.21. Rotating the GRF clockwise decreased the moment of the GRF acting about the knee joint. Changes in the knee and femur forces were not significant, but we see an increase in hip force of approximately 1.3 times bodyweight. Anti-clockwise rotation of the GRF increased the knee joint reaction

by 1 times bodyweight and the femur force by 2.7 times bodyweight. There was also a slight reduction in hip force as seen in Figure 3.21.

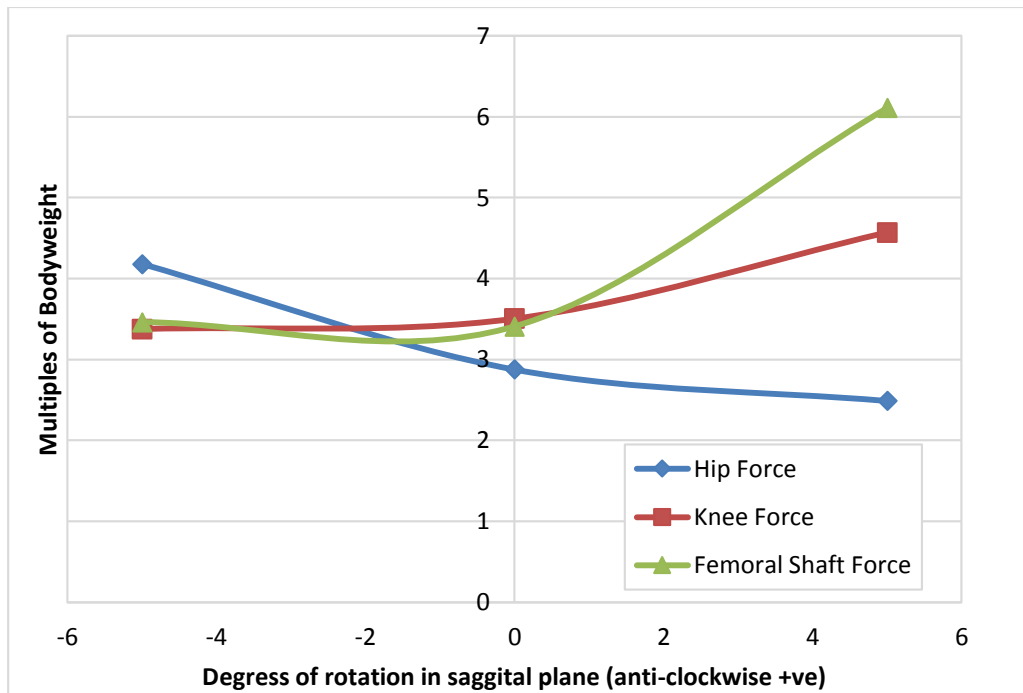


Figure 3.21 - Hip, knee, and femur forces with variations in direction of the GRF.

Study 4: Position of the spherical joint between femur segments in the transverse plane.

Knee joint reaction force was selected as the most appropriate output value to be reported in Study 4. The majority of muscles crossing the cut in the femur also cross the knee, and so the knee joint reaction force is significantly affected. By contrast, very little difference was observed in the hip joint reaction force with a shift in the femur joint. As highly detailed bone geometries were not available, the exact centre of mass of the cross section of the femoral shaft could not be calculated. It was therefore decided to vary the position of the joint in four directions. The results of this variation are seen in Table 3.4.

Table 3.4 - Impact on knee joint reaction force of moving the spherical joint between femur segments in the transverse plane

Knee Joint Reaction Force in Multiples of Bodyweight				
Direction		Posterior		Anterior
	Shift (mm)	- 2	0	+2
Medial	+ 2	-	3.45	-
	0	3.43	3.8	4.24
Lateral	- 2	-	4.24	-

3.6 Discussion

Study 1 shows that knee joint position has a significant impact on the performance of the model. The knee centre of rotation can be estimated by tracking the motion of the thigh and shank segments, but an accurate estimation of the point of contact would require more complicated methods. It is evident that the current knee model is over simplified and may not produce accurate results. This is owing to the fact the joint hinges on a single axis, about which the balance point is extremely sensitive.

Variations in position of the knee joint alter the muscle moment arms acting across the knee. Consequently, the muscle activation must change to compensate. Thus the total force across the knee joint is varied and this impacts in turn upon the joint reaction force. The femur joint is similarly affected as the majority of muscles crossing the knee joint also cross the femur joint as previously mentioned. Any changes in the activation of one muscle require compensatory action from other muscles and so we see that the muscles crossing the hip joint are also affected, but to a lesser degree. There are of course some muscles included in the model which cross both joints and contribute to the impact of a change in the knee joint affecting the hip.

The lack of anatomical accuracy in the modelling of the joints is a limitation of this study and care must be applied when interpreting the results. However, although the joint reaction forces are used as an indication of model performance, being directly influenced by the degree to which muscle forces are minimised, calculating accurate joint reaction forces is not the goal of this study.

The results of Study 2 show that the angle of the knee joint axis in the transverse plane is less sensitive to variation. Large rotations from the original position were not investigated due to the fact that the correct angle of the axis is somewhat easier to estimate by inspection than the antero-posterior position varied in Study 1. The small rotations applied here represent comparatively (compared to Study 1) small variations in muscle moment arms and consequently we see a smaller impact on joint forces.

The large impact of changing the GRF direction in Study 3 is somewhat predictable. Rotating the force to give a posterior bias (positive rotation) results in a large increase of the moment about the knee caused by the GRF. Increased activation of the knee extensors compensates for this change. As the muscle moment arms are small compared to the moment arm of the GRF, the increase in muscle action is substantial. Quadriceps muscle forces with a 5° positive rotation were approximately double those with a 5° negative rotation. Rotating the GRF in the anterior direction (negative rotation) reduced the moment of the GRF about the knee joint. The force was thus directed anterior to the hip joint, requiring increased activation of the gluteal muscles. This explains the increased hip force with anterior rotation of the GRF. The sensitivity to these changes highlights the importance of having accurate input data. The data used here was taken from the AnyBody Gait Lower Extremity model. This was later replaced with data collected in our own lab, as described in the following chapter

As with Studies 1 and 2, Study 4 examines a parameter which cannot be accurately determined in the current model. Due to this fact, limited conclusions can be drawn from the results obtained. It can be seen however, that the location of the joint between femur segments has an impact on the results, again due to variation in muscle moment arms as with Study 1.

If the muscles act to reduce or eliminate bending in bone in order to maintain compression, then the resultant force through the femoral shaft would pass directly through the centre of mass of the cross section. If we assume that the musculoskeletal system is designed efficiently, then it follows that the muscles should be capable of thus directing the load through the femur without placing undue strain on the surrounding joints.

We do see a variation in the knee joint reaction as a result of changes to the estimated centre of mass of the femoral cross section. The position of this centre of mass then becomes a parameter of some importance in this study as the study aims to determine to what extent muscles can maintain compression in the shaft of the femur during gait.

Lower knee joint reaction forces occur when the centre of mass of the femoral shaft cross section is shifted posteriorly and medially. Inspection of the cross section of real femurs suggests that this may be closer to the true centre of mass, thus showing that the musculoskeletal system may indeed be organised in such a way as to reduce bending in the femur and therefore maintain compression in the bone.

3.7 Conclusions

The model which has been developed is based on accurate anatomical data and provides opportunities to study the loading of the femur. The results collected thus far show that it is possible to maintain compression in the shaft of the femur at 15% of gait.

Many simplifications have been made in the development of this model which impact upon the validity of the results, and these will be discussed in greater detail in subsequent chapters of this thesis.

The model development process itself has been an incremental one, and developments to the model have been in response to various factors. These have included efforts to increase anatomical accuracy and improve results, as well as the need to overcome simulation errors. As the model had to be rebuilt at each position in the gait cycle, the model creation process was automated as much as was practical. The process of creating each model is outlined in Appendix A.

Much of the data used in this model came by necessity from external sources. As much as possible, this was supplemented with data collected in our lab. This allowed the origins of the data to be verified and documented. The next chapter describes the collection of gait data which was incorporated into this model, and then presents the results obtained using the updated subject specific model.

Chapter 4

Multibody Dynamics Gait Simulation

4.1 Introduction

The model described up to this point was based on the default gait data in the Anybody Model Repository. The origin and reliability of this data is unknown, therefore in the interests of thoroughness and traceability, gait data was collected in our own lab and fed into the model. The model was scaled to fit our subject in AnyBody using the standard built-in scaling feature (Schwartz et al. 2010). EMG data was also collected for comparison with model predictions of muscle activation.

This chapter includes a description of the data collected and its use. The process of scaling the model is outlined as well, with an explanation of the optimisation studies carried out.

4.2 Data Collection

Data was collected from a healthy 27 year old male using 10 Oqus infrared cameras (Qualysis, Gothenburg, Sweden) recording at 100 frames per second. Ground reaction forces were recorded using two Kistler force plates (Kistler, Winterthur, Switzerland) sampling at 2000Hz. Reflective markers were placed on the subject's lower limbs and pelvis similar to the Helen Hayes marker setup as shown in Figure 4.1 (Kadaba et al. 1990).

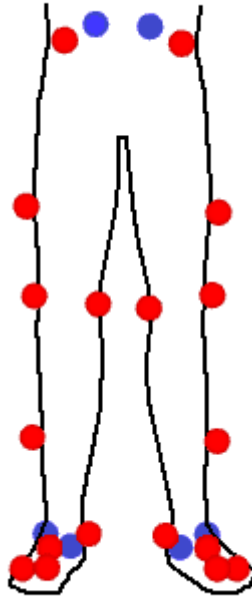


Figure 4.1 - Marker setup used for static trials. Red markers are those visible from the front of the body as shown here, blue markers are behind.

This marker setup was chosen due to the low number of markers used compared with other setups which use marker clusters on the thigh and shank segments. Less markers allowed space for EMG electrodes to be attached. Several of the markers shown in Figure 4.1 were removed during motion trials. The markers used in both static and motion trials are shown in Table 4.1. For each marker listed, one was placed on the right side of the body and one on the left.

Table 4.1 - List of marker locations and their inclusion in static/motion trials

Marker location	Static trials	Motion trials
Anterior superior iliac spine	Yes	Yes
Posterior superior iliac spine	Yes	Yes
Thigh	Yes	Yes
Lateral knee	Yes	Yes
Medial knee	Yes	No
Shank	Yes	Yes
Lateral malleolus	Yes	Yes
Medial malleolus	Yes	No
Calcaneus	Yes	Yes
5 th metatarsal head	Yes	Yes
2 nd metatarsal head	Yes	Yes
2 nd metatarsal base	Yes	No

The subject walked barefoot across the force plates at a self-selected pace. Qualysis Track Manager (Qualysis, Gothenburg, Sweden) was used to acquire the data.

Surface electrodes were placed on the skin over 10 muscles of the right lower limb according to SENIAM guidelines (www.seniam.org). The muscles included were GMax, GMed, TFL, ST, BFL, VL, RF, VM, GL, and GM (see Table 3.1 for a definition of these abbreviations). The skin was prepared by shaving and rubbing with alcohol prior to attachment of standard ECG electrodes made by Ambu (Ambu, Ballerup, Denmark).

The EMG data was recorded using an 8 channel wireless Noraxon system (Noraxon, Scottsdale, Arizona, USA). As only 8 EMG signals could be recorded at one time, two sets of trials were undertaken, with 2 channels being switched to other muscles in the second set of trials to collect all 10 EMG signals. Each set consisted of 5 trials and EMG measurements were collected as shown in table 4.2.

Table 4.2 - EMG data collected from 10 muscles using 8 channels over 2 sets of trials

EMG Channel	Muscle	
	Trial set 1	Trial set 2
1	GMax	GMax
2	GMed	GMed
3	TFL	TFL
4	RF	RF
5	VL	VL
6	VM	VM
7	ST	BFL
8	GM	GL

The EMG signal was recorded at 1500Hz and amplified with a gain of 1000 which was down sampled to 500Hz for transmission via the wireless system, and then interpolated back up to 1500Hz. Common mode rejection rate was 100dB and input impedance was 1mega-ohm.

The raw data was imported into Visual3D for processing (C-Motion, Germantown, Maryland, USA), and a fourth-order high-pass Butterworth filter (cut-off 50Hz) was applied to remove DC bias from the signal. This was then full-wave rectified and smoothed with a low-pass filter (fourth order Butterworth filter, cut-off 5Hz). Processed EMG signals were averaged over 5 trials.

EMG signals were normalised according to maximal voluntary contractions (MVC). These were tested by having the subject exert a maximal effort against resistance in a series of exercises designed to isolate each of the particular muscle groups being studied. The exercises and diagrams below follow guidelines described in “The ABC of EMG – A Practical Introduction to Kinesiological Electromyography” by Peter Konrad (2005), with the exception of the gastrocnemius test which was adapted according to the equipment available. Several of the exercises were completed with the subject lying on a physiotherapy table as shown in figures 4.2, 4.3, and 4.4. Figure 4.2 shows hip extension with a straight leg to isolate the gluteus maximus. Resistance was applied by investigators as indicated by the hollow arrows. The subject pushed against the resistance as indicated by the black arrow.

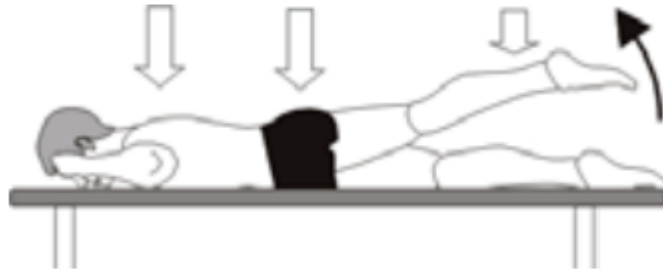


Figure 4.2 - Extension of the hip to test MVC of the gluteus maximus.

The gluteus medius was tested by abduction of the hip against resistance as shown in Figure 4.3. The tensor fascia lata muscle was difficult to isolate and so data for this muscle was collected during the abduction test. As before, the resistance to the movement was applied manually by the investigator as indicated by the hollow arrow. The subject pushed against the resistance in the direction indicated by the black arrow.

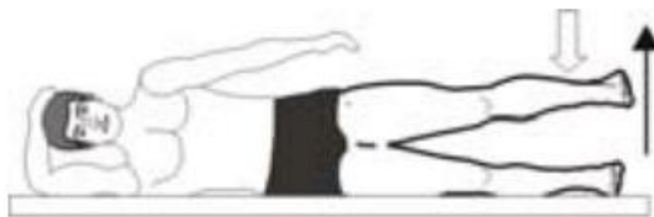


Figure 4.3 - MVC of the gluteus medius tested by abduction of the hip.

Hamstring MVC was tested by flexion of the knee (see Figure 4.4). Both biceps femoris and semitendinosus muscles were tested using this method. Resistance was again applied manually as indicated by the hollow arrows, with the subject pushing their foot in the direction indicated by the black arrow whilst keeping the knee stationary.

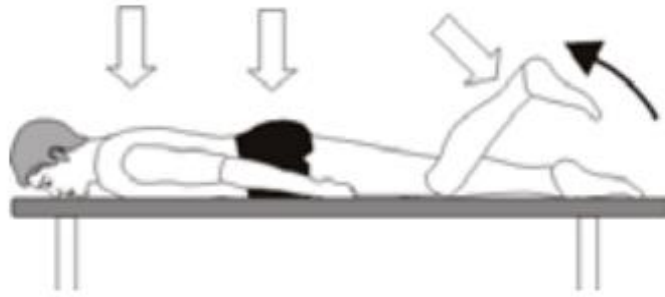


Figure 4.4 - Hamstring MVC tested by flexion of the knee with resistance applied as shown.

The quadriceps were tested as a single muscle group as shown in Figure 4.5. Resistance in this case was applied by having the subject sit facing a wall. An attempt to extend the knee was made by pushing the foot forward against the wall. During this exercise, electrodes were placed on the vastus medialis, rectus femoris and vastus lateralis muscles.



Figure 4.5 - MVC of quadriceps tested in a seated position by extension of the knee against fixed resistance.

The test for the gastrocnemius is shown in Figure 4.6. EMG was collected for the medial and lateral portions simultaneously. The investigator stood behind the subject and applied downward pressure on the shoulders as the subject attempted to raise the shoulders by plantarflexing the ankle and keeping the rest of the body straight.



Figure 4.6 - Gastrocnemius MVC tested by plantarflexion of the ankles against manually applied resistance on the shoulders.

MVC signals were processed in the same manner as the gait trials described previously. Three MVC trials were completed for each muscle group. The maximum value of the processed signal was taken for each trial and these were averaged. EMG amplitudes across the gait cycle were then expressed as a percentage of these MVC values. These are presented in Section 4.5 below.

4.3 Subject Specific Model

Model scaling is a relatively straightforward process in the AnyBody modelling system. Gait data was imported directly in the c3d file format, and the model setup file then modified to include the height and weight of the subject, in addition to an initial estimate of joint angles. Setup required some reorientation of the model to account for the difference between our lab coordinate system and that of the AnyBody model. Running a motion and parameter optimisation matched the model trajectory to the recorded marker trajectories whilst varying the size of the body segments to best match the model to the recorded data.

The force plate data was included in the model by specifying the type of force plate used and which data channels in the c3d file contained the relevant force components.

Once the AnyBody model was appropriately scaled and the force plate data incorporated, the model was exported for use in ADAMS as described in the previous chapter.

4.4 Simulations Carried Out

Static optimisations were carried out on the model for each set of constraints described in Chapter 3. These sets are designated as “Unconstrained femoral loading” and “Compression enforced”. In the case of unconstrained femoral loading, the resultant torques in the hip and knee joints were controlled (as per Constraint 1 in Chapter 3), but no constraint was placed on loading of the femur itself. In the compression enforced case, constraints were added to ensure that the load at the cut in the femur was only compressive and did not exceed a predefined limit.

The initial run of simulations was carried out using the minimised sum of muscle stresses cubed as the cost function. The optimal muscle loading pattern was calculated for each set of constraints in 20 different positions spread evenly across the gait cycle. Optimal in this case referred to the solution which best met the constraints and minimised the cost function. Note this is not necessarily representative of optimal conditions *in vivo*.

The simulations included 31 muscle strands, which required 6500 runs to build a response surface. The response surface was optimised to obtain an approximation of the best solution for each set of constraints. This initial optimisation was carried out in ADAMS Insight as described in Chapter 3.

Unfortunately the constraint for maintaining compression in the femur could not be accurately represented by the response surface. This was highlighted by a feature in the software which evaluates how well the response surface approximation matches the true output for each response. This was rechecked by feeding the muscle force values calculated in ADAMS Insight back into the ADAMS modelling environment. A single simulation was carried out with these muscle force values, which did indeed show different values for the resultant load at the cut in the femur than that predicted by the response surface.

To investigate this, the compression constraint was broken down into component parts and tested through the DOE optimisation process. It was found that although the

directly measured outputs (such as joint torques) were accurate, system responses which were a function of multiple outputs could not be represented accurately in the response surface. The compression constraint involved the combination of several torque components and an axial force. ADAMS technical support were consulted, including an expert in DOE and optimisation methods. However, no root cause for this problem was determined and therefore an alternative method was applied.

Instead of controlling the allowable levels of torque across the cut in the femur using a function, the torque components in the sagittal and frontal planes were simply set to zero. This ensured that the resulting muscle load pattern would not violate the constraints applied. However, the compression constraint was exceeded, which removed the solution from the optimal condition.

The response surface results were used as the starting point for a direct optimisation in HEEDS which included the correct constraint for maintaining compression and allowed the optimal solution to be found. Each optimisation study was set to complete 10000 runs, but these were monitored and stopped if 2000 runs had been completed without improving upon the best solution.

Joint load and muscle force data was collected for all simulations carried out. These results were collected and plotted using Microsoft Excel.

4.5 Results

The results of both the simulations and the EMG collection are presented here. A large number of model parameters were measured and consequently a massive amount of data was output from the model, hence the results presented here are those deemed to be most relevant. Results not included here are contained in Appendix B.

As previously described, the hip and knee joints in the model are highly simplified. Nevertheless, the hip and knee joint loads still yield useful information regarding the level of overall muscle activation and whether or not the loads predicted by the model are reasonable compared to those measured using instrumented prostheses.

Each graph of output from the model contains two data series, one with unconstrained femoral loading, and the other with compression enforced. These are designated by different colours as shown on each graph. The purpose of showing these together is to

highlight the differences in output under the two constraint conditions. As the model output was taken at only 20 points across the gait cycle, each data point is marked with a dot to make clear the data points which were examined.

Hip and knee joint reaction forces are shown in figures 4.7 and 4.8 respectively. We can see that there is little difference in hip joint reaction forces whether compression is enforced or not. In contrast, the knee joint load shows a significant difference throughout the stance phase of gait (0-60%) with a particularly pronounced peak at 50%. Even under conditions of unconstrained femoral loading, the knee joint load during push off is higher than expected.

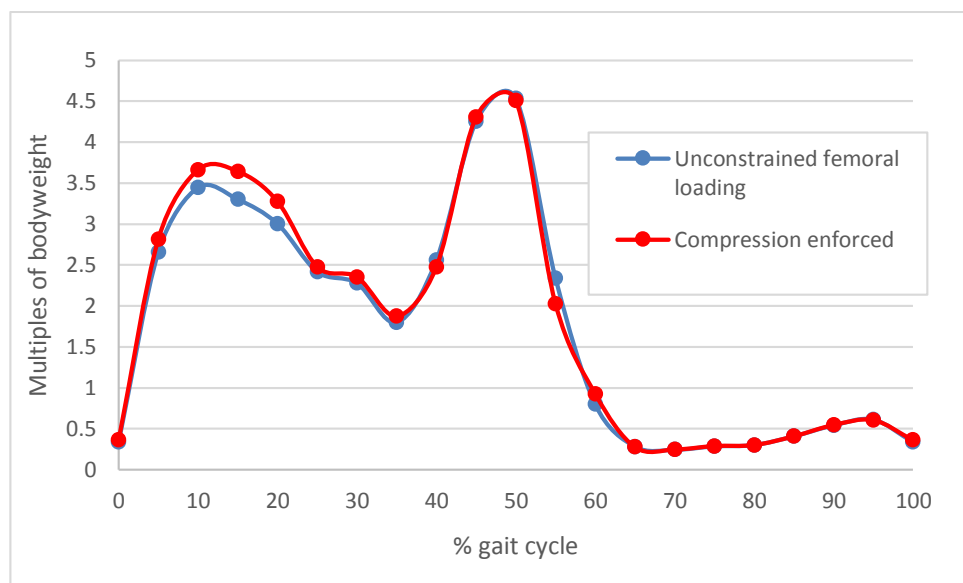


Figure 4.7 - Hip joint reaction force across the gait cycle for two constraint conditions.

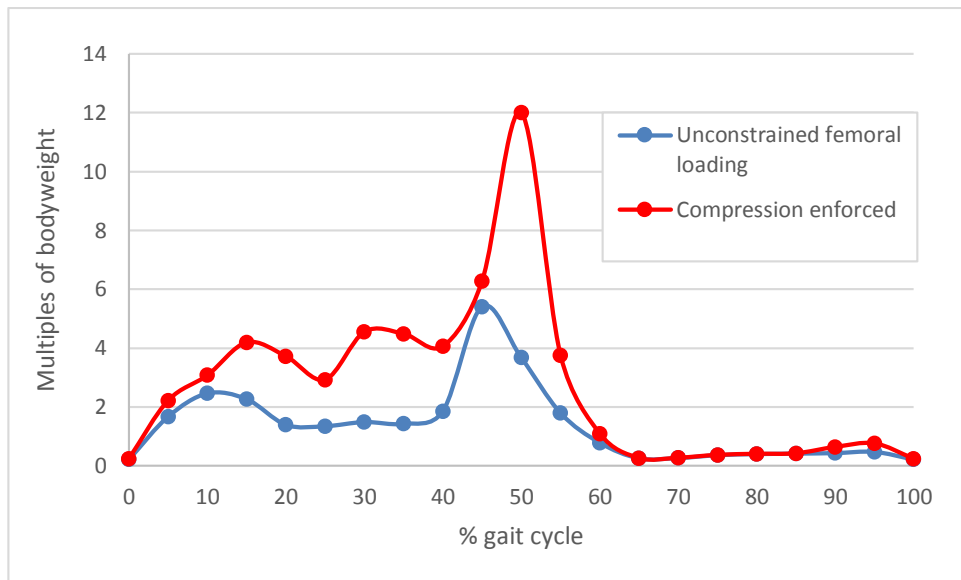


Figure 4.8 - Knee joint reaction force across the gait cycle for two constraint conditions.

Consideration of this unusually large peak led to examination of the measured ground reaction forces. A difference was discovered between the right and left sides, with the right side having a much higher ground reaction force during push off than the left side. This is presented graphically from the recorded data in Figure 4.9, where the results presented here were averaged across 3 trials. The results are shown with standard deviation included for each line. Unfortunately, kinetic data was only collected for a single stride and so no information is available on whether or not this asymmetry was repeated, or perhaps a result of making a single deliberate step to land on the force plates.

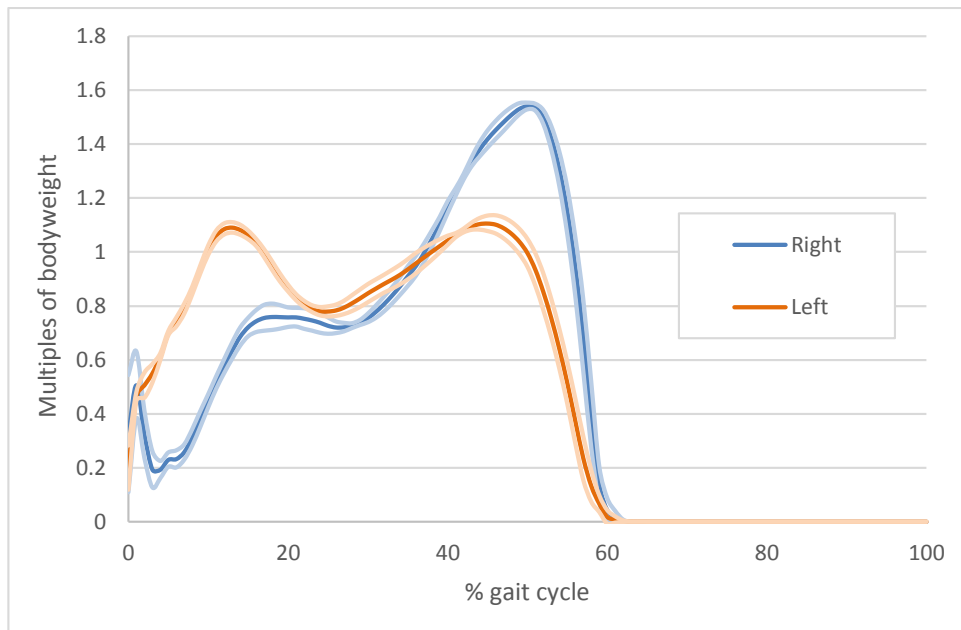


Figure 4.9 - Ground reaction forces for the right and left side across the gait cycle. These results were averaged across 3 trials and standard deviations are shown.

The following results show EMG profiles compared against model predictions of muscle activity. It should be noted that accurate MVC values are difficult to obtain and consequently, the shapes of the EMG profiles are of more interest than the magnitudes. In some cases the EMG signal recorded during gait exceeds the MVC value. This is most likely due to difficulty in isolating a single muscle, as many of the exercises used to determine MVC require the involvement of several muscles.

It is not expected that EMG profiles will match muscle activation profiles from the model, but that some similarities may be observed and provide stimulus for discussion. In spite of efforts to place electrodes on the belly of the muscle being studied, some cross-talk from nearby muscles may have occurred. With these points noted, the EMG and muscle activations predicted by the model will now be presented.

Figure 4.10 shows the EMG profile for the gluteus maximus muscle. Although a certain level of activity is recorded throughout, the most defined peaks occur during the loading response phase of gait, and just after toe off. The position of these peaks is repeated in the model predicted muscle activations shown in Figure 4.11, although with much more activity during the loading response phase than after toe off. The two curves shown in

Figure 4.11 are similar, with slightly higher muscle activation during loading response when compression is enforced.

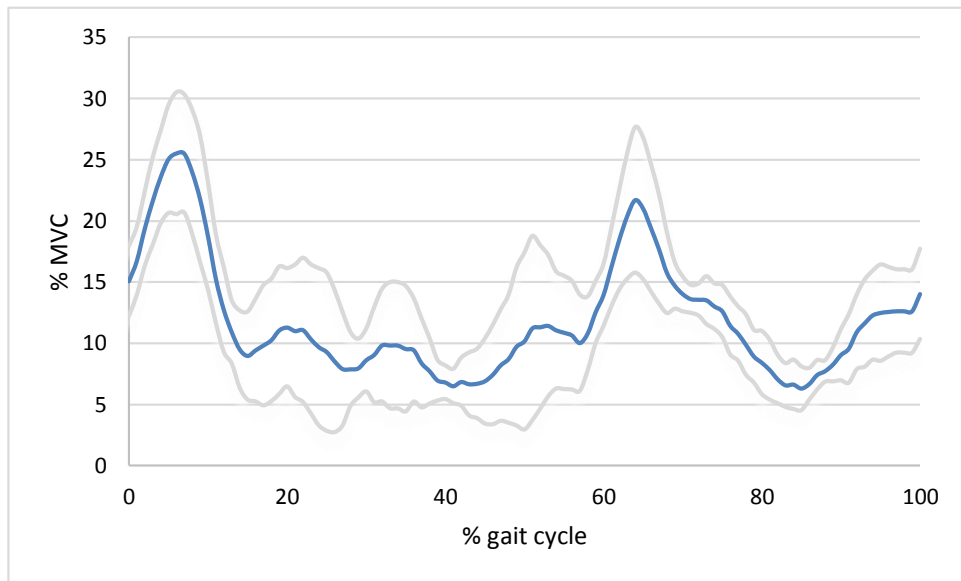


Figure 4.10 - Gluteus maximus EMG profile across the gait cycle from 5 trials with standard deviation.

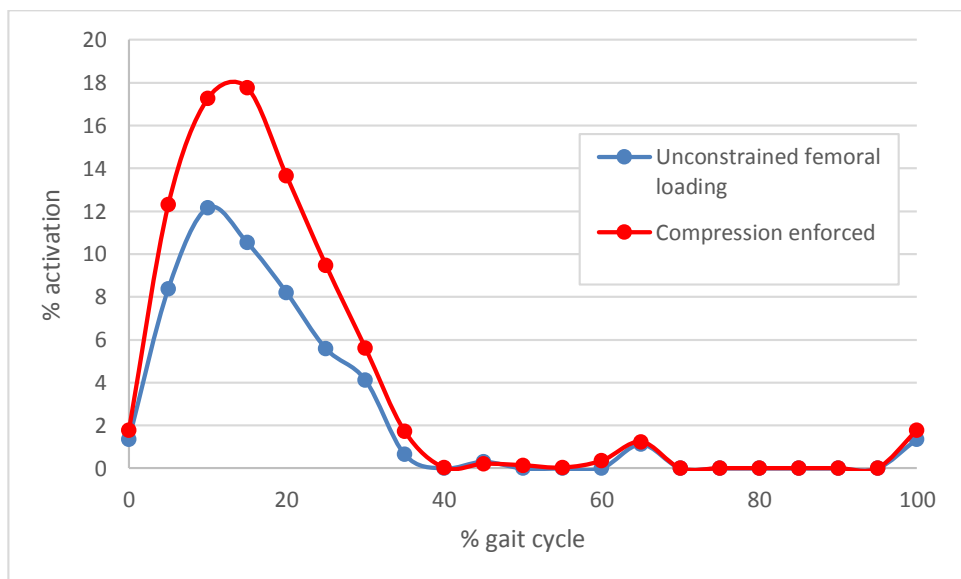


Figure 4.11 - Gluteus maximus activation as predicted by the model with each of two sets of constraints.

The gluteus medius EMG profile is similar to gluteus maximus but with the peaks occurring slightly earlier; immediately following heel strike, and during toe off (see

Figure 4.12). The first peak is also considerably larger than the second and the standard deviations are smaller.

Model-predicted gluteus medius activity bears little resemblance to the EMG profile save for the peak during loading response (see Figure 4.13). Figure 4.13 shows total gluteus medius activity, but it is worth considering that the gluteus medius is separated into anterior and posterior portions. These have been separated and presented in Figures 4.14 (anterior) and 4.15 (posterior).

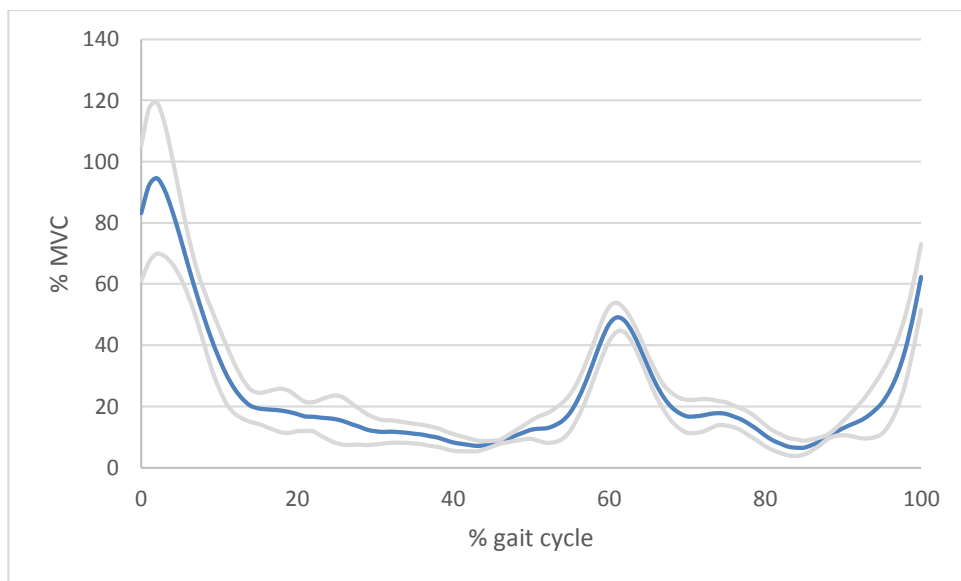


Figure 4.12 - Gluteus medius EMG profile across the gait cycle.

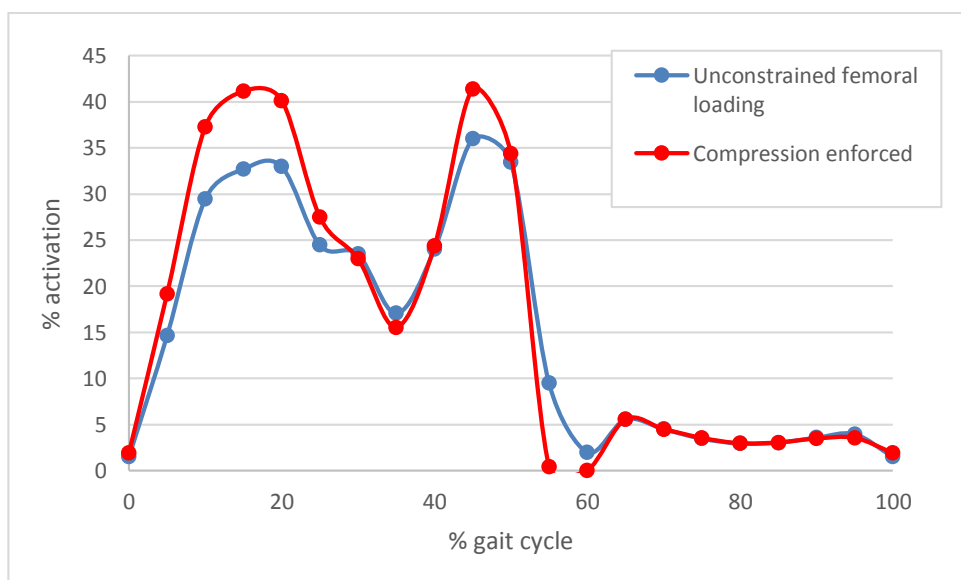


Figure 4.13 - Gluteus medius muscle activity as predicted by the model.

An examination of Figures 4.14 and 4.15 shows that the anterior portion of the gluteus medius is largely responsible for the second peak shown in Figure 4.13, and the posterior portion accounts for the first peak. Due to the placement of the electrodes used to collect EMG from the gluteus medius, it is likely that the EMG signal is dominated by the posterior portion of the gluteus medius. A comparison of Figures 4.12 and 4.15 shows similarities except that the model predicted much higher gluteus medius activity throughout the mid-stance phase of gait for both sets of constraints.

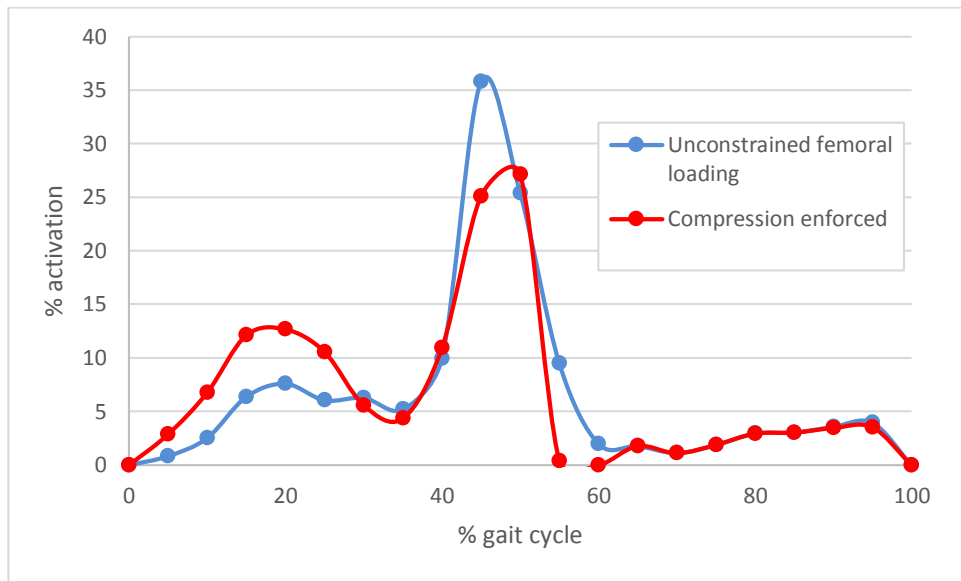


Figure 4.14 - Gluteus medius anterior muscle activity as predicted by the model.

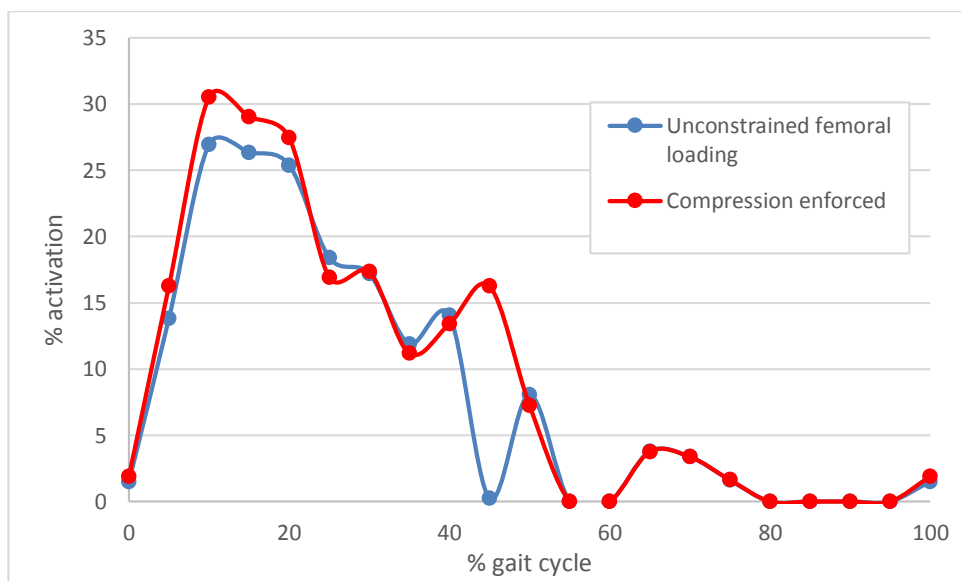


Figure 4.15 - Gluteus medius posterior muscle activity as predicted by the model.

Figures 4.16 and 4.17 show the EMG profile and model results for the tensor fascia lata muscle. This muscle has its origin on the anterior part of the iliac crest and inserts into the ilio-tibial band, which in turn inserts on the lateral epicondyle of the femur and lateral condyle of the tibia. There appears to be very little similarity between the EMG profile and model-predicted muscle activation. Although the magnitude of the model-predicted muscle force increases when compression is enforced, the muscle activation pattern has the same basic shape in both constraint conditions presented in Figure 4.17.

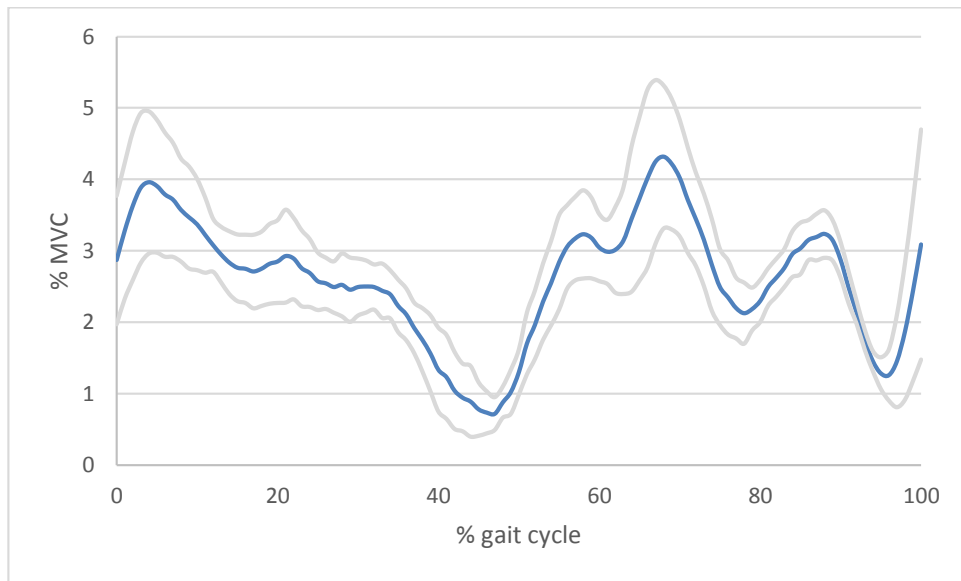


Figure 4.16 - Tensor fascia lata EMG profile across the gait cycle.

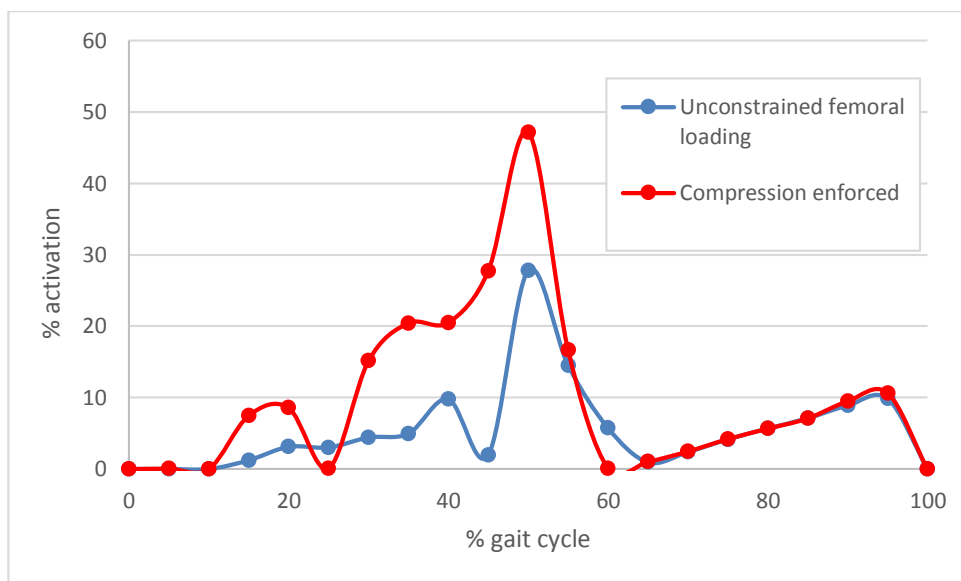


Figure 4.17 - Tensor fascia lata muscle activity as predicted by the model.

EMG data for the rectus femoris muscle is shown in Figure 4.18. It is evident that the MVC test for this muscle produced a very strong contraction as shown by the small percentage of MVC recorded across the gait cycle. The maximum contraction during gait occurs immediately following heel strike. We see activation increase towards the end of the cycle as the knee is extended and peak as the muscle contracts to prevent the knee from collapsing following heel strike.

The activation profile predicted by the model shows almost no resemblance to the EMG profile, with a very definite peak during the push-off phase of gait (see Figure 4.19). This is mirrored both when compression is enforced and when femoral loading is unconstrained.

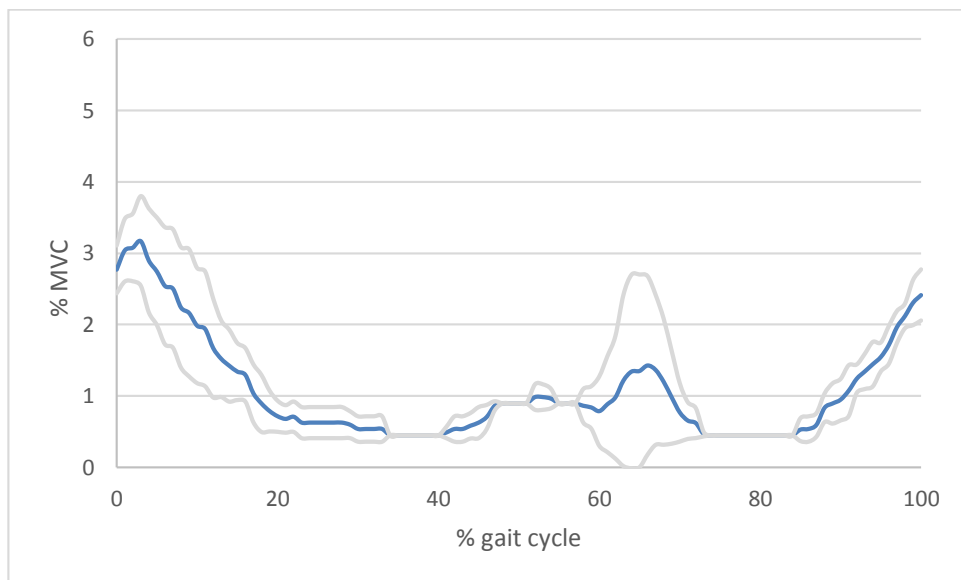


Figure 4.18 - Rectus femoris EMG profile across the gait cycle.

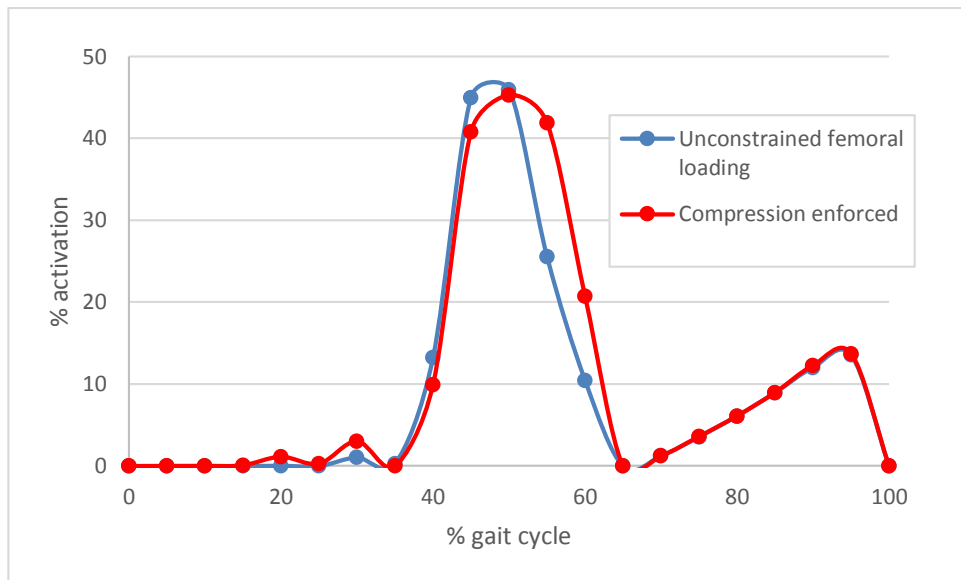


Figure 4.19 - Rectus femoris muscle activity as predicted by the model.

The vastus intermedius lies under the rectus femoris and acts with the rest of the quadriceps group as a knee extensor. EMG was not collected for this muscle due to its deep location. The model prediction of vastus intermedius activation shows greater activation when compression is enforced (see Figure 4.20). The muscle strand representing the vastus intermedius in the model lies lateral of the mid-line of the femur.

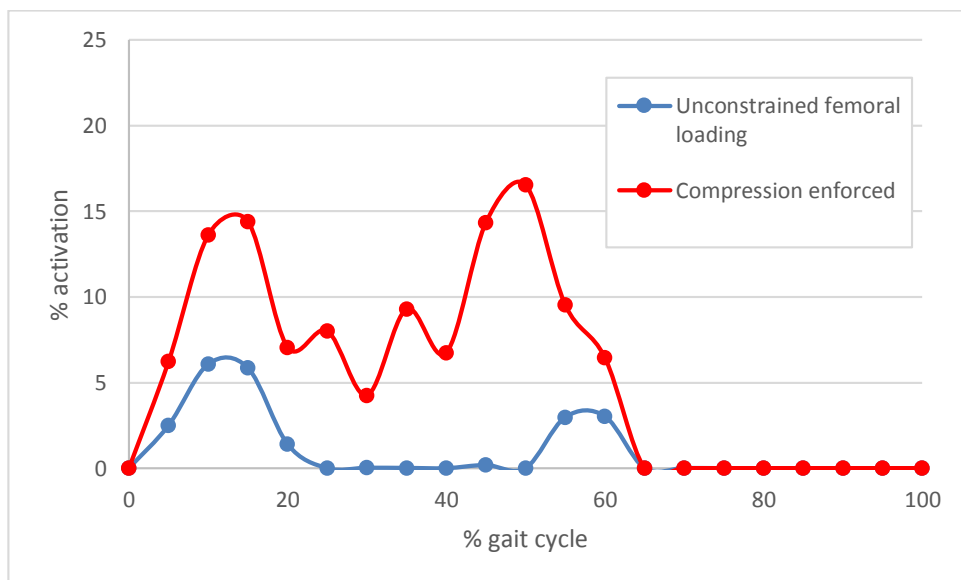


Figure 4.20 - Vastus intermedius muscle activity as predicted by the model.

Both the vastus lateralis (see Figure 4.21) and vastus medialis (see Figure 4.22) muscles show EMG profiles similar to the rectus femoris, but with a more definite lack of activity between 20 and 80% of the gait cycle. It appears from these results that the quadriceps group functions largely as a whole during the gait cycle to extend the knee prior to heel strike and control knee flexion during loading response.

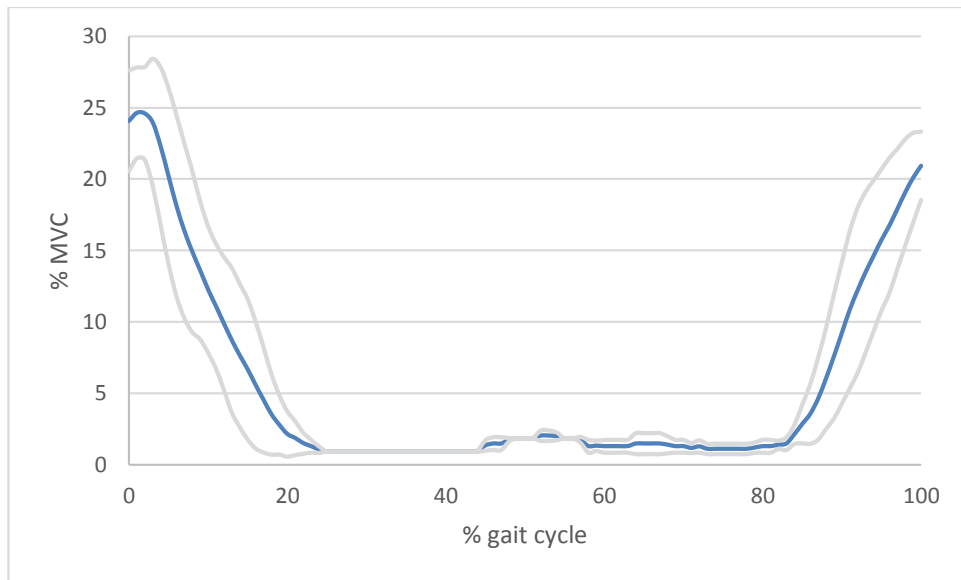


Figure 4.21 - Vastus lateralis EMG profile across the gait cycle.

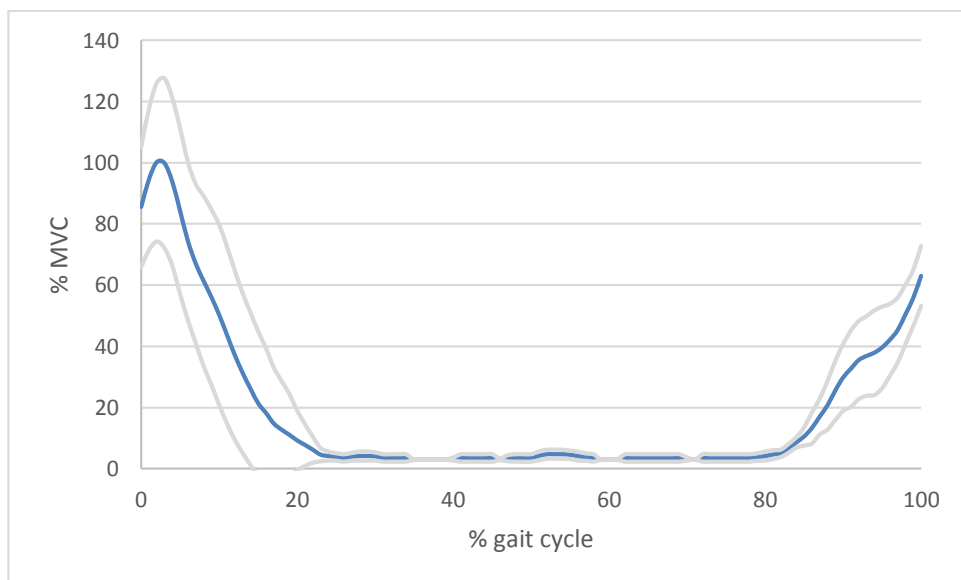


Figure 4.22 - Vastus medialis EMG profile across the gait cycle.

The model-predicted muscle data in Figure 4.23 does show activity during the first 20% of gait as in the EMG data but shows continued activation during the stance phase which

is not present in the EMG. There are also significant differences between the two sets of applied constraints. Where loading of the femur was unconstrained, activation of the vastus lateralis remains relatively low, with activity during loading response, push-off, and toe-off. Where compression of the femur was enforced, activation of the vastus lateralis is significantly higher and continues throughout the stance phase of gait.

The force produced in the vastus medialis under conditions of unconstrained femoral loading, is almost identical to the vastus lateralis under the same condition. This contrasts with the difference observed between the medial and lateral sides under enforced compression. When compression was enforced, activation of the vastus medialis was almost non-existent as shown in Figure 4.24. This difference between the medial and lateral muscles, shows that the vastus lateralis played a role in maintaining compression in the femur.

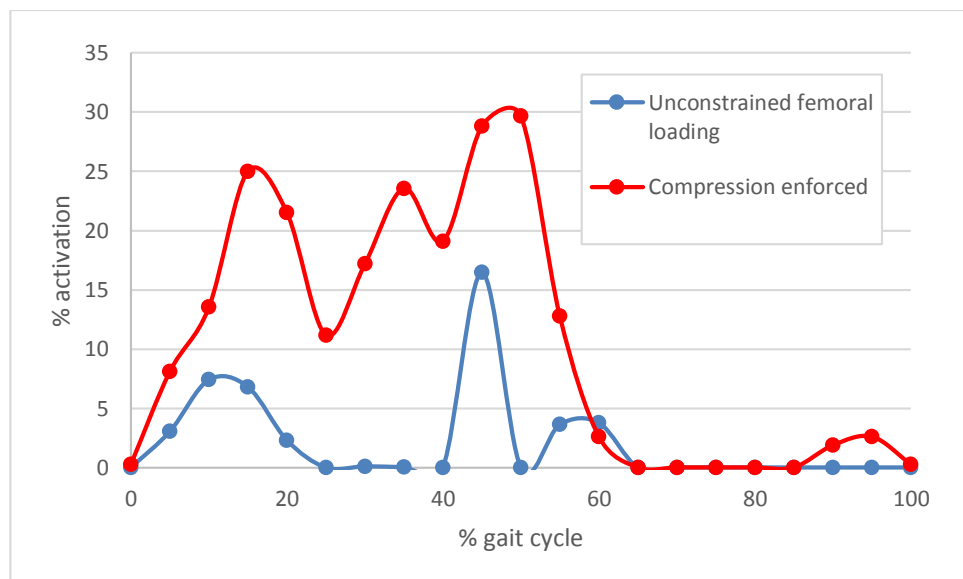


Figure 4.23 - Vastus lateralis muscle activity as predicted by the model.

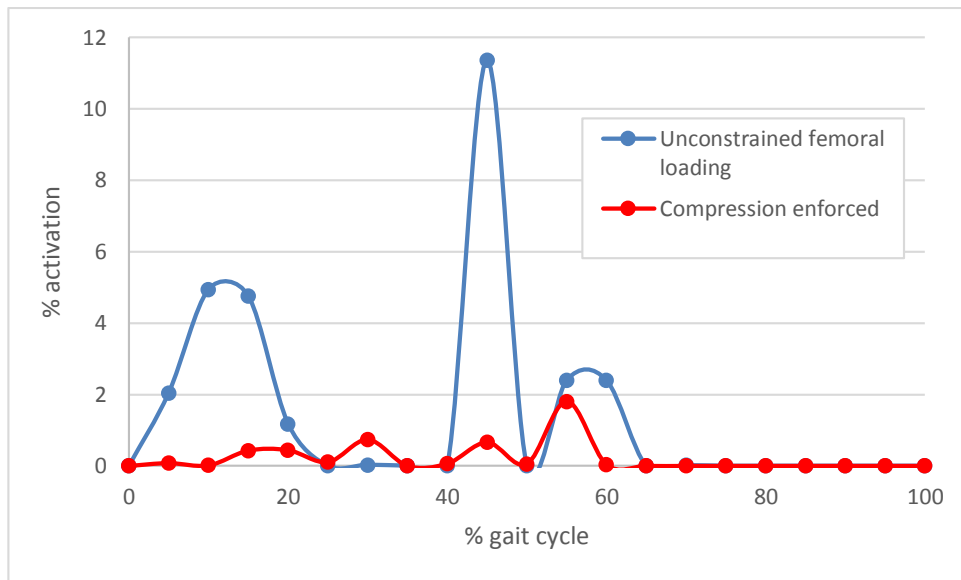


Figure 4.24 - Vastus medialis muscle activity as predicted by the model.

As previously mentioned, many of the exercises used to test MVC did not adequately isolate the muscle to be studied. This is evidenced by the fact that EMG activity in the semitendinosus muscle during gait far exceeded the MVC value against which it was normalised (see Figure 4.25). In terms of the shape of the graph, a similarity can be observed between the EMG profile in Figure 4.25 and the model-predicted muscle activity in Figure 4.26. Both graphs show activity during the loading response phase of gait (0-20 percent) and during the early swing phase (60-80 percent).

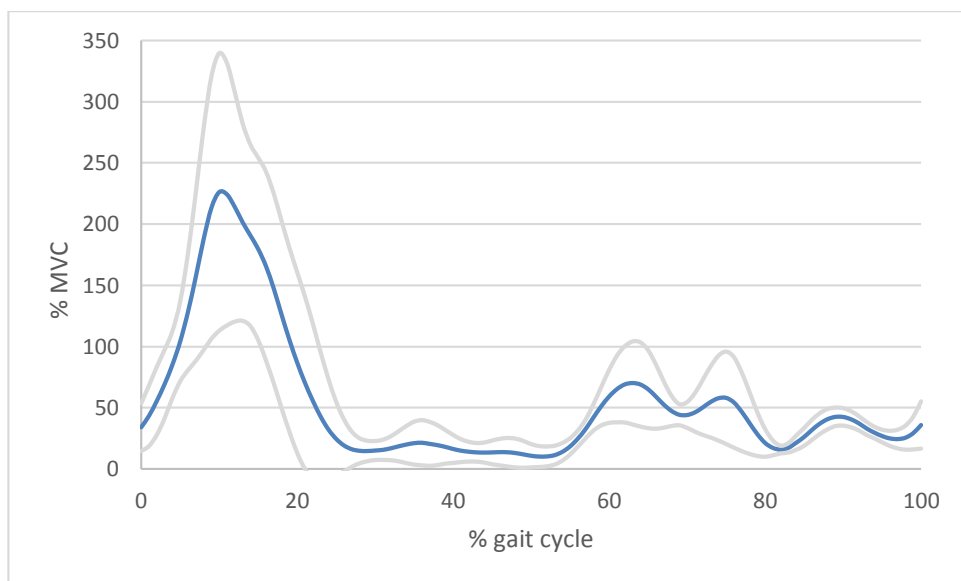


Figure 4.25 - Semitendinosus EMG profile across the gait cycle.

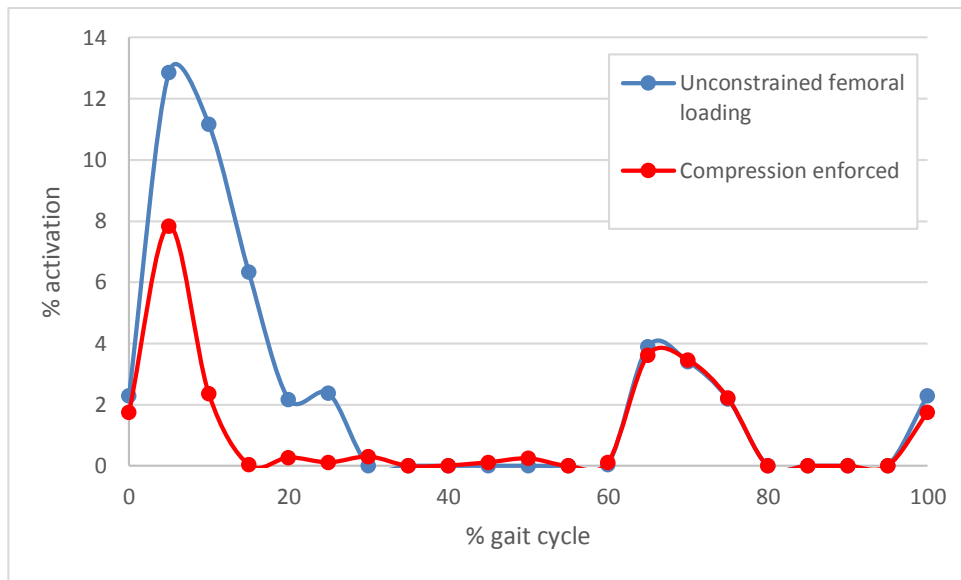


Figure 4.26 - Semitendinosus muscle activity as predicted by the model.

The biceps femoris muscle shows four peaks of activity spread across the gait cycle (see Figure 4.27). The largest peak occurs during the loading response phase of gait which also corresponds with the largest standard deviation. Figure 4.28 shows a similar initial peak of activity during loading response for both constraint conditions, with the burst of activity dropping off sooner when compression is enforced. The unconstrained femoral loading case matches the first three peaks of the EMG profile. The compression enforced case matches peaks one and three. It should be pointed out that the muscle loads given here for the model are for the long head of the biceps femoris muscle. The model showed very little activity for the short head of the muscle, and the EMG was collected from the more superficial long head. It is unknown to what extent the EMG signal may have been influenced by cross-talk from the deeper portion of the muscle.

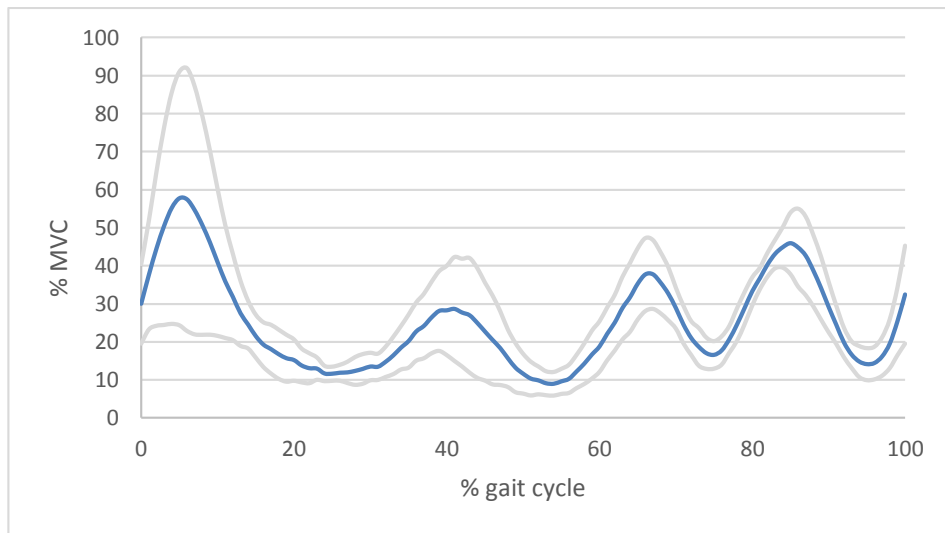


Figure 4.27 - Biceps femoris EMG profile across the gait cycle.

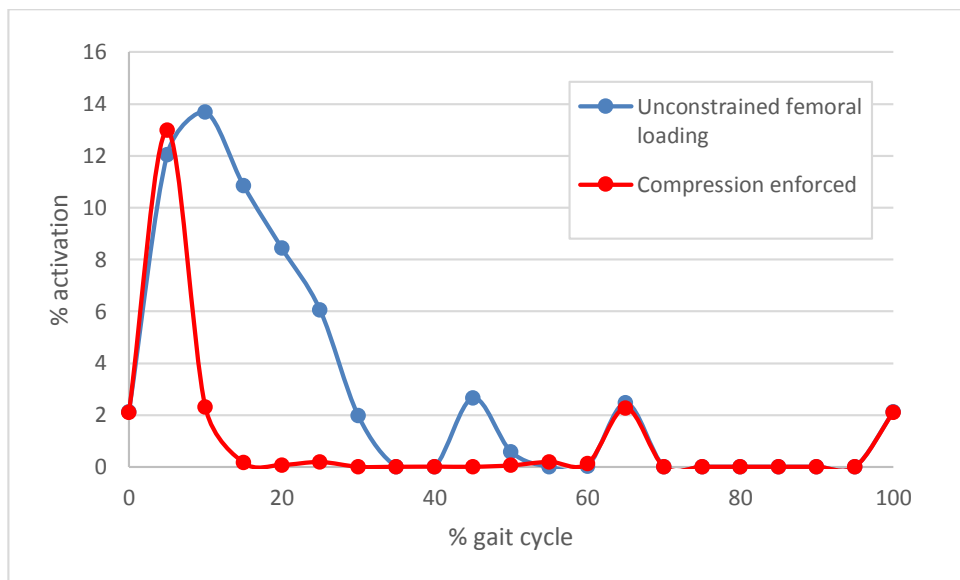


Figure 4.28 - Biceps femoris muscle activity as predicted by the model.

The final muscle to be considered is the gastrocnemius. Data was recorded separately for the medial and lateral portions. EMG collected for the medial portion is shown in Figure 4.29. The onset of activity occurs at approximately 10% of gait and increases gradually during the mid-stance phase before reaching a peak during push-off. The model shows similar muscle activity in the case of enforced compression (see Figure 4.30). The unconstrained femoral loading case is also similar, but with a later onset and earlier drop-off.

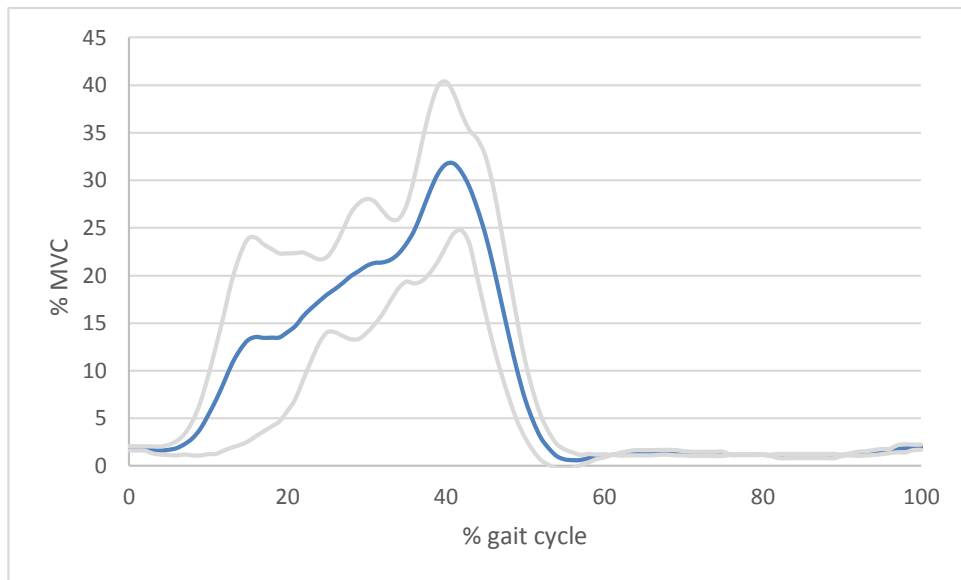


Figure 4.29 - Gastrocnemius medialis EMG profile across the gait cycle.

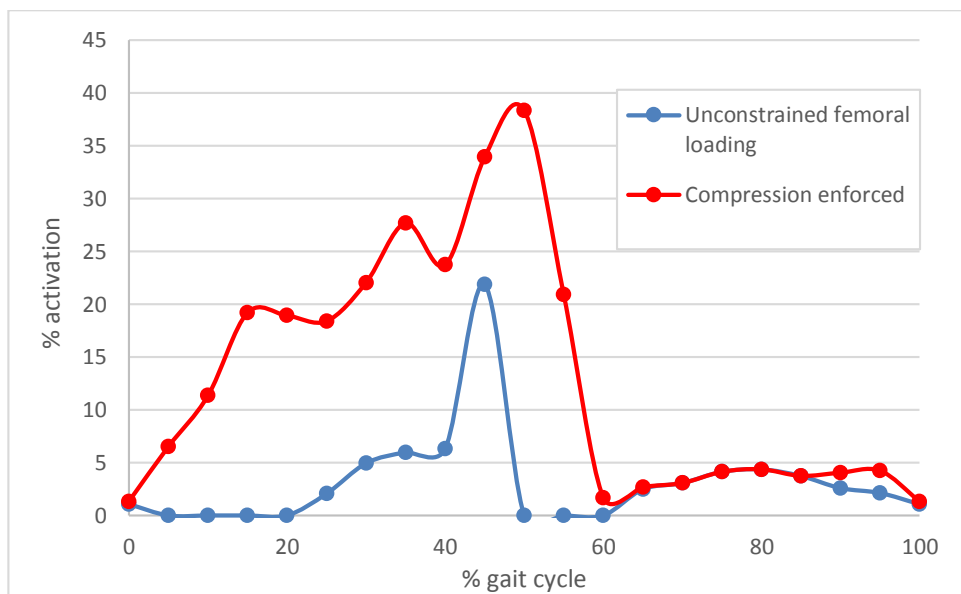


Figure 4.30 - Gastrocnemius medialis muscle activity as predicted by the model.

The lateral portion of the gastrocnemius (as shown in Figure 4.31) exhibits a similar EMG profile to the medial portion. This time however, the model prediction under enforced compression varies (see Figure 4.32). Although the duration of muscle activity is similar, there is a sharper rise and more sustained activation during the stance phase. Where femoral loading was not constrained, activity of the lateral portion of the muscle is identical to the medial portion. This medial-lateral difference further shows an overall increase in lateral muscle activity when compression is enforced.

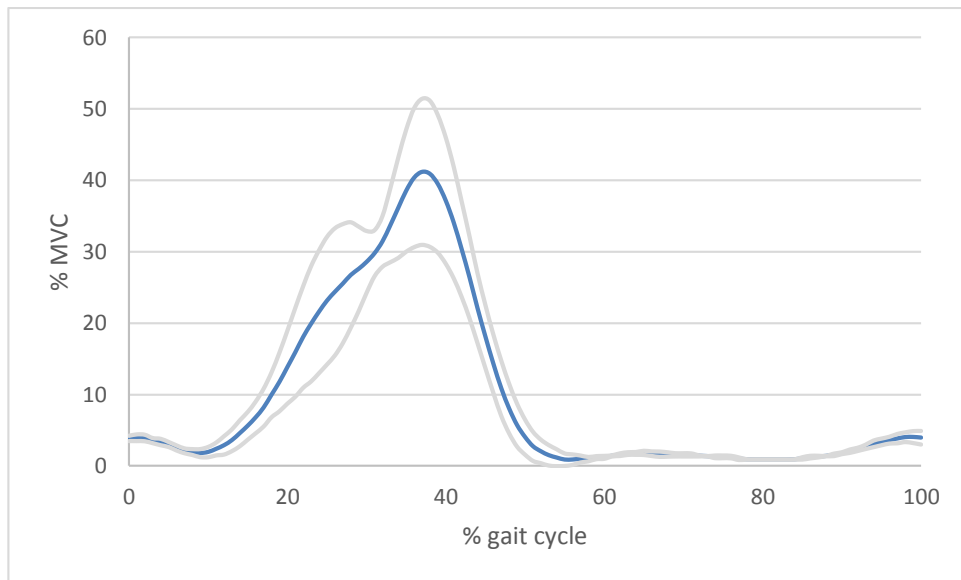


Figure 4.31 - Gastrocnemius lateralis EMG profile across the gait cycle.

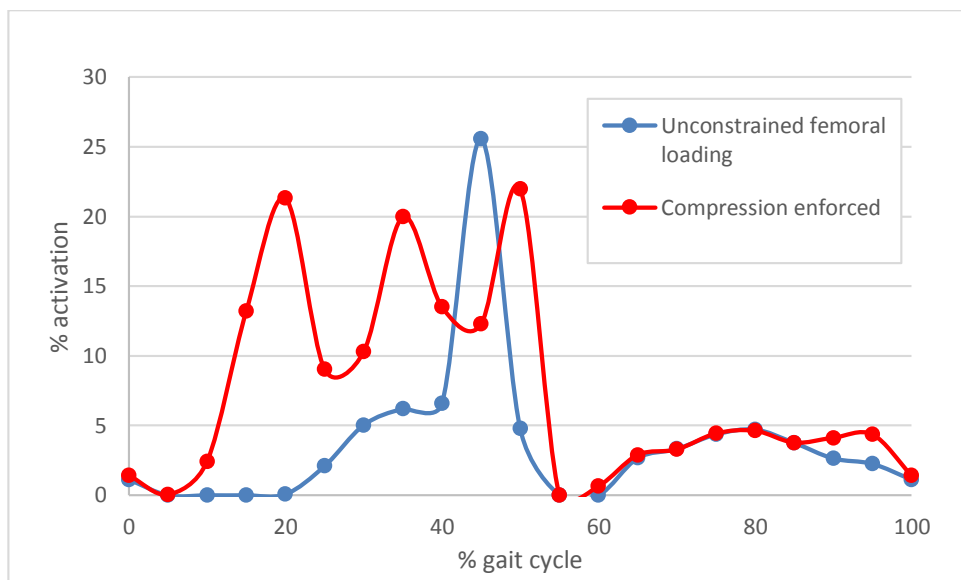


Figure 4.32 - Gastrocnemius lateralis muscle activity as predicted by the model.

These results prompted further examination of model performance and lead to identification of potential improvements which will be discussed in the following section.

4.6 Discussion

The primary purpose of the model which has been developed was not to replicate the workings of the musculoskeletal system perfectly. That would indeed be desirable but remains an elusive goal for the musculoskeletal modelling community. It is recognised that this model has several simplifications and limitations which have been described in the previous chapter. The purpose of this model is to evaluate whether or not compression of the femoral shaft enforced by muscular loading is feasible and if so, under what conditions is this state of loading achieved. With this goal in mind, evaluation of the results which have been presented will be more comparative than absolute.

Little difference is observed between the two constraint cases for the hip joint load. This is not unexpected, due to the fact that most of the muscles influencing the hip joint load do not cross the cut in the femur and do not influence the state of loading at that point.

Typical peak hip joint loads are in the region of 3 times bodyweight but may be higher or lower depending on the individual. The double peak pattern shown in Figure 4.7 is similar to the hip loading patterns collected using instrumented prostheses (Bergmann et al. 2001).

Figure 4.8 tells a different story regarding the knee joint. The additional constraints applied to the loading of the femur (compression enforced), result in greater activation of the muscles crossing the knee and consequently a higher knee force. This rises to a maximum of 12 times bodyweight during push-off, which is far above typical knee joint reaction force values. This can be explained in part by limitations to the model.

The results presented in Chapter 3 (study 1) highlighted the sensitivity of the model to correct placement of the hinge joint representing the knee. As pointed out then, the position of this joint was determined manually for each simulation and is almost certainly open to error. Even if the joint was positioned correctly, a single hinge point is a gross simplification which requires a fine balance of forces. This model included 31 muscle strands. This limitation in the number of strands required that some muscles act along a single line of action rather than being spread over larger areas. This caused the existing forces to increase in order to compensate for those absent from the model. An

increase in one force is followed by compensatory action by antagonistic forces and so we can see how this may result in unusually high knee joint reaction forces.

The problem caused by the limited number of muscle strands was the subject of further investigation which will be presented in the next chapter.

The reasons given thus far are not the only contributors to the large knee force. During processing of the recorded gait data, it was observed that ground reaction forces during push-off were higher during right-legged stance than during left-legged stance (see Figure 4.9). The peak GRF measured under the right leg was in excess of 1.5 times bodyweight, which exceeds typical GRF values in the literature (White et al. 1998, Cross 1999). A previous study measured GRF during gait of 18 adult males aged 18-38 years (Hunt et al. 2001) who walked over force plates at a self-selected pace. The results are shown in Figure 4.33. We see from this example that GRF patterns tend to match what was measured for the left leg of the current study, as shown in Figure 4.9. Thus, it would appear that the right leg GRF, which was used as input for the model, is unusual and contributes to the unusually high joint reaction forces seen during push-off.

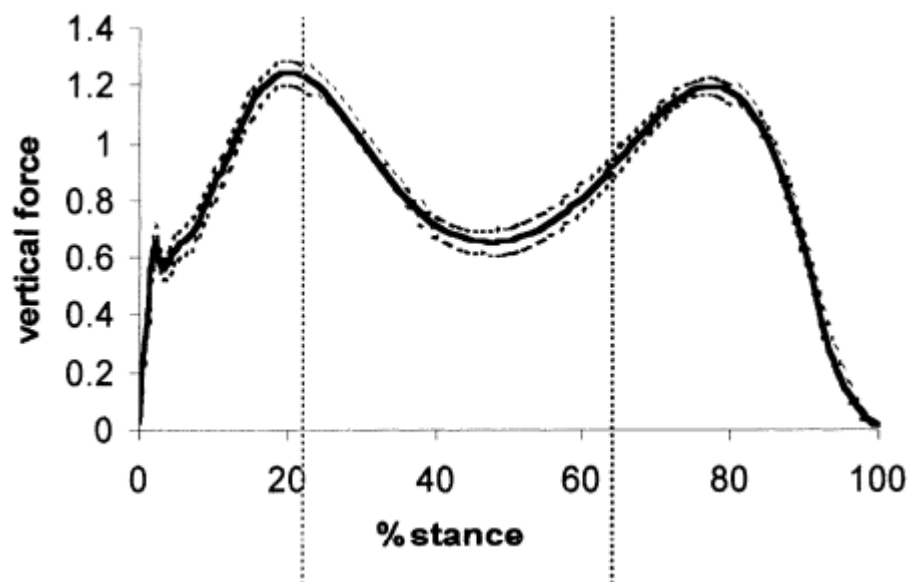


Figure 4.33 - GRF measured in 18 adult males by Hunt et al. (2001). Vertical GRF is given in units of bodyweight across the stance phase of gait.

Several of the measured EMG profiles show similarities in shape to model predictions of muscle activity, in particular the semitendinosus and gastrocnemius medialis. This helps

in making a case for the validity of the model. However, many of the predicted muscle forces are in stark contrast to EMG profiles. This in turn raises questions over whether or not these muscle force predictions are of value.

The most striking differences are seen in the quadriceps muscles. The rectus femoris, vastus medialis, and vastus lateralis, all show a peak of EMG activity at heel strike, with very little activity during the remainder of the gait cycle. The model-predicted muscle forces show activation of varying levels, particularly during the stance phase. The most obvious difference is the activation seen in the rectus femoris during push off. This large peak of activity is seen in both constraint conditions and so must be in response to the constraints applied to the hip and knee joints. In the case of the vastus intermedius, it is clear that almost all activation during the stance phase is in response to the constraint applied to enforce compression in the femur. If the large peak in rectus femoris activity was to support the knee, we would expect this load to be shared by the vastus intermedius which it is not. This suggests then that the model activates the rectus femoris during push-off to stabilise the hip.

Several other muscles show peaks of activity during the push-off phase. These are the gluteus medius anterior and TFL shown in Figures 4.14 and 4.17 respectively. Not shown in the results are the adductor longus, obturator externus, quadratus femoris, and sartorius muscles. All of these cross the hip and show their largest peaks of activity during the push-off phase. This period of the gait cycle is the time when the direction of the GRF is posterior to the hip joint.

As mentioned before, increase in one muscle force results in compensatory action by other muscle strands. The simplified hip joint model balances about a single point and so requires a very precise combination of muscle forces to keep the net joint moment within the limits specified in the constraint. In this case, some of the muscles activating to balance the hip also cross the knee. This has a knock on effect for the knee joint and additional muscle activation is required there. Of course, this push-off phase of gait is also where we see an unusually large GRF, further exacerbating the problem.

Further to the causes outlined above, a fundamental difference exists between the model and actual human gait. That difference is motion. The model seeks to keep the overall joint torques close to zero, whereas in reality a net moment exists about each

joint which produces the required motion. The largest joint torques calculated from the recorded gait data occur during the push-off phase. This is the point at which the model requirement of keeping the joint torques close to zero is furthest from the case encountered *in vivo*. Using the GRF as input does account for the movement of body mass but does not explain how torques are applied across each joint.

An examination of the gluteus maximus and TFL EMG profiles shows near constant activity throughout gait. These are the muscles which insert into the ITB. If the ITB acts as a tension band as has been suggested (Sverdlova & Witzel 2010), it may be reasonable to suggest that a level of tension is required whenever the femur is loaded and that this tension is provided by activation of the TFL and a portion of the gluteus maximus.

In addition, the ITB was represented in a simplified way in the model, as described in Chapter 3. No information was available on the portion of the gluteus maximus which inserts into the ITB and to what degree force is transferred between the two structures. This is therefore a limitation of the model. The way in which the TFL-ITB unit was modelled also varies from human anatomy. The load which originates in the TFL muscle does not pass independently in a perfectly straight line to the ITB point of insertion. It is unclear how the various loads applied to the ITB interact. Figure 4.34 shows a simplified representation of the current ITB model, and suggests a more anatomically accurate alternative. This alternative could have been implemented if accurate data had been available; it should be the focus of future work.

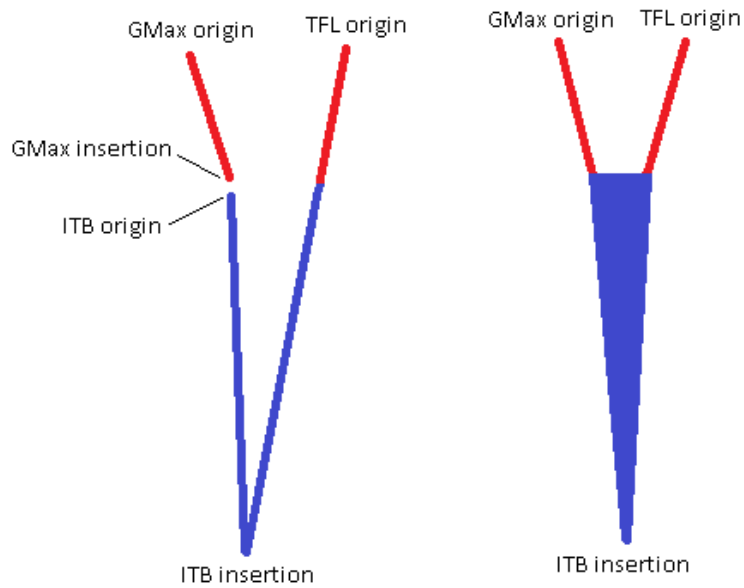


Figure 4.34 - Simplified diagrams of two options for modelling of the ITB imagined from a sagittal perspective. Muscles are shown in red and the ITB in blue. The image on the left shows how the ITB is represented in the current model. The gluteus maximus passes from its origin to insertion. A strand of the ITB originates at the point of insertion of the gluteus maximus but there is no load transfer between the two. The TFL and corresponding strand of the ITB are treated as a single unit, passing from the origin of the TFL to the insertion of the ITB. The image on the right shows a more accurate way of representing the ITB where the gluteus maximus and TFL insert into the thick band of the ITB.

Both the vastus lateralis and vastus intermedius muscles show increased activation when compression is enforced. Both of these muscles originate laterally to the mid-line of the femur and so may be acting to provide some of the tension band force normally attributed to the ITB. It is highly likely that changes to the way in which the ITB is modelled would alter the degree to which these lateral muscles activate under enforced compression.

Overall the results presented here show that compression can be maintained in the shaft of the femur throughout the gait cycle by coordinated muscle activation. Simplifications in the model - such as the limited number of muscle strands - increase the difficulty of producing an optimal muscle activation pattern. It is anticipated that a more complex

model with increased anatomical accuracy will have the capability to maintain compression without forcing large increases in joint loads.

With this in mind, a new simulation method was developed to allow the use of more muscle strands. The updated method will be presented in the next chapter along with the results it produced.

Chapter 5

Improved Model

5.1 Introduction

Results from the previous chapter raised the question of whether or not using a larger number of muscle strands would allow compression to be maintained in the femur without a large increase in overall muscle stress and joint loads. This chapter presents results obtained using a further improved simulation method which allowed the use of many more muscle strands.

The decision to repeat simulations using an improved model was taken after running exploratory trials with the new method at 15 and 50% of gait. These are the points where the peak GRF values occur. Both of these trial runs showed that compression could be achieved with a much lower knee joint reaction force than was previously seen in the 31 strand model. Figure 5.1 shows the difference in joint reaction forces between using 31 and 67 muscle strands at 50% of gait. Compression was enforced in both cases.

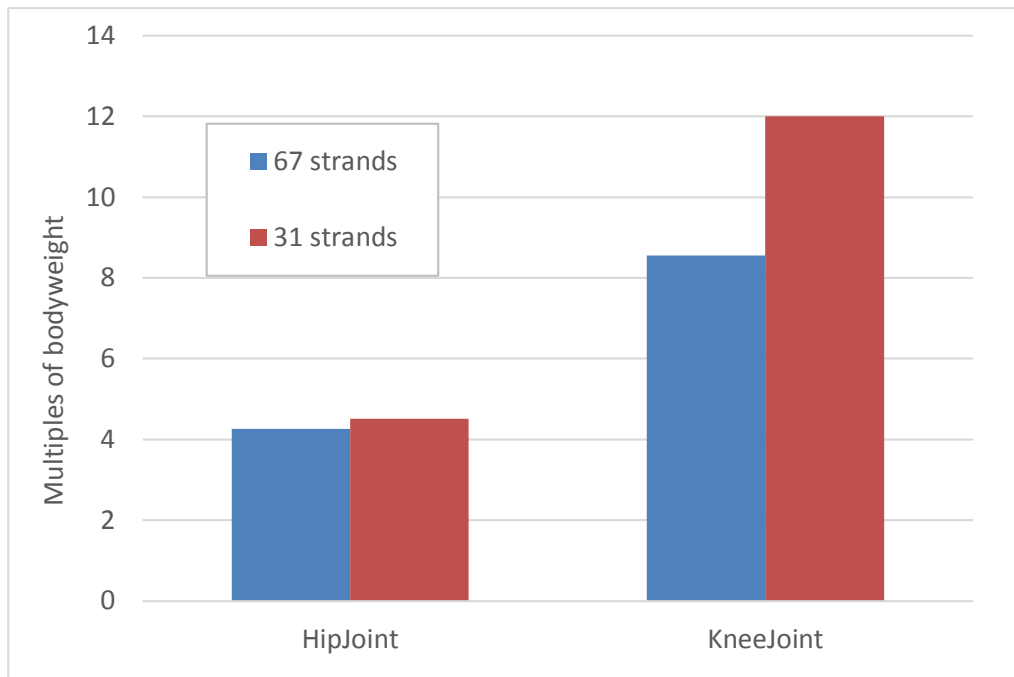


Figure 5.1 - Hip and knee joint loads at 50% of gait comparing the 67 and 31 strand models.

The rationale behind repeating simulations with 67 strands was that a more anatomically accurate model should produce more reliable results. If the model could maintain compression more efficiently with more muscle strands, then it might be reasonable to suppose that the human musculoskeletal system can maintain compression more efficiently still, provided muscle activation is appropriately coordinated. In this case maintaining compression efficiently means without large increases in muscle and joint loads.

As mentioned previously, running optimisations using 67 strands required some modification of the optimisation method. This will be outlined in the following section.

5.2 Method

A slight change to the simulation and optimisation method was implemented to allow the inclusion of additional muscle strands. The main constraint on the number of muscle strands in the previous model was the amount of runs required to build a response surface. The 31 strand model required a minimum of 5984 runs. This increased to 54740 using 67 strands and the same settings. This number of runs was not feasible for two reasons; the excessive amount of time required to build and run that many simulations,

and an inability to compute the response surface without software crashes. The cause of these crashes could not be determined by ADAMS technical support. It is possible that the software was unable to access sufficient memory to calculate such large response surfaces. Reducing the order of the response surface polynomials from cubic to quadratic allowed a 67 strand response surface to be built using only 2346 runs. The result of this was the potential for a less accurate initial response surface i.e. a larger difference between actual model output and model output approximated by the response surface.

However, this compromise was acceptable because the response surface method is merely used as a starting point for the HEEDS optimisation. The cost of this compromise was that the optimisation carried out in HEEDS had more to do to reach an optimal solution and this step in the process became critical. The optimisation settings were examined in an effort to improve the reliability of the optimisation.

Various optimisation parameters were tested in order to reach a suitable solution. This required varying normalisation factors and increasing the number of runs for each optimisation study. When running the 31 strand model the HEEDS optimisation was allowed to continue until 2000 design evaluations had been completed without improvement upon the best design. Following advice from the software developers it was decided to allow each optimisation study to complete the allocated number of runs. This is due to the fact that the search methods selected at various points during the study depend on the total number of runs specified at the outset. For example, global search methods will be employed earlier in the optimisation study, and local methods will become the focus during the final runs.

The next step was to determine the number of optimisation runs required to give confidence that the solution was optimal. Investigations were carried out at 50% of gait, being the point at which the fewest feasible solutions were found. Several optimisation studies were carried out with an increasing number of runs. The resolution of the muscle force values was also reduced to a maximum of 2 decimal places. This did not have a significant effect on the results obtained but greatly reduced the number of possible variations and therefore narrowed the design space. At 20000 runs and in the compression enforced case, the optimisation was found to consistently settle on an

optimal solution prior to its completion. When less constraints were applied, an optimal solution was reached faster and so 10000 runs were used in the case of unconstrained femoral loading.

The 67 strand model was also run with the alternative cost functions described in Chapter 3. These were run using the output from previous optimisations as a starting point and so were given only 5000 runs. This was deemed acceptable due to the fact that the starting point was already close to the optimum.

All the optimisation studies carried out using the 67 strand model are summarised in Table 5.1.

Table 5.1 - Optimisation studies carried out using 67 strand model

Cost function	Constraint condition	Starting values	Number of runs
Muscle stresses cubed	Unconstrained femoral loading	Response surface optimisation	10000
Muscle stresses cubed	Compression enforced	Response surface optimisation	20000
Hip and knee joint loads	Compression enforced	Muscle stresses cubed optimisation	5000
Muscle energy	Compression enforced	Muscle stresses cubed optimisation	5000

The results from the 31 strand model show very little variation in muscle loading during the swing phase of gait whether compression was enforced or not. As a result, the swing phase was excluded from the 67 strand study, and therefore all optimisations described in this chapter were carried out only for 0 to 60% of the gait cycle. Where muscle stress cubed was minimised, optimisations were completed at 5% increments to allow fair comparison with results from the 31 strand model. The other cost functions used were examined at 15% increments in order to reduce the already large number of optimisation studies required.

5.3 Results

The first set of results presented here used the muscle stresses cubed cost function and are similar in format to those shown in Chapter 4. This allows comparisons to be drawn which will demonstrate the effect of the changes made to the model and optimisation parameters. As before, additional results can be found in Appendix B.

Hip joint loads across the stance phase of gait are shown in Figure 5.2. Some differences are seen in the two constraint cases although they follow the same general trend. Values for unconstrained femoral loading are similar to what was seen in the 31 strand model but there appears to be more variation when compression is enforced. The difference between the two constraint cases shown here reaches a maximum of 1 times bodyweight at 45% of gait.

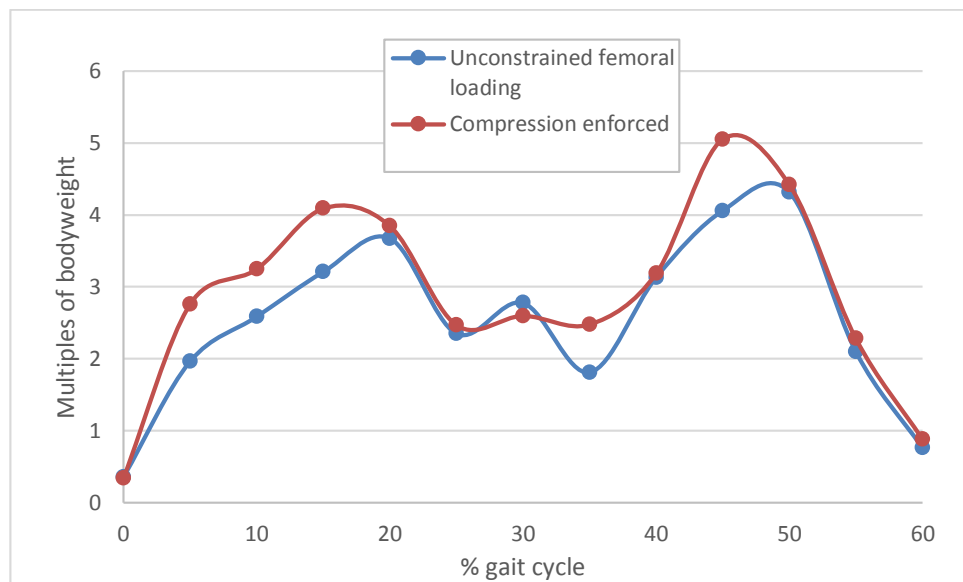


Figure 5.2 - Hip joint reaction forces across the stance phase of gait with and without enforced compression.

The calculated knee joint loads shown in Figure 5.3 display far less variation between the two constraint cases than was seen in the 31 strand model, with the exception of the large peak at 15% of gait when compression is enforced (this is discussed further in Section 5.4). The maximum load seen here at 50% of gait is just over 7 times bodyweight compared with 12 times bodyweight in the 31 strand model.

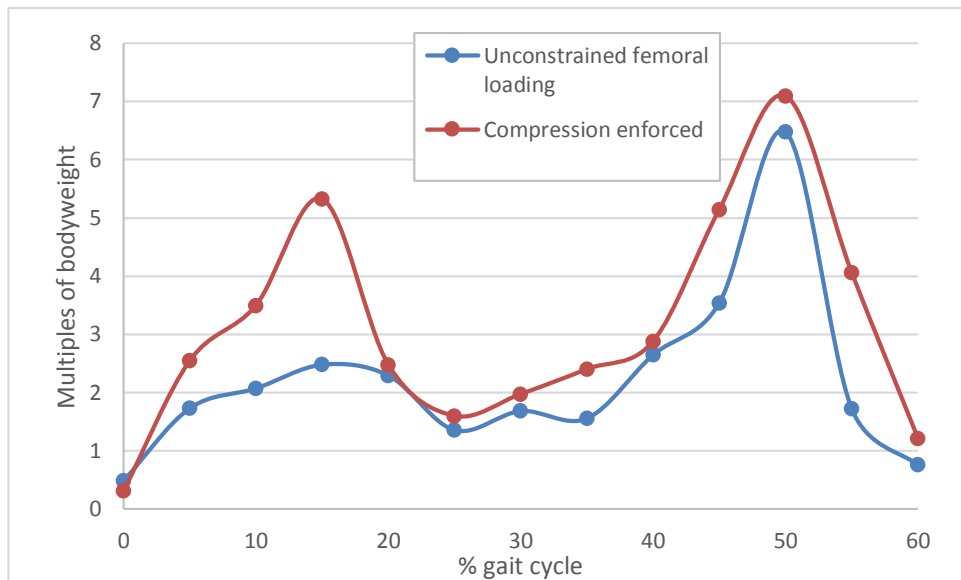


Figure 5.3 - Knee joint reaction forces across the stance phase of gait with and without enforced compression.

The activation profile of the gluteus maximus shown in Figure 5.4 is more in keeping with the recorded EMG in that muscle activity is more sustained across the stance phase of gait. The most obvious peak still occurs during the loading response phase of gait but there is also a much larger variation between the two constraint cases, with enforced compression causing an increase in muscle activation.

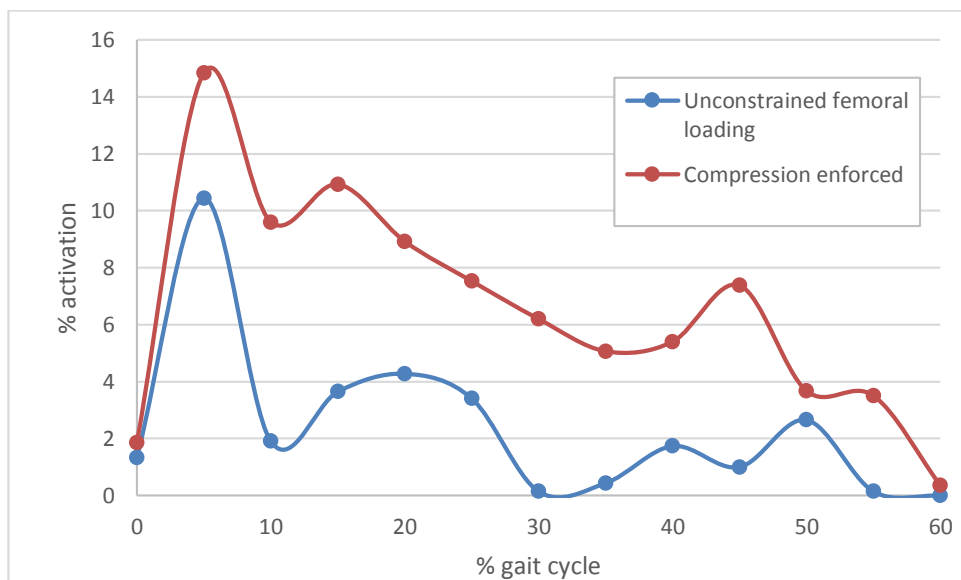


Figure 5.4 - Gluteus maximus muscle activation across the stance phase of gait with and without enforced compression.

The comparison between the 31 and 67 strand models with compression enforced is more clearly seen in Figure 5.5. The 67 strand model has an earlier peak and subsequent activity throughout the stance phase. It should also be noted that the peak activation is lower in the 67 strand model.

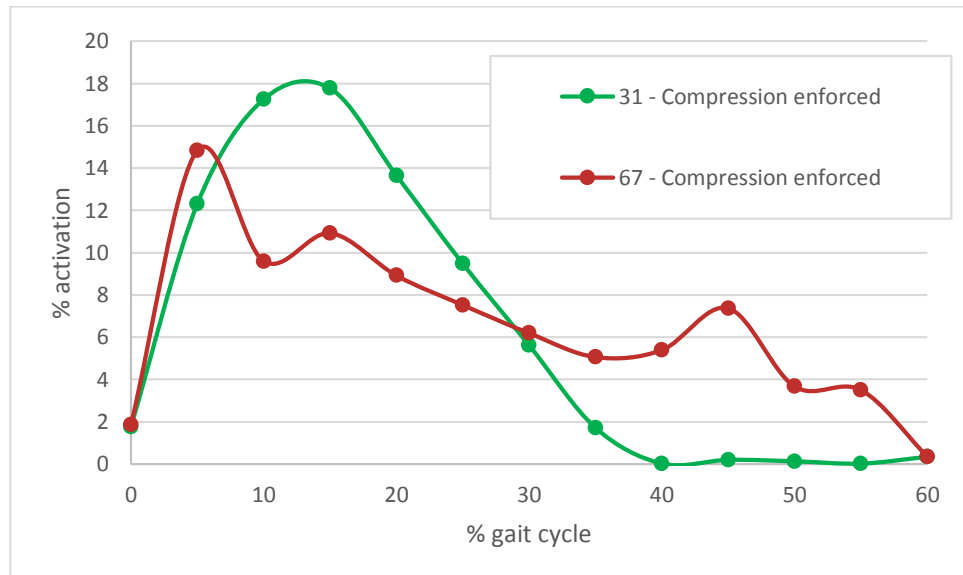


Figure 5.5 – Gluteus maximus activation with compression enforced in both the 31 and 67 strand models.

No significant difference is observed in the model-predicted muscle activation of the posterior gluteus medius whether compression is enforced or not (see Figure 5.6). A large initial peak is seen with continued activity which gradually reduces over the stance phase of gait. Model-predicted muscle activity of the anterior portion of the gluteus medius is shown in Figure 5.7. This muscle strand is active throughout the gait cycle with a peak at 45% of gait and a more pronounced difference between the two constraint sets than the posterior portion.

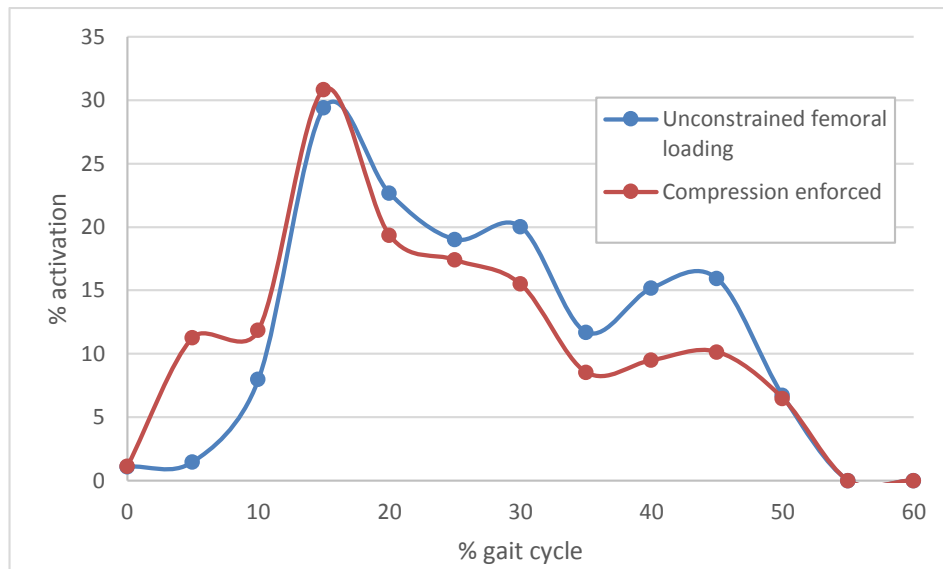


Figure 5.6 - Gluteus medius posterior muscle activation across the stance phase of gait with and without enforced compression.

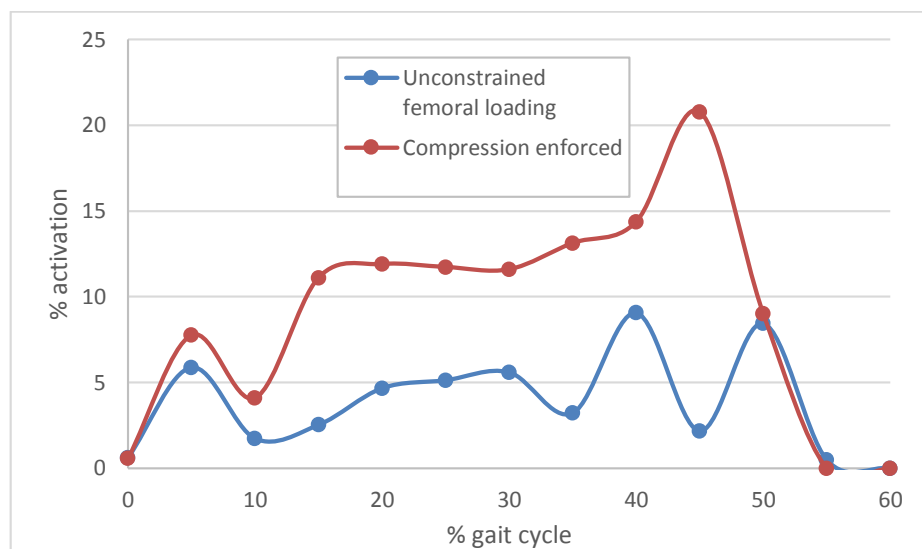


Figure 5.7 - Gluteus medius anterior muscle activation across the stance phase of gait with and without enforced compression.

Figures 5.8 and 5.9 compare muscle activation with compression enforced in the 31 and 67 strand models for the posterior and anterior portions of the gluteus medius respectively. In both cases the graphs show the same general trend although the anterior portion has a lower peak and more sustained activity in the 67 strand model.

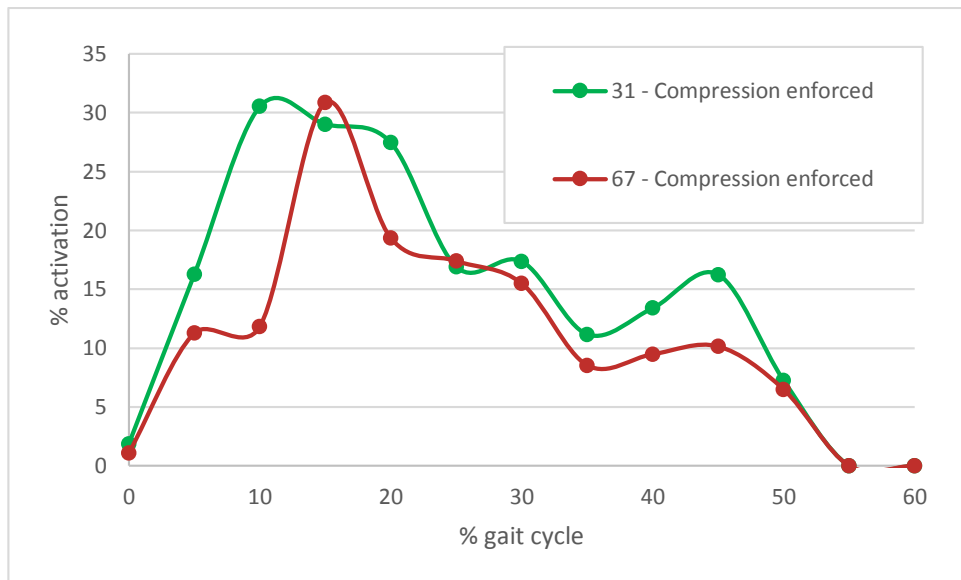


Figure 5.8 - Gluteus medius posterior activation with compression enforced in both the 31 and 67 strand models.

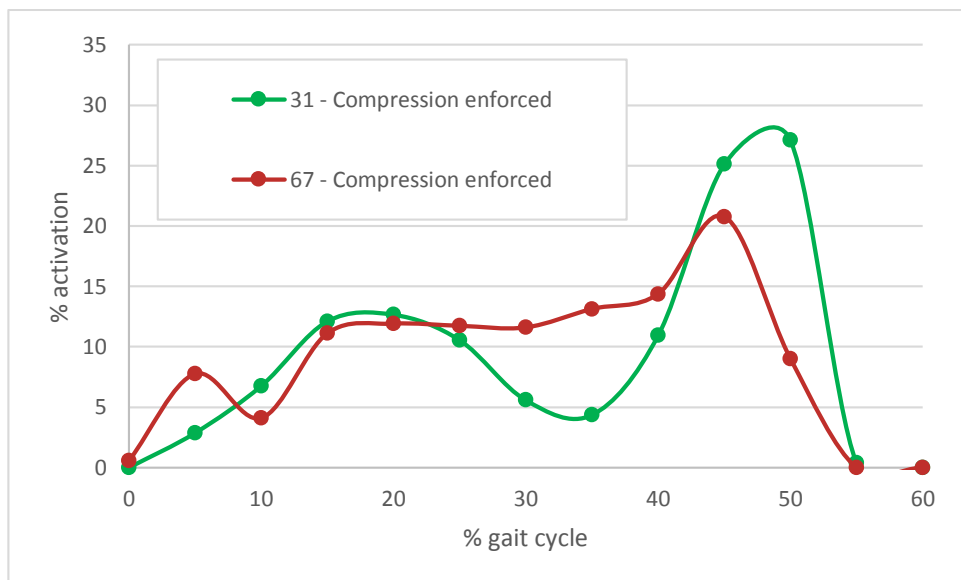


Figure 5.9 - Gluteus medius anterior activation with compression enforced in both the 31 and 67 strand models.

In the case of unconstrained femoral loading, the tensor fascia lata muscle (see Figure 5.10) shows a similar activation pattern to the 31 strand model. When compression is enforced there is a large additional peak at 10-20% of gait. Neither of the model-predicted muscle activation profiles are close to the EMG data. The limitations to the

way in which the tensor fascia lata and ilio-tibial band were modelled were discussed in the previous chapter and these limitations persist in the 67 strand model.

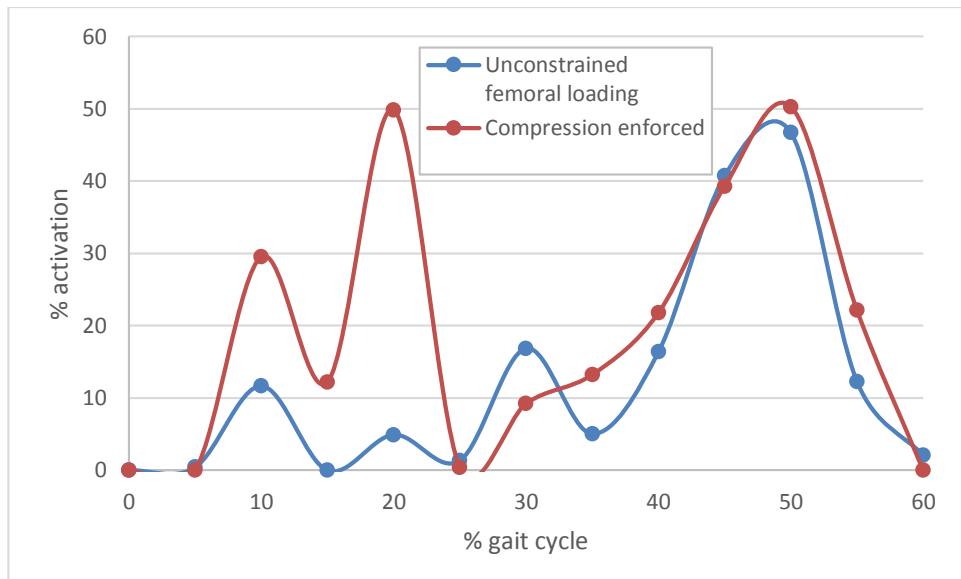


Figure 5.10 - Tensor fascia lata muscle activation across the stance phase of gait with and without enforced compression.

Rectus femoris muscle activity follows a similar pattern to that observed in the previous model with the addition of some activity between 10 and 20% of gait (see Figure 5.11). The large peak seen during the push-off phase of gait is mirrored using both sets of constraints and was discussed in detail in the previous chapter. It was noted that this differs significantly from the EMG profile which was recorded. The same is true of the entire quadriceps muscle group in both the 31 and 67 strand models.

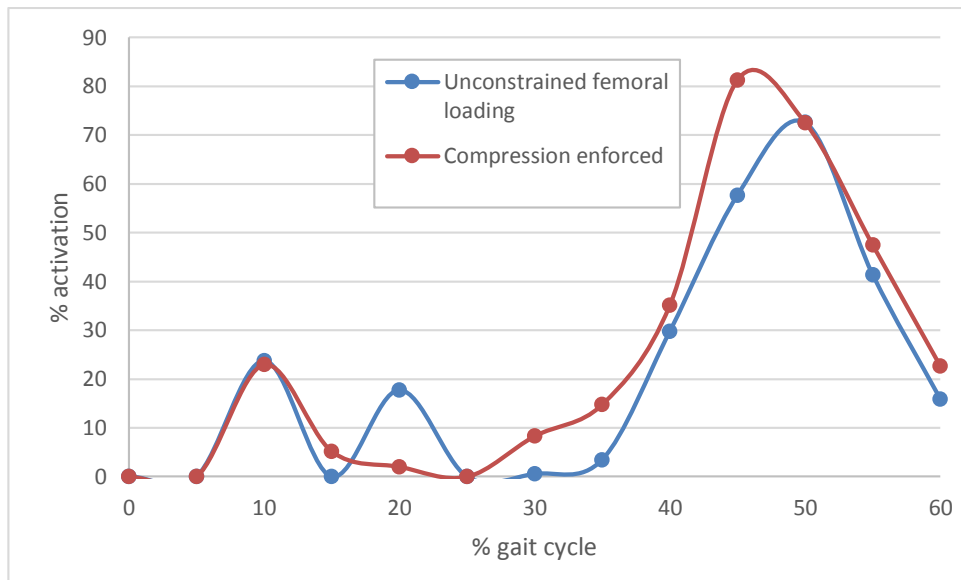


Figure 5.11 - Rectus femoris muscle activation across the stance phase of gait with and without enforced compression.

The model-predicted muscle activity of the vastus medialis and vastus lateralis muscles are shown in Figures 5.12 and 5.13 respectively. The vastus medialis appears somewhat erratic with sharp peaks and troughs spread across the stance phase of gait and little correlation between the compression enforced and unconstrained femoral loading case. It is worth noting that in the vastus medialis muscle, the magnitudes are relatively small with the highest peak being less than 10% of maximum muscle activation and so apparently large fluctuations in muscle activity are in fact somewhat minor. The vastus lateralis activation profile resembles the results from the 31 strand model, with the highest peaks occurring at 15 and 50% of gait. The results from this model differ from the previous one in that enforced compression has less of an effect on the magnitude of muscle activation.

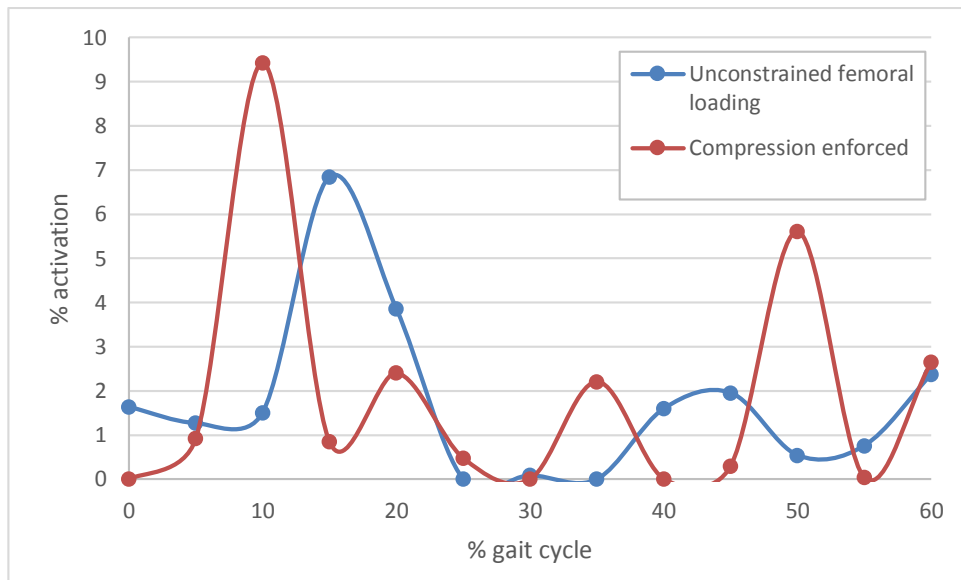


Figure 5.12 - Vastus medialis muscle activation across the stance phase of gait with and without enforced compression.

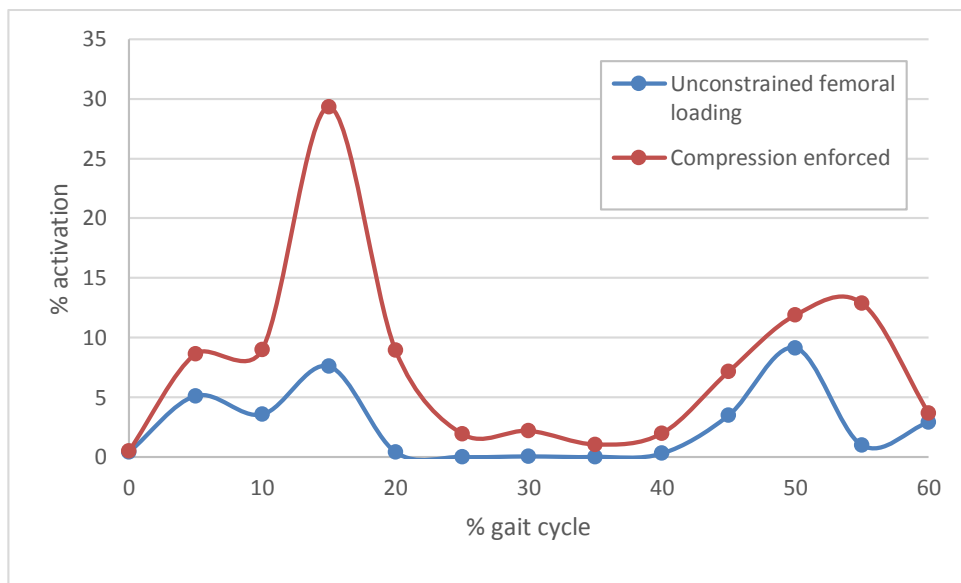


Figure 5.13 - Vastus lateralis muscle activation across the stance phase of gait with and without enforced compression.

Both the semitendinosus (see Figure 5.14) and biceps femoris (see Figure 5.15) muscles show muscle activation patterns similar to the EMG and the 31 strand model. In both cases muscle activity is evident during the first 20% of gait and reduced thereafter. In the case of unconstrained femoral loading, there is a small burst of activity in both the biceps femoris and semitendinosus at 40% of gait.

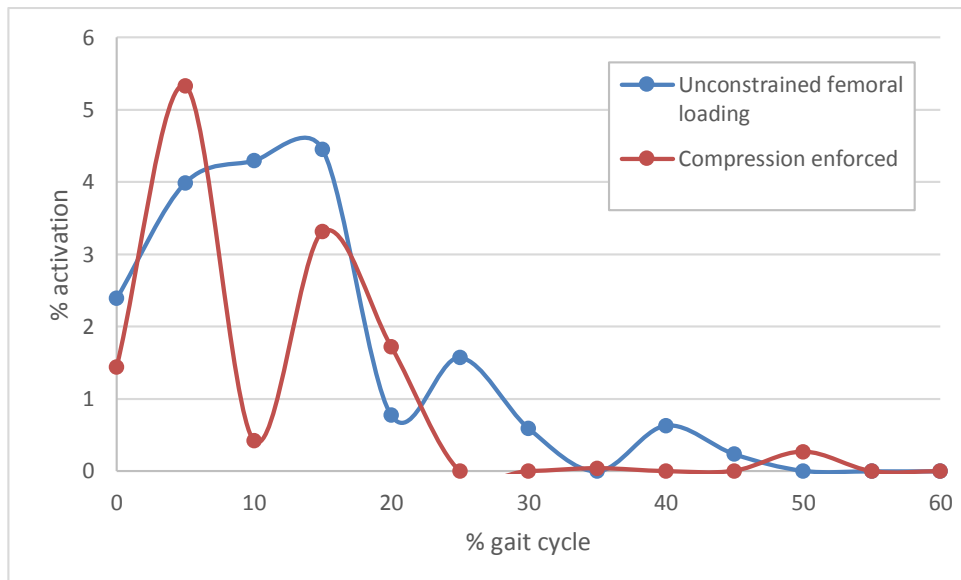


Figure 5.14 - Semitendinosus muscle activation across the stance phase of gait with and without enforced compression.

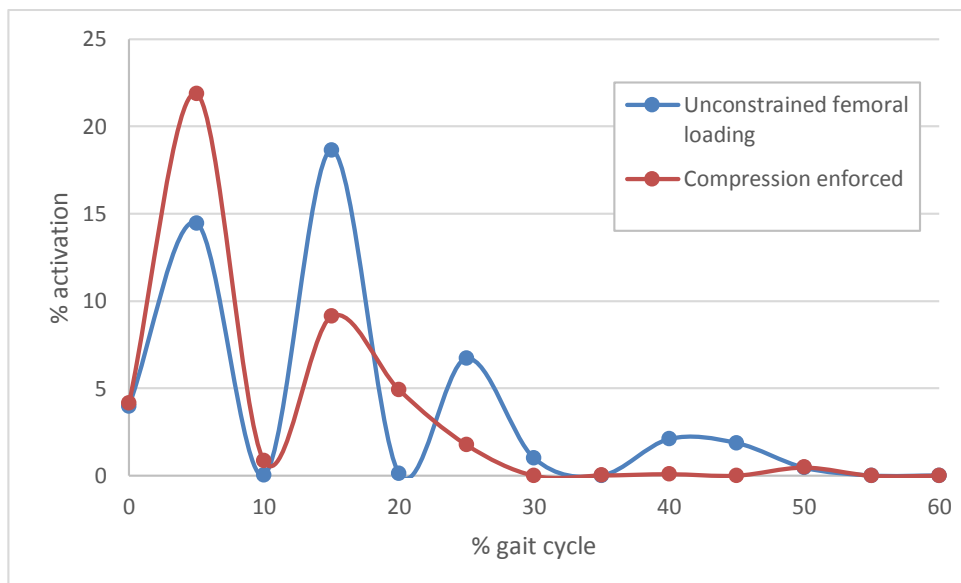


Figure 5.15 - Biceps femoris muscle activation across the stance phase of gait with and without enforced compression.

In the 31 strand model, gastrocnemius activity followed a similar pattern to the EMG. This pattern consists of gradually increasing muscle activity which reaches a peak during the push-off phase and drops off sharply thereafter. The 67 strand results follow this same pattern with the addition of unexpected peaks at 15 and 20% of gait.

Figure 5.16 shows the activity of the gastrocnemius lateralis which shows sharp peaks at 15% when compression is enforced and at 20% when femoral loading is unconstrained. Otherwise the muscle activation pattern is similar to that described above and seen in the previous model.

The gastrocnemius medialis displays increased activity from 10 to 15% of gait when compression is enforced (see Figure 5.17). There is a particularly sharp peak of activity at 50% using both sets of constraints.

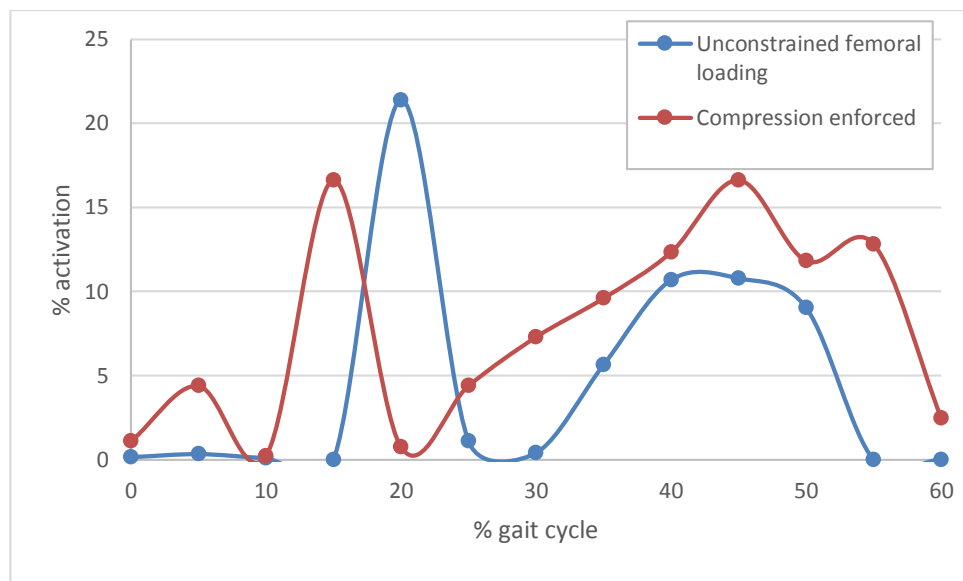


Figure 5.16 - Gastrocnemius lateralis muscle activation across the stance phase of gait with and without enforced compression.

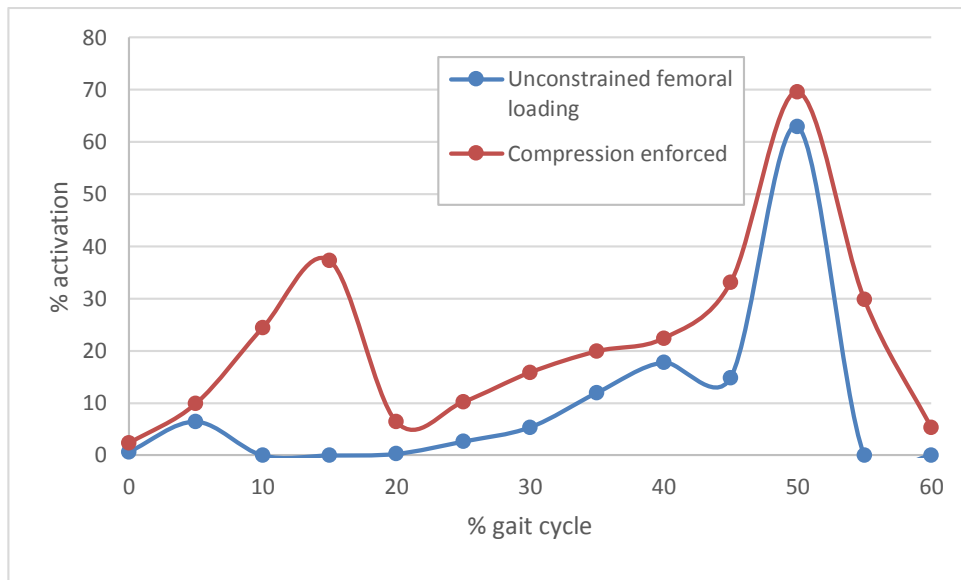


Figure 5.17 - Gastrocnemius medialis muscle activation across the stance phase of gait with and without enforced compression.

The overall sum of muscle stresses cubed across the stance phase of gait is shown in Figure 5.18. The first peak occurs at 15-20% of gait. At this point, enforcing compression causes a large increase in muscle stress. The largest difference between the two constraint cases occurs at 15% of gait where the sum of muscle stresses cubed is almost eight times higher than in the case of unconstrained femoral loading. The second peak occurs at 45-50% of gait, and although it is higher under enforced compression, the difference is less pronounced than the first peak.

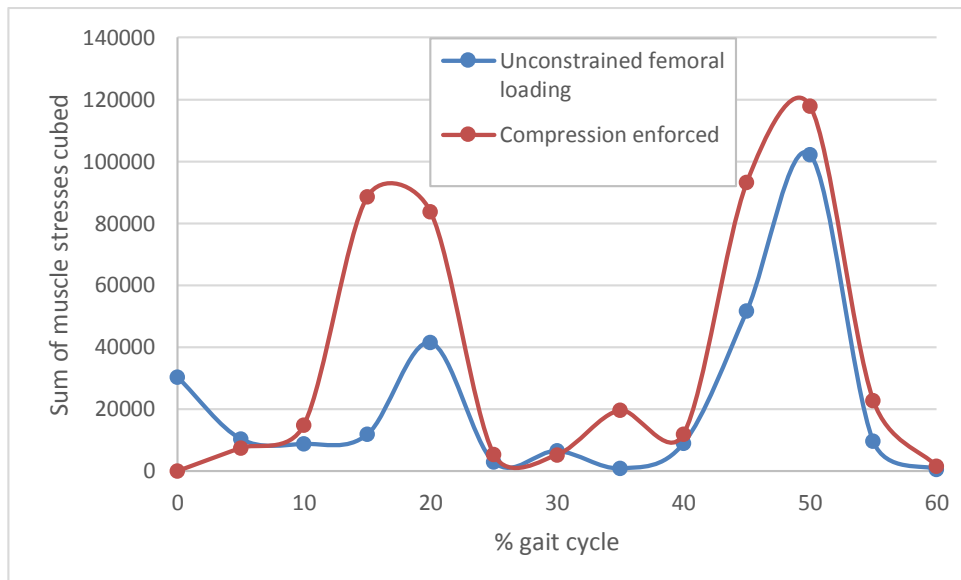


Figure 5.18 - The sum of muscle stresses cubed across the stance phase of gait with and without enforced compression.

Figure 5.19 shows what this increase in muscle activation does to the maximum principal stress at the cut in the femur. This is calculated based on an idealised cylinder geometry as described in Chapter 3. We can see that throughout the stance phase of gait, enforcing compression reduces the maximum stress in the bone at the point observed. At 30 and 40% of gait we see a significant reduction in bone stress where only a small difference in muscle stress was observed.

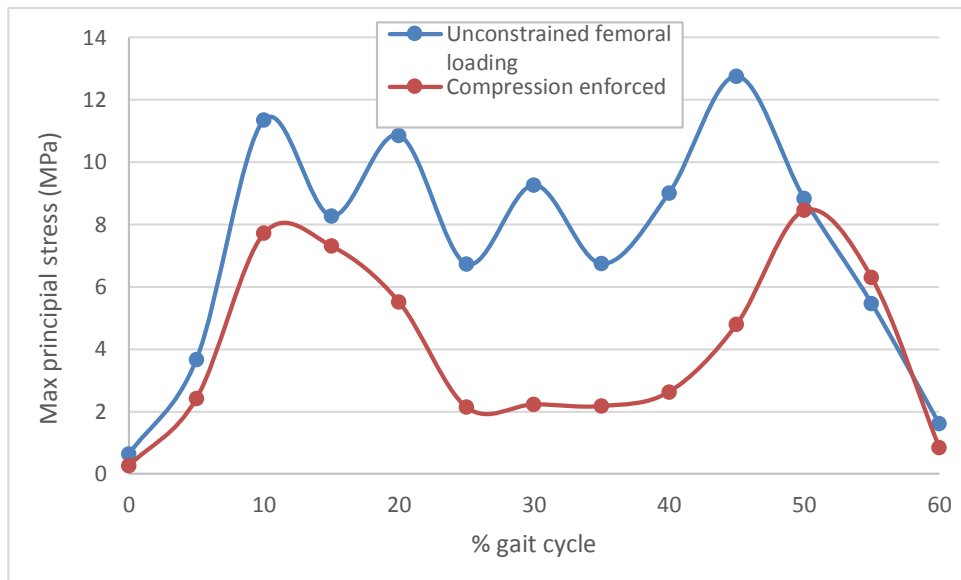


Figure 5.19 - Maximum principal stress at the cut in the femur with and without compression enforced. These values were calculated based on idealised geometry as described in Chapter 3 using torque measurements at the joint in the femur.

The remainder of the results to be presented here show a comparison between the three cost functions which were described in Chapter 3. These are the sum of muscle stresses cubed, the sum of muscle energy and joint loads. When presented in the graphs below these are abbreviated to “Stress”, “Energy”, and “Joints” for convenience. All comparisons are made in the case of enforced compression.

Figure 5.20 shows hip joint loads compared at 5 points spanning the stance phase of gait. Results are presented as columns due to the low number of points examined. In general there is very little difference between joint loads calculated using the different cost functions, although we do a slight increase in hip load when muscle stresses cubed are minimised compared to the other cost functions at 15 and 45% of gait.

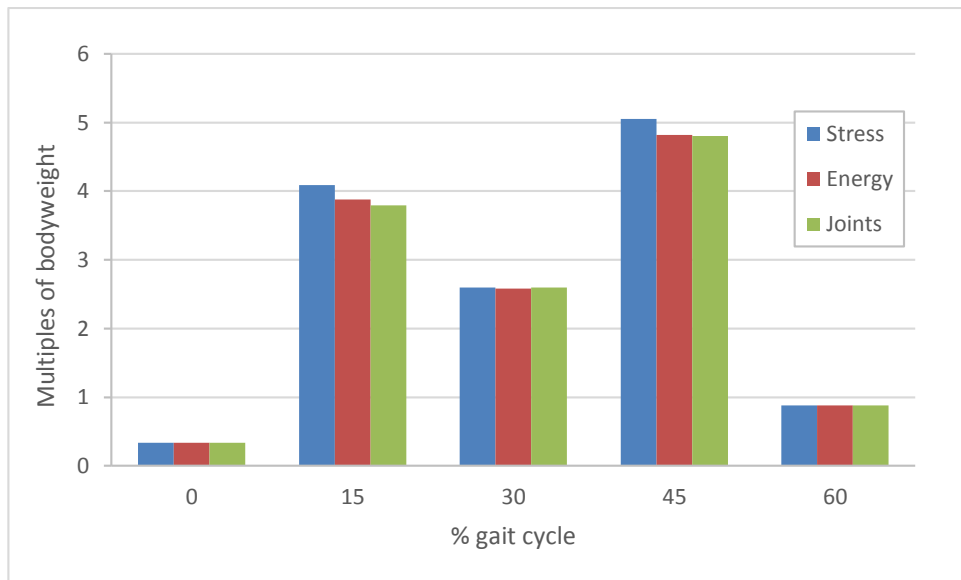


Figure 5.20 - Hip joint reaction forces across the stance phase of gait compared using three different cost functions.

A comparison of the knee joint loads is shown in Figure 5.21. The results are again very similar regardless of the cost function used. The exception is as 45% of gait where the knee force resulting from minimising muscle stresses cubed is larger than the values calculated using the other two cost functions. The difference between the “Stress” and “Energy” values at 45% of gait is 0.43 times bodyweight.

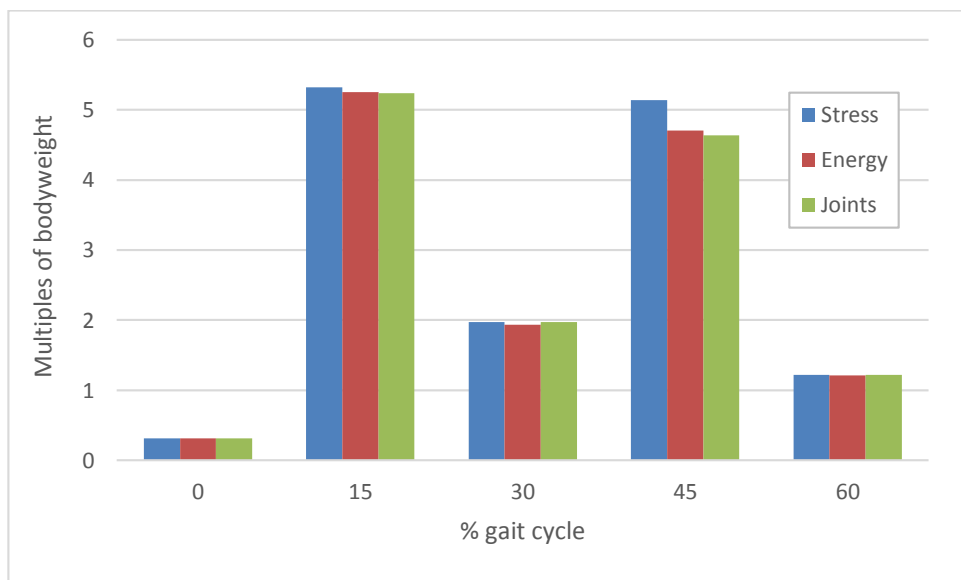


Figure 5.21 - Knee joint reaction forces across the stance phase of gait compared using three different cost functions.

The following series of graphs (Figures 5.22, 5.23, 5.24, and 5.25) show examples of muscle forces calculated using each of the three cost functions. The values are presented as a percentage of maximum muscle activation. For each of the muscles shown there is very little difference between the three cost functions across the points examined.

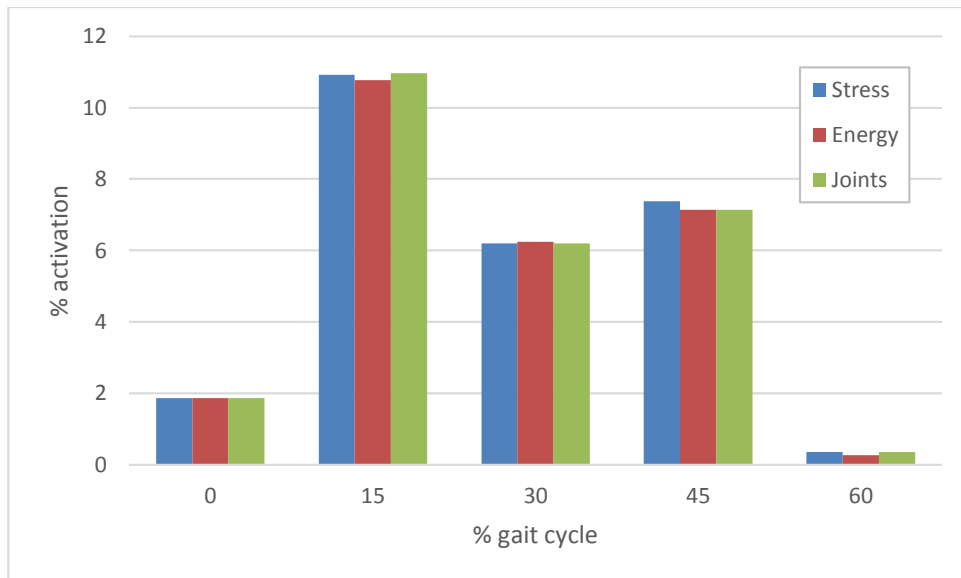


Figure 5.22 - Gluteus maximus muscle activation across the stance phase of gait compared using three cost functions.

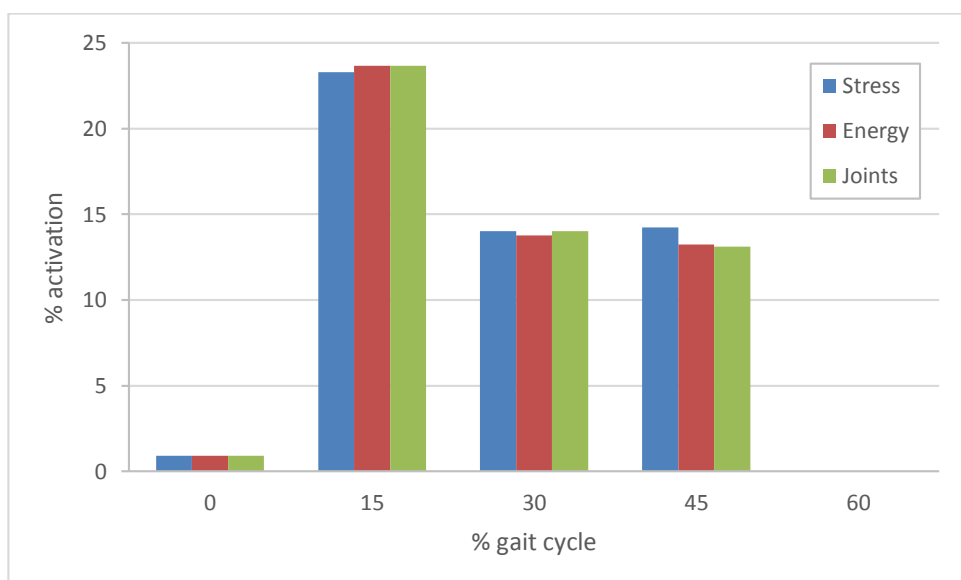


Figure 5.23 - Gluteus medius muscle activation across the stance phase of gait compared using three cost functions.

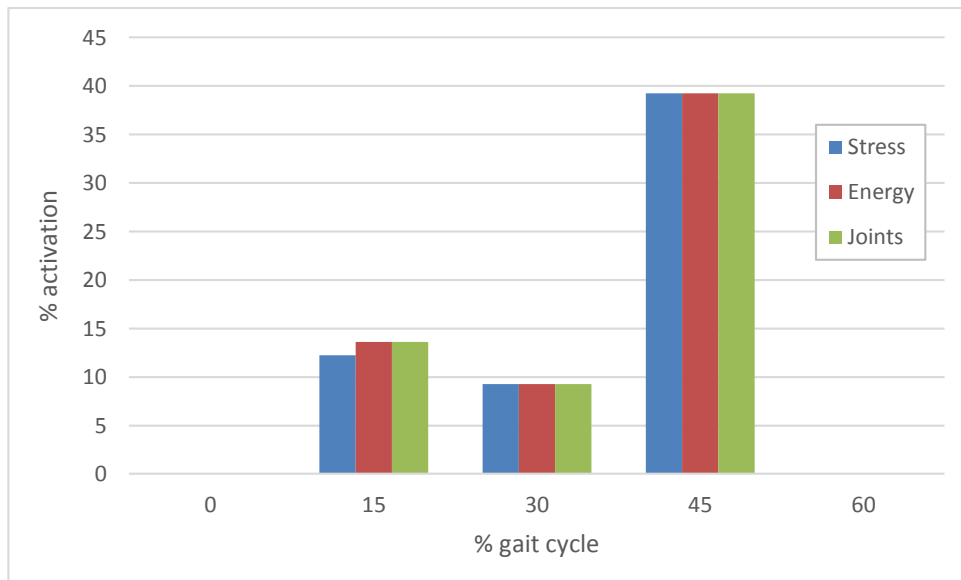


Figure 5.24 - Tensor fascia lata muscle activation across the stance phase of gait compared using three cost functions.

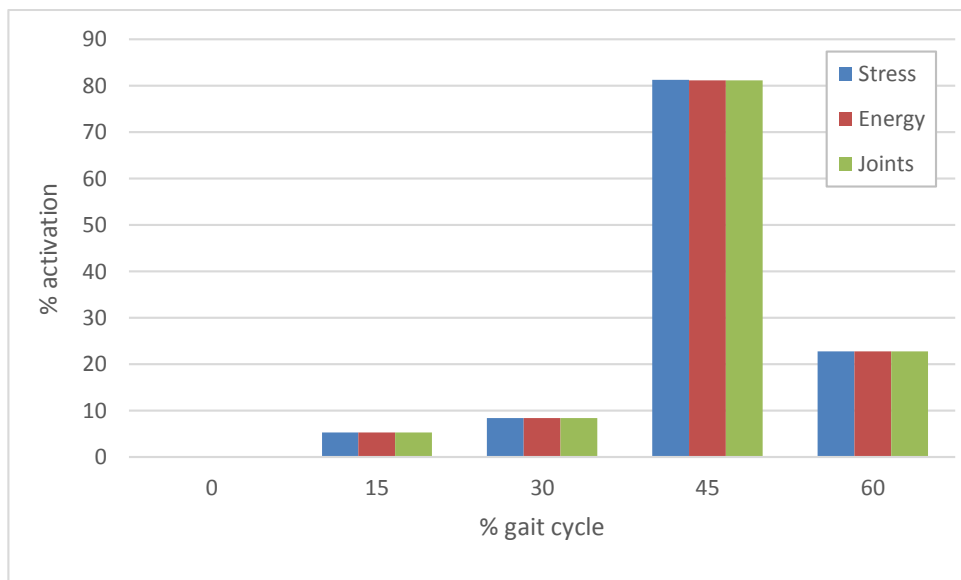


Figure 5.25 - Rectus femoris muscle activation across the stance phase of gait compared using three cost functions.

Figures 5.26 and 5.27 show muscle activation values for the semitendinosus and semimembranosus muscles respectively. These muscles follow a very similar line of action to one another. We can see in Figure 5.26 an increased level of activation in the semitendinosus at 15% of gait when minimising muscle stresses cubed. The semimembranosus (see Figure 5.27) shows a reduced level of activation in the same

circumstances. It should be noted that the maximum activations shown in these graphs are however only 3-4%, and so the variations between the cost functions are actually very small.

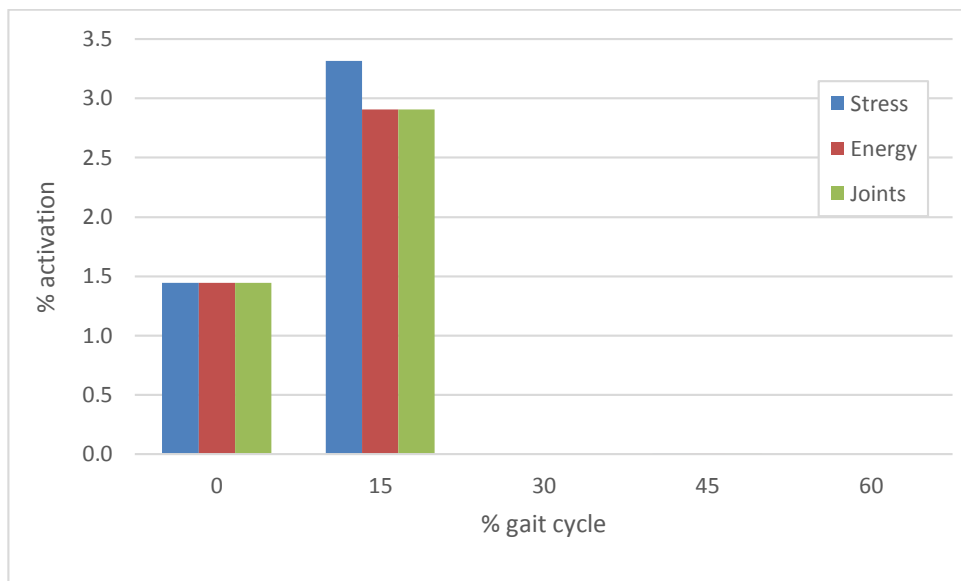


Figure 5.26 - Semitendinosus muscle activation across the stance phase of gait compared using three cost functions.

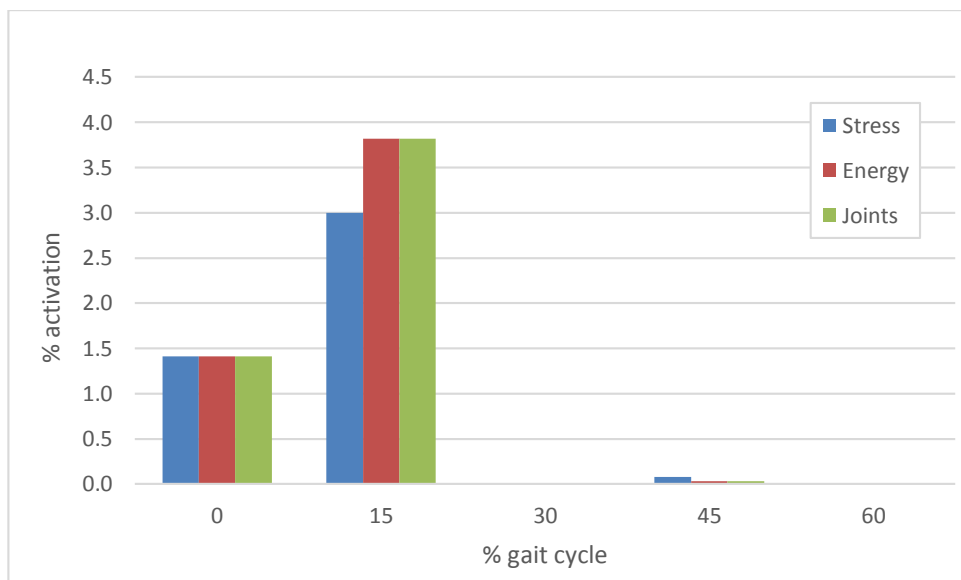


Figure 5.27 - Semimembranosus muscle activation across the stance phase of gait compared using three cost functions.

As with the previous chapter, the results which have been selected for presentation are those deemed to be most relevant. A more detailed discussion of the results presented here will be given in the following section.

5.4 Discussion

With the exception of the number of muscle strands used, and the optimisation method, the 67 and 31 strand models are identical. Simplifications made to the model and their potential impact on the results have been discussed in the previous two chapters, so they will not be discussed here. Instead, the impact of changes made to the model will be analysed.

In considering the results obtained by minimising muscle stresses cubed, there remains some doubt as to whether the optimisation method is capable of finding a single optimal solution. This is highlighted in the results at 15% of gait when compression was enforced (see Figure 5.3). The knee force given here is 5.32 times bodyweight. The equivalent knee force calculated by the 31 strand model (see Figure 4.8) was 4.20 times bodyweight. The 67 strand model includes all of the same strands as the 31 strand model, with an additional 36 strands. It would be expected that the increased options for direction of forces crossing the knee would result in lower magnitudes i.e. reduced overall muscle activation and consequently a lower knee force. At the very least we would expect an equivalent solution to be reached.

An important point to bear in mind is that the maximum activation for each muscle strand was different in the 67 strand model compared to the 31 strand model. This was due to the maximum allowable force in each muscle being divided by the number of strands representing that muscle. For example, if a single muscle strand in the 31 strand model had a maximum activation of 900N, and was represented by three strands in the 67 strand model, each of those strands would have a maximum force of 300N. The values for muscle PCSA were also divided in a similar manner. This would be expected to affect the behaviour of the minimised muscle stress cost function and may explain the differences observed between the 31 and 67 strand models.

In the 31 strand model, the output from ADAMS Insight was far closer to the optimal solution than in the 67 strand model owing to the fact that the response surfaces built

using cubic rather than quadratic polynomials were far more accurate. This meant that the HEEDS optimisation had more work to do to reach an optimal solution. The inclusion of more muscle strands added to this problem; although it increased the possible number of feasible solutions (muscle loading patterns which satisfied all constraints), it also added a significant number of infeasible solutions, resulting in a much larger design space to be searched by the optimisation algorithm. The combination of these two factors required a large increase in the number of runs to be completed for each optimisation study. The number of runs was determined using the method outlined in Section 5.2.

The compression enforced optimisation at 15% of gait was the only position which did not appear to settle on an optimal solution during the given number of runs. It is possible that increasing the number of runs may have improved the solution but due to long simulation times, it was not practical to do so indefinitely. Some additional optimisation runs were carried out, but the incremental improvements to the solution were sufficiently small that the result obtained was deemed to be acceptably close to the optimal solution.

With the exception of the point at 15% of gait, the knee joint load when compression is enforced (see Figure 5.3) matches the unconstrained loading case much more closely than in the 31 strand model (see Figure 4.8). In the 31 strand model, the knee joint load with compression enforced was on average 2.06 times bodyweight higher than with unconstrained femoral loading. This difference was reduced to 0.90 times bodyweight in the 67 strand model. The same values for the hip were 0.07 times bodyweight for the 31 strand model and 0.35 times bodyweight for the 67 strand model. Although, the difference in hip joint loads is slightly more pronounced in the 67 strand model, the difference in knee joint loads between the two models is significantly smaller in the 67 strand model. This shows that in general terms, the availability of more muscle strands allows compression to be maintained in the femur without large increases in joint loads.

Maintaining compression does result in increased overall muscle loading. Figure 5.18 shows increases in the sum of muscle stresses cubed. On average, this value increases by a factor of 3.32 when compression is enforced. This increase in muscle loading corresponds with a reduction in the maximum principal stress acting on the femur at the

point of interest (the cut in the femur as described in Chapter 3). This is shown in Figure 5.19. The stress on the femur at the point measured is reduced on average by a factor of 1.78. This supports the view that coordinated muscle activity may protect bone from high peak stresses due to bending.

The comparison of three different cost functions shows that when compression is enforced the different cost functions perform similarly. It may be that the added constraint of maintaining compression narrows the range of feasible solutions to a point where the cost function is of less importance. If the aim of the optimisation was to predict muscle forces accurately *in vivo*, the cost function used would be pivotal as this ultimately determines which muscle should be selected over another where both are capable of providing the required loading. This study aims to investigate the feasibility of maintaining compression in the femur by coordinated muscle activity. This is achieved by comparative analysis of results obtained by applying different constraints to the model. It is not within the scope of this study to provide accurate predictions of muscle loading patterns *in vivo*. With this in mind, it can be concluded that the minimised muscle stress function used in the majority of simulations is fit for purpose in the context of this study.

In summary, the results presented in this chapter show that compression can be maintained in the femur throughout the gait cycle. This loading regimen causes a reduction in peak stresses in the shaft of the femur, and where more muscle loading options are available, this can be achieved without any detrimental effect on joint reaction forces. The next step in this investigation is to assess the effect of limitations in muscle activity, for example as a result of ageing, on the ability to maintain compressive loading.

Chapter 6

Effect of Limited Muscle Activity on State of Loading in the Femur

6.1 Introduction

There are a variety of changes to the musculoskeletal system which may impact muscle function and bone loading. Surgical interventions caused by disease or in response to trauma may require removal of muscle, ligamentous tissue, or even bone. In addition to wide ranging musculoskeletal pathologies, changes to the musculoskeletal system also occur under physiological conditions as a natural consequence of ageing. One study reported a 20-30% loss of muscle strength over a 12 year period in men who were aged 65.4 ± 4.2 years at the start of the study (Frontera et al. 2000). A reduction of muscle size of up to 30% has also been observed in men between the ages of 50 and 80 years (Lexell et al. 1988). These studies examined changes occurring in the course of normal ageing. It is likely that this loss of muscle could be more severe under pathological conditions.

Loss of muscle function is associated with an increased risk of fragility fractures and it has been suggested that age related loss of muscle forms a vicious cycle with worsening osteoporosis (Perrini et al. 2010). This chapter aims to investigate the impact of reduced muscle activity on the ability to maintain compression in the femur.

6.2 Method

A set of optimisations was carried out to simulate age-related limitations to muscle activity. Maximum muscle forces were reduced by 50% to represent a worst case scenario. The muscle stresses cubed cost function was used and PCSA values were also

reduced by 50%. In reality, the loss of muscle strength is often more pronounced than the loss of muscle mass due to a reduced percentage of contractile tissue (Kent-Braun et al. 2000). However, precise data for the difference between the percentage losses of strength and mass was not available and so a uniform 50% reduction was applied to all muscles.

The GRF remained as recorded for our subject. People tend to gain weight with age and so we may expect GRF values to increase, although it has also been observed that there is an age-related redistribution of torques during gait (DeVita & Hortobagyi 2000).

Simulations were carried out from 0 to 60% of gait at 15% increments. The starting values used were taken from the previous 67 strand model results for minimised muscle stresses cubed. The purpose of these simulations was to determine whether or not compression can be maintained with reduced muscle forces and so all optimisation studies carried out were with compression enforced. Each optimisation was given 5000 runs.

6.3 Results

The results presented show a comparison between optimisation results carried out as described in Chapter 5 using the minimum muscle stresses cubed cost function, and otherwise identical optimisation results with maximum muscle forces and PCSA values reduced by 50%. These are designated on the graphs below as “100%” and “50%” respectively.

Figure 6.1 displays hip joint forces at the points studied with both sets of muscle force limits. There is very little difference in the hip joint loads at 0, 15, 30, and 60% of gait when muscle forces are limited. Where the joint load is highest at 45% of gait, we see an increased hip joint load as a result of limitations to muscle activity. At 45% the hip load increases by 0.82 times bodyweight.

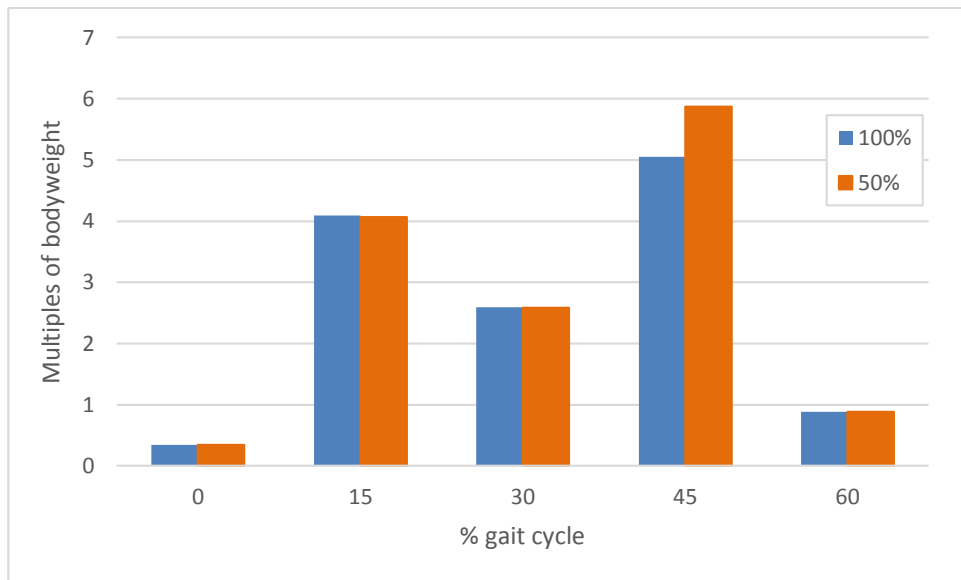


Figure 6.1 - Hip joint loads across the stance phase of gait with and without limitations to maximum muscle forces.

The knee joint loads for each set of muscle force limits are shown in Figure 6.2. Again, there is very little difference at 0, 30, and 60% of gait. Additionally, the difference at 45% of gait is small, with the limited muscle force case showing a knee joint load of 0.03 times bodyweight less than when muscle force values were allowed to vary up to their 100% max. The only notable difference is at 15% of gait where the knee joint load is 0.25 times bodyweight higher when muscle forces are limited.

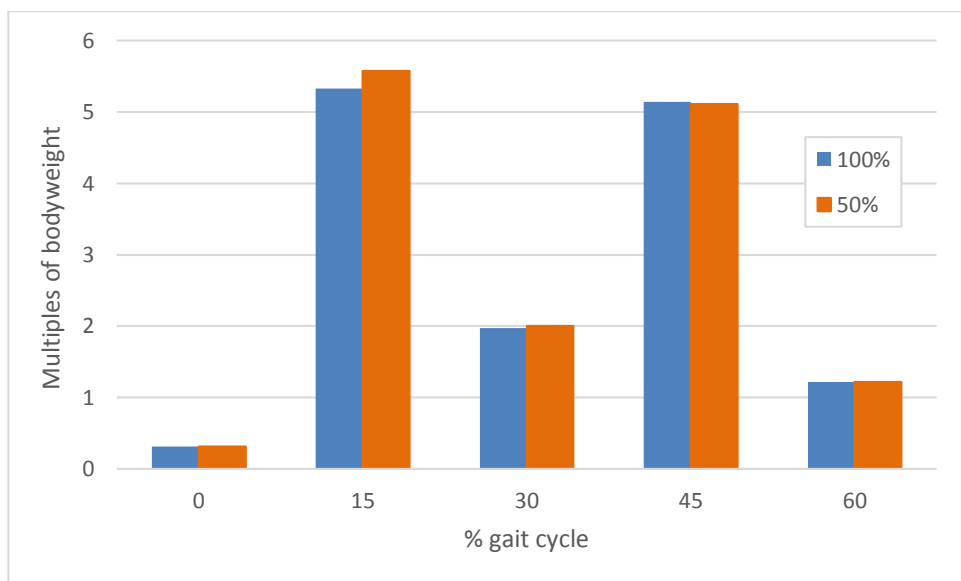


Figure 6.2 - Knee joint loads across the stance phase of gait with and without limitations to maximum muscle forces.

The starting values used when optimising with limited muscle forces were taken from previous optimisations carried out using full muscle force maximum values. This meant that some of the starting values were out of range when muscle forces were limited, i.e. values output from the previous optimisation were greater than 50% of muscle activation. The values which were out of range at 15% of gait were gluteus medius posterior, and vastus lateralis superior. At 45% of gait, the rectus femoris was the only muscle force value out of range.

These muscle force values were changed manually to fit within the limited range and other muscle strands had to compensate. The differences in muscle activation were more pronounced at 45% of gait. Some of the differences in muscle activation at 45% of gait are presented in Figures 6.3 and 6.4.

The labels for each muscle strand represented are as per Table 3.1. The suffixes added to some muscle designations are to differentiate between different portions of a muscle. These portions are proximal (Prox), distal (Dist), posterior (Post), anterior (Ant), superior (Sup), middle (Mid), and inferior (Inf). Where multiple muscle strands for one muscle portion are displayed separately, each strand is designated by a number. Although different values were used for the maximum force in each muscle, all forces were normalised as a percentage of the 100% maximum to allow comparison between the muscle forces in each case.

The reduction of the rectus femoris muscle was compensated for at the knee joint by activation of other muscle strands. The proximal sartorius and vastus lateralis inferior show large increases in their percentage activation. More modest increases are seen in the tensor fascia lata, vastus intermedius, vastus lateralis superior, and vastus medialis superior.

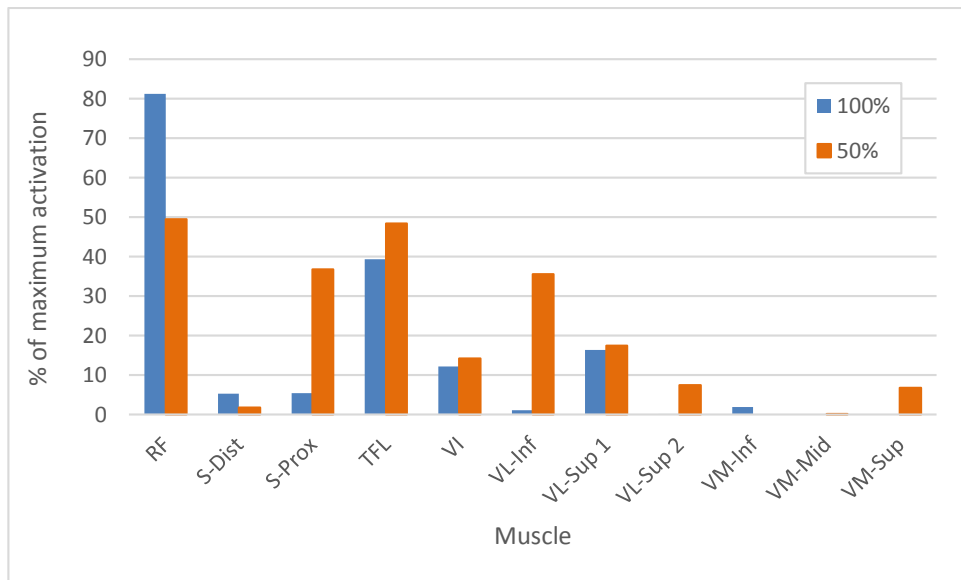


Figure 6.3 - Activation of the anterior muscles of the thigh at 45% of gait with and without limitations to maximum muscle forces.

The changes to activation of the muscles crossing the knee have a knock-on effect for muscles crossing the hip. In Figure 6.4 we see a slight increase of the gluteus maximus superior but little change in the gluteus medius posterior. The remaining 7 muscles shown here exhibit increased activation to compensate for changes in muscle force limits.

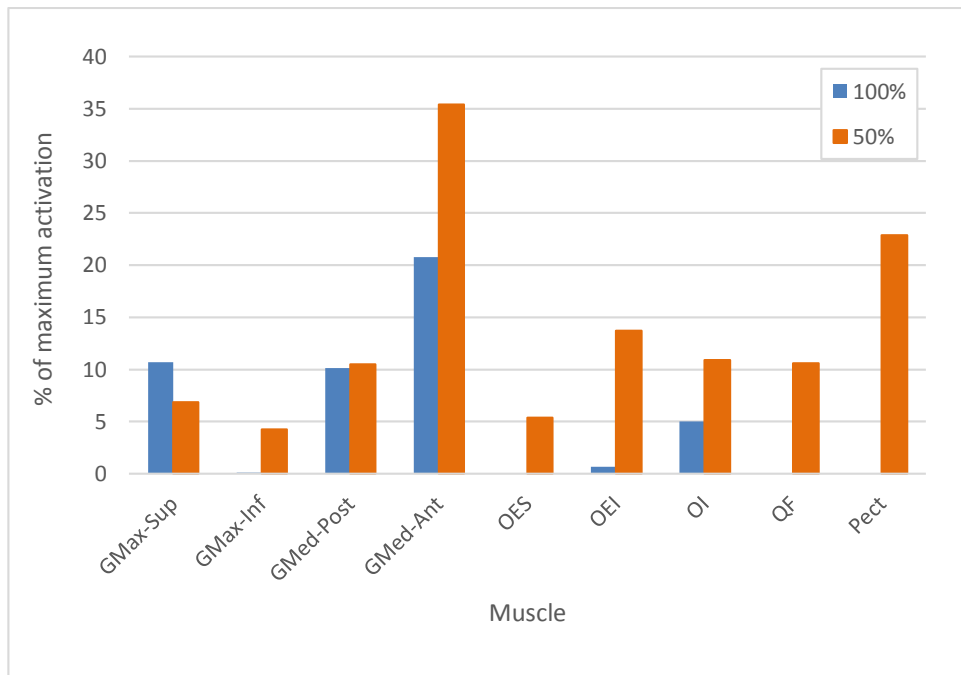


Figure 6.4 - Activation of the muscles surrounding the hip at 45% of gait with and without limitations to maximum muscle forces.

A point of interest in this study is the effect of these changes to muscular loading on stresses placed on bone. Figure 6.5 displays the maximum principal stress for each set of muscle force limits at each stage of gait studied. Negligible difference is observed at 0 and 60% of gait when overall loading is low. For all other points studied we see that limiting muscle activity results in increased stress on the bone at the point of measurement.

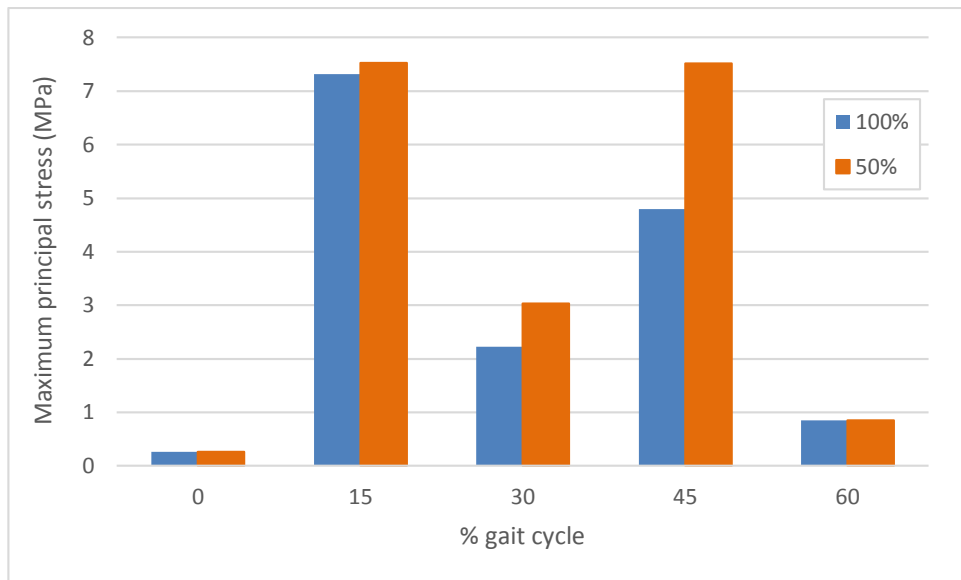


Figure 6.5 - Maximum principal stress in the femur with and without limitations to maximum muscle forces. These values were calculated at the cut in the femur and based in idealised cylindrical geometry.

6.4 Discussion

As with previous chapters, the results presented here should be evaluated comparatively. By comparing the results with and without limitations to maximum muscle forces, we can elicit several points for discussion.

Figures 6.1 and 6.2 show that reducing the maximum muscle forces results in relatively small changes in joint reaction forces. This is most likely due to the number of muscle loading patterns capable of producing the required net joint moments and in this case femoral state of loading. There is however an overall increase in joint loads at 15 and 45% of gait where the peak loads occur. This suggests that although muscle forces can activate differently to compensate for limitations, the efficiency with which they provide the required joint moments may be reduced. It is unclear whether or not this reduced efficiency is mirrored *in vivo*.

In Figures 6.3 and 6.4, we can see that more muscles are recruited to deal with limitations to muscle forces. Many of those muscles are activated at levels approaching their reduced maximum limit. This scenario if repeated *in vivo* would likely result in an increased metabolic cost of walking and cause muscle fatigue. Muscle fatigue may increase the risk of falls and therefore fractures.

The main point of concern in this investigation of limiting muscle forces is what this limitation means for the stresses placed on the femur. We can see in Figure 6.5 that the redistribution of muscle activation caused by limiting maximum muscle forces translates into higher levels of stress in the femoral shaft. It should be noted again that these results were produced with compression enforced and so we may expect maximum principal stress in the femur to be higher still in the case of unconstrained femoral loading. Additionally, the calculation of maximum principal stress was based on a cylinder of cortical bone with 20mm outer diameter and 10mm inner diameter. The values shown here remain far below the minimum effective strain described by Frost (Frost 1988) but it should be remembered that the shaft of the femur is not cylindrical and may be of varying wall thickness. Maximum principal stresses in the shaft of the femur *in vivo* will be different to what has been calculated here and may be much higher. This is particularly true in the case of advanced ageing where bone size and strength are reduced.

Even with a 50% reduction in the maximum allowable force in each muscle, compression of the femoral shaft was maintained in each of the five optimisation studies completed. In the case of limited muscle forces and where external loads were higher at 15-45% of gait, there was a cost associated with maintaining this state of loading. That cost was in terms of increased joint loads and femoral stress.

Chapter 7

Discussion

7.1 Background and Scope of This Study

The aims of this study as stated in Chapter 1 are to investigate the feasibility of maintaining compression in the femur as the dominant state of loading. The study also set out to explore the impact of changes to the musculoskeletal system on this loading regime. The method of investigation was by means of a multibody dynamics musculoskeletal model of the lower limb that was informed by a review of the relevant literature.

The literature presented in Chapter 2 provides a wealth of evidence for the adaptation of bone to its mechanical environment. Magnitude, frequency, and direction of loading are key components influencing the way in which bones adapt (Frost 1988, Robling et al. 2006, Lam et al. 2011, Saporin et al. 2011). The loads that a bone experiences *in vivo* result from a combination of joint reaction forces, ground reaction forces and muscle activation (Judex & Carlson 2009, Robling 2009). The latter of which produces the largest loads to which bones must adapt. As a consequence, the complex patterns of muscular loading are a key consideration in any study in the adaptation of bone.

There is a long standing theory that bone is loaded primarily in compression and that this is achieved by coordinated muscle activity (Pauwels 1980, Sverdlova & Witzel 2010). This study employed a model that compared optimisations of muscle loading with, and without, enforced compression in the shaft of the femur. The purpose of these optimisation studies was not to accurately predict patterns of muscle activation *in vivo*, but to comparatively assess the feasibility and cost of maintaining compression in the femur.

The remainder of this chapter provides a critical evaluation of the model and a detailed discussion of results obtained. The results are placed in context of the relevant literature relating to the compression theory of bone and neural feedback of bone loading. Finally, it discusses implications for healthy loading in the femur and disease conditions such as osteoporosis.

7.2 Limitations of the Study

Several limitations of this study have been discussed in previous chapters. These relate to gaps in the data available, practicalities of computer simulation, and boundaries guided by the scope of this research. Each of these will be briefly reviewed below before comment is made on the overall suitability of the model and implications for the interpretation of results.

The joints in the model, whether revolute or spherical, turn on a single infinitesimal point. This makes the model extremely sensitive to some variations in muscle forces. This sensitivity requires precise balance of muscle forces acting about the joints in question. The need for such precision resulted in increased joint reaction forces and increased the difficulty of finding feasible solutions to the optimisation problem. This was to some extent mitigated in the hip and knee joints by allowing a tolerance in the target value for joint torques. This tolerance was calculated to replicate the small amount of friction present in the joints *in vivo*.

No tolerance was set on the torque about the joint between the two parts of the femur. This was unnecessary due to the fact that when compression was enforced the target of the torque about this joint was not a set value, but was designed to exceed a threshold value dependent upon the axial loading of the joint. Nevertheless, the joint in the femur was sensitive to small perturbations in muscle forces as with the hip and knee, further increasing the difficulty of finding feasible optimisation solutions. When femoral loading was unconstrained torque about the joint in the femur was ignored.

The model only examined the state of loading at one precise point in the bone. Therefore, the results do not allow conclusions to be drawn on the feasibility of maintaining compression throughout the entire femur. The primary mechanism for maintaining compression is reduced bending. Even when measuring at a single point,

bending stress in adjoining areas of the same structure will naturally be reduced. We can therefore assume that some extrapolation of these results is appropriate at least insofar as the mid-section of the shaft of the femur is concerned.

Another point of discussion concerning the joint in the femur, is the position of the joint as it relates to the cross section of the femur in the transverse plane. This was the topic of Study 4 in Chapter 3. It was shown that a 2mm transverse shift of the position of the joint can result in a change to knee joint reaction force of 0.44 times bodyweight. This is of interest because if compression is to be maintained by reduced bending, the pivot point for this reduction should be the neutral axis of bending which corresponds with the centre of area of the cross-section. Whether or not the location of the joint in the femur corresponded with the neutral axis of bending could not be verified. This was due to several factors. Firstly, the centre of mass was calculated based on the solid shape bounded by the outer geometry of the femur. In reality, the shaft of the femur houses the medullary cavity and the wall thickness is not uniform. Unfortunately inner geometry of the femur was not available. Secondly, the bone geometries used in the model were representative only and did not match the subject from whom muscle origin and insertion points were mapped. It is therefore impossible to comment on the degree to which the spread of muscle moment arms about the pivot point in the femur matched the subject from whom data was sourced. Finally, even if the cadaver-collected muscle data from the Klein-Horsman data set perfectly matched the bone geometries in the model, there is no guarantee that this match would be preserved when the model was scaled to fit our gait data subject.

As loading of the femur was under consideration, only the muscles with an attachment on the femur were included in the model. However, variations in activation of muscles crossing one joint may result in compensatory effects in other muscles, causing a ripple effect throughout the model. This observation raises the question of whether or not it was acceptable to omit the ankle joint and its surrounding musculature. The gastrocnemius muscle has a function as a plantarflexor of the ankle which was ignored in the model. Changes to the activation of the gastrocnemius may have altered the overall muscle activation patterns predicted by the model. Inclusion of the ankle joint and associated muscles would have greatly increased the number of muscle strands in the model. This in turn would have increased the difficulties associated with the

optimisation procedure as outlined in Chapter 5. In the first paragraph of Section 4.6 it was explained that the goal of the model was not to reproduce accurate physiological muscle loading patterns, but to allow comparative assessment of whether or not compression can be maintained in the femur under varying conditions. With this rationale it was decided that inclusion of the musculature surrounding the ankle was not required. The ankle was therefore represented by a fixed joint, effectively creating a single unit comprised of foot and shank.

Various methods exist for the modelling of muscle. Rather than single dynamic simulations, this study comprised a series of static simulations. It was therefore deemed unnecessary to include details of muscle dynamics. Maximum forces were calculated as a function of muscle PCSA and each muscle strand was modelled as a point to point tensile force. In reality, maximum muscle forces during any given movement depend on a force-length relationship. The speed at which muscle activation reacts to changes in external forces may also come into play when considering ageing muscle, since fast twitch muscle activity is reduced. It is unlikely that muscles are activated close to their maximum potential during low level activity such as gait. It appears therefore that the sensitivity of the model has led to some over-estimation of muscle forces.

Gait data was collected from a single subject. Results in Chapter 4 showed large variability between the left and right sides of that subject. It is likely that significant inter-subject variability would be present in a model of this type due to variations in muscle moment arms about the joints. The different positions of the model and GRF across the gait cycle were extracted from a single trial run. It is possible that differences between trials may have resulted in significant variation of output from the model. However, results in Chapter 4 show a level of consistency between trials for ground reaction forces, and to a lesser extent EMG. The scope of this research called for an initial assessment of the feasibility of maintaining compression in the femur during gait and so it was not deemed necessary to create models based on numerous trials and different subjects.

Anatomical data was extracted from a cadaver study, which mapped origin and insertion points of muscles (Klein Horsman et al. 2007). These points were incorporated into the AnyBody model and scaled to fit bony landmarks to marker positions on our subject. It

is expected that although the scaled model is similar in size to our subject, some differences exist in muscle lines of action. This may cause differences between model predicted muscle activity and actual muscle activity in the subject.

The model used recorded GRF data as input. Chapter 3 (Study 3) showed that results were sensitive to the ground reaction forces and that large differences in joint reaction forces were produced by small variations in GRF direction. The methods of data collection used were outlined in Chapter 4. These methods are well established in biomechanics research and involved the use of highly sensitive specialised equipment. The recorded data is therefore assumed to be accurate and Chapter 4 showed that the results were consistent across trials.

Other limitations to the model exist and these have been discussed in previous chapters. It is evident that any interpretation of the results produced by the model should be made with caution. No assurance is given that predictions of muscle loading and the resulting joint reaction forces are consistent with those *in vivo*. However, when viewed comparatively across the range of simulations carried out, the results provide a useful stimulus for discussion and invite further research whether by improved computer modelling techniques or by experimental methods.

7.3 Compression in the Femur

The primary aim of this research was to determine the feasibility of maintaining compression in the femur during gait. The results presented in Chapter 4 collectively show that compression can be maintained in the shaft of the femur by coordinated muscle activity. This generally means an overall increase in muscle activation and the loads placed on joints, although increasing the number of muscle strands allows compression to be maintained with significantly less impact on joint loads. This was demonstrated in Chapter 5. If adding muscle strands to a simplified model can allow compression to be maintained more easily, then it follows that the even more complex human musculoskeletal system can maintain compression without placing undue strain on muscles and joints.

Compressive loading of bone is an attractive proposition in that it provides the best environment to allow lightweight optimised adaptation whilst maintaining a relatively

even strain distribution about the neutral axis of bending. Where tensile and compressive loading exist in tandem, there is an under-loaded area closer to the neutral axis of bending. We know from the extensive body of evidence that unloaded bone rapidly loses mass (Gross & Rubin 1995, Baldwin et al. 1996, Carmeliet et al. 2001). It is therefore desirable to force the neutral axis of bending away from the bone to avoid under-loaded areas. Figures 5.18 and 5.19 show that when compression is enforced, not only are under-loaded areas avoided, but the maximum principal stresses are reduced significantly. These results agree with the work undertaken by Sverdlova and Witzel who found that an optimised compression-enforced muscle load case produced a strain distribution which matched the material distribution in the femur and that the maximum stress in the bone was reduced under enforced compression (Sverdlova & Witzel 2010). They found that the ITB-TFL unit was an important contributor in maintaining the lateral tension required to counteract the bending load imposed by the weight of the body on the hip.

The current study also found a role for laterally placed muscle strands in maintaining compression in the femur. The TFL, ITB, vastus intermedius, and vastus lateralis all showed increased activation when compression was enforced. It is however impossible to draw firm conclusions from these results regarding the precise role of the ITB or any of these muscles. This is due to the fact that the modelling of the ITB-TFL unit, as discussed in Chapter 5, was found to be deficient. Strands of the ITB were allowed to vary between 0 and 5000N but no account was given for passive tension in the unloaded state and it is unclear how load is transferred by the TFL and gluteus maximus muscles. At the very least the model demonstrates that a tension force on the lateral aspect of the femur is essential in maintaining compression during gait. This supports the theory of a counter-bending force provided by a tension cord as described by Pauwels (Pauwels 1980).

Activation of the adductors changed very little when compression was enforced. The hamstrings showed reduced activation during the early stance phase of gait. This may have been to allow the increased lateral quadriceps forces to be more effective in maintaining compression. With increased quadriceps activity coupling with reduced activation of the hamstrings we would expect a change in the torque about the knee joint. This appears to have been compensated for by the increase in forces applied by

the gastrocnemius during the early stance phase. Reduced hamstring activity also results in a net increase in hip flexion moment, which itself was compensated for by an extension moment provided by the gluteus maximus.

Another muscle showing increased force production when compression was enforced was the anterior portion of the gluteus medius. This follows a line of action from the anterior superior iliac spine to the greater trochanter of the femur. As discussed in Chapter 5, the TFL-ITB unit does not pass in a straight line from its origin on the pelvis to its insertion on the tibia. The TFL is angled in a more posterior-lateral direction before meeting the ITB which extends distally to the tibia. This aligns the TFL more closely with the anterior portion of the gluteus medius. Compensation for the incorrect function of the TFL may explain why increased activation of the gluteus medius anterior is seen under enforced compression. The gluteus medius anterior and TFL are shown in Figure 7.1 highlighted in yellow and blue respectively.

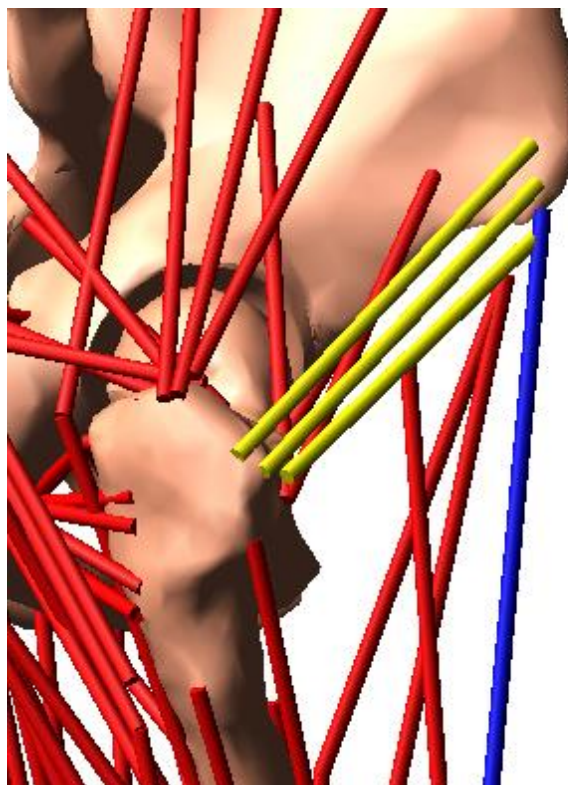


Figure 7.1 - Gluteus medius anterior (yellow) and TFL (blue) showing disparate lines of action which may not be replicated in vivo.

The model has demonstrated the possibility of maintaining compression in the femur throughout the gait cycle and suggested muscle activation patterns to achieve this.

Minimisation of a cost function governed the recruitment of various muscle strands provided constraints were met. Loading on the bone was measured computationally and constraint limits were set as targets for the optimisation.

If compression is maintained, the question remaining for the human musculoskeletal system is: how is the state of loading detected and what feedback mechanism exists to set targets for muscle activation?

7.4 Control of Muscular Loading

Chapter 2 explained the role of osteocytes as mechanosensors in bone. Osteocyte cell processes are strained by fluid drag on tethering filaments within canalicular tunnels (You et al. 2001). These strains elicit a biochemical response which is transmitted via the osteocyte network to the bone surface where bone remodelling activity is promoted or inhibited (Chen et al. 2010). The need for fluid flow to stimulate osteocytes offers an explanation for the lack of bone growth seen in the application of constant or low frequency loading (Lanyon & Rubin 1984).

Although this offers an explanation as to how bone loading is sensed to control bone remodelling, no explanation is offered by this process as to how bone loading is regulated in the first place. The detection of nerves in bone has led to investigations into their role and the influence of nerves on bone mass regulation. A review of some relevant literature was given in Section 2.3 which will be briefly summarised here.

Interestingly, the distribution of nerves in bone shows the highest concentration of nerve endings in the most highly stressed areas (McCredie 2007). This suggests a contribution of nerves to bone mass regulation but a 1971 study demonstrated no difference in bone's response to mechanical loading in the presence or absence of nerves (Hert et al. 1971). An experiment conducted on 246 rats found that loading of the right ulna caused increased bone mass in surrounding bones and the contralateral limb even though these were not loaded directly (Sample et al. 2008). This effect was cancelled by anaesthesia of the nerve supply to the right limb, suggesting a centrally controlled neural signalling mechanism based on feedback from the loaded bone.

The results from the model show that changes to muscular loading about one joint cause a ripple effect of compensatory muscle action which affects surrounding bones. It

follows that the response to a bone loading feedback signal would involve multiple muscles affecting multiple bones. An interruption to this feedback signal, would cause the loaded bone to respond directly to the load applied via the osteocyte network without any effect on nearby or distant bones. This suggests a double feedback loop. One loop controlling the response of a bone to its mechanical environment via osteocyte signalling to control modelling and remodelling. The other loop providing neural feedback to control bone's mechanical environment via appropriate muscle activation. A graphical representation of these feedback loops is shown below in Figure 7.2.

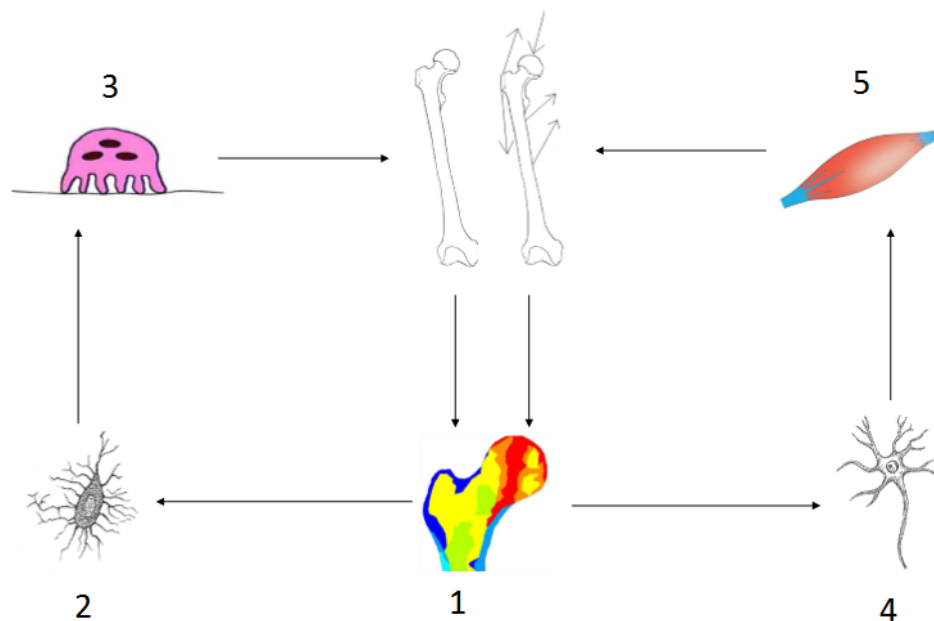


Figure 7.2 - A suggested double feedback loop for the regulation of healthy bone mass. Bone is loaded primarily in compression (1). Osteocytes (2) monitor bone's loading history and send biochemical signals to the bone surface where osteoclast cells (3) begin the remodelling process. By this method, bone geometry is maintained or altered to suit the bone's mechanical environment. On the other side of the loop, nerves (4) detect the state of loading in bone and provide feedback which governs muscle activation (5) and produces the loading pattern necessary to maintain compression in bone.

This is a suggested feedback mechanism and requires clarification through further research. What can be said with some certainty is that if compression is the dominant state of loading in the long bones and is achieved by coordinated muscle activity, then

there must be an appropriate feedback loop to control muscle activation. The correct operation of this feedback loop would then become of paramount importance in the maintenance of healthy bone.

7.5 Ageing and Osteoporosis

Maintenance of healthy bone requires the contribution of a number of factors. Many of these have been implicated in the development of osteoporosis including diet, hormone imbalances, vitamin D and calcium deficiency. Post-menopausal women are the group at highest risk of osteoporotic fractures. This is largely attributed to changes in circulating hormones but the sympathetic nervous system (SNS) has also been shown to play a role as discussed in Section 2.3. The literature presented in Section 2.3 provides evidence for a hormonal signalling pathway which influences bone mass regulation via the SNS. Reduced innervation of bone following ovariectomy in rats may be an indicator for post-menopausal bone loss (Elefteriou 2005, Burt-Pichat et al. 2005).

Of all the potential influences on the development of osteoporosis, this study is most interested in bone's mechanical environment. The speed of bone loss which occurs in the case of inadequate loading makes this a key consideration. Muscle loads are essential in maintaining bone mass and therefore age related weakening of the muscles, or sarcopenia, is the main point of interest in this study as it relates to bone mass.

The review presented in Section 2.4 highlighted the fact that muscle force producing capability is reduced with age. This is caused by reduced muscle mass and changes to the innervation of muscle motor units. Changes to the way in which motor units are innervated may cause deficiencies in motor control (Williams et al. 2002). In the context of the current work, this has implications for the ability of muscles to maintain compression of bone. The difference between the 31 and 67 strand models shows that limited loading options may result in higher loads being placed on bony structures.

Figure 5.19 shows the consequences of bone being loaded without any feedback. Peak stresses are increased and in the case of bending, unloaded areas of bone will be introduced. If nerves provide this feedback then reduced innervation of bone has implications for increasing peak stresses. The effectiveness of the osteocyte network is diminished with ageing as apoptosis causes interruptions in cell communication

(Bonewald 2007). These factors combined suggest a vicious cycle of declining ability, to provide both ideal loading conditions, and to respond appropriately to the loading applied.

The muscle atrophy associated with ageing is more pronounced in type II muscle fibres (Lexell et al. 1988). Terracciano et al. discovered a prevalence of type II fibre atrophy in osteoporosis over and above normal age related atrophy (Terracciano et al. 2013). This suggests that the frequency and rate of loading provided by muscles may be equally if not more important than loading magnitudes. Research on loading frequencies applied using dynamic muscle stimulation found that muscles stimulated at 20-50Hz were most effective in maintaining bone mass (Lam & Qin 2008). Slower muscle firing rates may not be capable of adapting to changes in bone loading with sufficient speed to maintain compression, resulting in momentary high bending loads. Sudden large loads may be the result of a stumble or fall. The loss of type II muscle fibres is associated with a loss of muscle power (Izquierdo et al. 1999). This is in turn related with a higher risk of falling (Skelton et al. 2002).

Not all fractures are associated with falls however, and spontaneous fractures have been reported (Viceconti et al. 2012). Martelli found that sub-optimal motor control can result in large increases in hip reaction forces (Martelli et al. 2011). A follow up study determined that where weakened bone due to osteoporosis and sub-optimal motor control exist together, spontaneous fractures are possible (Viceconti et al. 2012). The results taken from the current model show increased stresses on bone in the case of sub-optimal muscle activation – assuming that overall compression is the goal of optimal loading patterns.

Activation of a larger number of muscles is required to maintain compression in the femur when maximum muscle forces are reduced. This was shown in Figures 6.3 and 6.4. The reduction in maximum forces means that those active muscles are functioning at a higher percentage of their maximum activity. The combination of more muscles being active at a higher percentage of their maximum, is likely to cause muscle fatigue and increase the relative metabolic cost of walking. A person with fatigued muscles is also more likely to stumble, leading to falls.

Several intervention methods have been demonstrated to mitigate the effects of age related changes to the musculoskeletal system. There are many commonly used pharmacological treatments which have been shown to have some positive impact on bone mass (MacLean et al. 2008, Chen & Sambrook 2012). These do not address changes to muscle or neuromuscular control. The overwhelming evidence showing that bone adapts to its mechanical environment, points to the fact that no treatment for osteoporosis will be entirely successful without consideration of the mechanical loading of bone.

The differences in bone loading and corresponding muscle activation observed with and without compression show that coordination of muscle activity is a key factor in maintaining a particular state of loading in bone. Comparing the results between the 31 and 67 strand models we see that less options for muscle loading increase the difficulty of maintaining compression. This was evidenced by the large difference in knee joint reactions between the two constraint cases (unconstrained femoral loading vs compression enforced) seen in Figure 4.8 compared with the smaller differences observed in Figure 5.3. Figure 7.3 contains the same data as Figure 6.1 with the addition of hip joint loads from the 31 strand model with full maximum muscle forces. The 31 strand model results show slightly lower hip joint loads throughout the mid-stance phase of gait.

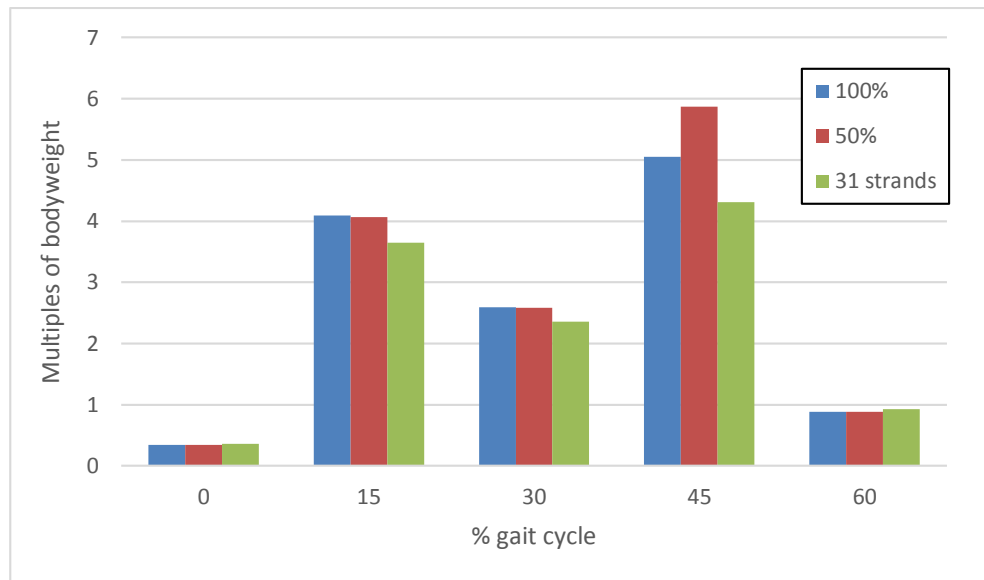


Figure 7.3 - Hip joint reaction force across the stance phase of gait. Results from three models are compared; the 67 strand model with original maximum muscle force values, the 67 strand model with muscle force values limited to 50 percent, and the 31 strand model with original maximum muscle force values.

The same data for the knee joint is shown in Figure 7.4. This time we see increased loads across the mid-stance phase of gait with the 31 strand model, except at 15% of gait. The potential reasons for the apparently poor performance of the 67 strand model at 15% of gait were discussed in Chapter 5.

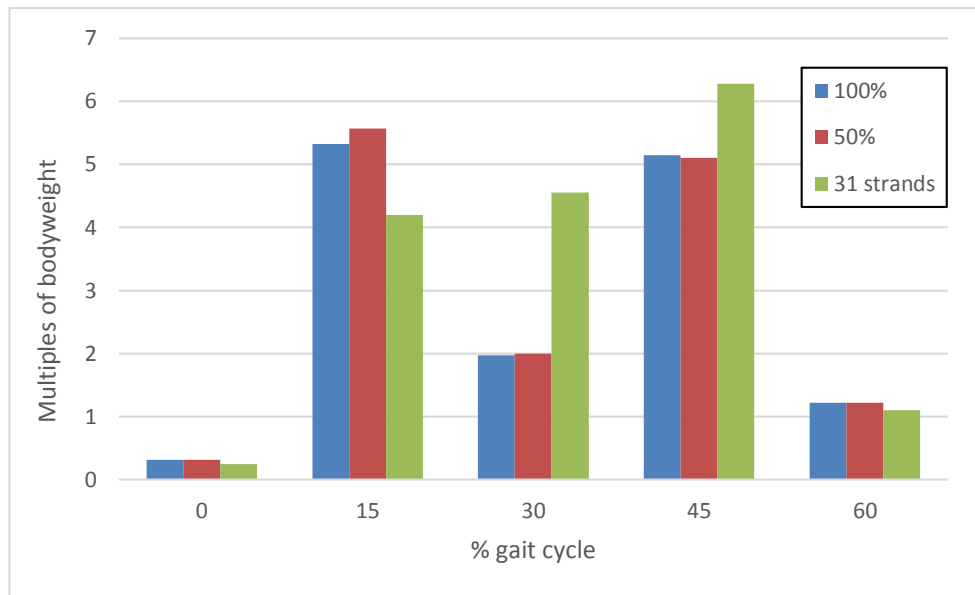


Figure 7.4 - Knee joint reaction force across the stance phase of gait. Results from three models are compared; the 67 strand model with original maximum muscle force values, the 67 strand model with muscle force values limited to 50 percent, and the 31 strand model with original maximum muscle force values.

The more interesting point of this comparison is the effect of reducing the number of strands on the stress in the femur. This is shown in Figure 7.5. Although both hip and knee reaction loads were lower in the 31 strand model at 15% of gait, the resultant stress on the bone at the point measured differs very little. At 30 and 45% of gait, the stress in the femur is higher in the 31 strand model than even the limited muscle loading case from the 67 strand model. This suggests that limiting options for muscle recruitment is more detrimental than limiting loading magnitudes.

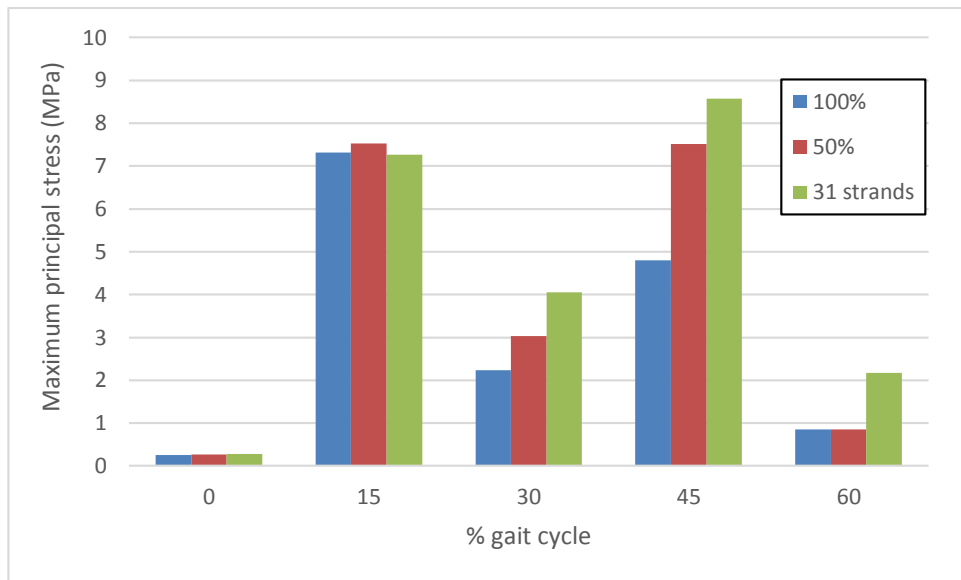


Figure 7.5 - Maximum principal stress at the cut in the femur across the stance phase of gait. Results from three models are compared; the 67 strand model with original maximum muscle force values, the 67 strand model with muscle force values limited to 50 percent, and the 31 strand model with original maximum muscle force values.

Re-innervation of denervated muscle fibres by adjacent motor units in the elderly results in fewer but larger motor units (Campbell et al. 1973). This effect is crudely simulated by reducing the number of available muscle strands in the model and the effects on bone loading are seen in Figure 7.5. It is possible that the reduced number of motor units in aged muscle causes difficulties for the fine-tuning of muscular loading required to maintain a particular state of loading such as compression.

Muscle strengthening weight bearing exercise has been shown to be of some benefit by mitigating loss of muscle strength (Coggan et al. 1992b, Rogers & Evans 1993, Hurley & Hagberg 1998). During the early stages of training, neural adaptations cause the greatest gains in muscles' force-producing capability (Kraemer et al. 1996). In the context of the current discussion, this effect is likely to be more important than strength gains caused by increased muscle mass. Tai Chi as a form of exercise has been linked with improved outcomes for osteoporosis, although one review found no consensus on the effects of Tai Chi on BMD (Lee et al. 2008). A study by Murphy and Singh found that regular practice of Tai Chi resulted in increased balance confidence and performance, functional strength, and mobility (Murphy & Singh 2008). It is proposed that this type of low-impact

coordinated exercise improves neuromuscular control, but fails to provide sufficient skeletal loading to stimulate bone mass gains.

Dynamic muscle stimulation has been proven effective in combating muscle and bone atrophy caused by disuse (Lam & Qin 2008, Qin et al. 2010). A positive effect on bone mass has also been demonstrated through the use of vibrating platforms (Judex & Rubin 2010). Although these treatments are effective in maintaining or improving bone mass when administered, the author is unaware of any lasting improvements on neuromotor control which is an essential factor in autonomous maintenance of healthy bone.

The study by Terracciano et al. uncovered a potential cause of muscle atrophy in osteoporosis independent of changes caused by age or disuse (Terracciano et al. 2013). They found reduced levels of protein kinase Akt in osteoporotic subjects which interacts with insulin-like growth factor 1 (IGF-1) to promote muscle protein synthesis and prevent muscle atrophy. As concluded in that study, this may invite the development of pharmacological interventions which target muscle atrophy rather than bone as a treatment for osteoporosis.

Thus, there are several mechanisms which appear to be responsible for the development of osteoporosis. It is difficult to determine which of these prevail over the others, whether they be hormonal, neural, or mechanical. It is clear however that muscular loading should be a key consideration in the development of treatments. The results discussed in this chapter show that muscles are capable of coordinated activity to maintain compression in the shaft of the femur, and demonstrate the benefit of such a loading regimen. Limitations to muscle activity simulated by reduced maximum muscle forces and fewer muscle strands show the threat posed by age-related muscular changes to the control of femoral loading, and by extension general loading of the long bones.

Chapter 8

Conclusions and Future Work

8.1 Conclusions

The aims of this research were to better understand muscular loading of the femur and its impact on bone health particularly as it relates to osteoporosis. The simplified nature of the model demands that care be taken in the interpretation of results. We cannot assume that model predictions of muscle activity or bone loading reflect conditions *in vivo*. However, proceeding with this cautionary caveat in mind we can make a reasoned comparative assessment of the results and, with support from the literature, draw tentative conclusions and invite further work.

Maintenance of overall compression of the femur has obvious benefits in terms of lightweight optimisation and reduction of peak stresses as described by Pauwels (Pauwels 1980). This research shows that compression can be maintained in the shaft of the femur throughout the gait cycle and it is associated with a reduction in peak stresses at the point of measurement. These results are an example of stress reduction by counter-bending or “active unloading” as this principle has been described (Munih et al. 1992). There is perhaps insufficient evidence to unequivocally declare that bones are preferentially loaded in compression, but the evidence provided both in this study and wider literature suggests that compressive loading of the long bones by coordinated muscle activity is not only a logical scenario but a likely one.

Reduction in muscle force producing capability was associated with increased difficulty in maintaining compression in the shaft of the femur. Limitations to the number of muscle loading options available (i.e. muscle strands) also inhibited the stress reducing effect of maintaining compression. These results promote the idea that compressive loading of the femur, if indeed the preferred loading scenario, would be less effective in reducing peak stresses where limitations to muscle strength or neuromuscular control exist. These limitations occur as a consequence of ageing, pointing to potential difficulties in maintaining compressive loading of the long bones in the elderly.

The prevalence of type II muscle fibre atrophy observed in osteoporotic subjects (Terracciano et al. 2013) highlights an osteoporosis-specific limitation to muscle activity. In the context of the current study, this muscular deficiency is likely to reduce the ability of the musculoskeletal system to react to changes in bone loading. The combined evidence shows muscular loading and neuromotor control of the same to be key considerations in the development of osteoporosis. It is suggested that understanding osteoporotic changes in muscle loading may provide a clearer picture of what causes the disease and how it can be treated more effectively. The remainder of this chapter focuses on possible areas of future research which are suggested as a means to improve understanding of the loading of bone and potential causes of osteoporosis.

8.2 Musculoskeletal Modelling

Detailed discussion of limitations to the current model has been presented throughout this thesis. Many of these limitations were the result of gaps in the available data. Others were simplifications imposed in order to comply with the realities of computer modelling. Barriers presented by limitations in technology are gradually being eroded and making way for more complex anatomically accurate models. This section highlights several areas for future development of the current model.

Modelling of the ITB was shown to be lacking detail in the current model. This was discussed in Section 4.6. A detailed anatomical study would be required to yield usable information on the load transferred to the ITB by the TFL and gluteus maximus muscles. This should include all attachments of the ITB, the degree to which it is pre-tensioned, and the way in which load is transferred to the distal femur and proximal tibia. This would allow more accurate modelling of the ITB as a single unit, following the correct

path over the lateral surface of the thigh, and avoiding the confounding factor of incorrect ITB modelling on the surrounding muscles.

The muscles themselves should be represented more accurately. The results from the current model show significant differences caused by changing the number of muscle strands. Even with a large number of strands, representing muscles as a point to point tensile force is still a gross simplification and this has been found to be insufficient to represent the complex and varying directions of muscle loading (Röhrle & Pullan 2007). More detailed muscle models have been developed based on magnetic resonance images and implemented in musculoskeletal models (Blemker & Delp 2005, Teran et al. 2005). It is recommended that future studies of the effect of muscular loading on bone consider implementing a more anatomical approach to the modelling of muscle.

The main obstacle to including more detailed muscle models in this work was limitations in the optimisation method. A more computationally efficient method of simulating the model and a more focused optimisation problem would allow more detail to be included. This may be more effective as a multi-stage process which uses simpler models to narrow the design space for more detailed models and analyses.

Another component of the current model which is lacking in detail is the modelling of the hip and knee joints. Studies which include detailed contact geometries of joints tend to focus on a single joint due to the computational cost of modelling contact forces between deformable structures with varying properties. The simplified joint models used in this study increased the sensitivity of the model to variations in joint position. Future models should aspire to include detailed contact geometry of the hip and knee joints including ligaments and menisci. This would likely force the need for realistic articulation of the joints which would in turn improve the accuracy of muscle force predictions.

Consideration of realistic articulation of the joints leads to a need to model dynamic motion. This study consisted a series of static simulations. Although the GRF input to the model accounts for acceleration of the body towards the ground, the specific dynamic requirements of each joint were not specified. Optimisation of a forward dynamics gait simulation to match recorded gait data is an alternative method to ensure that the predicted muscle forces produce the effect of muscle forces *in vivo*.

A dynamic simulation of gait provides the platform to consider muscle activation dynamics. This is particularly important in the context of osteoporosis and ageing. It may be possible to determine whether or not changes in muscle activation dynamics hinder the ability of muscles to maintain compressive loading of the femur. If so, there may be observable consequences such as momentary high peak stresses as muscles react to changes in loading.

The state of loading in the femur was measured in this study at a single point in the mid-shaft. This does not allow conclusions to be drawn about the state of loading elsewhere in the bone and whether or not it is possible to maintain compressive loading throughout the entire femur simultaneously. Future work may consider several points of interest, or include a finite element analysis of the entire femur similar to the work by Sverdlova and Witzel (Sverdlova & Witzel 2010). It would be desirable to combine such analysis with a dynamic simulation of gait. The time and computing power required to resolve detailed finite element models makes it difficult to perform simulations involving large deformations. The solution may be to perform a multibody dynamics analysis using a low resolution flexible femur. This would allow stress patterns to be measured throughout the bone and fed into more detailed finite element analyses of key positions.

Several possible modelling improvements have been touched upon which would potentially improve the accuracy and reliability of the model. The ideal situation would be to combine each of these improvements into a single study, provided the identified gaps in anatomical data could be accounted for. Accurate muscle and bone geometry matching gait subjects would lead to a significant improvement on model accuracy and outcomes.

8.3 Compression of Bone

Computer modelling studies can provide comparative data and comment on the effect of varying certain parameters, but definite conclusions require the support of experimental data. Further development of the compression theory of bone demands demonstration of the principle of coordinated muscle activity *in vivo*. A carefully designed animal study may allow demonstration of this principle by introduction of a bending load on a long bone and concurrent monitoring of surrounding musculature to

detect a reactionary counter-bending load with and without resection of the nerve supply to the bone under study. There are several difficulties anticipated with this type of study, not least of which is a way to introduce the required bending load without disturbing the surrounding musculature. In addition, there is the question of anaesthesia and whether or not muscle function can be preserved without causing undue stress to the animal.

An alternative may be to conduct a human study using functional muscle stimulation. By stimulating a certain muscle in an otherwise relaxed limb and monitoring EMG activity in surrounding muscles, it may be possible to map agonist-antagonist pairs and recognise a pattern of bending reduction. A great deal of care would be required to measure each individual muscle accurately and this would likely require the use of fine-wire EMG. The difficulty associated with fine-wire EMG is the highly localised nature of the recorded measurement of a single point within a muscle. Imaging methods such as ultrasound may be able to detect muscle contraction in a less invasive and potentially more reliable way. A study of this type would likely benefit from a concomitant modelling study using detailed muscle geometry and contraction characteristics to simulate observed muscle activation patterns and assess their impact on bone loading.

8.4 Changes to the Musculoskeletal System

The changes which occur in the musculoskeletal system due to ageing and osteoporosis have been discussed in Chapters 1, 2, and 7. Two significant changes have been identified which impact muscle function and control. The first is re-innervation of denervated muscle fibres by adjacent motor units, resulting in fewer but larger motor units. The model showed that more muscle strands with lower maximum forces were more effective in loading the femur in compression than fewer muscle strands. It would be useful to determine what level of neuromotor control is lost by the creation of larger motor units, what impact this has on bone loading, and what could be done to prevent this change.

The second change which was identified is atrophy of type II muscle fibres. It is anticipated that a reduction in fast-twitch muscle activity may slow the response of muscle to changes in bone loading. This could be tested by a study involving detection of agonist-antagonist muscle activity similar to that described in Section 8.3. The

difference would be the time between stimulation of the agonist muscle and activation of the antagonist. Some effort should then be made to quantify the level or lack of type II muscle fibre atrophy in each subject and correlate with the agonist-antagonist response times.

These suggestions are offered to stimulate further thought and identify possible avenues of research. Although osteoporosis is a large and growing problem, it is only one of many musculoskeletal disorders which could be helped by an increased understanding of the musculoskeletal system. It is hoped that continued research will lead to better treatments and better quality of life for those affected.

Appendix A

Model Creation

This appendix gives a step by step account of the creation and simulation process for each model.

The GaitLowerExtremity model was opened in AnyBody and linked to the appropriate recorded gait data. The .c3d file containing the gait data was previously trimmed so that the final frame of the AnyBody simulation would be the frame of interest to be studied, be it at 0, 5, 10 percent of gait etc. The correct data file was included by modifying “TrialSpecificData.any” as highlighted below in Figure A.1.

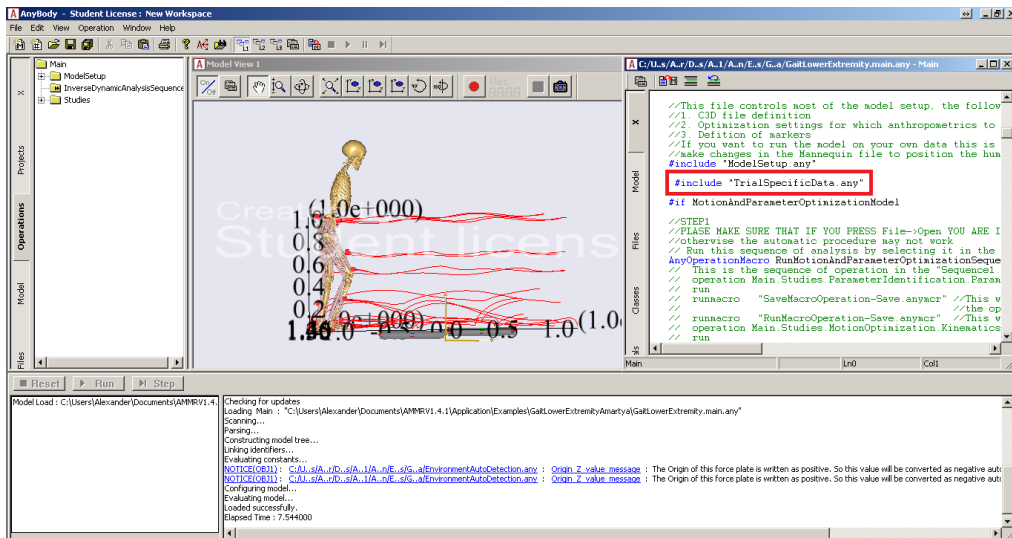


Figure A.1 – Editing AnyBody model to match recorded data.

The name of the file to be used was inserted as shown below in Figure A.2.

Figure A.2 - Editing the trial specific data.

Some manipulation of the other parameters shown here (body mass, height, and segment lengths) was required initially in order to fit the AnyBody model to the recorded data. A motion and parameter optimisation was run in AnyBody, followed by an inverse dynamics simulation. Bone geometries were exported from AnyBody in the final position (frame of interest) and saved as .stl files.

A line of text was added to the AnyBody model for each data point to be extracted. These data points included the origin and insertion points of muscles, joint locations, and centre of pressure under the foot. These were automatically saved into a spreadsheet. The text added to the AnyBody model is shown in Figure A.3.

```
AnyFloat gastroclatfemur =
  ..Main.Studies.HumanModel.BodyModel.Right.Leg.Mus.Gastroc
nemiusLateralis1.Org.r;
```

Figure A.3 - Code to export muscle origin and insertion points from AnyBody.

Data points were reorganised in Microsoft Excel into lists of X, Y, and Z coordinates. Lists of coordinates for all the points attached to each bone segment were saved as .dat files.

Bone geometries were imported into a new database in ADAMS and a command file was run which called a macro to import the points listed in the .dat files. A portion of the command file is shown in Figure A.4. This portion was repeated for each bone segment.

```
!---import macro
macro read &
  macro_name = .MAC &
  file_name = "point_macrofemurprox.mac" & !---calls the relevant macro
  wrap_in_undo = yes &
  create_panel = yes

!---execute macro
run_point &
  data_prox = "femurprox.dat" & !---references the data points to be drawn
  part_prox = .Femur_basic_solid.Femur_prox & !---the target part in the
model
  part_nom = .Femur_basic_solid.Ground
```

Figure A.4 - Command file to manage creation of data points In ADAMS.

The macro "point_macrofemurprox.mac" called by the above command file is shown in Figure A.5. This was modified from a macro provided on the ADAMS knowledge base.

```
!USER_ENTERED_COMMAND run_point
!WRAP_IN_UNDO NO
!$data_prox:T=file(*.dat)
!$part_prox:T=part

defaults model model_name=( $part_prox.parent)
analysis create analysis_name = ajs_scr

!---create working variables
var set var=$_self.my_name string="$data_prox"
```

```

var set var=$_self.find_spot &
  int= (STR_FIND_N($_self.my_name, "/", STR_FIND_COUNT($_self.my_name, "/")))
var set var=$_self.fname &

str=(STR_SUBSTR($_self.my_name,($_self.find_spot+1),STR_LENGTH($_self.my_name)-$_self.find_spot-4))

!--import the 3 column data
file testdata read measures &
  file_name = $data_prox &
  analysis=ajs_scr &
  units = length,length,length &
  use_file_column_labels = yes

!--set default part as point destination part
defaults model part_name=$part_prox

!--loop and create points
for variable=h start=1 inc=1 end=(COLS(ajs_scr.X.Q.values))
marker create marker = (UNIQUE_NAME((eval($_self.fname))/"_PT")) &
  location = &
  (eval(
    (STACK((STACK((ajs_scr.X.Q.values[h]),(ajs_scr.Y.Q.values[h]])),
    ((ajs_scr.Z.Q.values)[h])))) ) &
  rel=$part_nom
end

!--delete analysis representing input data
analysis delete analysis_name=ajs_scr
measure delete measure_name=X, Y, Z

!--clean-up temporary variables
var del var = $_self.*

```

```
!
```

Figure A.5 - Macro to create points in ADAMS.

Another ADAMS command file was used to create muscle via points around the newly created points. As the complete file is large, a section of this for one muscle via point is shown in Figure A.6.

```
!----- PART_10 -----!  
!  
!  
defaults coordinate_system &  
  default_coordinate_system = .Femur_basic_solid.ground  
!--details of the part to be created  
part create rigid_body name_and_position &  
  part_name = .Femur_basic_solid.PART_10 &  
  adams_id = 10 &  
  location = 0.0, 0.0, 0.0 &  
  orientation = 0.0d, 0.0d, 0.0d  
!  
defaults coordinate_system &  
  default_coordinate_system = .Femur_basic_solid.PART_10  
!  
! ***** Markers for current part *****  
!--centre of mass of the part and also position for rotational joint  
marker create &  
  marker_name = .Femur_basic_solid.PART_10.cm &  
!--location referenced to existing point  
  location = (.Femur_basic_solid.ground.viac_PT_7) &  
!--orientation defined to ensure the joint created is orientated correctly  
  orientation = 0.0d, 0.0d, 0.0d  
!--marker to allow rotational joint between via part and relevant bone  
segment
```

```

marker create &
  marker_name = .Femur_basic_solid.TIBIA.MARKER_vp7 &
  location = (.Femur_basic_solid.ground.viac_PT_7) &
  orientation = 0.0d, 0.0d, 0.0d
!--via point through which muscle strand will attach
marker create &
  marker_name = .Femur_basic_solid.PART_10.via_PT_7 &
  adams_id = 100 &
  location = (.Femur_basic_solid.ground.via_PT_7) &
  orientation = 0.0d, 0.0d, 0.0d
!
part create rigid_body mass_properties &
  part_name = .Femur_basic_solid.PART_10 &
  material_type = .Femur_basic_solid.steel
!
! ***** Graphics for current part *****
!
geometry create shape ellipsoid &
  ellipsoid_name = .Femur_basic_solid.PART_10.ELLIPSOID_46 &
  center_marker = .Femur_basic_solid.PART_10.cm &
  x_scale_factor = 50.0 &
  y_scale_factor = 50.0 &
  z_scale_factor = 50.0
!
part attributes &
  part_name = .Femur_basic_solid.PART_10 &
  color = RED &
  name_visibility = off
!
!*****
!--create rotational joint
constraint create joint revolute &

```

```
joint_name = .Femur_basic_solid.JOINT_1 &
adams_id = 1 &
!--creates a joint between two previously created markers
i_marker_name = .Femur_basic_solid.PART_10.cm &
j_marker_name = .Femur_basic_solid.TIBIA.MARKER_vp7
!--generic information regarding the joint
constraint attributes &
  constraint_name = .Femur_basic_solid.JOINT_1 &
  visibility = on &
  name_visibility = off &
  size_of_icons = 20.0
!
```

Figure A.6 - Creation of muscle via points.

Following this, the ground reaction force was created manually using the recorded value and direction.

This was followed by creation of the knee joints as described in Chapter 3.

Torsional springs around the hip, knee, and femur joints were placed manually.

The ADAMS model at this point is shown in Figure A.7. The red spheres are the muscle via points.

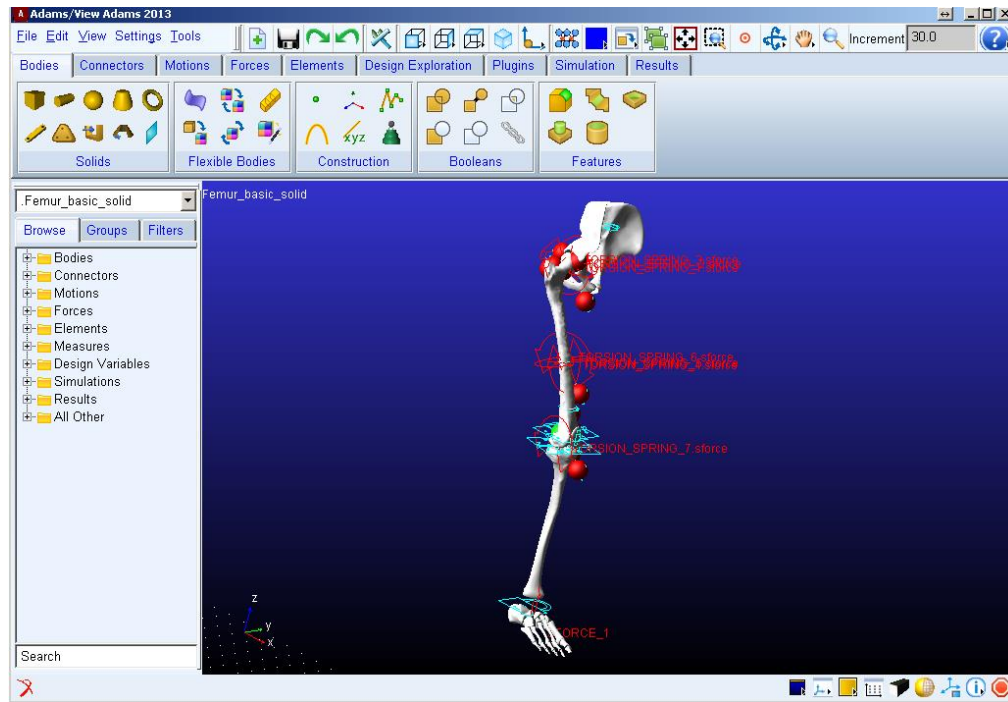


Figure A.7 - ADAMS model ready for import of remaining model components

The following command file was then imported which created all remaining components of the model. A sample of the command file is shown here (Figure A.8) which has been reduced to show the content of the file without repeating the script for every muscle strand and objective.

```

!----- Requests -----!

!--creates output requests
!--as with all sections of this sample script, this was repeated many times but is only
!--shown here once.
output_control create request &
  request_name = .Femur_basic_solid.HipT1 &
  adams_id = 2 &
  comment = hip1 &
  f2 = ""
!

!----- Adams/View Variables -----!

!--creates design variables and assigns a range
!--the range for each variable was determined by muscle PCSA

```

```

variable create &
  variable_name = .Femur_basic_solid.VasMedSup_10 &
  units = "no_units" &
  range = -1345.0, 0.0 &
  use_allowed_values = no &
  real_value = 0.0
!
!
!----- Adams/View UDE Instances -----!
!--this section creates a spring to represent a muscle strand
!
defaults coordinate_system &
  default_coordinate_system = .Femur_basic_solid.ground
!
undo begin_block suppress = yes
!
ude create instance &
  instance_name = .Femur_basic_solid.TFL2 &
  definition_name = .MDI.Forces.spring &
  location = 0.0, 0.0, 0.0 &
  orientation = 0.0, 0.0, 0.0
!
ude attributes &
  instance_name = .Femur_basic_solid.TFL2 &
  color = BLUE
!
!
!----- Adams/View UDE Instance -----!
!--this section assigns properties to a muscle strand/spring
!--the points listed below are the origin and insertion points of the muscle
variable modify &u
  variable_name = .Femur_basic_solid.TFL2.i_marker &

```

```

object_value = (.Femur_basic_solid.PELVIS.pelvis_PT_22)
!
variable modify &
  variable_name = .Femur_basic_solid.TFL2.j_marker &
  object_value = (.Femur_basic_solid.TIBIA.tibia_PT_8)
!--the remainder of spring parameters are as default with one exception
!-- highlighted below
variable modify &
  variable_name = .Femur_basic_solid.TFL2.stiffness_mode &
  string_value = "linear"
!
variable modify &
  variable_name = .Femur_basic_solid.TFL2.stiffness_coefficient &
  real_value = 0.0
!
variable modify &
  variable_name = .Femur_basic_solid.TFL2.stiffness_spline &
  object_value = (NONE)
!
variable modify &
  variable_name = .Femur_basic_solid.TFL2.damping_mode &
  string_value = "linear"
!
variable modify &
  variable_name = .Femur_basic_solid.TFL2.damping_coefficient &
  real_value = 0.0
!
variable modify &
  variable_name = .Femur_basic_solid.TFL2.damping_spline &
  object_value = (NONE)
!
variable modify &

```

```

variable_name = .Femur_basic_solid.TFL2.free_length_mode &
string_value = "Design_Length"
!
variable modify &
variable_name = .Femur_basic_solid.TFL2.free_length &
real_value = 1.0
!--the preload value is tied to the relevant variable for each muscle strand
variable modify &
variable_name = .Femur_basic_solid.TFL2.preload &
real_value = (.Femur_basic_solid.TFL_2)
!
variable modify &
variable_name = .Femur_basic_solid.TFL2.i_dynamic_visibility &
string_value = "On"
!
variable modify &
variable_name = .Femur_basic_solid.TFL2.j_dynamic_visibility &
string_value = "Off"
!
variable modify &
variable_name = .Femur_basic_solid.TFL2.spring_visibility &
string_value = "depends"
!
variable modify &
variable_name = .Femur_basic_solid.TFL2.damper_visibility &
string_value = "depends"
!
ude modify instance &
instance_name = .Femur_basic_solid.TFL2
!
!-----REQUESTS-----
!--the requests previously created are referenced to a function or measure

```

```

output_control modify request &
  request_name = .Femur_basic_solid.HipT1 &
  f2 = ".Femur_basic_solid.TORSION_SPRING_1.torque"
!
!
!----- Measures -----!
!--all measures and functions are defined here
!--a measure such as the one below was created for each design variable in
!--order to facilitate calculations at the optimisation stage
measure create function &
  measure_name = .Femur_basic_solid.FUNCTION_MEA_AddBrevDist_6 &
  function = "" &
  units = "no_units" &
  create_measure_display = no
!
data_element attributes &
  data_element_name = .Femur_basic_solid.FUNCTION_MEA_AddBrevDist_6 &
  color = WHITE
!
!--other measures are referenced to functions such as the one below
measure create function &
  measure_name = .Femur_basic_solid.FUNCTION_COMPRESSION_RESULTANT &
  function = "" &
  units = "no_units"
!
data_element attributes &
  data_element_name = .Femur_basic_solid.FUNCTION_COMPRESSION_RESULTANT
&
  color = WHITE
!
!--torque in joints is measured by means of the torsional springs in the model
measure create computed &

```

```

measure_name = .Femur_basic_solid.TORSION_SPRING_1_MEA_1 &
text_of_expression = "0" &
create_measure_display = no
!
entity attributes &
  entity_name = .Femur_basic_solid.TORSION_SPRING_1_MEA_1 &
  color = WHITE
!
!----- Adams/View Optimization Objective -----!
!
!--objectives are defined in this section and referenced to measures
optimize objective create &
  objective_name = .Femur_basic_solid.OBJECTIVE_HIP1 &
  measure_name = .Femur_basic_solid.TORSION_SPRING_1_MEA_1 &
  output_characteristic = last_value
!
!----- Function definitions -----!
!
!--here functions are defined
!--in the function below the design variable measure is referenced to the relevant
!--variable
measure modify function &
  measure_name = .Femur_basic_solid.FUNCTION_MEA_AddBrevDist_6 &
  function = ".Femur_basic_solid.AddBrevDist_6"
!--the function to calculate the resultant state of loading in the femur is given
!--as an example below
measure modify function &
  measure_name = .Femur_basic_solid.FUNCTION_COMPRESSION_RESULTANT &
  function
  =
"SQRT(((.Femur_basic_solid.TORSION_SPRING_4.torque/1000)*(.Femur_basic_solid.
TORSION_SPRING_4.torque/1000))+((.Femur_basic_solid.TORSION_SPRING_5.torqu

```

```

e/1000)*(.Femur_basic_solid.TORSION_SPRING_5.torque/1000)))-
((.Femur_basic_solid.FEMUR_JOINT_MEA_X*1.1781E-7)/1.88496E-5)"
!
measure_display create &
    mea_display = .Femur_basic_solid.FUNCTION_COMPRESSION_RESULTANT_display
&
    measure_name = .Femur_basic_solid.FUNCTION_COMPRESSION_RESULTANT
!--the example below shows the muscle stress cubed for only one muscle strand
!--in the complete file, this calculation is repeated and summed for all muscle
!--strands
measure_modify function &
    measure_name = .Femur_basic_solid.FUNCTION_MUSCLE_STRESS_cubed &
function
=
"((.Femur_basic_solid.FUNCTION_MEA_AddBrevDist_6/3.2)*(.Femur_basic_solid.FU
NCTION_MEA_AddBrevDist_6/3.2)*(.Femur_basic_solid.FUNCTION_MEA_AddBrevD
ist_6/3.2))+", &
!
!WRAP_IN_UNDO NO
variable_set variable_name=Model_Name &
object=(eval(db_default(.system_defaults,"model")))
!#####
!#####right muscle
!--the code below changes the spring graphic to a cylinder
for var=a object_name=* TYPE=spring_damper_graphic
geometry_modify shape spring_damper &
    spring_damper_name = (eval(a)) &
    diameter_of_spring = 0 &
    damper_diameter_at_ij = 5,5 &
    tip_length_at_ij = 0.0,0.0
end !for

```

Figure A.8 - Command script to import main components of the model.

The point of insertion of the ITB was moved manually to attach on the lateral epicondyle of the femur. The reason for this was outlined in Chapter 3. This is shown in Figure A.9.

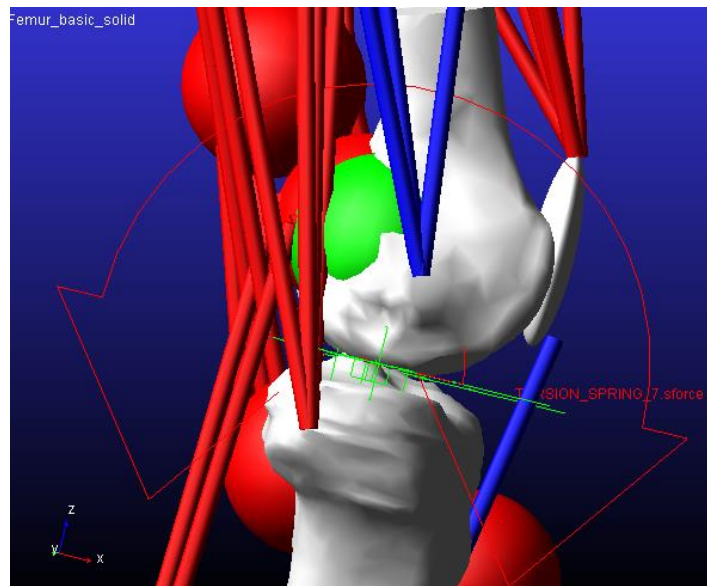


Figure A.9 - Final position of ITB insertion.

With the model complete, the solver output settings were modified by selecting the menu options shown in Figure A.10. The model was set to output results files for the ADAMS Insight study and request files for the HEEDS optimisation.

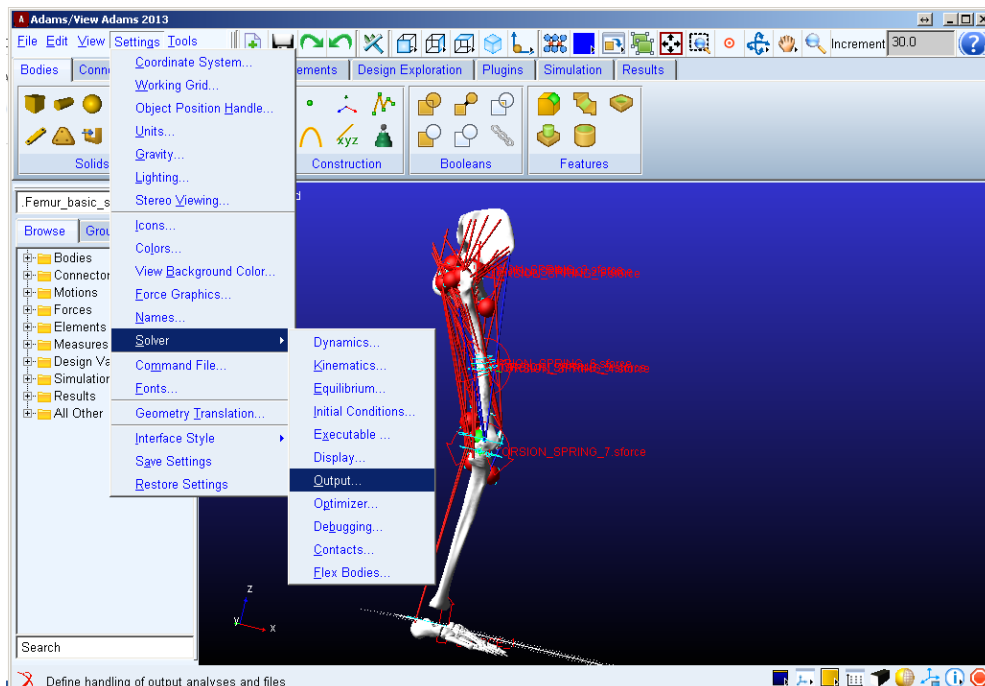


Figure A.10 - Editing solver output settings.

Due to a recurring error, completed models were exported in their entirety as a command file and then re-imported into a new model database. This prevented errors in the database from causing crashes during simulation. Another command script was then run to allow a set of simulation runs to continue if one run failed. This was obtained from the ADAMS knowledge base.

Under the design exploration tab, the model was exported to ADAMS Insight. The relevant button is shown by the mouse pointer in Figure A.11.

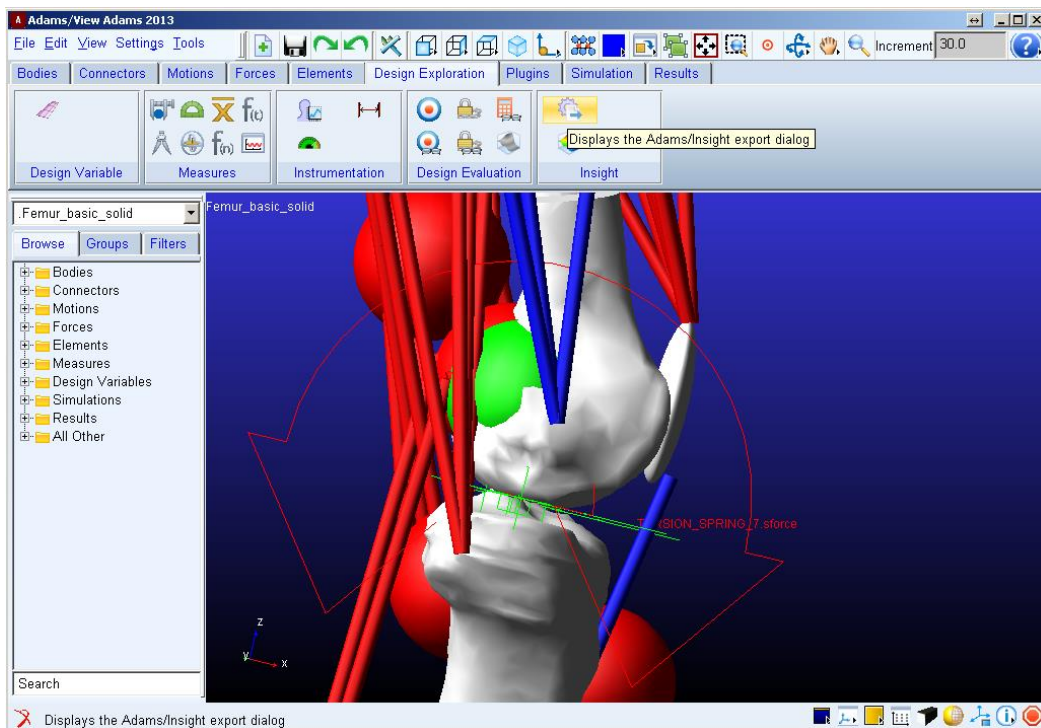


Figure A.11 - Preparing to export the model to ADAMS Insight.

When prompted, a new simulation script was created to carry out a static calculation using ADAMS Solver commands.

The experiment file was then created in ADAMS Insight and the factor and response values to be included in the study were selected. The design specification was selected from the options available as shown in Figure A.12. At this point the number of runs to be completed in preparation of the response surface was given.

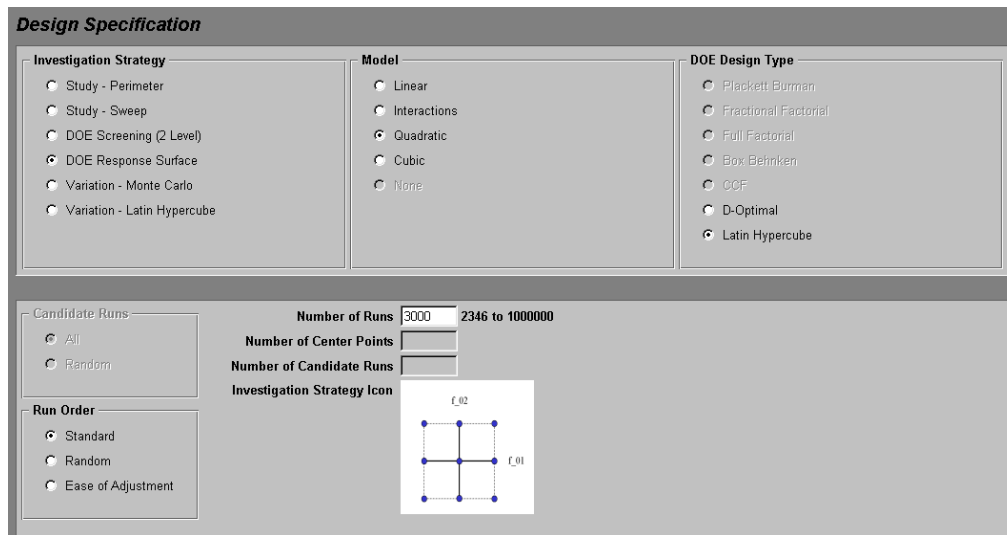


Figure A.12 - Selection of design specification for ADAMS Insight study.

The next step was to generate the workspace, which maps out the factor values to be used for each simulation run. When this was complete, the experiment file was saved and ADAMS Insight was closed, returning to ADAMS View.

The following menu path was used to begin the design study by launching the process of building the model files for each run:

Tools>command navigator>mdi>insight>build

This opened a dialog box where the experiment file previously created in ADAMS Insight was selected. A model file for each simulation run was then created in the working directory including a master batch file to run all the simulations. When the batch file was run, output files for each simulation run were written into the working directory.

The following menu path was then used to load the results back into ADAMS Insight:

Tools>command navigator>mdi>insight>load

When the loading process was complete, ADAMS Insight was opened and the response surface was created by clicking “fit results”.

Completion of this process then allowed the response surface to be optimised by setting targets for response values as shown in Figure A.13.

Optimize model 'Model_01'

Design Variables

	Minimum		Maximum	Value	Fixed
f_01	-1345		0	-1.2506e-12	<input type="checkbox"/>
f_02	-1200		0	-1200	<input type="checkbox"/>
f_03	-295		0	-2.2737e-12	<input type="checkbox"/>
f_04	-631.67		0	-97.264	<input type="checkbox"/>
f_05	-631.67		0	-153.93	<input type="checkbox"/>
f_06	-1013.3		0	-525.68	<input type="checkbox"/>
f_07	-1013.3		0	-240.35	<input type="checkbox"/>
f_08	-196.67		0	-1.7053e-13	<input type="checkbox"/>
f_09	-196.67		0	-35.226	<input type="checkbox"/>
f_10	-855		0	-7.9012e-12	<input type="checkbox"/>

Design Objectives

	Minimum		Maximum	Value	Oper	Target	Weight	Cost
r_01	-5.8962e+05		3.6937e+05	-0.68422	Equal	0	1	
r_02	-3.7208e+05		2.4326e+05	-0.030954	Equal	0	1	
r_03	-1.9012e+05		1.6893e+05	0.12405	Equal	0	1	
r_07	-2.3969e+05		3.4628e+05	0.14703	Equal	0	1	
r_09	-155.18		7811.5	3131.2	Ignore	0	1	
r_10	225.58		8919.8	4643.2	Ignore	0	1	
r_11	-2.4799e+05		1.6326e+05	65218	Ignore	0	1	
r_12	-1.3834e+05		16514	-0.66352	Ignore	0	1	
r_13	-5.3185e+05		1.6863e+05	9.6424	Ignore	0	1	
r_14	3.7736e-09		1.6974e+05	18373	Ignore	0	1	

Figure A.13 - ADAMS Insight response surface optimisation.

Results from this optimisation were exported into a spreadsheet to be used as the starting point for optimisation studies in HEEDS.

An ADAMS Solver Dataset (.adm) file was exported from ADAMS View for each model to act as the main input file for the HEEDS optimisation.

This was associated with a command file to call the simulation script, which referenced the .adm file and output the results into a request file. A list of variables and responses was created in HEEDS to match those in the model. The variable values were then tagged in the .adm file and the response values were tagged in the request file. The constraints and objectives to be used in each study were specified along with the number of optimisation runs to be completed. Figure A.14 shows a HEEDS study running with minimum, maximum, and best values shown on the right, other studies available on the left, the details about the current study in the middle.

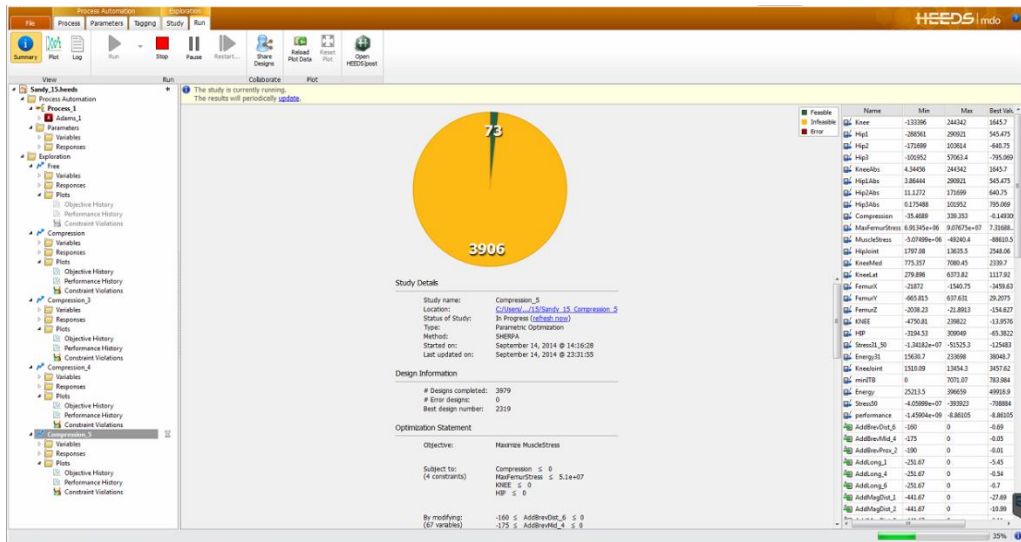


Figure A.14 - Example of a HEEDS study running.

Results from completed optimisation studies were copied into spreadsheets for further analysis.

This is a very brief description of the creation and simulation process relating to the final version of the model to supplement what is contained in the thesis.

Appendix B

Additional Results

This appendix contains results from the model which were not included in the thesis. Although many results were included and discussed, it was not practical to show model-predicted muscle activation for every muscle. Although the content of each figure is clearly indicated, no detailed explanation of the results is given as these are provided for information only.

B. 1 Thirty-One Strand Model

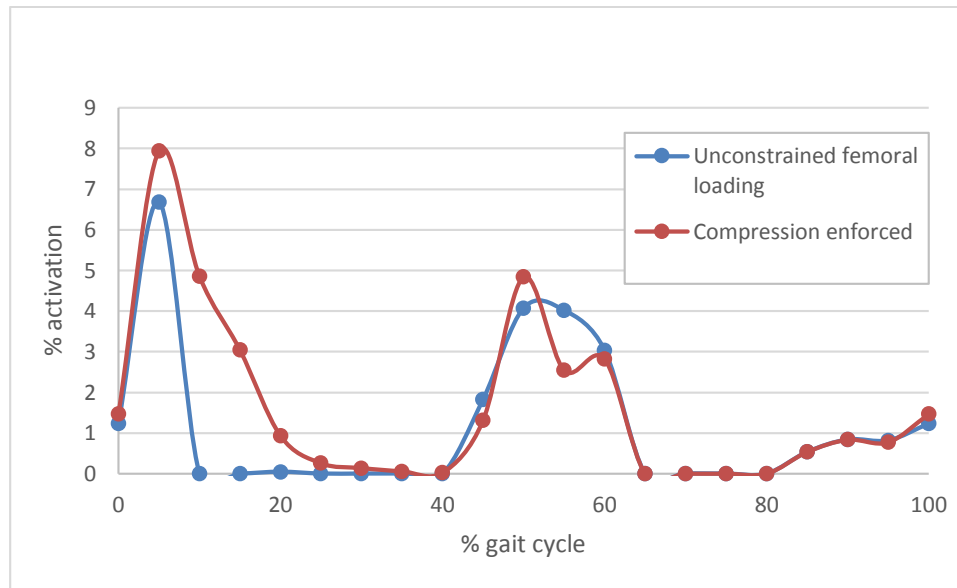


Figure B.1 - Activation of adductors across the gait cycle with and without compression in the femur.

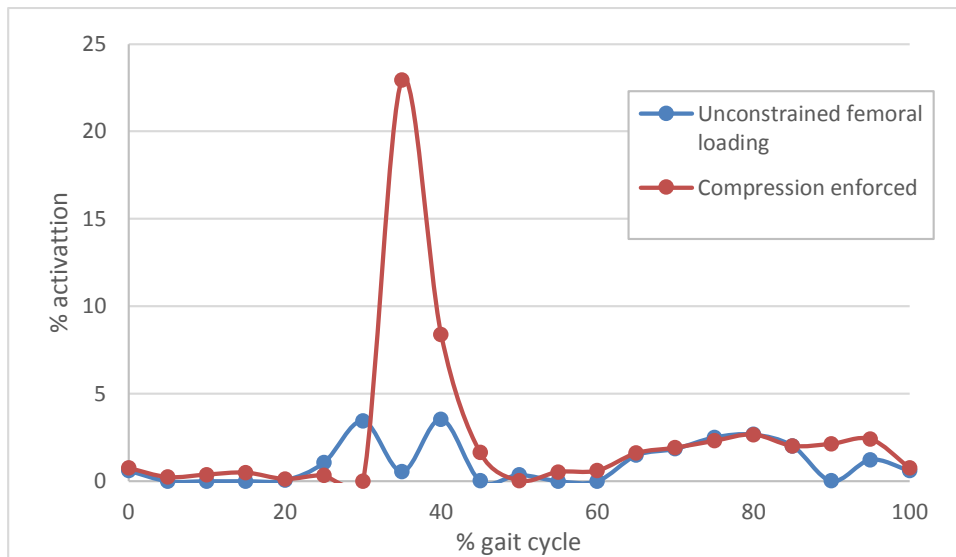


Figure B.2 - Activation of bicep femoris short head across the gait cycle with and without compression in the femur.

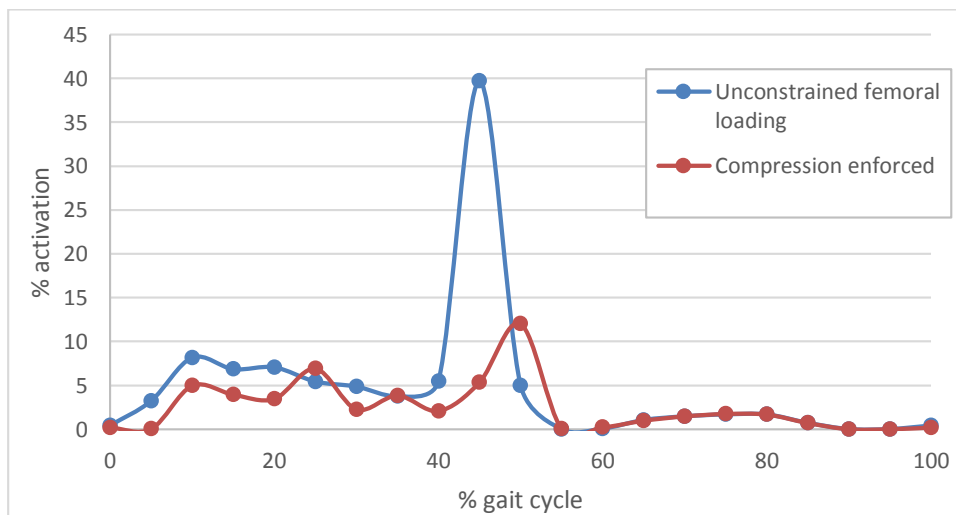


Figure B.3 - Activation of gemellus across the gait cycle with and without compression in the femur.

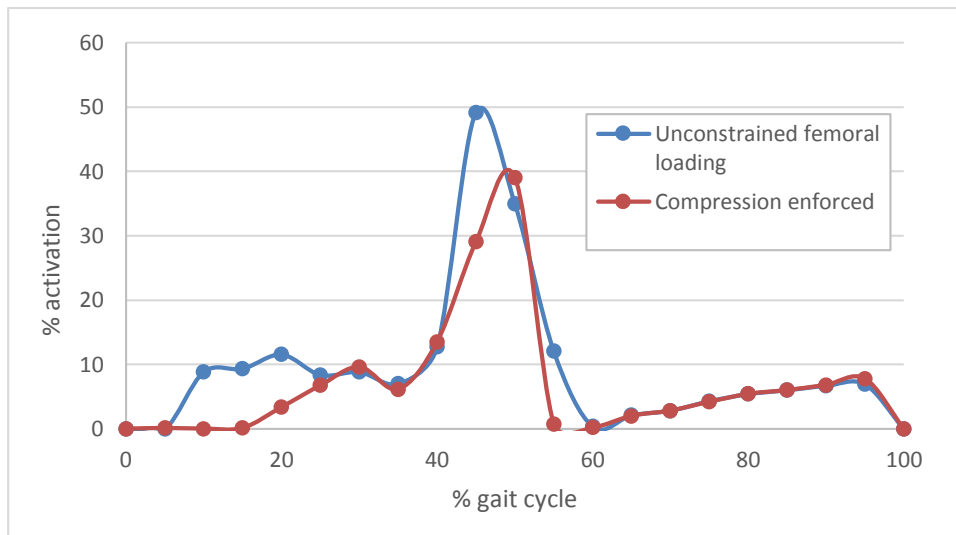


Figure B.4 - Activation of gluteus minimus anterior across the gait cycle with and without compression in the femur.

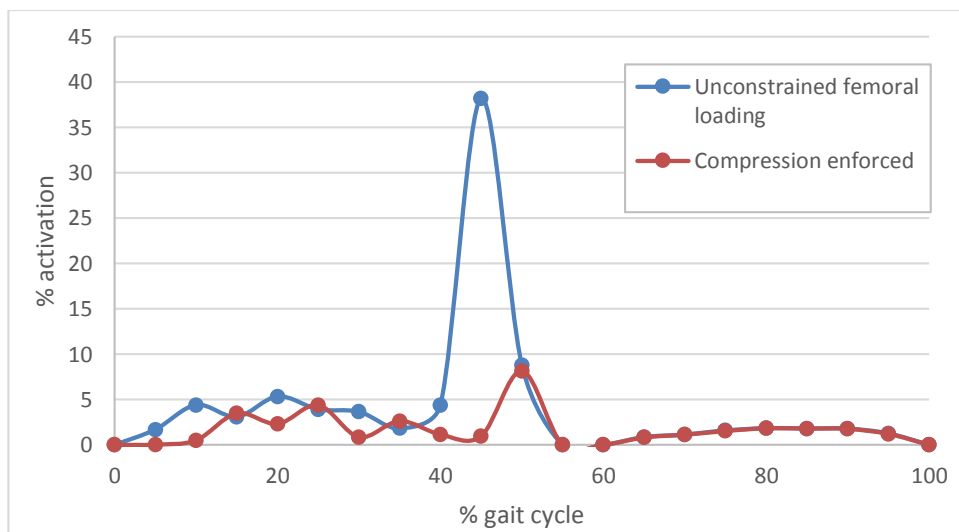


Figure B.5 - Activation of gluteus minimus posterior across the gait cycle with and without compression in the femur.

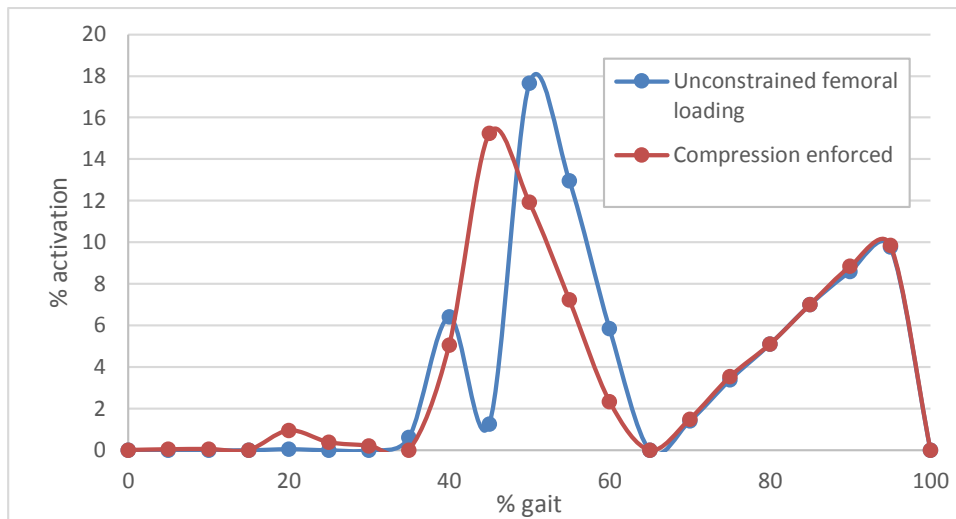


Figure B.6 - Activation of iliacus across the gait cycle with and without compression in the femur.

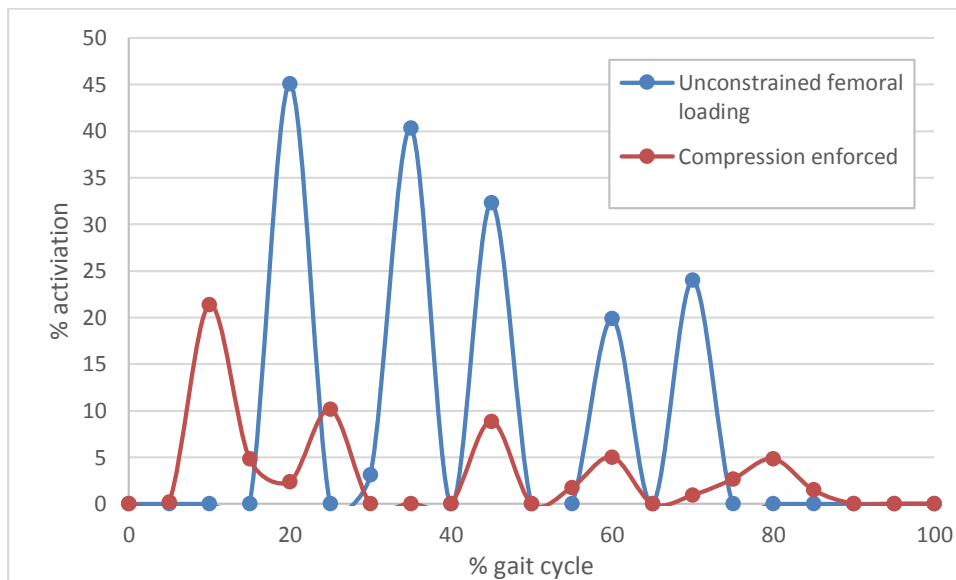


Figure B.7 - Activation of ITB 1 across the gait cycle with and without compression in the femur.

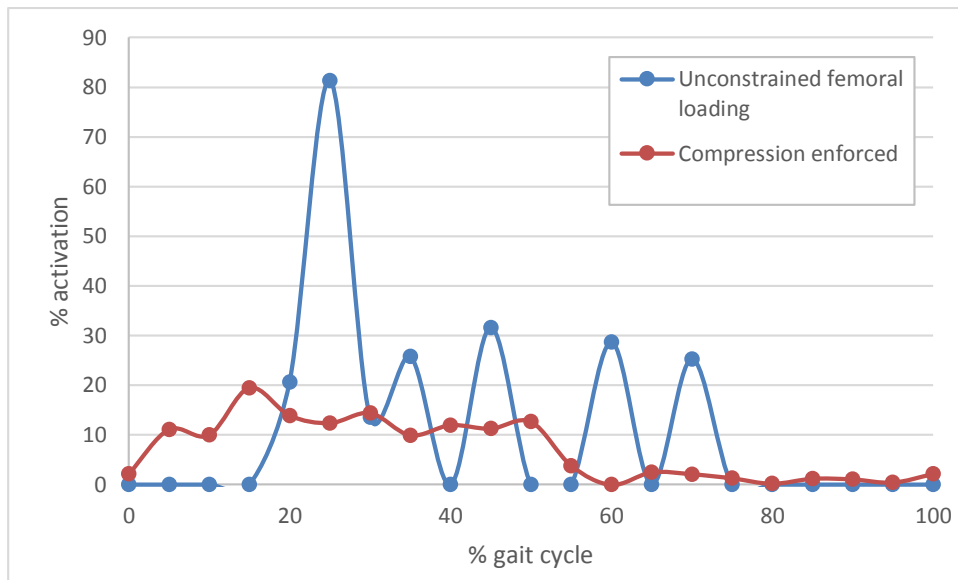


Figure B.8 - Activation of ITB 2 across the gait cycle with and without compression in the femur.

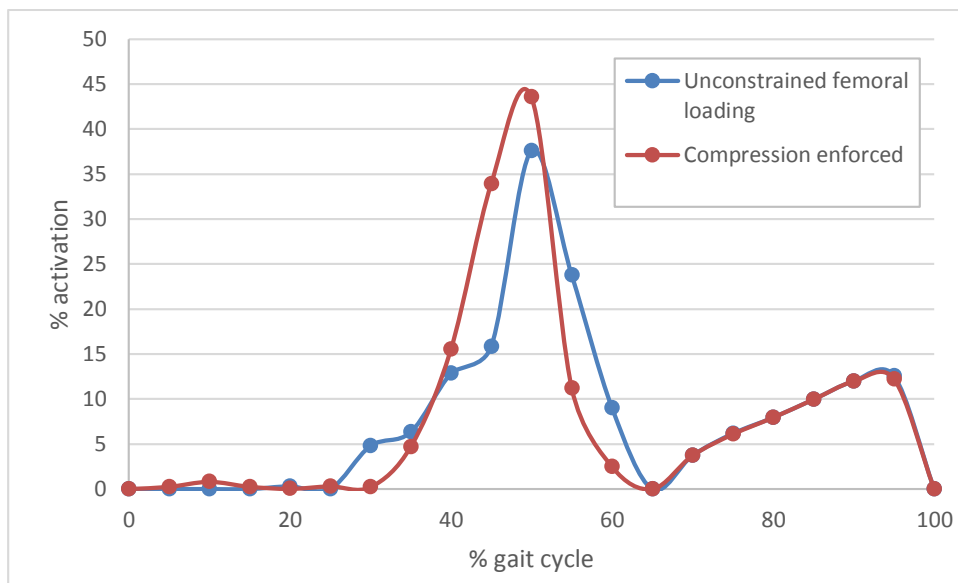


Figure B.9 - Activation of obturator externus across the gait cycle with and without compression in the femur.

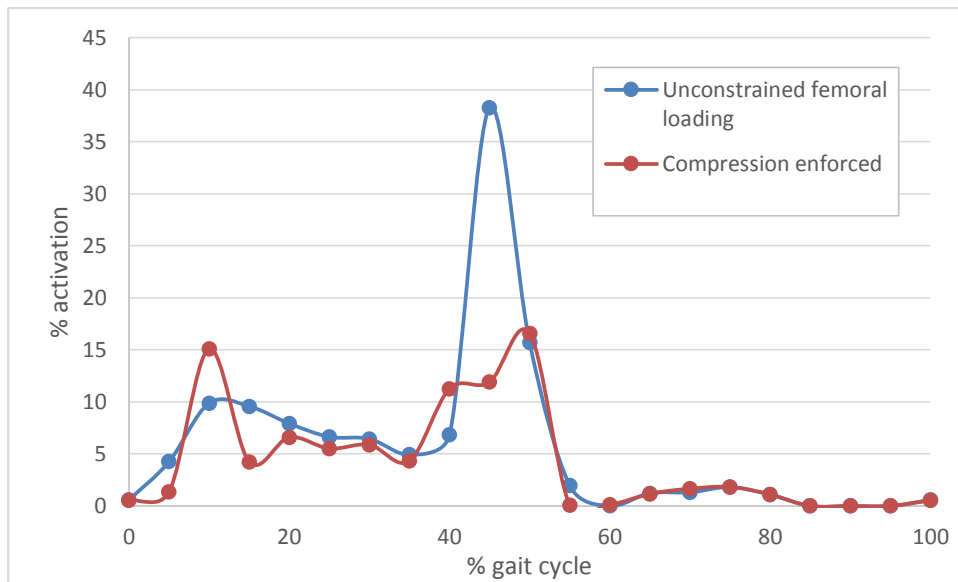


Figure B.10 - Activation of piriformis across the gait cycle with and without compression in the femur.

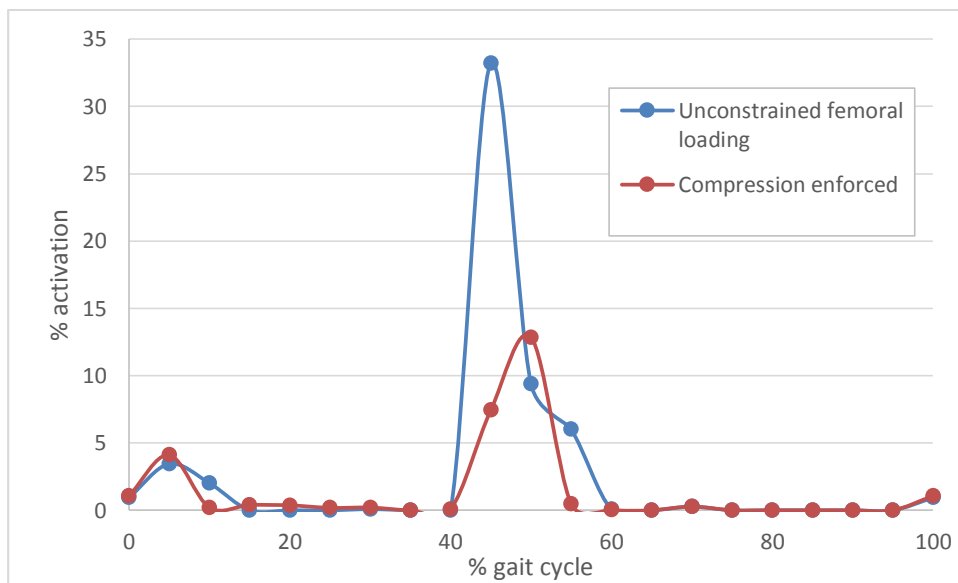


Figure B.11 - Activation of quadratus femoris across the gait cycle with and without compression in the femur.

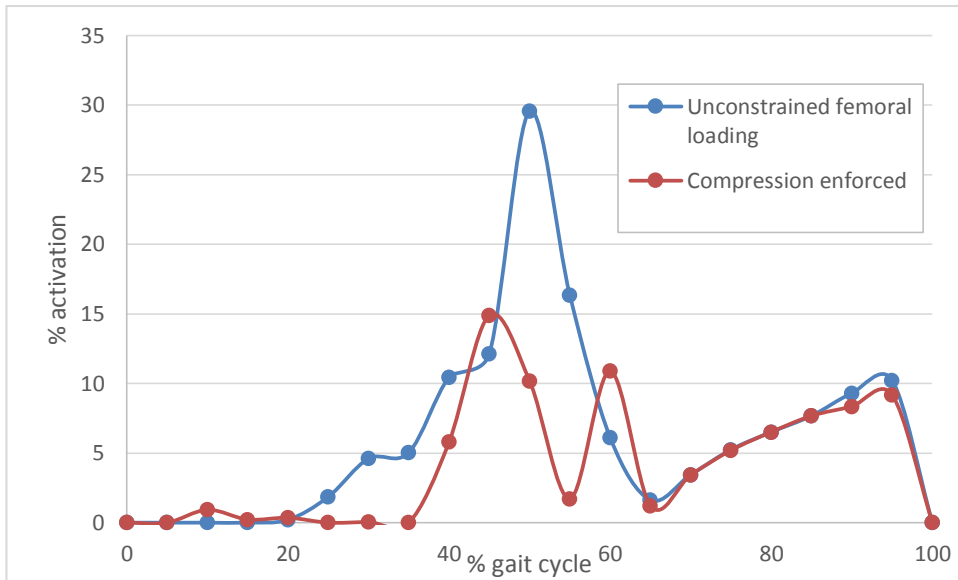


Figure B.12 - Activation of Sartorius across the gait cycle with and without compression in the femur.

B. 2 Sixty-Seven Strand Model

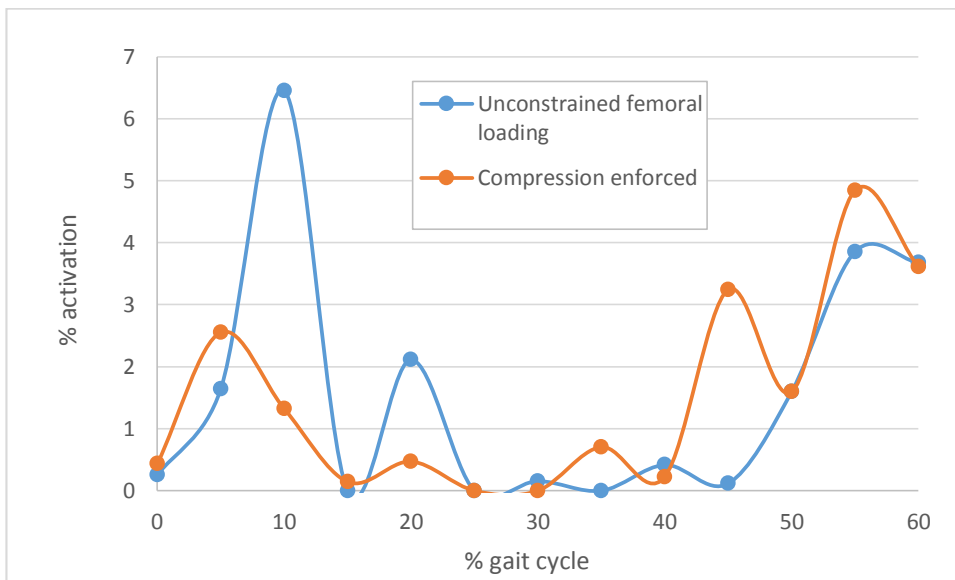


Figure B.13 - Activation of adductor brevis across the stance phase of gait with and without compression in the femur.

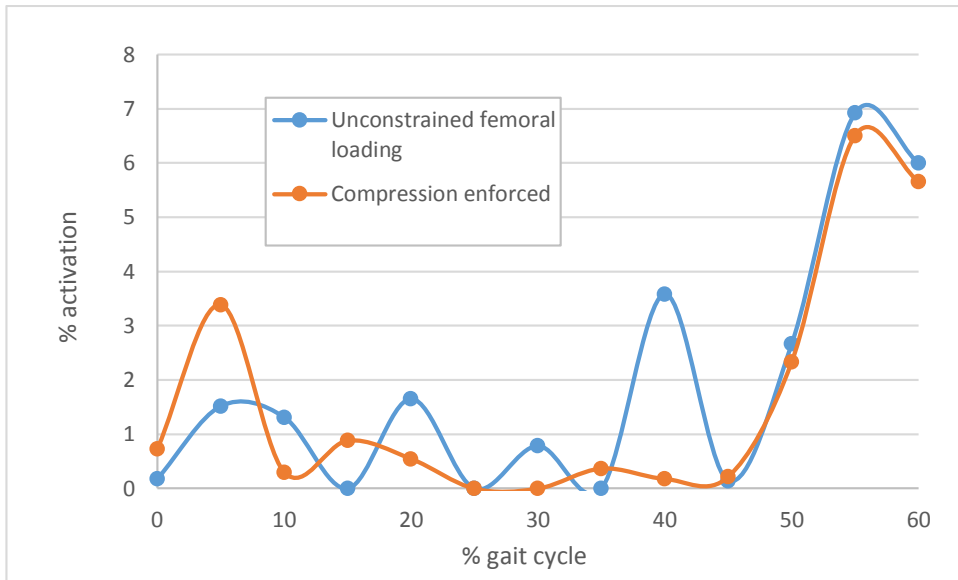


Figure B.14 - Activation of adductor longus across the stance phase of gait with and without compression in the femur.

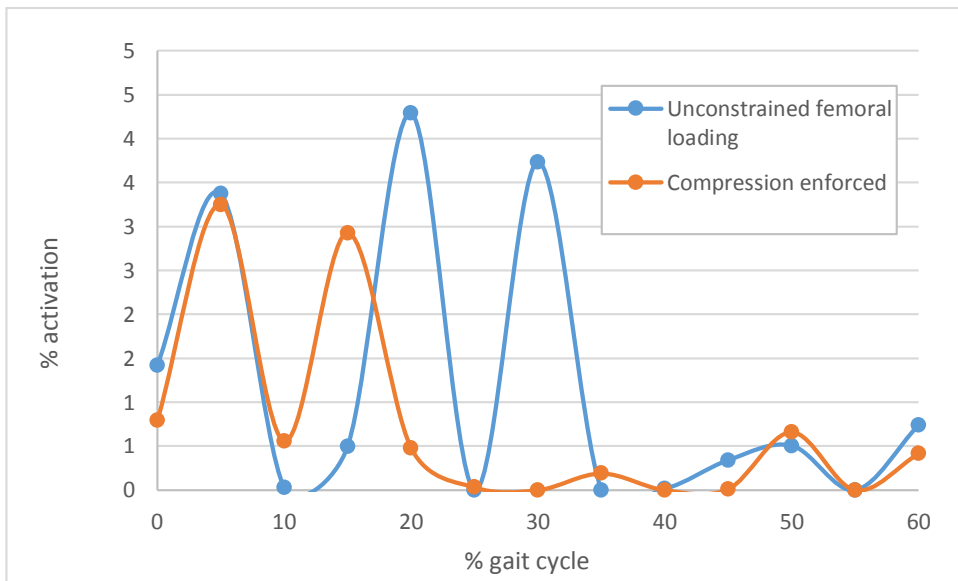


Figure B.15 - Activation of adductor magnus distal across the stance phase of gait with and without compression in the femur.

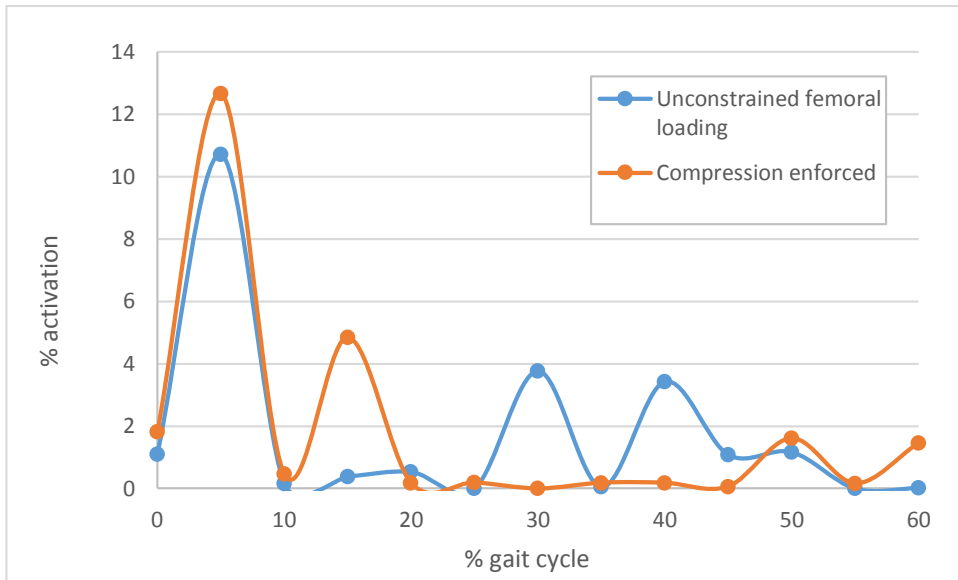


Figure B.16 - Activation of adductor magnus middle across the stance phase of gait with and without compression in the femur.

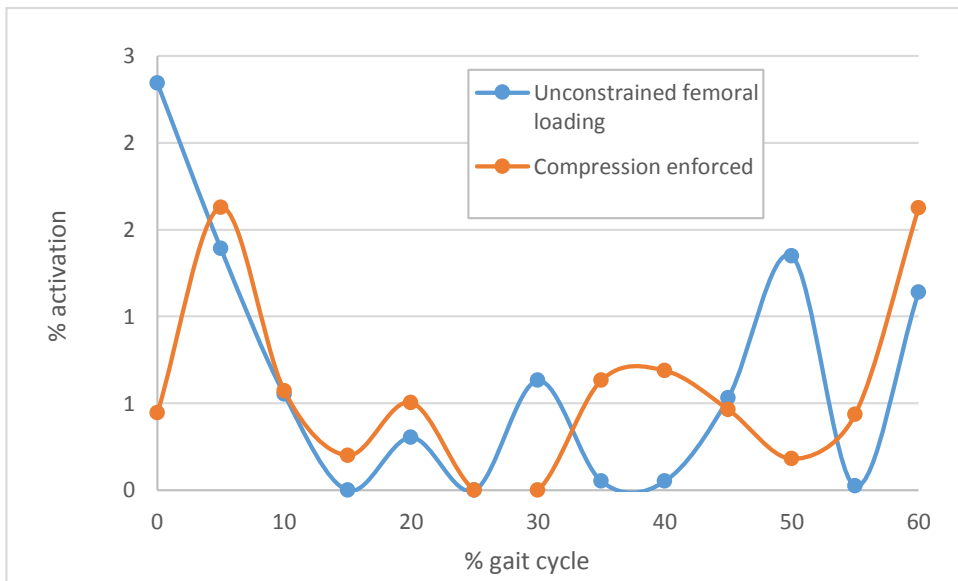


Figure B.17 - Activation of adductor magnus proximal across the stance phase of gait with and without compression in the femur.

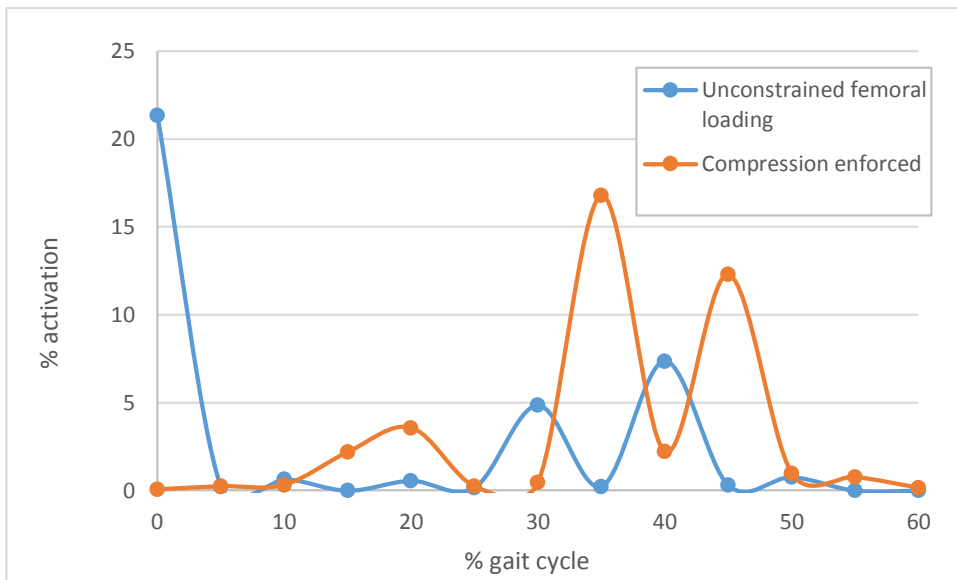


Figure B.18 - Activation of biceps femoris caput breve across the stance phase of gait with and without compression in the femur.

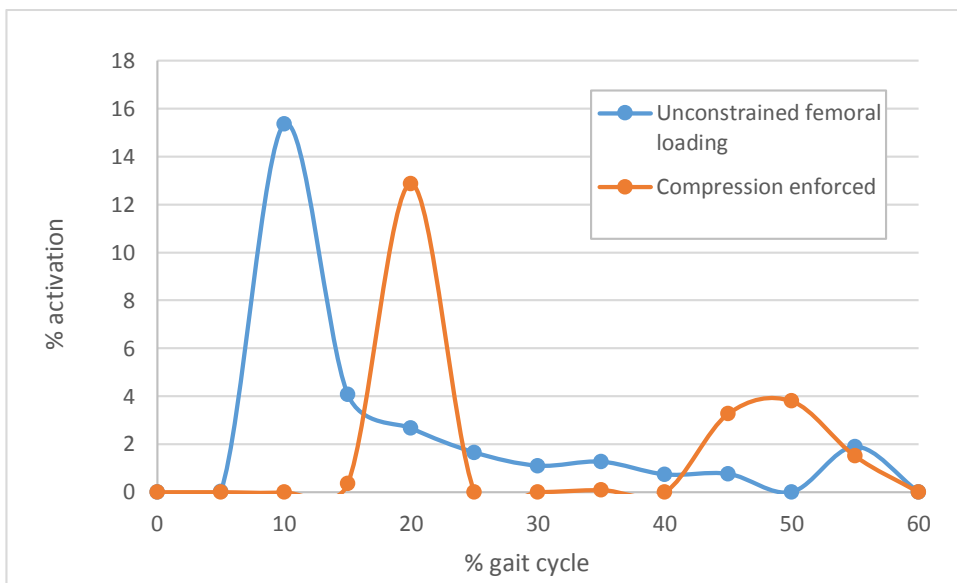


Figure B.19 - Activation of gemellus inferior across the stance phase of gait with and without compression in the femur.

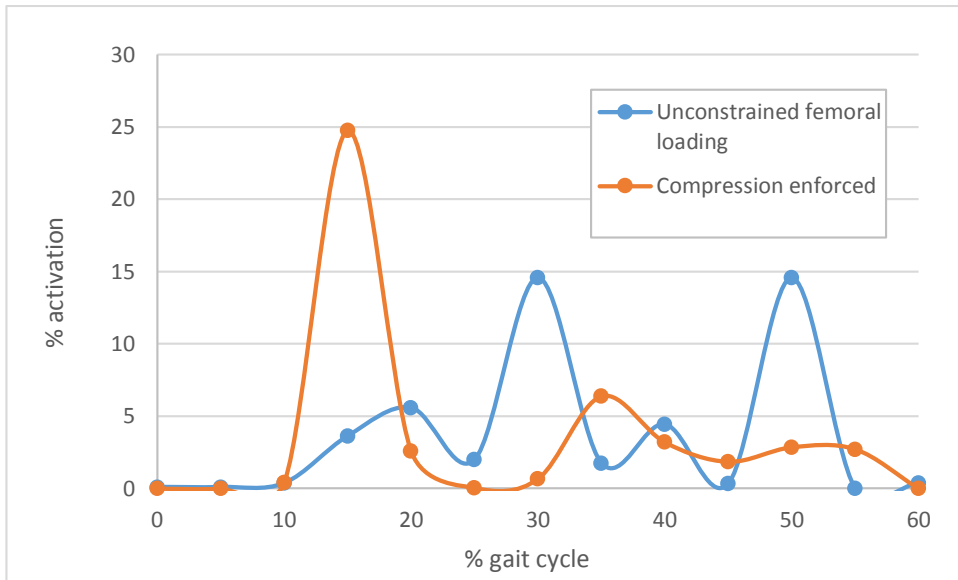


Figure B.20 - Activation of gemellus superior across the stance phase of gait with and without compression in the femur.

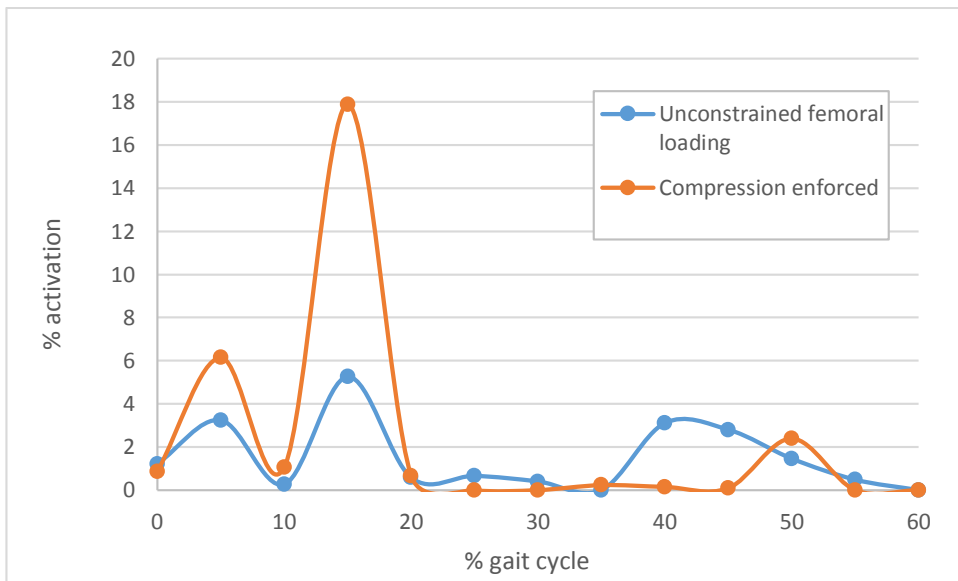


Figure B.21 - Activation of gluteus maximus inferior across the stance phase of gait with and without compression in the femur.

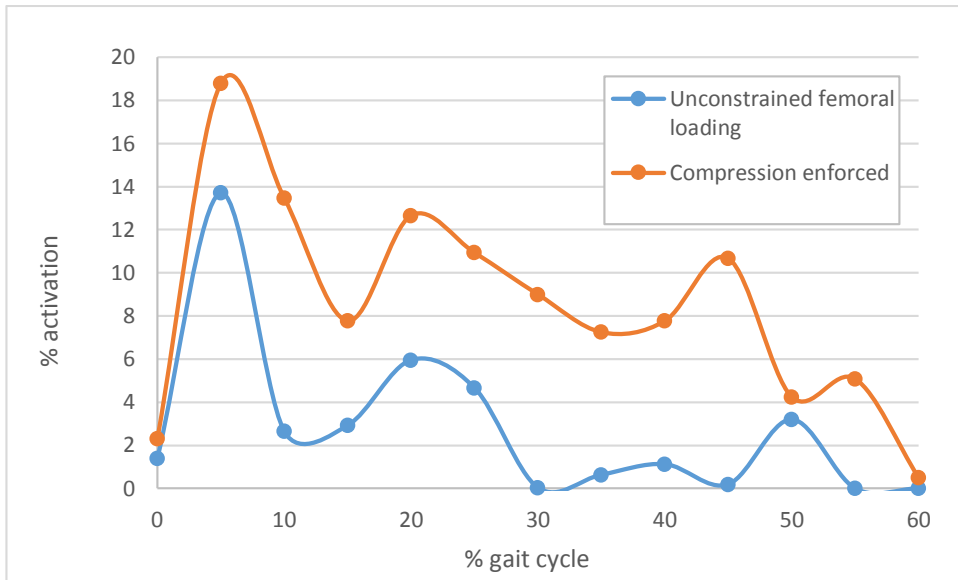


Figure B.22 - Activation of gluteus maximus superior across the stance phase of gait with and without compression in the femur.

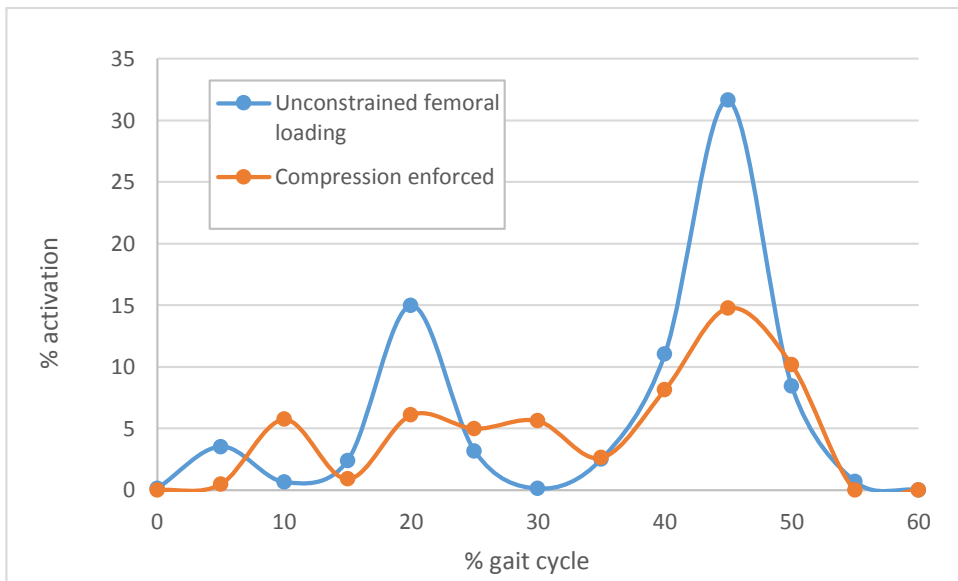


Figure B.23 - Activation of gluteus minimus anterior across the stance phase of gait with and without compression in the femur.

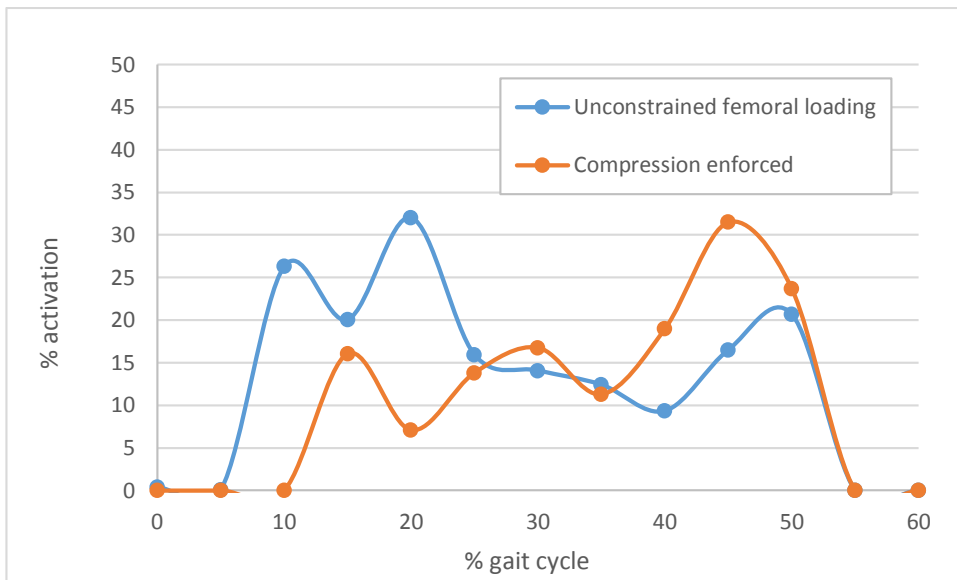


Figure B.24 - Activation of gluteus minimus posterior across the stance phase of gait with and without compression in the femur.

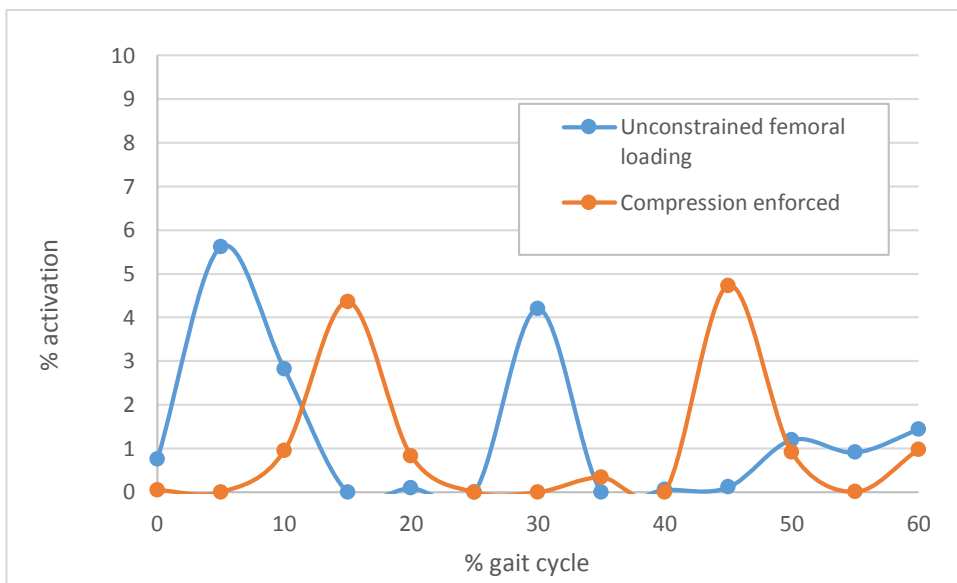


Figure B.25 - Activation of gracilis across the stance phase of gait with and without compression in the femur.

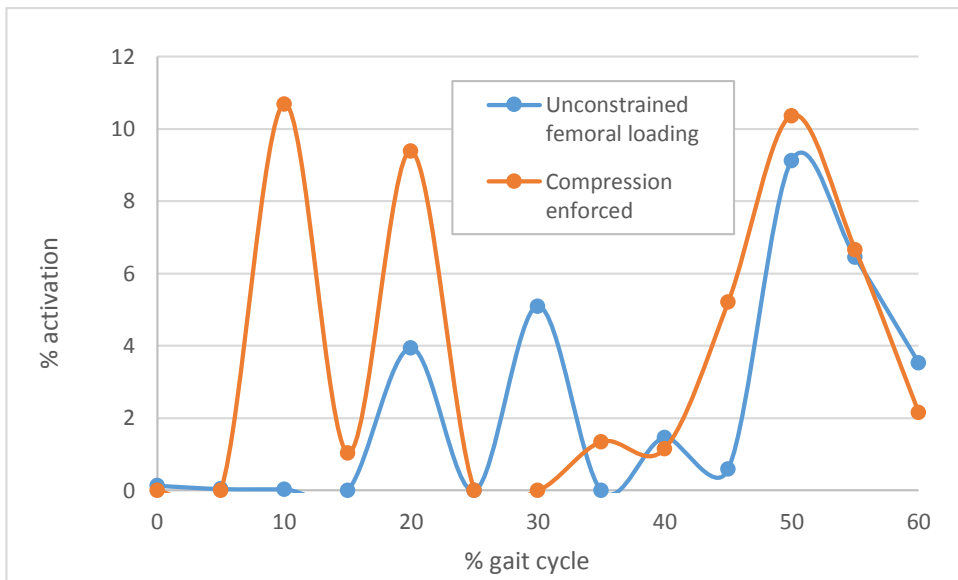


Figure B.26 - Activation of iliacus across the stance phase of gait with and without compression in the femur.

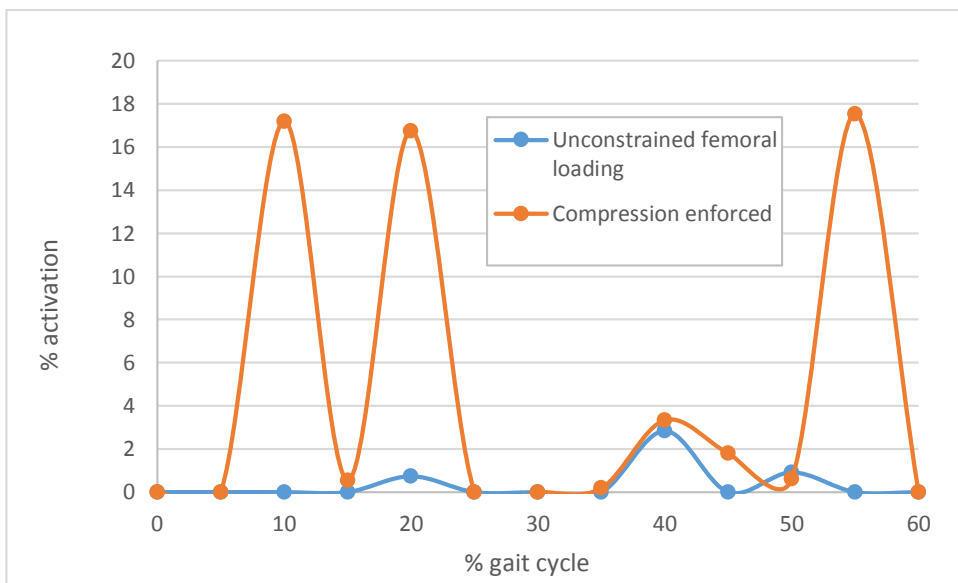


Figure B.27 - Activation of ITB 1 across the stance phase of gait with and without compression in the femur.

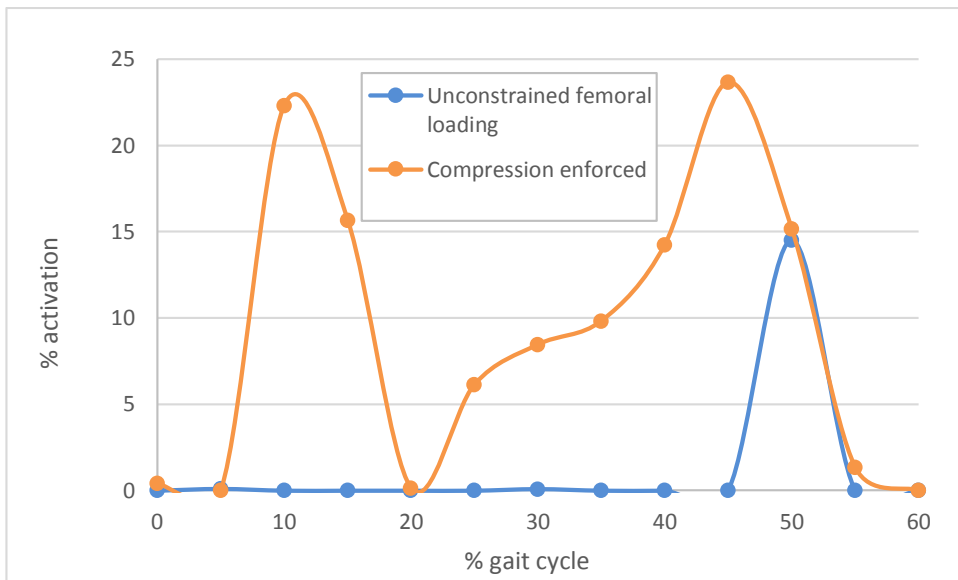


Figure B.28 - Activation of ITB 2 across the stance phase of gait with and without compression in the femur.

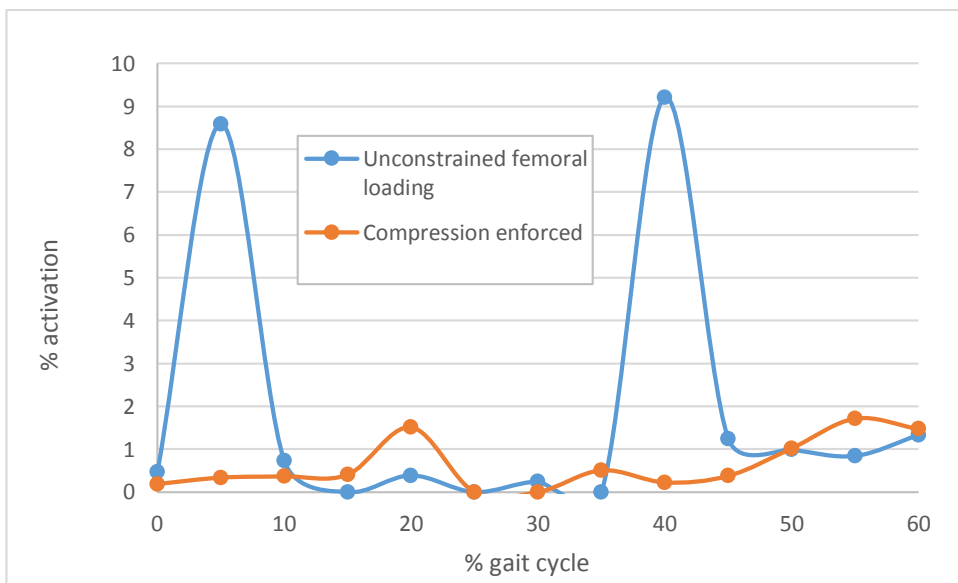


Figure B.29 - Activation of obturator externus inferior across the stance phase of gait with and without compression in the femur.

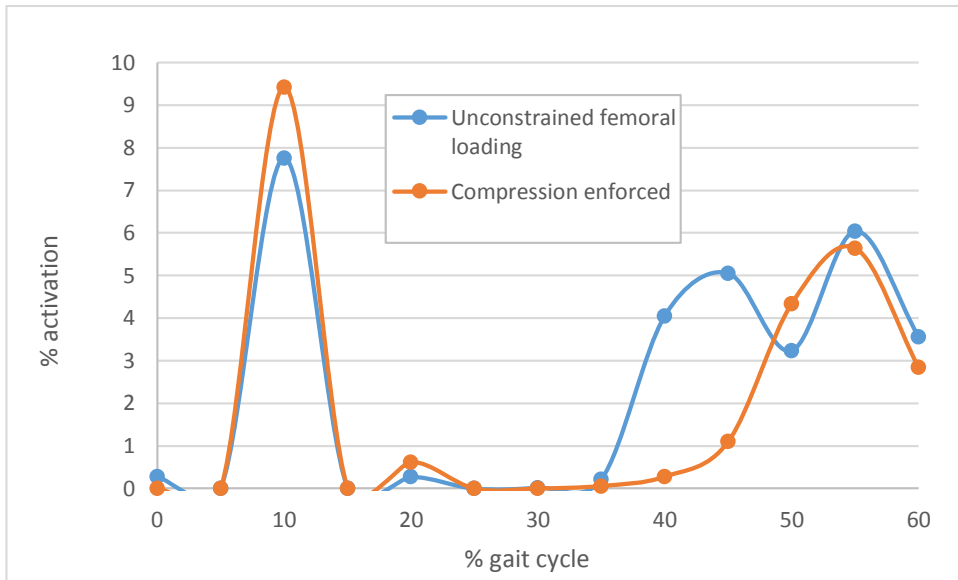


Figure B.30 - Activation of obturator externus superior across the stance phase of gait with and without compression in the femur.

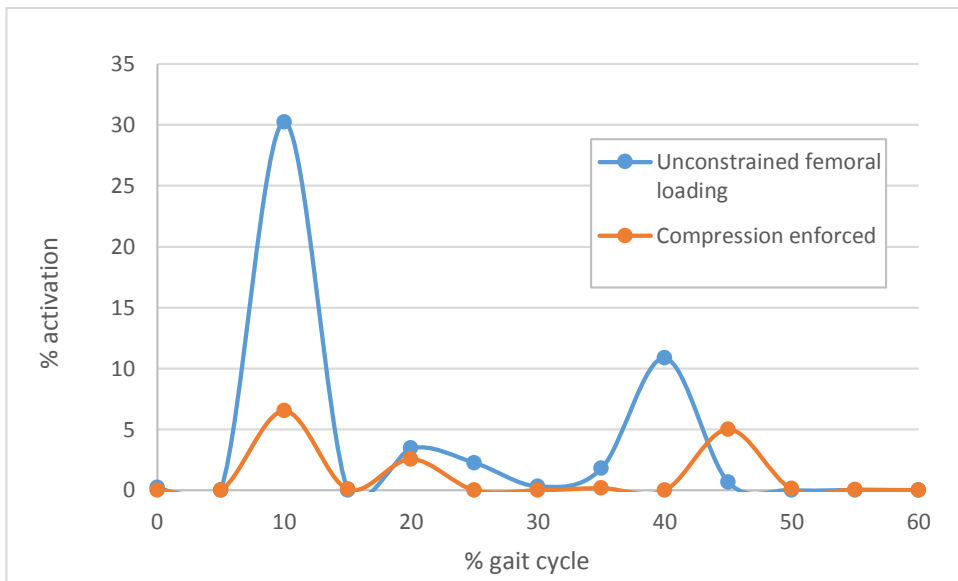


Figure B.31 - Activation of obturator internus across the stance phase of gait with and without compression in the femur.

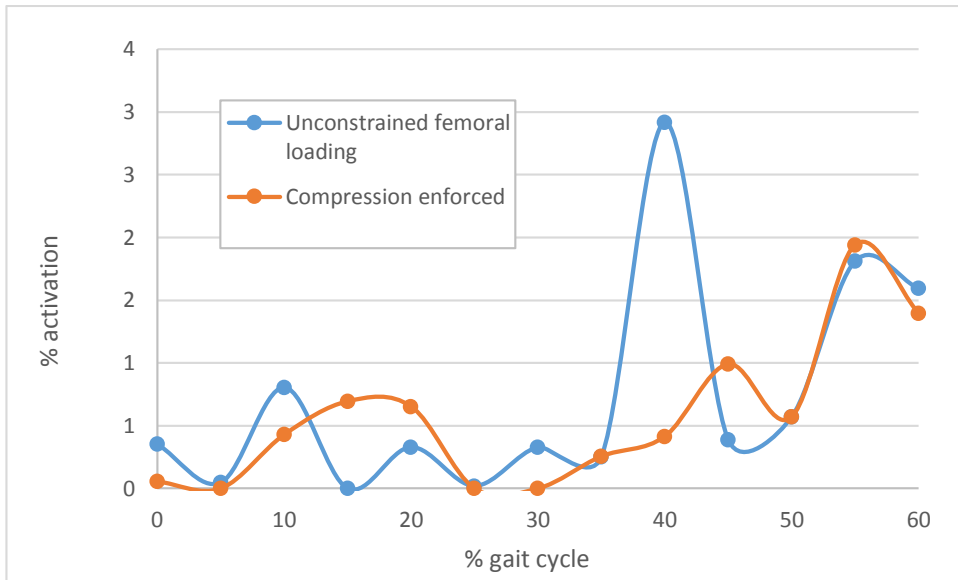


Figure B.32 - Activation of pectineus across the stance phase of gait with and without compression in the femur.

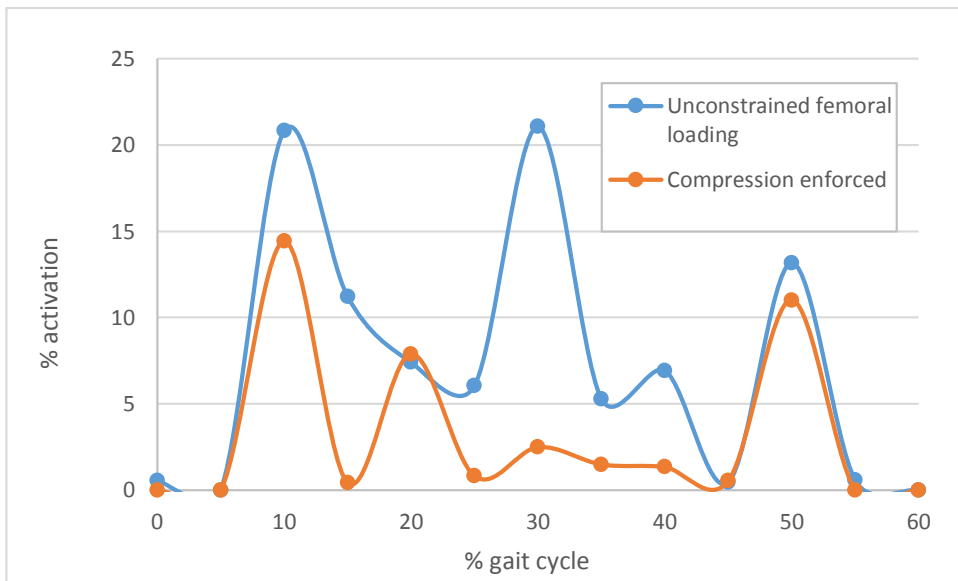


Figure B.33 - Activation of piriformis across the stance phase of gait with and without compression in the femur.

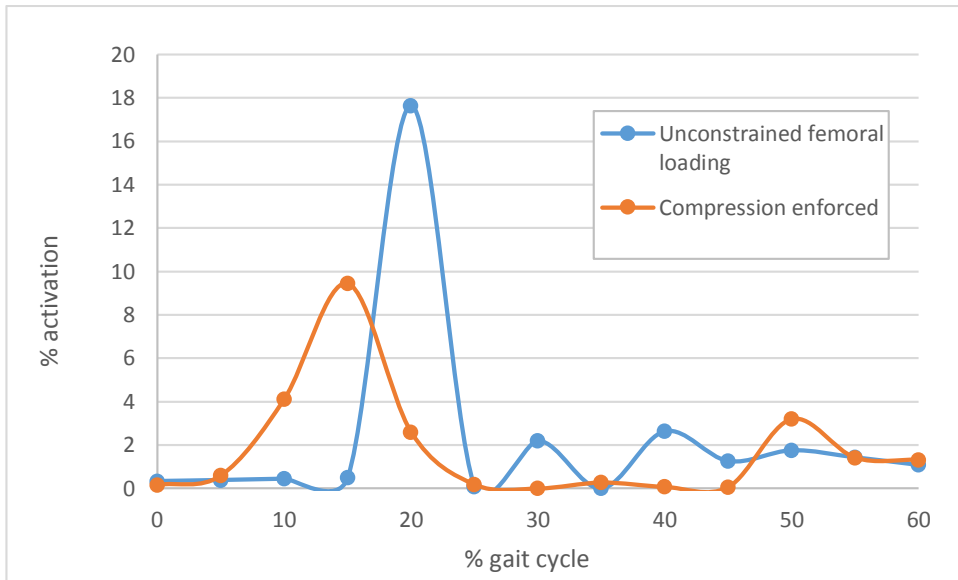


Figure B.34 - Activation of quadratus femoris across the stance phase of gait with and without compression in the femur.

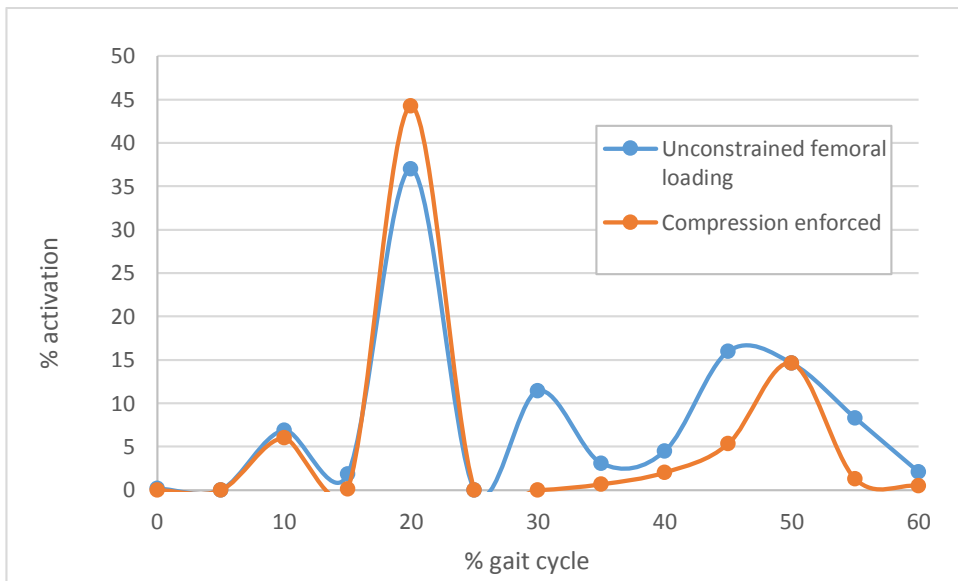


Figure B.35 - Activation of sartorius across the stance phase of gait with and without compression in the femur.

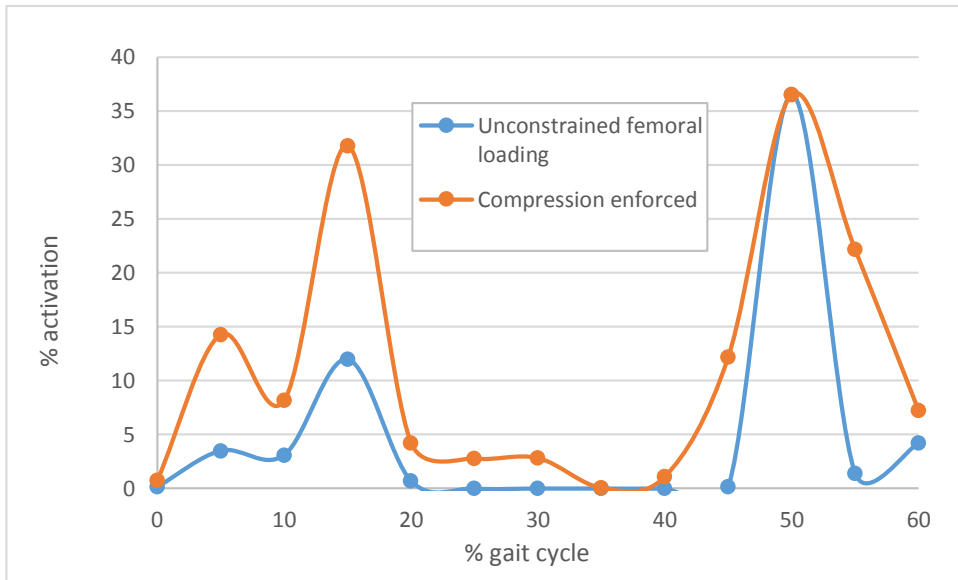


Figure B.36 - Activation of vastus intermedius across the stance phase of gait with and without compression in the femur.

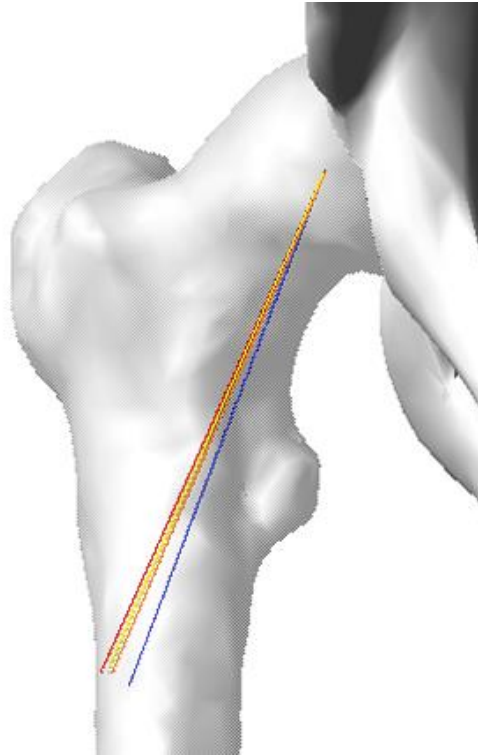


Figure B.37 - Direction of hip joint reaction force in frontal plane at 15 % of gait in various loading conditions. Direction is indicated by a line originating at the centre of the hip and extending in the direction of the hip reaction force. Each coloured line corresponds with a particular simulation type. Blue: Unconstrained femoral loading in 67 strand model, Orange: Compression enforced in 67 strand model, Red: Compression enforced in 67 strand model with max muscle forces reduced by 50%, Yellow: Compression enforced in 31 strand model.

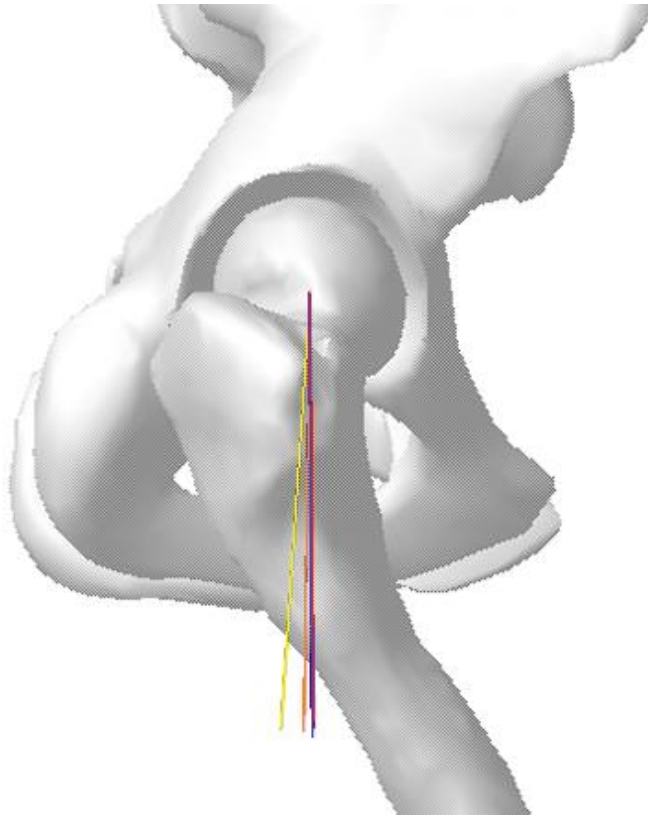


Figure B.38 - Direction of hip joint reaction force in sagittal plane at 15 % of gait in various loading conditions. Direction is indicated by a line originating at the centre of the hip and extending in the direction of the hip reaction force. Each coloured line corresponds with a particular simulation type. Blue: Unconstrained femoral loading in 67 strand model, Orange: Compression enforced in 67 strand model, Red: Compression enforced in 67 strand model with max muscle forces reduced by 50%, Yellow: Compression enforced in 31 strand model.

References

- ABRAHAMSEN B (2012) Atypical femur fractures: Refining the clinical picture. *Journal of Bone and Mineral Research* **27**, 975-976.
- ANDERSEN MS, DE ZEE M, DENDORFER S, MACWILLIAMS B & RASMUSSEN J (2009) Validation of a detailed lower extremity model based on the klein horsman data set. In: *Proceedings of the 12th International Symposium on Computer Simulation in Biomechanics*, Cape Town, South Africa.
- ARNOLD EM, WARD SR, LIEBER RL & DELP SL (2010) A Model of the Lower Limb for Analysis of Human Movement. *Annals of Biomedical Engineering* **38**, 269-279.
- AUWERX J & BOUILLON R (1986) Mineral and bone metabolism in thyroid disease: a review. *The Quarterly journal of medicine* **60**, 737-52.
- BALDWIN KM, WHITE TP, ARNAUD SB, et al. (1996) Musculoskeletal adaptations to weightlessness and development of effective countermeasures. *Medicine and Science in Sports and Exercise* **28**, 1247-1253.
- BERGMANN G, DEURETZBACHER G, HELLER M, et al. (2001) Hip contact forces and gait patterns from routine activities. *Journal of Biomechanics* **34**, 859-871.
- BEZERRA MA, SANTELLI RE, OLIVEIRA EP, VILLAR LS & ESCALEIRA LA (2008) Response surface methodology (RSM) as a tool for optimization in analytical chemistry. *Talanta* **76**, 965-977.
- BLEMKER SS, ASAKAWA DS, GOLD GE & DELP SL (2007) Image-based musculoskeletal modeling: Applications, advances, and future opportunities. *Journal of Magnetic Resonance Imaging* **25**, 441-451.
- BLEMKER SS & DELP SL (2005) Three-dimensional representation of complex muscle architectures and geometries. *Annals of Biomedical Engineering* **33**, 661-673.
- BONEWALD LF (2007) Osteocyte messages from a bony tomb. *Cell Metabolism* **5**, 410-411.
- BONNET N, BENHAMOU CL, MALAVAL L, et al. (2008) Low Dose Beta-Blocker Prevents Ovariectomy-induced Bone Loss in Rats Without Affecting Heart Functions. *Journal of Cellular Physiology* **217**, 819-827.
- BONNET N, LAROCHE N, VICO L, DOLLEANS E, BENHAMOU CL & COURTEIX D (2006) Dose effects of propranolol on cancellous and cortical bone in ovariectomized adult rats. *Journal of Pharmacology and Experimental Therapeutics* **318**, 1118-1127.
- BOUXSEIN ML, DEVLIN MJ, GLATT V, DHILLON H, PIERROZ DD & FERRARI SL (2009) Mice Lacking beta-Adrenergic Receptors Have Increased Bone Mass but Are Not Protected from Deleterious Skeletal Effects of Ovariectomy. *Endocrinology* **150**, 144-152.
- BRAND RA, PEDERSEN DR & FRIEDERICH JA (1986) The sensitivity of muscle force predictions to changes in physiological cross-sectional area. *Journal of Biomechanics* **19**, 589-596.
- BRAZIER M, KAMEL S, MAAMER M, et al. (1995) Markers of bone remodeling in the elderly subject: Effects of vitamin D insufficiency and its correction. *Journal of Bone and Mineral Research* **10**, 1753-1761.
- BURT-PICHAT B, LAFAGE-PROUST MH, DUBOEU F, et al. (2005) Dramatic decrease of innervation density in bone after ovariectomy. *Endocrinology* **146**, 503-510.
- CALBET JAL, MOYSI JS, DORADO C & RODRIGUEZ LP (1998) Bone mineral content and density in professional tennis players. *Calcified Tissue International* **62**, 491-496.

- CALIGARIS M & ATESHIAN GA (2008) Effects of sustained interstitial fluid pressurization under migrating contact area, and boundary lubrication by synovial fluid, on cartilage friction. *Osteoarthritis and Cartilage* **16**, 1220-1227.
- CAMPBELL MJ, MCCOMAS AJ & PETITO F (1973) Physiological changes in aging muscles. *Journal of Neurology Neurosurgery and Psychiatry* **36**, 174-182.
- CARBONE V, VAN DER KROGT MM, KOOPMAN HFJM & VERDONSCHOT N (2012) Sensitivity of subject-specific models to errors in musculo-skeletal geometry. *Journal of Biomechanics* **45**, 2476-2480.
- CARMELIET G, VICO L & BOUILLON R (2001) Space flight: A challenge for normal bone homeostasis. *Critical Reviews in Eukaryotic Gene Expression* **11**, 131-144.
- CARTER ND, KANNUS P & KHAN KM (2001) Exercise in the prevention of falls in older people - A systematic literature review examining the rationale and the evidence. *Sports Medicine* **31**, 427-438.
- CHAPUY MC, ARLOT ME, DUBOEU F, et al. (1992) Vitamin D3 and calcium to prevent hip fractures in elderly women. *New England Journal of Medicine* **327**, 1637-1642.
- CHEN JH, LIU C, YOU LD & SIMMONS CA (2010) Boning up on Wolff's Law: Mechanical regulation of the cells that make and maintain bone. *J. Biomech.* **43**, 108-118.
- CHEN JS & SAMBROOK PN (2012) Antiresorptive therapies for osteoporosis: a clinical overview. *Nature Reviews Endocrinology* **8**, 81-91.
- CHENU C (2004) Role of innervation in the control of bone remodeling. *Journal of Musculoskeletal & Neuronal Interactions* **4**, 132-134.
- CHENU C & MARENZANA M (2005) Sympathetic nervous system and bone remodeling. *Joint Bone Spine* **72**, 481-483.
- COGGAN AR, SPINA RJ, KING DS, et al. (1992a) Histochemical and enzymatic comparison of the gastrocnemius-muscle of young and elderly men and women. *Journals of Gerontology* **47**, B71-B76.
- COGGAN AR, SPINA RJ, KING DS, et al. (1992b) Skeletal-muscle adaptations to endurance training in 60-yr-old to 70-yr-old men and women. *Journal of Applied Physiology* **72**, 1780-1786.
- COOPER C (1997) The crippling consequences of fractures and their impact on quality of life. *American Journal of Medicine* **103**, 12S-19S.
- COURTBROWN CM & MCBIRNIE J (1995) The epidemiology of tibial fractures. *Journal of Bone and Joint Surgery-British Volume* **77B**, 417-421.
- CROSS R (1999) Standing, walking, running, and jumping on a force plate. *American Journal of Physics* **67**, 304-309.
- CROWNINSHIELD RD & BRAND RA (1981) A physiologically based criterion of muscle force prediction in locomotion. *Journal of Biomechanics* **14**, 793-801.
- CUNHA-HENRIQUES S, COSTA-PAIVA L, PINTO-NETO AM, FONSECHI-CARVESAN G, NANNI L & MORAIS SS (2011) Postmenopausal women with osteoporosis and musculoskeletal status: a comparative cross-sectional study. *Journal of clinical medicine research* **3**, 168-76.
- CUPPONE M, SEEDHOM BB, BERRY E & OSTELL AE (2004) The longitudinal Young's modulus of cortical bone in the midshaft of human femur and its correlation with CT scanning data. *Calcified Tissue International* **74**.
- CURTIS N, KUPCZIK K, O'HIGGINS P, MOAZEN M & FAGAN M (2008) Predicting skull loading: Applying multibody dynamics analysis to a macaque skull. *Anatomical Record-Advances in Integrative Anatomy and Evolutionary Biology* **291**, 491-501.

- DE LUCA CJ (1997) The use of surface electromyography in biomechanics. *Journal of Applied Biomechanics* **13**, 135-163.
- DE SOUZA RL, PITSILLIDES AA, LANYON LE, SKERRY TM & CHENU C (2005) Sympathetic nervous system does not mediate the load-induced cortical new bone formation. *Journal of Bone and Mineral Research* **20**, 2159-2168.
- DELP SL, ANDERSON FC, ARNOLD AS, et al. (2007) OpenSim: open-source software to create and analyze dynamic Simulations of movement. *Ieee Transactions on Biomedical Engineering* **54**, 1940-1950.
- DENNISON E, COLE Z & COOPER C (2005) Diagnosis and epidemiology of osteoporosis. *Current Opinion in Rheumatology* **17**, 456-461.
- DEVITA P & HORTOBAGYI T (2000) Age causes a redistribution of joint torques and powers during gait. *Journal of Applied Physiology* **88**, 1804-1811.
- DUCHEN LW (1970) Changes in motor innervation and cholinesterase localization induced by botulinum toxin in skeletal muscle of mouse - differences between fast and slow muscles. *Journal of Neurology Neurosurgery and Psychiatry* **33**, 40
- DUL J, JOHNSON GE, SHIAMI R & TOWNSEND MA (1984) Muscular synergism .2. A minimum-fatigue criterion for load sharing between synergistic muscles. *Journal of Biomechanics* **17**, 675-684.
- EBACHER V, TANG C, MCKAY H, OXLAND TR, GUY P & WANG R (2007) Strain redistribution and cracking behavior of human bone during bending. *Bone* **40**, 1265-1275.
- ELEFTERIOU F (2005) Neuronal signaling and the regulation of bone remodeling. *Cellular and Molecular Life Sciences* **62**, 2339-2349.
- ELEFTERIOU F, AHN JD, TAKEDA S, et al. (2005) Leptin regulation of bone resorption by the sympathetic nervous system and CART. *Nature* **434**, 514-520.
- ELMQUIST JK & STREWLER GJ (2005) Physiology - Do neural signals remodel bone? *Nature* **434**, 447-448.
- ERDEMIR A, MCLEAN S, HERZOG W & VAN DEN BOGERT AJ (2007) Model-based estimation of muscle forces exerted during movements. *Clinical Biomechanics* **22**, 131-154.
- FRONTERA WR, HUGHES VA, FIELDING RA, FIATARONE MA, EVANS WJ & ROUBENOFF R (2000) Aging of skeletal muscle: a 12-yr longitudinal study. *Journal of Applied Physiology* **88**, 1321-1326.
- FROST HM (1963) *Bone Remodelling Dynamics.* Charles C. Thomas, Springfield, IL.
- FROST HM (1988) Vital biomechanics - proposed general concepts for skeletal adaptations to mechanical usage. *Calcified Tissue International* **42**, 145-156.
- GILSANZ V, AL WREN T, SANCHEZ M, DOREY F, JUDEX S & RUBIN C (2006) Low-level, high-frequency mechanical signals enhance musculoskeletal development of young women with low BMD. *Journal of Bone and Mineral Research* **21**, 1464-1474.
- GLITSCH U & BAUMANN W (1997) The three-dimensional determination of internal loads in the lower extremity. *Journal of Biomechanics* **30**, 1123-1131.
- GRADOS F, BRAZIER M, KAMEL S, et al. (2003) Effects on bone mineral density of calcium and vitamin D supplementation in elderly women with vitamin D deficiency. *Joint Bone Spine* **70**, 203-208.
- GREGORY JS & ASPDEN RM (2008) Femoral geometry as a risk factor for osteoporotic hip fracture in men and women. *Medical Engineering & Physics* **30**, 1275-1286.

- GRONING F, JONES MEH, CURTIS N, et al. (2013) The importance of accurate muscle modelling for biomechanical analyses: a case study with a lizard skull. *Journal of the Royal Society Interface* **10**.
- GROSS TS & RUBIN CT (1995) Uniformity of resorptive bone loss induced by disuse. *Journal of Orthopaedic Research* **13**, 708-714.
- HAMMER A (2010) The structure of the femoral neck: A physical dissection with emphasis on the internal trabecular system. *Annals of Anatomy-Anatomischer Anzeiger* **192**, 168-177.
- HE J-Y, JIANG L-S & DAI L-Y (2011) The roles of the sympathetic nervous system in osteoporotic diseases: A review of experimental and clinical studies. *Ageing Research Reviews* **10**, 253-263.
- HELTON JC & DAVIS FJ (2003) Latin hypercube sampling and the propagation of uncertainty in analyses of complex systems. *Reliability Engineering & System Safety* **81**, 23-69.
- HELTON JC, JOHNSON JD, SALLABERRY CJ & STORLIE CB (2006) Survey of sampling-based methods for uncertainty and sensitivity analysis. *Reliability Engineering & System Safety* **91**, 1175-1209.
- HERT J, SKLENSKA A & LISKOVA M (1971) Reaction of bone to mechanical stimuli. 5. Effect of intermittent stress on the rabbit tibia after resection of the peripheral nerves. *Folia Morphologica* **19**, 378-387.
- HORTOBAGYI T, ZHENG DH, WEIDNER M, LAMBERT NJ, WESTBROOK S & HOUMARD JA (1995) The influence of aging on muscle strength and muscle-fiber characteristics with special reference to eccentric strength. *Journals of Gerontology Series a-Biological Sciences and Medical Sciences* **50**, B399-B406.
- HUANG RP, RUBIN CT & MCLEOD KJ (1999) Changes in postural muscle dynamics as a function of age. *J. Gerontol. Ser. A-Biol. Sci. Med. Sci.* **54**, B352-B357.
- HUANG T-H, LIN H-S, CHEN H-I & YANG R-S (2011) The effects of systemic chemical sympathectomy on local bone loss induced by sciatic neurectomy. *Journal of Orthopaedic Science* **16**, 629-637.
- HUNT AE, M. SMITH R, TORODE M & KEENAN A-M (2001) Inter-segment foot motion and ground reaction forces over the stance phase of walking. *Clinical Biomechanics* **16**, 592-600.
- HURLEY BF & HAGBERG JM (1998) Optimizing health in older persons: Aerobic or strength training? *Exercise and Sport Sciences Reviews*, Volume 28, 1998 **26**, 61-89.
- IZQUIERDO M, IBANEZ J, GOROSTIAGA E, et al. (1999) Maximal strength and power characteristics in isometric and dynamic actions of the upper and lower extremities in middle-aged and older men. *Acta Physiologica Scandinavica* **167**, 57-68.
- JUDEX S & CARLSON KJ (2009) Is Bone's Response to Mechanical Signals Dominated by Gravitational Loading? *Medicine and Science in Sports and Exercise* **41**, 2037-2043.
- JUDEX S & RUBIN CT (2010) Is bone formation induced by high-frequency mechanical signals modulated by muscle activity? *Journal of Musculoskeletal & Neuronal Interactions* **10**, 3-11.
- KADABA MP, RAMAKRISHNAN HK & WOOTTEN ME (1990) Measurement of lower extremity kinematics during level walking. *Journal of Orthopaedic Research* **8**, 383-392.

- KENT-BRAUN JA, NG AV & YOUNG K (2000) Skeletal muscle contractile and noncontractile components in young and older women and men. *Journal of Applied Physiology* **88**, 662-668.
- KLEIN HORSMAN MD, KOOPMAN HFJM, VAN DER HELM FCT, PROSE LP & VEEGER HEJ (2007) Morphological muscle and joint parameters for musculoskeletal modelling of the lower extremity. *Clin Biomech (Bristol, Avon)* **22**, 239-47.
- KRAEMER WJ, FLECK SJ & EVANS WJ (1996) Strength and power training: physiological mechanisms of adaptation. *Exercise and sport sciences reviews* **24**, 363-97.
- LAM H, HU MY & QIN YX (2011) Alteration of contraction-to-rest ratio to optimize trabecular bone adaptation induced by dynamic muscle stimulation. *Bone* **48**, 399-405.
- LAM H & QIN YX (2008) The effects of frequency-dependent dynamic muscle stimulation on inhibition of trabecular bone loss in a disuse model. *Bone* **43**, 1093-1100.
- LANYON LE & RUBIN CT (1984) Static vs dynamic loads as an influence on bone remodeling. *Journal of Biomechanics* **17**, 897-905.
- LASDON LS, FOX RL & RATNER MW (1974) Nonlinear optimization using generalized reduced gradient method. *Revue Francaise D Automatique Informatique Recherche Operationnelle* **8**.
- LEE MS, PITTLER MH, SHIN BC & ERNST E (2008) Tai chi for osteoporosis: a systematic review. *Osteoporosis International* **19**, 139-146.
- LERNER ZF, HAIGHT DJ, DEMERS MS, BOARD WJ & BROWNING RC (2014) The Effects of Walking Speed on Tibiofemoral Loading Estimated Via Musculoskeletal Modeling. *Journal of Applied Biomechanics* **30**, 197-205.
- LEXELL J, DOWNHAM D & SJOSTROM M (1986) Distribution of different fiber types in human skeletal-muscles - fiber type arrangement in m-vastus lateralis from 3 groups of healthy-men between 15 and 83 years. *Journal of the Neurological Sciences* **72**, 211-222.
- LEXELL J, TAYLOR CC & SJOSTROM M (1988) What is the cause of the aging atrophy - total number, size and proportion of different fiber types studied in whole vastus lateralis muscle from 15-year-old to 83-year-old men. *Journal of the Neurological Sciences* **84**, 275-294.
- LIU D, ZHAO C-Q, LI H, JIANG S-D, JIANG L-S & DAI L-Y (2008) Effects of spinal cord injury and hindlimb immobilization on sublesional and supralesional bones in young growing rats. *Bone* **43**, 119-125.
- LUND ME, DE ZEE M, ANDERSEN MS & RASMUSSEN J (2012) On validation of multibody musculoskeletal models. *Proceedings of the Institution of Mechanical Engineers Part H-Journal of Engineering in Medicine* **226**, 82-94.
- MACLEAN C, NEWBERRY S, MAGLIONE M, et al. (2008) Systematic review: Comparative effectiveness of treatments to prevent fractures in men and women with low bone density or osteoporosis. *Annals of Internal Medicine* **148**, 197-213.
- MANSKE SL, BOYD SK & ZERNICKE RF (2011) Vertical ground reaction forces diminish in mice after botulinum toxin injection. *J. Biomech.* **44**, 637-643.
- MARENZANA M, DE SOUZA RL & CHENU C (2007) Blockade of beta-adrenergic signaling does not influence the bone mechano-adaptive response in mice. *Bone* **41**, 206-215.
- MARTELLI S, TADDEI F, CAPPELLO A, VAN SINT JAN S, LEARDINI A & VICECONTI M (2011) Effect of sub-optimal neuromotor control on the hip joint load during level walking. *Journal of Biomechanics* **44**, 1716-1721.
- MCCREDIE J (2007) Nerves in bone: the silent partners. *Skeletal Radiology* **36**, 473-475.

- MCKAY MD, BECKMAN RJ & CONOVER WJ (1979) A comparison of three methods for selecting values of input variables in the analysis of output from a computer code. *Technometrics* **21**.
- MOAZEN M, CURTIS N, EVANS SE, O'HIGGINS P & FAGAN MJ (2008) Combined finite element and multibody dynamics analysis of biting in a *Uromastix hardwickii* lizard skull. *Journal of Anatomy* **213**, 499-508.
- MOAZEN M, CURTIS N, O'HIGGINS P, EVANS SE & FAGAN MJ (2007) Musculoskeletal modelling and finite element analysis of lizard skulls. *Journal of Morphology* **268**, 1108-1108.
- MODENESE L, GOPALAKRISHNAN A & PHILLIPS ATM Application of a falsification strategy to a musculoskeletal model of the lower limb and accuracy of the predicted hip contact force vector. *Journal of Biomechanics* **46**, 1193-1200.
- MODENESE L, GOPALAKRISHNAN A & PHILLIPS ATM (2013) Application of a falsification strategy to a musculoskeletal model of the lower limb and accuracy of the predicted hip contact force vector. *Journal of Biomechanics* **46**, 1193-1200.
- MOORE KL, AGUR AMR & DALLEY AF (2011) *Essential Clinical Anatomy*. Lippincott Williams & Wilkins.
- MORSE L, TENG YD, PHAM L, et al. (2008) Spinal cord injury causes rapid osteoclastic resorption and growth plate abnormalities in growing rats (SCI-induced bone loss in growing rats). *Osteoporosis International* **19**, 645-652.
- MULLER ME & NAZARIAN S (1981) Classification of fractures of the femur and its use in the ao index. *Revue De Chirurgie Orthopedique Et Reparatrice De L Appareil Moteur* **67**, 297-309.
- MUNIH M & KRALJ A (1997) Modelling muscle activity in standing with considerations for bone safety. *J. Biomech.* **30**, 49-56.
- MUNIH M, KRALJ A & BAJD T (1992) Bending moments in lower-extremity bones for 2 standing postures. *Journal of Biomedical Engineering* **14**, 293-302.
- MURPHY L & SINGH BB (2008) Effects of 5-Form, Yang Style Tai Chi on older females who have or are at risk for developing osteoporosis. *Physiotherapy Theory and Practice* **24**, 311-320.
- NGUYEN TV, CENTER JR & EISMAN JA (2000) Osteoporosis in elderly men and women: Effects of dietary calcium, physical activity, and body mass index. *Journal of Bone and Mineral Research* **15**, 322-331.
- OJEDA J, MAYO J & MARTINEZ-REINA J (2011) Cost Function in Muscle Redundancy Problems: Computational Aspects. *Mechanics Based Design of Structures and Machines* **39**, 268-284.
- PAUWELS F (1980) *Biomechanics of the Locomotor Apparatus*. Springer-Verlag.
- PERRINI S, LAVIOLA L, CARREIRA MC, CIGNARELLI A, NATALICCHIO A & GIORGINO F (2010) The GH/IGF1 axis and signaling pathways in the muscle and bone: mechanisms underlying age-related skeletal muscle wasting and osteoporosis. *Journal of Endocrinology* **205**, 201-210.
- PIERROZ DD, BONNET N, BIANCHI EN, et al. (2012) Deletion of β -adrenergic receptor 1, 2 or both leads to different bone phenotypes and response to mechanical stimulation. *Journal of Bone and Mineral Research*, n/a-n/a.
- PITSILLIDES AA, RAWLINSON SCF, SUSWILLO RFL, BOURRIN S, ZAMAN G & LANYON LE (1995) Mechanical strain-induced NO production by bone cells: A possible role in adaptive bone (re)modeling? *Faseb J.* **9**, 1614-1622.

- POLIACHIK SL, BAIN SD, THREET D, HUBER P & GROSS TS (2010) Transient muscle paralysis disrupts bone homeostasis by rapid degradation of bone morphology. *Bone* **46**, 18-23.
- PRAAGMAN M, CHADWICK EKJ, VAN DER HELM FCT & VEEGER HEJ (2006) The relationship between two different mechanical cost functions and muscle oxygen consumption. *Journal of Biomechanics* **39**, 758-765.
- PRENDERGAST PJ & HUISKES R (1995) The biomechanics of wolff law - recent advances. *Irish Journal of Medical Science* **164**, 152-154.
- PRILUTSKY BI, HERZOG W & ALLINGER TL (1997) Forces of individual cat ankle extensor muscles during locomotion predicted using static optimization. *Journal of Biomechanics* **30**, 1025-1033.
- QIN YX, LAM H, FERRERI S & RUBIN C (2010) Dynamic skeletal muscle stimulation and its potential in bone adaptation. *Journal of Musculoskeletal Neuronal Interactions* **10**, 12-24.
- ROBLING AG (2009) Is Bone's Response to Mechanical Signals Dominated by Muscle Forces? *Medicine and Science in Sports and Exercise* **41**, 2044-2049.
- ROBLING AG, CASTILLO AB & TURNER CH (2006) Biomechanical and molecular regulation of bone remodeling. *Annual Review of Biomedical Engineering* **8**, 455-498.
- ROGERS MA & EVANS WJ (1993) Changes in skeletal muscle with aging: effects of exercise training. *Exercise and sport sciences reviews* **21**, 65-102.
- ROOS MR, RICE CL & VANDERVOORT AA (1997) Age-related changes in motor unit function. *Muscle & Nerve* **20**, 679-690.
- ROUX W (1885) Beitrage zur Morphologie der funktionellen Anpassung. *Arch Anat. Physiol. Anat.*, 120-158.
- RUBIN C, RECKER R, CULLEN D, RYABY J, MCCABE J & MCLEOD K (2004) Prevention of postmenopausal bone loss by a low-magnitude, high-frequency mechanical stimuli: A clinical trial assessing compliance, efficacy, and safety. *Journal of Bone and Mineral Research* **19**, 343-351.
- RUBIN J, RUBIN C & JACOBS CR (2006) Molecular pathways mediating mechanical signaling in bone. *Gene* **367**, 1-16.
- RUDMAN KE, ASPDEN RM & MEAKIN JR (2006) Compression or tension? The stress distribution in the proximal femur. *Biomedical Engineering Online* **5**.
- RÖHRLE O & PULLAN AJ (2007) Three-dimensional finite element modelling of muscle forces during mastication. *Journal of Biomechanics* **40**, 3363-3372.
- SALAMOUN MM, KIZIRIAN AS, TANNOUS RI, et al. (2005) Low calcium and vitamin D intake in healthy children and adolescents and their correlates. *European Journal of Clinical Nutrition* **59**, 177-184.
- SAMPLE SJ, BEHAN M, SMITH L, et al. (2008) Functional adaptation to loading of a single bone is neuronally regulated and involves multiple bones. *Journal of Bone and Mineral Research* **23**, 1372-1381.
- SAPARIN P, SCHERF H, HUBLIN JJ, FRATZL P & WEINKAMER R (2011) Structural Adaptation of Trabecular Bone Revealed by Position Resolved Analysis of Proximal Femora of Different Primates. *Anat. Rec.* **294**, 55-67.
- SCHWARTZ C, LUND ME, DE ZEE M, RASMUSSEN J & ASME (2010) Prediction of knee loads using a lower extremity model based on the klein horsman data set. *Proceedings of the Asme Summer Bioengineering Conference*, 2010.

- SELLERS WI & CROMPTON RH (2004) Using sensitivity analysis to validate the predictions of a biomechanical model of bite forces. *Annals of Anatomy-Anatomischer Anzeiger* **186**, 89-95.
- SHI J, CURTIS N, FITTON L, O'HIGGINS P & FAGAN M (2008) Musculoskeletal modelling of a macaque skull - sensitivity studies. *Journal of Vertebrate Paleontology* **28**, 141A-141A.
- SHI JF, CURTIS N, FITTON L, O'HIGGINS P & FAGAN MJ (2009) The effect of variations in muscle positions in a complex biomechanical model of a macaque skull. *American Journal of Physical Anthropology*, 238-238.
- SINAKI M, WOLLAN PC, SCOTT RW & GELCZER RK (1996) Can strong back extensors prevent vertebral fractures in women with osteoporosis? *Mayo Clinic Proceedings* **71**, 951-956.
- SKEDROS JG & BAUCOM SL (2007) Mathematical analysis of trabecular 'trajectories' in apparent trajectorial structures: The unfortunate historical emphasis on the human proximal femur. *Journal of Theoretical Biology* **244**, 15-45.
- SKELTON DA, KENNEDY J & RUTHERFORD OM (2002) Explosive power and asymmetry in leg muscle function in frequent fallers and non-fallers aged over 65. *Age and Ageing* **31**, 119-125.
- SUGIYAMA T, PRICE JS & LANYON LE (2010) Functional adaptation to mechanical loading in both cortical and cancellous bone is controlled locally and is confined to the loaded bones. *Bone* **46**, 314-321.
- SUTHERLAND DH (2001) The evolution of clinical gait analysis part I: kinesiological EMG. *Gait & Posture* **14**, 61-70.
- SUTHERLAND DH (2005) The evolution of clinical gait analysis part III - kinetics and energy assessment. *Gait & Posture* **21**, 447-461.
- SVRDLOVA NS & WITZEL U (2010) Principles of determination and verification of muscle forces in the human musculoskeletal system: Muscle forces to minimise bending stress. *Journal of Biomechanics* **43**, 387-396.
- TATSUMI S, ISHII K, AMIZUKA N, et al. (2007) Targeted ablation of Osteocytes induces osteoporosis with defective mechanotransduction. *Cell Metabolism* **5**, 464-475.
- TAYLOR ME, TANNER KE, FREEMAN MAR & YETTRAM AL (1996) Stress and strain distribution within the intact femur: Compression or bending. *Medical Engineering & Physics* **18**, 122-131.
- TERAN J, SIFAKIS E, BLEMKER SS, NG-THOW-HING V, LAU C & FEDKIW R (2005) Creating and simulating skeletal muscle from the visible human data set. *IEEE Transactions on Visualization and Computer Graphics* **11**, 317-328.
- TERRACCIANO C, CELI M, LECCE D, et al. (2013) Differential features of muscle fiber atrophy in osteoporosis and osteoarthritis. *Osteoporosis international : a journal established as result of cooperation between the European Foundation for Osteoporosis and the National Osteoporosis Foundation of the USA* **24**, 1095-100.
- TOBIN WJ (1955) The internal architecture of the femur and its clinical significance; the upper end. *The Journal of bone and joint surgery. American volume* **37-A**, 57-72; passim.
- VAN STAA TP, DENNISON EM, LEUFKENS HGM & COOPER C (2001) Epidemiology of fractures in England and Wales. *Bone* **29**, 517-522.
- VICECONTI M, TADDEI F, CRISTOFOLINI L, MARTELLI S, FALCINELLI C & SCHILEO E (2012) Are spontaneous fractures possible? An example of clinical application for

- personalised, multiscale neuro-musculo-skeletal modelling. *Journal of Biomechanics* **45**, 421-426.
- VIEIRA ELC, VIEIRA EA, DA SILVA RT, BERLFEIN PAD, ABDALLA RJ & COHEN M (2007) An anatomic study of the iliotibial tract. *Arthroscopy-the Journal of Arthroscopic and Related Surgery* **23**, 269-274.
- WHITE SC, YACK HJ, TUCKER CA & LIN HY (1998) Comparison of vertical ground reaction forces during overground and treadmill walking. *Medicine and Science in Sports and Exercise* **30**, 1537-1542.
- WILLIAMS GN, HIGGINS MJ & LEWEK MD (2002) Aging skeletal muscle: Physiologic changes and the effects of training. *Physical Therapy* **82**, 62-68.
- WOLFF J (1986) *The law of bone remodelling.* Springer-Verlag, Berlin, 3-22.
- YOU J, YELLOWLEY CE, DONAHUE HJ, ZHANG Y, CHEN Q & JACOBS CR (2000) Substrate deformation levels associated with routine physical activity are less stimulatory to bone cells relative to loading-induced oscillatory fluid flow. *Journal of Biomechanical Engineering-Transactions of the Asme* **122**, 387-393.
- YOU LD, COWIN SC, SCHAFFLER MB & WEINBAUM S (2001) A model for strain amplification in the actin cytoskeleton of osteocytes due to fluid drag on pericellular matrix. *Journal of Biomechanics* **34**, 1375-1386.
- ZEBAZE RMD, JONES A, KNACKSTEDT M, MAALOUF G & SEEMAN E (2007) Construction of the femoral neck during growth determines its strength in old age. *Journal of Bone and Mineral Research* **22**, 1055-1061.
- ZHANG WP, KANEHARA M, ZHANG YJ, WANG XM & ISHIDA T (2007) beta-blocker and other analogous treatments that affect bone mass and sympathetic nerve activity in ovariectomized rats. *American Journal of Chinese Medicine* **35**, 89-101.